A Molecular Investigation of the Isoform-Specific Activities of *Dictyostelium discoideum* Class I PI3Ks During Macropinocytic Cup Formation

Ana Paula Guevara-Cerdán

A thesis submitted in partial fulfilment of the requirements for the degree of Doctor of Philosophy

The University of Sheffield
Faculty of Science
School of Biosciences

2025

To my Parents

To my Grandparents

To my Husband

To my Brother

To my Teachers and Mentors

Abstract

Class I phosphoinositide 3-kinases (PI3Ks) are central regulators of membrane dynamics and actin remodelling in most eukaryotic cells, yet the isoform-specific roles of these enzymes remain poorly understood. In *Dictyostelium discoideum*, the Class I PI3K isoforms PikA and PikF are both essential for macropinocytosis, but the molecular basis of their non-redundant activities has not been resolved. This thesis investigates their distinct contributions to macropinocytic cup formation through a multidisciplinary approach combining structural biology, genetic engineering, live-cell imaging, and proteomics.

We demonstrate that PikA and PikF share highly conserved catalytic domains but differ substantially in their N-terminal regions, which likely drive their isoform-specific localisation and function. Spinning Disk Confocal and Lattice Light Sheet Microscopy reveal that PikA is enriched at the base of macropinocytic cups, where it plays a critical role in initiating cup formation and coordinating early actin assembly. In contrast, PikF localises throughout the entire cup, extending into the rim, and plays a key role in restricting Rac1 activity, thereby facilitating proper cup extension and closure. Live-cell imaging further reveals divergent trafficking behaviours, with PikA undergoing vesicular recycling and PikF remaining cytosolic when not membrane-bound.

Affinity Purification-Mass Spectrometry (AP-MS) reveals largely distinct interactomes: PikA associates with microtubule motors, myosins, and actin nucleators, while PikF interacts with actin disassembly factors, IQGAP scaffolds, and GTPase regulators. These isoform-specific networks suggest that PI3K function is not solely determined by lipid kinase activity, but also by spatially organised protein-protein interactions.

Together, these findings support a revised model of *D. discoideum* Class I PI3Ks, where isoform specificity arises from domain-dependent localisation and scaffolding roles that coordinate actin dynamics at distinct stages of macropinocytosis – extending beyond the traditional view of Class I PI3Ks as mere PIP_3 producers. This work advances our understanding of PI3K-driven large-scale endocytosis and offers broader insight into how spatial signalling architectures govern cellular behaviour in eukaryotes.

Table of Contents

Abstract **2**

Table of Contents **4**

List of Figures **7**

List of Tables **13**

List of Supplementary Movies **15**

Chapter 1: Introduction **18**

1.1 Macropinocytosis 19

1.1.1 What is Macropinocytosis? 19

1.1.2 How Does Macropinocytosis Differ from Other Endocytic Pathways? 19

1.1.3 Macropinocytosis in Human Health and Disease 22

1.2 Phosphoinositide 3-Kinases (PI3Ks) 24

1.2.1 What are Phosphoinositides? 24

1.2.2 The Three Classes of PI3K 24

1.2.3 Mammalian Class I PI3Ks in Cell Signalling 28

1.2.4 Mammalian Class I PI3Ks in Membrane Dynamics 29

1.2.5 Class I PI3Ks in Human Health & Disease 30

1.3 The Cytoskeletal Mediation of Membrane Remodeling 30

1.3.1 The Role of the Cytoskeleton in Membrane Dynamics 30

Cytoskeletal Components 30

Cytoskeletal Motor Proteins 32

1.3.2 The Mechanical Drivers of Membrane Dynamics: Actin Regulators 33

Actin Nucleation 33

Branched versus Linear Actin Filaments 34

Actin Filament Cross-Linking 35

Actin Filament Disassembly and Turnover 35

1.3.3 The Orchestrators of Membrane Dynamics: Small GTPases 36

1.4 Dictyostelium discoideum: A Model for Investigating Class I PI3K Function in Macropinocytosis 37

1.4.1 Dictyostelium discoideum as a Model Organism 37

1.4.2 Molecular Basis of Macropinocytosis in Dictyostelium discoideum 37

Genomic and Structural Complexity of Signalling Networks 37

Regulation of Rac Activity by GEFs and GAPs 38

Downstream Effectors: PAK Kinases and Class I Myosins 38

PI3Ks and the Spatial Organisation of Macropinocytic Cups 39

1.5 Summary Remarks 40

1.6 Project Aims and Hypothesis 41

Overall Aim....41
Specific Aims....41
Central Hypothesis....41
1.7 References....42

Chapter 2: Methods....52
2.1 Bioinformatics and Cloning....53
2.1.1 Dictyostelium discoideum PI3K Isoform Sequence Analysis....53
2.1.2 PikA and PikF Protein Structure Prediction and Visualisation....53
2.1.3 Construction of Extrachromosomal Expression Vectors....53
2.1.4 Tagging PikA and PikF with N-terminal GFP....54
2.1.5 Protein Design: PikA/PikF Chimeras....54
2.1.6 Protein Design: Kinase-inactive PikF....57
2.2 Dictyostelium discoideum Strains and Cell Culture....57
2.2.1 Growth of D. discoideum in Axenic and Non-Axenic Culture....57
2.2.2 D. discoideum Transformations with Plasmid DNA....58
2.3 Cellular Uptake Assays....59
2.3.1 Macropinocytosis Assay....59
2.3.2 Phagocytosis Assay....60
2.3.3 Preparation of TRITC-Dextran and Alexa405/594-Labelled Yeast....60
2.3.4 Statistical Analysis....60
2.4 Protein-Based Assays....61
2.4.1 Western Blotting....61
2.4.2 Rac1 Pull-Down and Detection....61
2.4.3 Affinity Purification Mass Spectrometry (AP-MS)....62
2.5 Live-Cell Microscopy....62
2.5.1 General Sample Preparation and Image Analysis....62
2.6 References....63

Chapter 3: Class I PI3K Isoform Specificity in Dictyostelium discoideum Macropinocytosis....64
3.1 Introduction....65
Research Questions Addressed in this Chapter....66
3.2 Results....67
3.2.1 PikA and PikF Mutants Display Impaired Macropinocytosis....67
3.2.2 PikA and PikF Perform Distinct, Non-Redundant Functions....68
3.2.3 Isoform-Specific Function Is Independent of the Catalytic Domain....69
3.2.4 Proteasomal Regulation of PI3K Isoform Expression....74
3.2.5 Differential Localisation of PikA and PikF in Macropinocytic Cups....75
3.2.6 Challenges in Visualising Phosphoinositide Dynamics....84
3.2.7 Morphological Differences Between PikA/B- and PikF- Cells....85
3.3 Discussion....88
Beyond catalysis: structural basis of PikA and PikF functional divergence....88
Isoform-specific localisation patterns during macropinocytic cup formation....91

Interpreting phosphoinositide probe specificity....92
Comparative morphology of PikA/B- and PikF- cells....93
3.4 References....94

Chapter 4: Isoform-Specific Regulation of GTPase Signalling and Actin Dynamics by Class I PI3Ks in Dictyostelium discoideum....96
4.1 Introduction....97
Research Questions Addressed in this Chapter....97
4.2 Results....98
4.2.1 Class I PI3Ks Influence Ras and Rac Signalling Pathways....98
Ras and Rac Signalling in Macropinocytic Cups....98
Ras and Rac Signalling in Basal Waves....103
Rac1 Pull-Down Assays....108
4.2.2 Altered F-actin and PIP3 Dynamics in PikA and PikF Mutant Cells....109
4.2.3 F-actin and PIP3 Dynamics in Phagocytic Cup Formation....116
4.3 Discussion....126
Rim feedback fails in PikF- cells, expanding Rac activity beyond the cup rim...126
Rac1 pull-down assays: technical challenges and interpretative caution....126
Basal waves may not be a reliable proxy for cup dynamics....126
PikA/B loss impairs cup initiation, whereas PikF loss disrupts rim confinement 127
Basal-wave behaviour exposes isoform-specific defects in initiation and confinement....127
Phagocytosis reveals isoform-specific roles and competition with macropinocytosis....127
4.4 References....129

Chapter 5: Proteomic Dissection of PikA and PikF Isoform-Specific Interactors in Dictyostelium discoideum Macropinocytosis....130
5.1 Introduction....131
Research Questions Addressed in this Chapter....131
5.2 Results....132
5.2.1 Shared PikA and PikF Interactors....134
5.2.2 PikA-Specific Interactors....146
5.2.3 PikF-Specific Interactors....156
5.3 Discussion....166
Isoform-specific cytoskeletal interactomes of PikA and PikF revealed by AP-MS...166
PikA-specific interactors: microtubule and motor protein complexes....166
PikF-specific interactors: actin disassembly and turnover....167
The role of IQGAP scaffolds in spatial PI3K signalling coordination....169
MyoB, ForG, P80 and LimC are of particular interest....169
5.4 References....171

Chapter 6: Discussion....176
References....181

List of Figures

Figure 1.1 “Overview of the primary mechanisms of uptake into cells” (Rennick et al., 2021)

Figure 1.2 The chemical structure of phosphatidylinositol

Figure 1.3 Mammalian Class I PI3K isoforms and their respective regulatory subunits

Figure 1.4 Mammalian Class II PI3K isoforms

Figure 1.5 Mammalian Class III PI3K (VPS34)

Figure 1.6 Domain arrangement of the 11 PI3K/PI4K catalytic domain-containing proteins found in the *Dictyostelium discoideum* proteome

Figure 1.7 The distribution of the three cytoskeletal filament networks and their formation from monomeric components

Figure 2.1 Design of PikA/PikF Chimeras 1-8

Figure 2.2 Confirmation of A to G mutation in pDM1043-K3356R (pAP73)

Figure 3.1 Domain arrangements and tertiary structures of PikA and PikF

Figure 3.2 Macropinocytosis defects in PikA^{-}, PikA/B^{-}, and PikF^{-} cells

Figure 3.3 Rescue of PikA/B^{-} and PikF^{-} macropinocytosis defects by GFP-PikA and GFP-PikF

Figure 3.4 Schematic representation of PikA/PikF chimeras (Chimeras 1-8)

Figure 3.5 Rescue of PikA/B^{-} macropinocytosis defect by GFP-PikA, GFP-PikF and GFP-tagged Chimeras 1 to 4

Figure 3.6 Rescue of PikF$^-$ macropinocytosis defect by GFP-PikA, GFP-PikF and GFP-tagged Chimeras 1 to 4

Figure 3.7 Amino acid sequence alignment of conserved regions within the PI3K catalytic domains of PikA, PikB, and PikF

Figure 3.8 Rescue of PikF$^-$ macropinocytosis defect by GFP-tagged kinase-inactive PikF (GFP-K3356R)

Figure 3.9 Western blot analysis of PikF$^-$ cells expressing GFP-PikA, GFP-PikF and GFP-tagged Chimeras 1 to 4

Figure 3.10 Representative images of macropinocytic cups in PikA/B$^-$ and PikF$^-$ cells expressing GFP-PikA and GFP-PikF, respectively, used for quantitative analysis

Figure 3.11 Localisation patterns of PikA and PikF throughout macropinocytic cups

Figure 3.12 Co-localisation of GFP-PikA with the PIP_3 probe PkgE-PH-mCherry at macropinocytic cups in PikA/B$^-$ cells

Figure 3.13 Time-lapse filmstrip (6 seconds) showing co-localisation of GFP-PikA with the PIP_3 probe PkgE-PH-mCherry at the macropinocytic cup in PikA/B$^-$ cells

Figure 3.14 Time-lapse filmstrip (15 seconds) showing co-localisation of GFP-PikA with the PIP_3 probe PkgE-PH-mCherry at the macropinocytic cup in PikA/B$^-$ cells

Figure 3.15 Co-localisation of GFP-PikF with the PIP_3 probe PkgE-PH-mCherry at macropinocytic cups in PikF$^-$ cells

Figure 3.16 Time-lapse filmstrip (3 seconds) showing co-localisation of GFP-PikF with the PIP_3 probe PkgE-PH-mCherry at the macropinocytic cup in PikF$^-$ cells

Figure 3.17 Representative examples of GFP-PikF co-localisation with the PIP_3 probe PkgE-PH-mCherry in PikF$^-$ cells

Figure 3.18 3D projections of wild-type (Ax2), PikA/B$^-$ and PikF$^-$ cells expressing $PI(3,4)P_2$ and PIP_3 probes

Figure 3.19 Cell area, perimeter, and circularity measurements in wild-type (Ax2), PikA/B$^-$, and PikF$^-$

Figure 3.20 Representative images of spike-like membrane protrusions in wild-type (Ax2), PikA/B$^-$, and PikF$^-$ cells expressing Rac and Ras activity probes

Figure 3.21 Quantification of spike-like membrane protrusions in wild-type (Ax2), PikA/B$^-$, and PikF$^-$ cells

Figure 3.22 Structural superimposition of PikA and PikF catalytic domains highlighting conserved features

Figure 3.23 Phylogram of the 11 PI3K/PI4K catalytic domains in the *Dictyostelium discoideum* proteome

Figure 3.24 Structural superimposition of individual PikA and PikF domains

Figure 3.25 Schematic representation of PikA/PikF Chimeras 9-12

Figure 4.1 Representative line scans used to measure Rac and Ras signal distribution across macropinocytic cups in wild-type (Ax2), PikA/B$^-$, and PikF$^-$ cells

Figure 4.2 Relative intensity profiles of Ras and Rac signals across macropinocytic cups in wild-type (Ax2) cells

Figure 4.3 Relative intensity profiles of Ras and Rac signals across macropinocytic cups in PikA/B$^-$ cells

Figure 4.4 Relative intensity profiles of Ras and Rac signals across macropinocytic cups in PikF$^-$ cells

Figure 4.5 Representative line scans used to measure Rac and Ras signal distribution across basal patches in wild-type (Ax2), PikA/B$^-$, and PikF$^-$ cells

Figure 4.6 Relative intensity profiles of Ras and Rac signals across basal membrane patches in wild-type (Ax2) cells

Figure 4.7 Relative intensity profiles of Ras and Rac signals across basal membrane patches in PikA/B$^-$ cells

Figure 4.8 Relative intensity profiles of Ras and Rac signals across basal membrane patches in PikF$^-$ cells

Figure 4.9 Western blot analysis of Rac1 Pull-Down samples from wild-type (Ax2), PikA/B$^-$ and PikF$^-$ cells

Figure 4.10 Representative pinocytic events in wild-type (Ax2), PikA/B$^-$, PikF$^-$ and PikA/B/F$^-$ cells

Figure 4.11 Macropinocytic cup formation in wild-type (Ax2) cells

Figure 4.12 Pinocytic events in PikA/B$^-$ cells

Figure 4.13 Pinocytic events in PikA/B/F$^-$ cells

Figure 4.14 Pinocytic events in PikF$^-$ cells

Figure 4.15 Localisation of F-actin and PIP_3 at basal waves in wild-type (Ax2), PikA/B$^-$, PikF$^-$ and PikA/B/F$^-$ cells

Figure 4.16 Localisation of F-actin and PIP_3 at basal waves in wild-type (Ax2) cells

Figure 4.17 Localisation of F-actin and PIP_3 at basal waves in PikA/B$^-$ cells

Figure 4.18 Localisation of F-actin and PIP_3 at basal waves in PikF$^-$ cells

Figure 4.19 Localisation of F-actin and PIP_3 at basal waves in PikA/B/F$^-$ cells

Figure 4.20 Phagocytosis defects in PikA/B$^-$ compared to wild-type (Ax2) and PikF$^-$ cells

Figure 4.21 Rate of successful phagocytic cup closure events in wild-type (Ax2), PikA/B$^-$, PikF$^-$, and PikA/B/F$^-$ cells

Figure 4.22 Failure of phagocytic cup formation in favour of macropinocytic cup closure in wild-type (Ax2) cells

Figure 4.23 Successful and unsuccessful phagocytic cup formation in wild-type (Ax2) cells

Figure 4.24 Post-engulfment disassembly of F-actin around a budding yeast particle in a wild-type (Ax2) cell

Figure 4.25 Successful and unsuccessful phagocytic cup formation in PikA/B$^-$ cells

Figure 4.26 Successful and unsuccessful phagocytic cup formation in PikF$^-$ cells

Figure 4.27 Successful and unsuccessful phagocytic cup formation in PikA/B/F$^-$ cells

Figure 4.28 Examples of F-actin and PIP_3 localisation at phagocytic cups in PikA/B/F$^-$ cells

Figure 5.1 Variability in GFP-trap pull-down yields across technical repeats

Figure 5.2 Reactome Pathway enrichment analysis of the 203 interactors shared between GFP-PikA and GFP-PikF

Figure 5.3 Protein-protein interaction network of interactors shared between GFP-PikA and GFP-PikF associated with the 'RHO GTPase Cycle' pathway

Figure 5.4 Protein-protein interaction network of interactors shared between GFP-PikA and GFP-PikF associated with the 'RAC1 GTPase Cycle'

Figure 5.5 Protein-protein interaction network of interactors shared between GFP-PikA and GFP-PikF associated with 'Signal Transduction'

Figure 5.6 Cellular Component enrichment analysis of interactors shared between GFP-PikA and GFP-PikF associated with 'Cytoskeleton'

Figure 5.7 Biological Process enrichment analysis of interactors shared between GFP-PikA and GFP-PikF associated with 'Cytoskeleton'

Figure 5.8 Cellular Component enrichment analysis of interactors shared between GFP-PikA and GFP-PikF associated with 'Endosome'

Figure 5.9 Biological Process enrichment analysis of interactors shared between GFP-PikA and GFP-PikF associated with 'Endosome'

Figure 5.10 Subcellular Localisation enrichment analysis of GFP-PikA-specific interactors associated with 'Cytoskeleton'

Figure 5.11 Biological Process enrichment analysis of GFP-PikA-specific interactors associated with 'Cytoskeleton'

Figure 5.12 Molecular Function enrichment enrichment analysis of GFP-PikA-specific interactors associated with 'Cytoskeleton'

Figure 5.13 Local Network Cluster enrichment analysis of GFP-PikA-specific interactors associated with 'Cytoskeleton'

Figure 5.14 Protein Domains and Features enrichment analysis of GFP-PikA-specific interactors associated with 'Cytoskeleton Organisation'

Figure 5.15 Biological Process enrichment analysis of GFP-PikA-specific interactors associated with 'Endocytosis'

Figure 5.16 Molecular Function enrichment analysis of GFP-PikF-specific interactors associated with 'Cytoskeleton'

Figure 5.17 Subcellular Localisation enrichment analysis of GFP-PikF-specific interactors associated with ‘Cytoskeleton’

Figure 5.18 Biological Process enrichment analysis of GFP-PikF-specific interactors associated with ‘Cytoskeleton’

Figure 5.19 Local Network Cluster enrichment analysis of GFP-PikF-specific interactors associated with ‘Cytoskeleton Organisation’

Figure 5.20 Biological Process enrichment analysis of GFP-PikF-specific interactors associated with ‘Regulation of Cytoskeleton Organisation’

Figure 5.21 Local Network Cluster enrichment analysis of GFP-PikF-specific interactors associated with ‘Regulation of Cytoskeleton Organisation’

Figure 5.22 Protein Domains and Features enrichment analysis of GFP-PikF-specific interactors associated with ‘Regulation of Cytoskeleton Organisation’

Figure 6.1 Schematic illustration of PikA and PikF localisation within macropinocytic cups, shown in relation to F-actin, SCAR/WAVE and RGBARG

Figure 6.2 Model illustrating the effects of PikF loss on Rac regulation and actin dynamics during macropinocytic cup formation

Figure 6.3 Model illustrating the coordinated regulation of branched and linear actin networks during macropinocytic cup formation in wild-type *D. discoideum* cells

List of Tables

Table 2.1 Oligos used for the amplification of PikA and PikF from *D. discoideum* gDNA

Table 2.2 Oligos used for fragment amplification in the construction of Chimeras 1-8

Table 2.3 Oligos used to join fragments together in the construction of Chimeras 1-8

Table 2.4 *D. discoideum* expression vectors used in this study

Table 5.1 Summary of Affinity Purification-Mass Spectrometry (AP-MS) output

Table 5.2 GFP-PikA and GFP-PikF shared interactors associated with ‘Cytoskeleton’

Table 5.3 GFP-PikA and GFP-PikF shared interactors associated with ‘Cytoskeleton Organisation’

Table 5.4 GFP-PikA and GFP-PikF shared interactors associated with ‘Endosome’.

Table 5.5 GFP-PikA-specific interactors associated with ‘Cytoskeleton’

Table 5.6 GFP-PikA-specific interactors associated with ‘Cytoskeleton Organisation’

Table 5.7 GFP-PikA-specific interactors associated with ‘Endocytosis’

Table 5.8 GFP-PikA-specific interactors associated with ‘Endosome’

Table 5.9 GFP-PikF-specific interactors associated with ‘Cytoskeleton’

Table 5.10 GFP-PikF-specific interactors associated with ‘Cytoskeleton Organisation’

Table 5.11 GFP-PikF-specific interactors associated with ‘Regulation of Cytoskeleton Organisation’

Table 5.12 GFP-PikF-specific interactors associated with ‘Endosome’

Table 5.13 Tentative PikA- and PikF-enriched interactors with enrichment values below 2x

List of Supplementary Movies

SM1 Time-lapse filmstrip (6 seconds) showing co-localisation of GFP-PikA with the PIP_3 probe PkgE-PH-mCherry at the macropinocytic cup in PikA/B$^-$ cells

SM2 Time-lapse filmstrip (15 seconds) showing co-localisation of GFP-PikA with the PIP_3 probe PkgE-PH-mCherry at the macropinocytic cup in PikA/B$^-$ cells

SM3 Time-lapse filmstrip (3 seconds) showing co-localisation of GFP-PikF with the PIP_3 probe PkgE-PH-mCherry at the macropinocytic cup in PikF$^-$ cells

SM4 Macropinocytic cup formation in Ax2 cells

SM5 Pinocytic events in PikA/B$^-$ cells

SM6 Pinocytic events in PikF$^-$ cells

SM7 Pinocytic events in PikA/B/F$^-$ cells

SM8 Localisation of F-actin and PIP_3 at basal waves in wild-type (Ax2) cells

SM9 Localisation of F-actin and PIP_3 at basal waves in PikA/B$^-$ cells

SM10 Localisation of F-actin and PIP_3 at basal waves in PikF$^-$ cells

SM11 Localisation of F-actin and PIP_3 at basal waves in PikA/B/F$^-$ cells

SM12 Failure of phagocytic cup formation in favour of macropinocytic cup closure in wild-type (Ax2) cells – Example 1

SM13 Failure of phagocytic cup formation in favour of macropinocytic cup closure in wild-type (Ax2) cells – Example 2

SM14 Successful phagocytic cup formation in wild-type (Ax2) cells

SM15 Unsuccessful phagocytic cup formation in wild-type (Ax2) cells

SM16 Post-engulfment disassembly of F-actin around a budding yeast particle in a wild-type (Ax2) cell

SM17 Successful phagocytic cup formation in PikA/B^{-} cells

SM18 Unsuccessful phagocytic cup formation in PikA/B^{-} cells

SM19 Successful phagocytic cup formation in PikF^{-} cells

SM20 Unsuccessful phagocytic cup formation in PikF^{-} cells

SM21 Successful phagocytic cup formation in PikA/B/F^{-} cells

SM22 Unsuccessful phagocytic cup formation in PikA/B/F^{-} cells

Declaration

I, Ana Paula Guevara-Cerdán, confirm that this thesis is my own work.

I am aware of the University's Guidance on the Use of Unfair Means (www.sheffield.ac.uk/ssid/unfair-means).

This work has not previously been presented for an award at this, or any other, university.

Chapter 1: Introduction

1.1 Macropinocytosis

1.1.1 What is Macropinocytosis?

Cell drinking as “the act of sipping adjacent fluid” was first theorised by S. J. Meltzer in 1904 (Lewis, 1937). However, the term pinocytosis, composed of the Greek words πίνω (pino) ‘to drink’ and κύτταρο (kýttaro) ‘cell’, was first used in 1931 by W. H. Lewis when he published the first morphological description of macropinocytosis, which up to that point had been known amongst colleagues as “hydrophagocytosis” or “the Lewis phenomenon” (Chapman-Andresen, 1984). Lewis first observed and described the engulfment of extracellular fluid through movements of the cell surface membrane of rat macrophages, and he later noticed this same phenomenon in malignant cells from rat and mouse tumours (Lewis, 1937). The term *macro*pinocytosis was later devised to differentiate the process first described by Lewis from small-scale cellular fluid uptake (Lim and Gleeson, 2011; Palm, 2019). In the present day, macropinocytosis is defined as the cellular uptake of fluid and solutes into vesicles larger than 0.2 μm in diameter (Kerr and Teasdale, 2009). After nearly a century since its first documented morphological description, many aspects of the molecular mechanisms enabling large-scale fluid uptake in eukaryotic cells, including the intricacies of signalling and regulatory pathways, remain undefined. Since the early studies in the 1930s, macropinocytosis has slowly become recognised as a biological process relevant to health and disease worthy of investigation (Chapman-Andresen, 1984). Macropinocytosis research is a growing field which continues to attract attention, and is currently studied in relation to viral and bacterial pathogenesis, immunology, inflammation, cancer metabolism, neurodegeneration, and the development of novel drug delivery mechanisms (Bloomfield and Kay, 2016; Palm, 2019; Qiu et al., 2022; Stow et al., 2020; Swanson and Watts, 1995; Zeineddine and Yerbury, 2015).

1.1.2 How Does Macropinocytosis Differ from Other Endocytic Pathways?

Endocytosis is the cellular process by which extracellular material is internalised. Endocytic processes can be classified under macroscale or microscale endocytosis. Macroscale (large-scale) endocytosis encompasses both phagocytosis - the cellular uptake of solid particles larger than 0.5 μm in diameter (Flannagan et al., 2012) - and macropinocytosis. Microscale (small-scale) endocytosis, on the other hand, is defined by the uptake of extracellular material into vesicles smaller than 0.2 μm in diameter (Kumari et al., 2010). Microscale endocytosis can be subdivided into two categories: the coat protein-mediated pathways known as Clathrin- and Caveolin-mediated endocytosis, which are associated with Dynamin-mediated vesicle scission, and the coat protein-independent endocytic pathway most commonly known as Clathrin-independent (CI) endocytosis, which can be Dynamin-dependent or independent (Kumari et al., 2010; Mayor and Pagano, 2007). Because phagocytosis and macropinocytosis are Clathrin-independent, they may sometimes be described as CI endocytic pathways as well. However, it is important to differentiate these as their own class of large-scale endocytosis. Small-scale CI endocytosis includes two subtypes of endocytic processes known as FEME and CLIC/GEEC: fast endophilin-mediated endocytosis (clathrin-independent, dynamin-dependent), which is a

ligand-driven process specific for the internalisation of membrane proteins (Rennick et al., 2021), and clathrin-independent carrier/glycosylphosphatidylinositol-anchored protein-enriched early endocytic compartment endocytosis (clathrin- and dynamin-independent), which is also a process by which a range of transmembrane proteins are internalised (Mechanobiology Institute, National University of Singapore, 2023). In total, including all macroscale and microscale endocytic pathways, there is now a consensus for six forms of endocytosis: Phagocytosis, Macropinocytosis, Clathrin-mediated endocytosis (CME), Caveolin-mediated endocytosis (Caveolae), FEME and CLIC/GEEC (Rennick et al., 2021) (Figure 1.1).

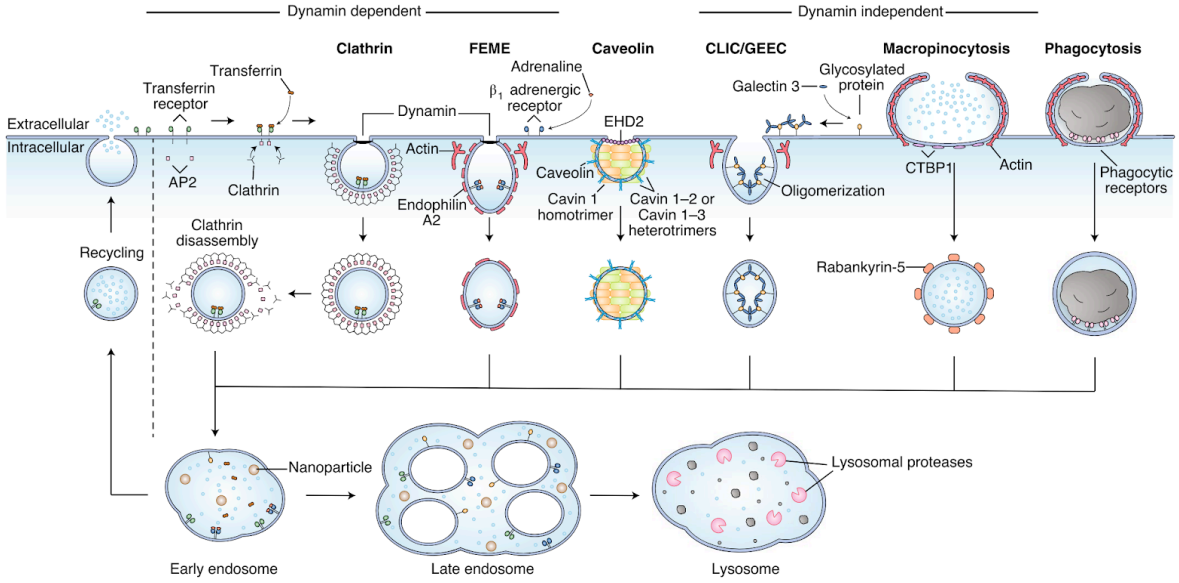

Figure 1.1 "Overview of the primary mechanisms of uptake into cells" (Rennick et al., 2021). From left to right: Adaptor Protein Complex 2 (AP2) recruits Clathrin to cytosolic receptors leading to the formation of Clathrin-coated pits (CCPs) (Lacruz et al., 2013). Endophilin A2 is recruited to FEME pits following receptor activation by the binding of ligand molecules; FEME is regulated by Edophilin A2 and Actin polymerisation. Caveolin and Cavin proteins lead to the formation of Caveolae, which are stabilised and regulated by Eps15 homology domain-containing 2 (EHD2) at the neck of the pit (Torrino et al., 2018). Constitutive CLIC/GEEC happens independently of receptor-ligand binding and is regulated by Actin dynamics; Galectin proteins cluster glycoproteins and glycolipids driving carrier formation with incorporated cargo. Macropinocytosis is an Actin-driven process that leads to the uptake of large volumes of fluid and solutes. In human carcinoma cells, during epidermal growth factor (EGF)-mediated macropinocytosis, macropinosome membrane fission is independent of Dynamin GTPase activity, and instead involves C-terminal-binding protein-1 (CTBP1) activity driven by p21-activated kinase (PAK) phosphorylation (Liberali et al., 2008). Phagocytosis occurs upon receptor-binding to a solid particle, which triggers actin polymerisation and drives the engulfment of the bound particle into a phagocytic vesicle. After internalisation, endosomes from all pathways merge into early endosomes. Thereafter, material can be recycled back to the cell surface or continues onwards to the late endosome and lysosome for processing (Rennick et al., 2021).

As well as the difference in size between macropinosomes and smaller fluid-filled vesicles, macropinocytosis (0.2-5 μm), CME (~0.1 μm), Caveolae (~0.06 μm), FEME (0.06-0.08 μm) and CLIC/GEEC (~0.1 μm) differ in function. Macropinocytosis is an unselective feeding mechanism evolutionarily conserved from the last common ancestor of the amoebozoa and metazoa, which enables cells to ingest nutrients from their extracellular environment (Kay, 2021). CME is recognised as the principal route for mammalian cells to obtain receptor-bound nutrients including iron and cholesterol (Rennick et al., 2021), and in neuronal cells, CME contributes to the formation of synaptic vesicles (Royle and Lagnado, 2003; Takei and Haucke, 2001). Caveolae are uniquely evolved in metazoa (Kirkham et al., 2008); they provide cells with mechanoprotection in response to increased membrane tension, are involved in mechanosensing and mechanotransduction, can modify the extracellular matrix through the modulation of exosome deposition, and serve as specialised lipid domains (Parton et al., 2020; Sotodosos-Alonso et al., 2023). FEME is a rapid, GPCR-specific endocytic pathway specialised in the movement of ligand-stimulated GPCR receptors towards the cell centre within seconds (Boucrot et al., 2015). And lastly, in mammalian cells and *Drosophila*, CLIC/GEEC is a constitutive pathway that mediates the uptake of various types of cargo including fluid, membrane and membrane-anchored proteins, and is also involved in the regulation of plasma membrane tension homeostasis through the mechanotransducer Vinculin (Rennick et al., 2021).

As illustrated in Figure 1.1, the six consensual endocytic pathways are driven by pathway-specific molecules, as well as overlapping cellular machinery. CME is initiated by the formation of the Clathrin complex, which is dependent on the accumulation of Adaptor Protein (AP) complexes mediated by $PI(4,5)P_2$ binding (Mousavi et al., 2004); thereafter, Clathrin-coated pit (CCP) growth is driven by Actin nucleation by the Arp2/3 complex, stabilised by negatively-charged-lipid-interacting BAR domain proteins (Dawson et al., 2006), and terminated by membrane fission through Dynamin GTPase activity (Ferguson et al., 2009). $PI(4,5)P_2$ is also known to be enriched inside Caveolae structures, and Caveolae-associated proteins such as Cavins, EHD2 and Dynamin have $PI(4,5)P_2$-binding properties (Parton et al., 2020; Sotodosos-Alonso et al., 2023). FEME on the other hand, which is Actin-driven like CME, requires Class I PI3K activity for the production of PIP_3 from $PI(4,5)P_2$, allowing for the production of $PI(3,4)P_2$ by SHIP phosphatase activity throughout the inside of the FEME pit, and in turn enabling the recruitment of Endophilin for membrane scission aided by Dynamin (Boucrot et al., 2015). CLIC/GEEC is also Actin-driven by the Arp2/3 complex, and is regulated by the small GTPases Arf1 and Cdc42, and the BAR domain protein IRSp53 (Sathe et al., 2018). As well as phosphoinositide signalling and Actin-driven dynamics, other commonalities might be shared between CI endocytic pathways, for example, Cholesterol perturbation was found to affect Caveolae, FEME and CLIC/GEEC (Rennick et al., 2021).

The macroscale endocytic processes - phagocytosis and macropinocytosis - also share overlapping cellular machinery between them and with the different forms of microscale endocytosis. The most evident difference between macroscale and microscale endocytosis is the greater degree of cytoskeletal rearrangements required for the larger endocytic processes; however, Actin dynamics regulated through small GTPase and phosphoinositide signalling remain at the centre of these. Phagocytosis primarily differs from macropinocytosis in the way that it relies on directional Actin polymerisation guided in a zipper-like manner by the shape of a membrane-bound solid particle through surface receptor interactions. In RAW

264.7 cells, this process has been shown to require the coordination of both Actin polymerisation and depolymerisation through the sequential signalling events mediated by the production of $PI(4,5)P_2$, $PI(3,4,5)P_3$, $PI(3,4)P_2$ membrane domains, and Rac1/Cdc42 activation (Montaño-Rendón et al., 2022; O'Reilly et al., 2003; Scott et al., 2005). The contribution of enzymes such as Phosphoinositide 5-Phosphatases and Phospholipase C (PLC) to phagocytic cup formation has been recognised, but their precise roles remain unclear (Montaño-Rendón et al., 2022). Macropinocytic cup formation, on the other hand, is spatiotemporally coordinated independently of a physical guide. In *Dictyostelium discoideum* amoebae, this is believed to be a process driven by the spontaneous formation of Actin protrusions (Vines and King, 2019). In human cells, constitutive macropinocytosis, which is specific to macrophages and dendritic cells, is triggered by the activation of calcium-sensing GPCR receptors (CaSRs) upon Ca^{2+} binding, leading to the formation of Actin-driven membrane ruffles through $PI(4,5)P_2$, $PI(3,4,5)P_3$, and $PI(3,4)P_2$ dynamics, as well as Rac1/Cdc42 signalling (Canton et al., 2016; Maekawa et al., 2014). In parallel, the production of diacylglycerol (DAG) by the hydrolysis of $PI(4,5)P_2$, as well as the phosphorylation of DAG into phosphatidic acid (PA or PtdOH), is known to be important for Rac1 recruitment and activation (Bohdanowicz et al., 2013). Moreover, Cholesterol has also been shown to be important for Rac1 localisation and activity during macropinocytic cup formation (Grimmer et al., 2002). A similar sequence of events as what triggers constitutive macropinocytosis in macrophages and dendritic cells happens upon growth factor receptor stimulation in other cell types, and macropinocytosis can be induced as a nutrient-acquisition mechanism in these (Commisso et al., 2013). The formation of lipid and phosphoinositide domains at the plasma membrane allow for the spatiotemporal coordination of effector recruitment, resulting in the large membrane deformations driven methodically by carefully orchestrated Actin dynamics that result in macropinocytic cup formation. Macropinocytosis can therefore be described as a lipid raft-dependent endocytic process (Kirkham and Parton, 2005), and so can phagocytosis by the same principle.

1.1.3 Macropinocytosis in Human Health and Disease

The field of macropinocytosis research is vast and still expanding. In relation to human health, macropinocytosis is most commonly known to be active in cells of the immune system, where it is an instrumental mechanism of defence. As well as phagocytosis for the engulfment and elimination of pathogens, immune cells rely on macropinocytosis to perform various roles including immune surveillance, antigen capture, antigen presentation, and the delivery of pattern recognition receptors (PRRs) to intracellular compartments of primary innate immune cells (Canton, 2018; Kerr and Teasdale, 2009). Most recently, macropinocytosis has also been found to contribute to T cell growth and activation through mTORC1 signalling, evidencing that the promotion of cell growth by macropinocytosis is not exclusive to malignant cells (Charpentier et al., 2020; Charpentier and King, 2021). In relation to other areas of human health, macropinocytosis continues to be found in association with various biological processes; an example of this is how macropinocytosis is now known to contribute to neural morphogenesis during brain development, where it modulates the internalisation of the growth factor receptor TrkB (Powers et al., 2022). Similarly, in the kidneys, macropinocytosis has been found to contribute to the maintenance of the glomerular filtration barrier (Chung et al., 2015). On the other hand, macropinocytosis

in the kidneys may lead to nephrotic syndrome if persistently active, and calcium oxalate (CaOx) crystal internalisation by renal tubular cells - an important initiator of kidney stone formation - has also been shown to be primarily mediated by macropinocytosis (Kanlaya et al., 2013).

However, in relation to human disease, macropinocytosis research is most commonly associated with cancer metabolism and progression. As mentioned above, the first observation of malignant cells performing macropinocytosis was published in 1937 (Lewis, 1937). At present, macropinocytosis is recognised as a pathway by which tumour cells can access nutrients such as amino acids from the extracellular environment (Commisso et al., 2013). Other nutrients available to cancer cells from the extracellular environment are those found in necrotic cell debris; these result from cells that have starved and died in the harshness of the tumour microenvironment, which in turn favour the surrounding malignant cells that are able to perform macropinocytosis and feed of them (Kim et al., 2018). This allows cancer cells to meet their high metabolic demands and thrive over cells from the surrounding healthy tissues. Additionally, pancreatic cancer cells have been shown to enhance their metastatic ability by increasing migration-associated membrane receptor uptake through macropinocytosis (Nikolaou et al., 2024), also promoting cancer progression.

As well as cancer, neurodegenerative diseases including Alzheimer's, Parkinson's, Huntington's, and Amyotrophic Lateral Sclerosis (ALS) have been associated with macropinocytosis. These diseases are caused by defects in proteostasis and protein folding, leading to the formation of misfolded protein aggregates in neuronal cells, which eventually result in irreparable cell death (Zeineddine et al., 2015). The prion-like cell-to-cell propagation of these protein aggregates has been shown to be mediated by macropinocytosis. After protein aggregates are released into the extracellular environment by affected cells, they bind to cell surface receptors and stimulate macropinocytosis through Rac1 activation, continuing the spread of pathogenic protein aggregation in neighbouring cells (Yerbury, 2016; Zeineddine et al., 2015).

Macropinocytosis can also be induced by bacterial, viral and parasitic pathogens to gain entry into host cells and establish intracellular infections across a range of tissues. A bacterial example of this is the causing agent of neonatal meningitis, *Escherichia coli* K1, which has been shown to invade cells of the blood-brain barrier (BBB) endothelium by modulating macropinocytic membrane ruffling through the activation of Rho GTPases and downstream effectors including PI3K (Loh et al., 2017). Similarly, *Salmonella enterica* was found to hijack Rho GTPase signalling networks at the plasma membrane to promote its invasion of HeLa cells via macropinocytosis (Brooks et al., 2017). In viral studies, the Ebola virus, *Zaire ebolavirus*, was shown to depend on PI3K and Rac1 activity for cell entry, and it colocalised with internalised Dextran upon its induction of fluid uptake in HEK293T cells (Saeed et al., 2010). Furthermore, *Trypanosoma cruzi*, *Entamoeba histolytica*, and *Toxoplasma gondii* are examples of protozoan parasites that have been shown to modulate cytoskeletal dynamics to exploit macropinocytosis for cellular invasion (de Carvalho et al., 2015; Portes et al., 2020; Shimoyama et al., 2024). These examples provide us with an insight into the relevance of macropinocytosis to immunity from two sides of the same coin: it is a mechanism of defence, as well as a widely exploitable entry point for intracellular pathogens, which in turn may be harnessed for novel means of drug and vaccine delivery.

1.2 Phosphoinositide 3-Kinases (PI3Ks)

1.2.1 What are Phosphoinositides?

The term phosphoinositide refers to all phosphorylated derivatives of phosphatidylinositol (PI) (Figure 1.2). PI is a type of phospholipid found in eukaryotic cell membranes, which is unique in its ability to be transiently phosphorylated by phosphoinositide kinases (PIKs) at three free hydroxyl positions in its inositol head group - 3', 4' and 5' - individually or in different combinations. In total, seven different phosphoinositides have been identified in living cells, which can be derived from a single PI molecule through a series of phosphorylation and dephosphorylation events: PI(3)P, PI(4)P, PI(5)P, PI(3,4)P_2, PI(3,5)P_2, PI(4,5)P_2, and PI(3,4,5)P_3 (Fruman et al., 1998). Although phosphoinositides comprise a small percentage of cellular phospholipids, they play a central role in the regulation of cellular processes including cytoskeletal rearrangements and vesicular trafficking (Araki et al., 2007). Phosphoinositides can be described as lipid second messengers, since they are the molecules by which PIKs act as signal transducers and exert effects on the cell by recruiting effector proteins to membrane domains of their phosphoinositide products (Toker and Cantley, 1997). In fact, different membrane compartments contain characteristic phosphoinositide compositions, which result from the activity of localised phosphoinositide kinases and phosphatases at specific membrane sites, in turn working to localise the activity of downstream effector proteins (Bohdanowicz and Grinstein, 2013).

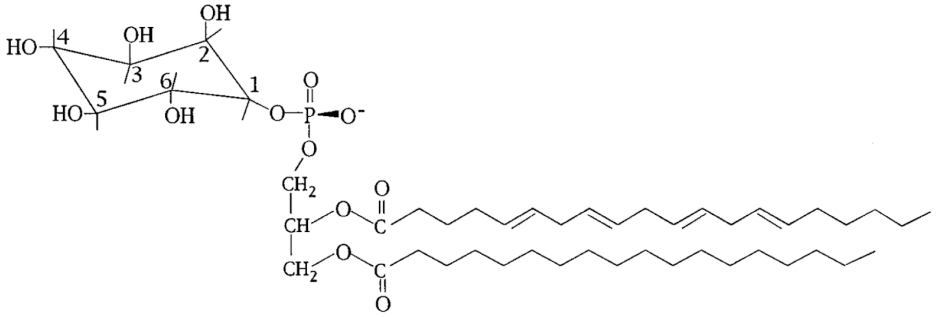

Figure 1.2 The chemical structure of phosphatidylinositol. Adapted from Fruman *et al*., 1998. "The myo-D-enantiomer of inositol is shown, in which the 2'-hydroxyl is axial and the other hydroxyls are equatorial."

1.2.2 The Three Classes of PI3K

Phosphoinositide 3-kinases (PI3Ks) are enzymes that catalyse the phosphorylation of phosphatidylinositol and phosphoinositides at the 3' position of the inositol head group; they produce PI(3)P, PI(3,4)P_2 and PI(3,4,5)P_3 from PI, PI(4)P and PI(4,5)P_2, respectively. PI3Ks have been categorised into three main Classes - I, II and III - based on their sequence conservation, regulation and substrate preference (Vanhaesebroeck et al., 1997).

Mammalian Class I PI3Ks phosphorylate PI(4,5)P_2 into PI(3,4,5)P_3, more commonly referred to as PIP_3, and exist as heterodimeric complexes whose adaptor/regulatory subunits mediate the interactions with upstream regulators such as activated receptors. However, the Class I PI3K Ras Binding Domain (RBD) is also able to mediate its own interactions with regulators such as the GTP-bound small GTPases Ras, Rac1 and Cdc42. (Fritsch et al., 2013; Fritsch and Downward, 2013). Additionally, although this is an area less well characterised to date, Class I PI3Ks have been found to play important scaffolding roles and possess secondary protein kinase activity (Bilanges et al., 2019; Hirsch et al., 2009; Leevers et al., 1999). There are four mammalian Class I PI3K catalytic subunit isoforms (p110α, p110β, p110δ, p110γ) which can be further subdivided into Class IA (p110α, p110β, p110δ) and Class IB (p110γ) according to the specific regulatory subunit they bind to (Figure 1.3). Class IA isoforms form heterodimeric complexes with one of five p85 regulatory subunits (p85α, p55α, p50α, p85β, p55γ) and remain in a cytosolic, self-inhibited dimeric state when inactive (Bilanges et al., 2019). The single Class IB isoform, on the other hand, forms heterodimeric complexes with p84/p87 and p101 regulatory subunits (Bilanges et al., 2019); the functional consequences of which remain not well understood (Fritsch and Downward, 2013). Interestingly, in lower eukaryotes such as the soil amoebae *Dictyostelium discoideum*, putative Class I PI3Ks (PikA, PikB, PikC, PikF, PikG), which are believed to also catalyse the phosphorylation of PI(4,5)P_2 into PIP_3 (Merlot and Firtel, 2003), are not known to bind regulatory subunits, but they do conserve the domain arrangement of mammalian Class I PI3K catalytic subunits (Takeda et al., 2007) (Figure 1.6).

Mammalian Class II PI3Ks (PI3KC2α, PI3KC2β, PI3KC2γ) seem to have evolved from earlier versions of Class I PI3Ks to specialise in the regulation of separate biological processes. The Class II PI3K lipid products have been long disputed, but these are now recognised to include both PI(3)P and PI(3,4)P_2, and like all PI3Ks, Class II isoforms play scaffolding roles besides their catalytic activities (Lo et al., 2022). Class II PI3Ks conserve the same catalytic core as Class I PI3Ks (RBD, C2 Domain, Helical Domain, Catalytic Domain) (Figure 1.4). However, they exist as monomers and do not bind regulatory subunits; instead, they contain a predictably disordered N-terminal region - much like *D. discoideum* Class I PI3Ks (see Chapter 3) - as well as a C-terminus PX domain and an additional C2 Domain at the far-end of their C-terminus (Bilanges et al., 2019; Gulluni et al., 2019) (Figure 1.4). The single mammalian Class III PI3K (VPS34), on the other hand, exclusively produces PI(3)P and is only composed of a C2 Domain, a Helical Domain, and a Catalytic Domain, albeit in the same order as in Class I and Class II PI3Ks, which is known as the ‘signature motif’ of all PI3Ks (Gulluni et al., 2019) (Figure 1.5).

The conserved domain structure of PI3Ks in the model organism and lower eukaryote *D. discoideum*, hints at how PI3Ks may have evolved from single-celled organisms through to Mammals. Whilst no Class II PI3Ks have been explicitly identified in *D. discoideum* amoebae, they do possess at least five putative Class I PI3K homologues and a single Class III PI3K homologue (PikE) (Vanhaesebroeck et al., 1997) (Figure 1.6). It is worth noting that Class I and Class II PI3Ks are absent from plant and fungal proteomes (Clark et al., 2014), however, these do possess VPS34 homologues (Domin et al., 2000; Lee et al., 2008). Could this be indicative of how mammalian Class II PI3Ks evolved from class I PI3Ks in single-celled eukaryotes, which in turn evolved from the primordial Class III PI3K of an earlier common ancestor shared between amoebae, plants and yeast?

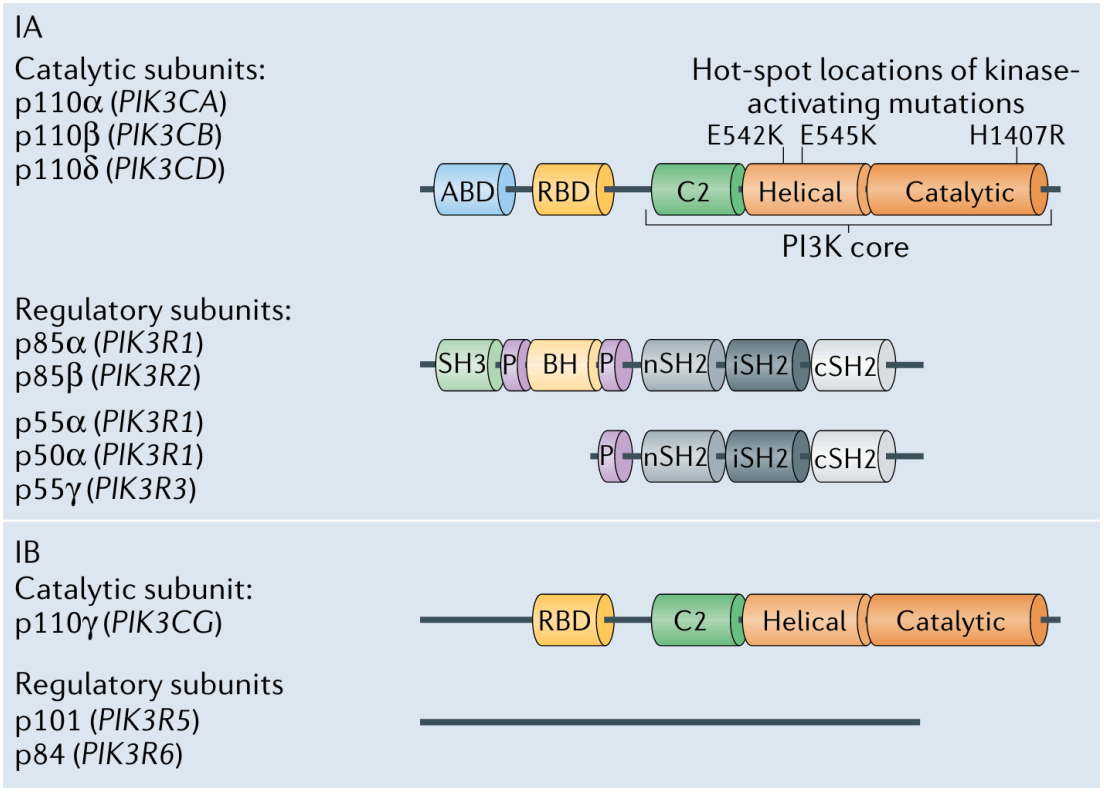

Figure 1.3: Mammalian Class I PI3K isoforms and their respective regulatory subunits. Adapted from Bilanges *et al*., 2019. Domains in order of appearance: Adapter Binding Domain (ABD), Ras Binding Domain (RBD), Protein Kinase C Conserved Domain (C2), Helical Domain (Helical), Catalytic Domain (Catalytic), Src Homology 3 Domain (SH3), Proline-rich Region (P), BCR Homology Domain (BH), Src Homology 2 Domain [n: N-terminal, i: Intermediate, c: C-terminal] (SH2).

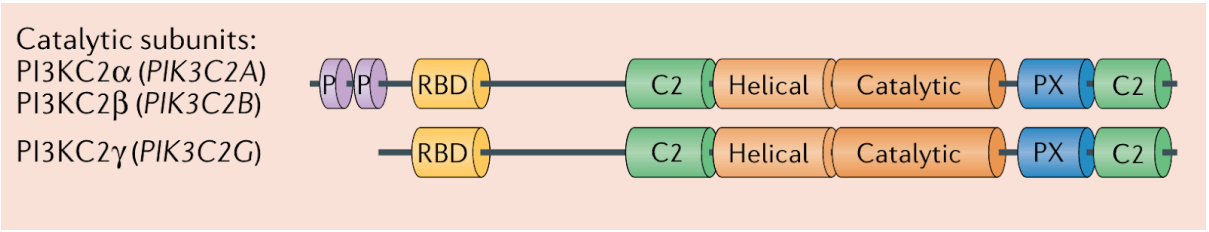

Figure 1.4: Mammalian Class II PI3K isoforms. Adapted from Bilanges *et al*., 2019. Domains in order of appearance: Proline-rich Region (P), Ras Binding Domain (RBD), Protein Kinase C Conserved Domain (C2), Helical Domain (Helical), Catalytic Domain (Catalytic), PX, Phox Homology Domain (PX).

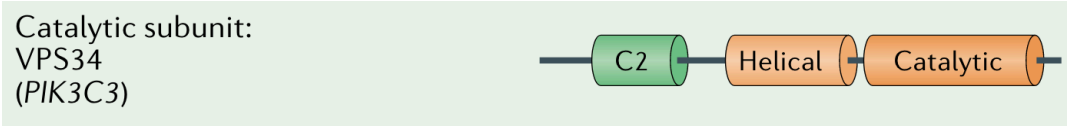

Figure 1.5: Mammalian Class III PI3K (VPS34). Adapted from Bilanges *et al*., 2019. Domains in order of appearance: Protein Kinase C Conserved Domain (C2), Helical Domain (Helical), Catalytic Domain (Catalytic).

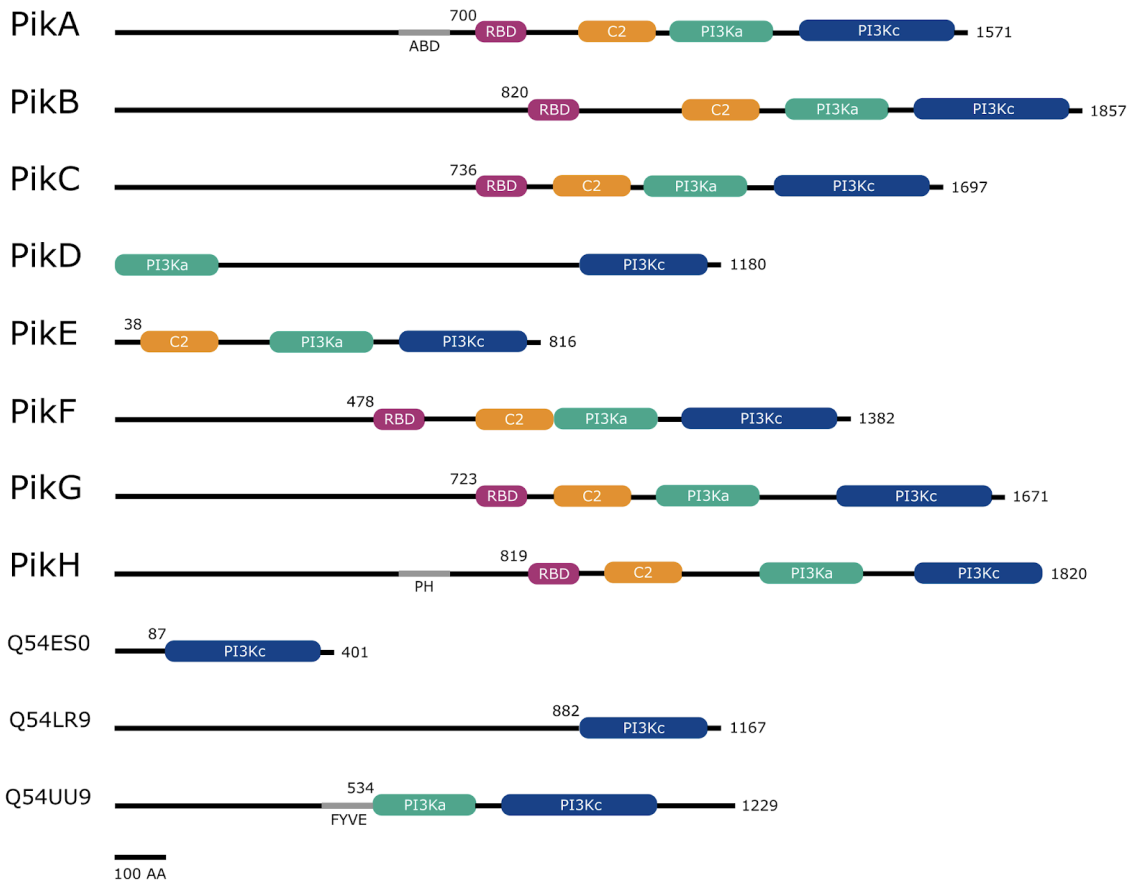

Figure 1.6: Domain arrangement of the 11 PI3K/PI4K catalytic domain-containing proteins found in the *Dictyostelium discoideum* proteome. The full protein sequences and annotations were obtained from UniProt. The total protein lengths as well as the length of each isoform's N-terminal tail are shown at their respective positions. PikA, PikH and uncharacterised protein Q54UU9 possess additional domain annotations within their N-terminal regions (highlighted in grey). ABD: Adapter Binding Domain. PH: Pleckstrin Homology Domain. FYVE: FYVE-like Domain. RBD: Ras Binding Domain. C2: Protein Kinase C conserved region, C2 Domain. PI3Ka: Accessory/Helical Domain. PI3Kc: PI3K/PI4K Catalytic Domain. Illustration created with Inkscape.

1.2.3 Mammalian Class I PI3Ks in Cell Signalling

Mammalian Class IA PI3K heterodimers are recruited to the plasma membrane through the binding of p85 SH2 domains to tyrosine-phosphorylated sites of activated surface receptors, such as receptor tyrosine kinases (RTKs), leading to the disinhibition of p85-p110 dimers. Once at the plasma membrane, the catalytic subunit of a Class IA PI3K heterodimer can bind and phosphorylate its lipid substrate (Bilanges et al., 2019). On the other hand, Class IB p110γ heterodimers are activated by interacting with membrane-anchored Gβγ subunits released upon G protein-coupled receptor (GPCR) activation through both their regulatory and catalytic subunits (Fritsch and Downward, 2013). Interestingly, the Class IA p110β heterodimer can interact with Gβγ subunits through a linker region of its C2 Domain (Erami et al., 2017), as well as active Rab5 through its Helical Domain (Salamon et al., 2015), making it unique in its ability to interact with tyrosine-phosphorylated proteins, GPCRs, and active Rab5 (Bilanges et al., 2019). Notwithstanding, all mammalian Class I PI3Ks interact with GTP- and membrane-bound small GTPases through the RBDs of p110 catalytic subunits, although it remains unclear whether GTPase-binding is enough to drive in vivo Class I PI3K activation independently of parallel receptor-mediated activities. p110β heterodimers preferentially interact with Rac1 and Cdc42, which are members of the Rho GTPase family, whilst p110α, p110δ and p110γ bind the more classical members of the Ras superfamily (Fritsch et al., 2013). The binding of activated small GTPases is believed to enhance Class I PI3K recruitment, activation, and potentially, lipid substrate-specificity (Fritsch and Downward, 2013). For example, in the case of p110β activation, the Dock180/Elmo1 Rac1-GEF complex is itself activated by Gβγ proteins; this leads to the indirect reinforcement of 110β activation through the additional interaction of active Rac1 with the p110β RBD at a localised site of GPCR activation in the plasma membrane (Fritsch et al., 2013).

Following the activation of Class I PI3Ks downstream of cell surface receptors, protein effectors can further transduce and amplify signalling cascades to modulate a variety of biological processes. Class I PI3K activity centres on the downstream recruitment of specific effector molecules to PIP_3-enriched membrane domains. This is mediated through effector protein PIP_3-binding domains such as the Pleckstrin homology (PH) domain, or by physical interactions through the less well documented role of PI3Ks as scaffolding proteins. It has been predicted that there are 44 PIP_3-regulated effector proteins in humans and 15 in *D. discoideum* (Park et al., 2008), alluding to the conservation of PIP_3-mediated signal transduction from *D. discoideum* amoeba to humans. Human Class I PI3K effectors most notably include protein kinases (e.g. Akt), scaffolding proteins (e.g. GAB1), and various small GTPase activating proteins (GAPs) and guanine nucleotide exchange factors (GEFs) (Bilanges et al., 2019). As an example of how far PIP_3-mediated signalling cascades may travel through interconnected signalling networks, it is worth considering that Akt alone has been reported to have well over 100 different substrates (Manning and Toker, 2017), including the widely influential mTOR complexes (Laplante and Sabatini, 2009). Hence, Class I PI3K activity influences biological processes ranging from cytoskeletal rearrangements to cell metabolism, survival, growth, proliferation, and differentiation.

1.2.4 Mammalian Class I PI3Ks in Membrane Dynamics

Class I, II, and III PI3Ks play instrumental roles in the orchestration of membrane dynamics at both the plasma membrane and intracellular membrane compartments. In mammalian cells, Class I and II PI3K isoforms are primarily involved in the spatiotemporal coordination of macro- and microscale endocytic processes, respectively, whilst VPS34, the sole member of Class III, is a key modulator of intracellular vesicular dynamics (Bilanges et al., 2019). In mammalian cells, Class II PI3Ks have been implicated in CME but not macropinocytic cup formation (Gozzelino et al., 2020; Salloum et al., 2023). Accordingly, in the context of this thesis, Sections 1.2.3 and 1.2.4 focus on the mechanisms of action of Class I PI3Ks.

Since early studies in the 1990s, mammalian Class I PI3Ks have been identified to be key regulators of macroscale endocytic processes. In 1995, the pan-PI3K inhibitor Wortmannin was first found to inhibit fluid uptake in baby hamster kidney (BHK) cells (Clague et al., 1995). Most recently, constitutive macropinocytosis in dendritic cells and macrophages has been found to be modulated by the GPCR activity of Calcium-sensing receptors (CaSRs) via PI3Kɣ (p110ɣ) signalling, which promotes membrane ruffling at sites of receptor stimulation (Canton et al., 2016). Similarly, growth factor-stimulated macropinocytosis in fibroblasts and breast cancer cells has been found to require PI3Kβ (p110β) activity for the formation of the Actin-rich circular dorsal ruffles (CRDs) that precede macropinocytic cup formation (Salloum et al., 2019). Moreover, PI3Kβ (p110β) activity was found to be required for effective macropinocytic cup closure in cells expressing constitutively active Rac1, which alone induce membrane ruffling, suggesting a secondary role for PI3Kβ downstream of Rac1 during macropinocytic cup formation (Salloum et al., 2019). Interestingly, it was previously shown that Rac1 activity is in fact sufficient to induce membrane ruffling, whilst in later stages of macropinocytic cup formation, Rac1 inactivation is essential for cup closure (Fujii et al., 2013). Could PI3Kβ activity in the late stages of macropinocytic cup formation be influencing Rac1 inactivation through an unidentified feedback mechanism?

It has similarly been reported that Rac and Cdc42 inactivation is required for phagocytic cup closure in the internalisation of large particles, and that this requires Class I PI3K activity for the recruitment of specific RhoGAPs to large phagocytic cups (Schlam et al., 2015). Interestingly, Fcγ receptor (FcγR)-mediated phagocytosis of 6μm antibody-coated beads was previously found to be inhibited by Wortmannin, whilst no effect was seen on the phagocytosis of 2μm antibody-coated beads (Cox et al., 2002). In 1994, it was first identified that Class I PI3Ks are activated downstream of FcγRs during mammalian FcγR-mediated phagocytosis (Ninomiya et al., 1994). The binding of ligand-coated (IgG-opsonised) particles to FcγRs results in the clustering of these receptors at discrete regions of the plasma membrane. The close proximity of clustered FcγRs enables their phosphorylation by Src family tyrosine kinases, in turn allowing spleen tyrosine kinase (Syk) to bind via SH2 domains to phosphorylated tyrosine residues on FcγR cytoplasmic domains. The binding of Syk to activated FcγRs results in Syk activation and the recruitment of additional signaling proteins (Cox and Greenberg, 2001). Amongst the proteins recruited to sites of FcγR activation in this way is the p85 regulatory subunit of Class I PI3K via its own SH2 domains (Flannagan et al., 2012). It was initially thought that PI3K signalling promoted actin polymerisation at sites of receptor stimulation on the plasma membrane (Toker and Cantley, 1997). However, consistent with the more recent findings (Schlam et al., 2015), actin was

found to be successfully polymerised at the base of phagocytic cups in macrophages of Syk-null mice, whilst they were unable to complete particle internalisation (Crowley et al., 1997), and Wortmannin inhibition was shown to disrupt the contractile activity that is required for phagocytic cup closure without hindering pseudopod extension (Swanson et al., 1999). This body of evidence supports the hypothesis first postulated by Araki, Johnson and Swanson in 1996, where they argue for the contribution of PI3K activity to the late stages of both phagocytic and macropinocytic cup formation including closure (Araki et al., 1996).

1.2.5 Class I PI3Ks in Human Health & Disease

Similarly to the relevance of macropinocytosis in human health and disease discussed in Section 1.1.3, Class I PI3Ks have been largely associated with cancer (Thorpe et al., 2015) and neurodegenerative diseases (Desale et al., 2021), as well as human overgrowth disorders, obesity, type 2 diabetes, cardiovascular diseases, inflammatory and autoimmune disorders, and primary immunodeficiencies such as Activated p110delta Syndrome (APDS) and p110δ-activating mutation causing Senescent T cells, Lymphadenopathy and Immunodeficiency (PASLI) (Vanhaesebroeck et al., 2016). Therefore, the investigation of Class I PI3K signaling pathways holds significant value across diverse medical disciplines. Moreover, on an organismal level and under physiological conditions, Class I PI3Ks contribute to immunity, insulin signalling, spermatogenesis, angiogenesis and platelet function (Bilanges et al., 2019). Hence, given the central role of Class I PI3Ks in regulating immune, metabolic, and proliferative processes, understanding isoform-specific functions under specific contexts may enable the development of targeted therapies with fewer harmful side effects, which is what for many years has hindered the progress of PI3K inhibitors through clinical trials (Yu et al., 2023).

1.3 The Cytoskeletal Mediation of Membrane Remodeling

1.3.1 The Role of the Cytoskeleton in Membrane Dynamics

Cytoskeletal Components

The cytoskeleton is the network of tubules and filaments that provides cells with shape and structural support, and drives cellular movement through the generation of mechanical forces. There are three types of cytoskeletal tubules and filaments: microtubules, intermediate filaments (IFs), and actin filaments. These are built from three types of cytoskeletal proteins, respectively: tubulin monomers, ‘IF proteins’ (>70) and actin monomers (Etienne-Manneville, 2018; Hohmann and Dehghani, 2019) (Figure 1.7). The individual properties of these proteins, once polymerised, enable the cytoskeletal structures to fulfill distinct cellular functions. In general terms, microtubules serve as tracks for intracellular transport, intermediate filaments provide a scaffold that anchors organelles and maintains spatial organisation, and the actin cytoskeleton drives dynamic structural changes (Hohmann and Dehghani, 2019; Li et al., 2019). The interplay and crosstalk between the three filament networks are not well researched. However, emerging evidence suggests that

these networks may function in a more integrated and interdependent manner than previously understood (Etienne-Manneville, 2018; Fletcher et al., 2000). In the context of this thesis, it is important to highlight not only filamentous actin (F-actin) but also other cytoskeletal components, and to consider how all three networks may contribute to the formation of macropinocytic cups.

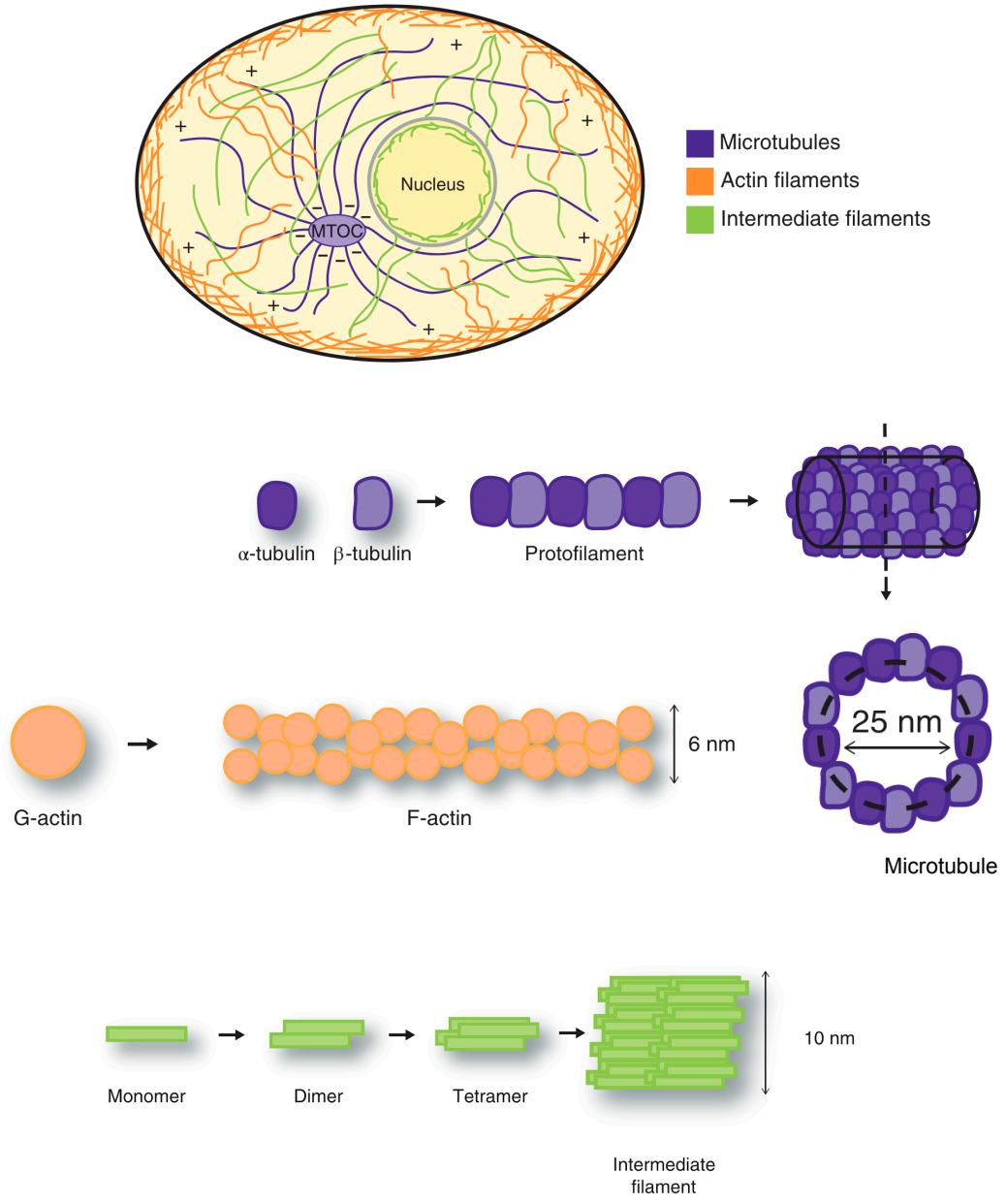

Figure 1.7: The distribution of the three cytoskeletal filament networks and their formation from monomeric components. Adapted from Río-Bergé *et al*., 2023. MTOC: Microtubule-organising center.

Additionally, it is also important to bring attention to motor proteins and how these contribute to the generation of forces that modulate cytoskeletal rearrangements. Motor proteins are ATP hydrolases that actively travel along cytoskeletal filaments in a stepwise, “walking” motion. There are three superfamilies of motor proteins: kinesins, dyneins, and myosins (Río-Bergé et al., 2023). Kinesins and dyneins bind to microtubules, whilst Myosins bind to actin filaments (Fletcher and Mullins, 2010). Although intermediate filaments do not serve as tracks for motor protein movement, they can interact with both microtubules and actin filaments - as well as their associated motor proteins - through plakins (Jefferson et al., 2004). This interconnection is thought to be important for the coordinated activity of cytoskeletal components during cellular movements.

Kinesins carry a variety of materials across the cell including protein complexes, vesicles (e.g. lysosomes and endosomes), and organelles (e.g. mitochondria, the endoplasmic reticulum, and the Golgi apparatus) (Hirokawa et al., 2009). Kinesins can bind to cargo directly or through adaptor and scaffolding proteins, and most commonly, they transport cargo towards microtubule plus ends (Figure 1.7), away from the cell centre and towards the plasma membrane. Interestingly, some kinesin isoforms contain lipid-binding domains, such as PX and PH domains, which in different contexts have been shown to directly interact with the phosphoinositides PI(3)P, PI(3,4)P_2, PI(4,5)P_2, and PIP_3 (Klopfenstein et al., 2002). For example, the PX domain of the kinesin-3 family member KIF16B can directly bind to PI(3)P, PI(3,4)P2, and PIP_3 molecules, and it localises to early endosomes to modulate the recycling of cargo to the plasma membrane (Hoepfner et al., 2005). Moreover, kinesins can also bind phosphoinositides through adaptor proteins; an example of this is another member of the kinesin-3 family, KIF13B, which binds to the PIP_3-binding protein centaurin α1 (CENTA1) in neuronal cells and contributes to axonal development by mediating the polarised transport of PIP_3-coated vesicles (Tong et al., 2010).

Dyneins, specifically referred to as cytoplasmic dyneins to distinguish them from axonemal dyneins of cilia and flagella, transport cargo toward the microtubule minus ends (Figure 1.7). As such, they can carry cargo such as endosomes, phagosomes, and lysosomes, as well as cytoskeletal filaments and peripheral material requiring degradation or recycling, away from the plasma membrane and toward the cell center (Roberts et al., 2013). The binding of cytoplasmic dyneins to cargo is mediated by adaptor proteins. For example, during T cell calcium-stimulated endocytosis, the RabGTPase and dynein adapter CRACR2a recruits dynein to cortical puncta where it facilitates the mechanical pulling and extraction of newly formed endosomes from the actin cortex (Wang et al., 2019). Furthermore, cytoplasmic dyneins have been reported to localise to the leading edge of migrating cells, where they exert pulling forces on the microtubule cytoskeleton that help coordinate the movement of microtubules and the cortical actin network (Dujardin et al., 2003; Levy and Holzbaur, 2008).

Myosins play essential roles in actin-based biological processes, ranging from membrane trafficking to muscle contraction (Kendrick-Jones and Buss, 2016). A number of myosins possess lipid-binding PH domains. Myosin-X (Myo10) is of particular interest in the context of this thesis, since its $PH1_N$-PH2-$PH1_C$ domain arrangement specifically recognises and binds to PIP_3, allowing for the release of its autoinhibition and enabling its motor activity (Lu

et al., 2011). Myo10 has been identified in regions of dynamic actin remodeling, such as membrane ruffles and phagocytic cups (Berg et al., 2000; Cox et al., 2002), and has been proposed to function downstream of Cdc42 to induce filopodia formation through the actin-nucleating Arp2/3 complex and formins, as well as promoting actin bundling (Bohil et al., 2006).

1.3.2 The Mechanical Drivers of Membrane Dynamics: Actin Regulators

Membrane dynamics refer to the sequence of events that reshape and remodel cellular membranes. For example, the formation of membrane protrusions requires force generation through the outward polymerisation of actin networks against the plasma membrane (Lappalainen et al., 2022). Coordinated membrane deformation is essential for the success of actin-driven processes such as phagocytosis and macropinocytosis. Thus, the precise orchestration of membrane dynamics by phosphoinositide and GTPase signaling pathways is central to the efficiency of these processes. In addition, motor proteins contribute supportive forces during dynamic membrane remodelling: they deliver membrane components to facilitate membrane extension and subsequently produce contractile tension against cytoskeletal filaments to drive retraction. Moreover, additional mechanisms such as vesicle scission are required in the final stages of endocytic membrane remodelling processes.

Actin Nucleation

The formation of protrusive force-generating actin networks involves multiple steps coordinated by distinct protein complexes. Once actin monomers (globular actin, G-actin) self-assemble into unstable dimers and trimers, a step known as “nucleation”, short, stable tetrameric filaments can form, and these can be further elongated from their ends (Sept and McCammon, 2001). Actin monomer-binding proteins, including thymosin-β4 (Tβ4) and profilin, must prevent spontaneous actin nucleation at sites where filament formation is not required, particularly because this step is highly sensitive to the local concentration of actin monomers. Whilst Tβ4-bound actin monomers are unable to bind any existing filaments, profilin-bound monomers (profilin-actin) can be added to the “barbed” end of actin filaments facing the plasma membrane (Lappalainen et al., 2022). However, because spontaneous actin nucleation is thermodynamically unfavorable (Sept and McCammon, 2001), this process is structurally aided by proteins called actin nucleators, which can generate either linear or branched actin filaments.

Linear filaments are formed by formins and Ena/VASP family proteins, whereas branched filaments are produced by the Arp2/3 complex. Formins exist as autoinhibited homodimers that become activated by signalling cascades such as those mediated by Rho GTPases (Kovar, 2006); VASP proteins exist as tetrameric structures that interact with several regulatory proteins, as well as profilin-actin complexes (Faix and Rottner, 2022); and Arp2/3 is a heptameric complex whose activation is mediated by nucleation-promoting factors (NPFs), such as proteins of the WASP and SCAR/WAVE families. These NPFs are normally maintained in an autoinhibited conformation that prevents them from activating Arp2/3.

Activation occurs when Rho family GTPases such as Rac1 and Cdc42 bind to their regulatory domains, often with the assistance of adaptor proteins including WIP in the case of WASP or Abi1 in the case of WAVE (Takenawa and Suetsugu, 2007; Innocenti et al., 2004). For example, Rac1 binding remodels the WAVE regulatory complex to expose the C-terminal VCA (verprolin-homology, central, acidic) domain (Chen et al., 2010), which then directly engages the Arp2/3 complex to promote branched filament nucleation (Lappalainen et al., 2022).

Although canonical nucleators account for most actin network assembly, additional factors broaden this repertoire. Amongst these are Spire and Cordon-bleu (Cobl), which rely on tandem Wiskott-Aldrich syndrome protein-homology 2 (WH2) domains to promote filament nucleation. Spire contains four WH2 domains, whilst Cobl contains three. In both cases, these motifs bind multiple actin monomers in sequence to stabilise a nucleus. This mode of action differs from that of formins, which remain associated with barbed ends to drive processive elongation, or the Arp2/3 complex, which generates new branches from existing filaments (Renault et al., 2008). Spire and Cobl have been studied mainly in developmental and neuronal contexts, where they contribute to processes such as oocyte axis determination and dendritic branching (Quinlan et al., 2005; Ahuja et al., 2007; Haag et al., 2012). Although they appear less directly implicated in macropinocytosis, they exemplify the diversity of nucleation strategies available to cells (Renault et al., 2008). By contrast, in the context of membrane remodelling events such as macropinocytosis, the canonical nucleators formins, Ena/VASP and the Arp2/3 complex are of greatest significance, as the coordination of branched and linear filament systems is central to the formation and closure of macropinocytic cups (Insall and Machesky, 2009; Veltman et al., 2016).

Branched versus Linear Actin Filaments

The assembly of long, linear actin filaments leads to the emergence of spike-like protrusions from the plasma membrane (Insall and Machesky, 2009), such as filopodia. Formins and VASP proteins, positioned at the membrane, capture the barbed ends of existing filaments and promote their linear elongation by facilitating the sequential addition of G-actin or profilin-actin monomers (Lappalainen et al., 2022). On the other hand, branched actin filament networks play a critical role in driving the formation of sheet-like protrusive membrane structures (Insall and Machesky, 2009), such as those that give rise to macropinocytic cups. Branched actin networks are generated when the Arp2/3 complex is activated by the simultaneous binding of two NPFs and two actin monomers. This binding induces a conformational change in the Arp2/3 complex and enables it to nucleate a new actin filament at a characteristic 70° angle from the side of an existing filament (Mullins et al., 1998). As branches form on existing branches, a dense and highly branched actin network emerges (Lappalainen et al., 2022). It has been suggested that branch formation is forward-oriented due to an intrinsic mechanosensing property of actin filaments, resulting in the generation of outward protrusive forces (Risca et al., 2012; Svitkina, 2012). In recent years, it has become increasingly evident that linear and branched actin networks are not entirely independent, but rather functionally integrated within the same biological processes. Branched actin filaments can emerge from the sides of linear filament networks, while linear elongation can reinforce and sustain the force generation of branched networks. For

example, it has been demonstrated that formins contribute to the stability and sustained force generation required for the effective formation of lamellipodia, functioning in support of the Arp2/3 complex (Kage et al., 2017).

Actin Filament Cross-Linking

Following the nucleation and elongation of both linear and branched actin filaments, the spatial organisation and three-dimensional stabilisation of the actin network are reinforced by actin bundling proteins. Bundling involves the cross-linking of individual filaments into tight, ordered arrays, which contributes to the mechanical integrity of dynamic cellular structures such as filopodia and macropinocytic cups. Actin bundlers characterised to date include Filamins, Fimbrins, Cortexillins, and Villin-domain-containing proteins (Faix et al., 1996; Lappalainen, 2016; Skau et al., 2011; Trösch, 2025). Their activity is often regulated by phosphoinositide signalling and they operate in coordination with contractile actin-associated motor proteins, as well as actin filament disassembly factors, to shape cytoskeletal architecture and membrane tension. Therefore, actin-bundling proteins are key downstream effectors of PI3Ks and small GTPases, playing central roles in the maturation and resolution of actin-based structures. In *D. discoideum*, Cortexillins I and II are well-studied examples of actin bundlers with PI(4,5)P_2-binding motifs that generate robust three-dimensional actin meshworks (Faix et al., 1996).

Actin Filament Disassembly and Turnover

To maintain cell shape and membrane homeostasis, the negative regulation of F-actin polymerisation is just as critical as its promotion. The effective formation of defined membrane protrusions depends not only on actin assembly at specific sites but also on the suppression of errant extensions in surrounding regions of the plasma membrane. Beyond their roles in filament bundling, Cortexillins and Villin-domain-containing proteins have been implicated in the inhibition of actin assembly, thereby contributing to the spatial restriction of actin polymerisation to designated protrusive zones. In *D. discoideum*, Cortexillin I forms a complex with IQGAP-related scaffolding proteins DGAP1 and GAPA, and they collectively limit actin assembly to specific membrane regions (Cha and Jeon, 2011). Villin-domain proteins, meanwhile, enhance cytoskeletal organisation by acting both as bundling and severing agents (severing is the fragmentation of actin filaments, which in turn promotes the dissociation of actin monomers). Together, these proteins integrate spatial and mechanical cues, enabling the regulation of cell shape and protrusive activity (Trösch, 2025).

Within dynamic membrane protrusions, the disassembly of actin filaments is also essential for the efficient remodelling of the cytoskeleton (Pollard and Borisy, 2003). This process is tightly regulated by a suite of actin-modulatory proteins that mediate filament disassembly to ensure rapid cytoskeletal turnover within dynamic structures. Among these, cofilin plays a central role ensuring the recycling of actin monomers. Cofilin binds preferentially to relaxed, ADP-bound actin filaments and promotes their breakage, working together with three types of cofactors to enhance its activity: AIP1, CAP and coronin (Goode et al., 2023). For example, coronin enhances cofilin-mediated filament severing by accelerating cofilin’s

association with actin filaments (Mikati et al., 2015). In *D. discoideum*, Coronin A (CorA) localises to cell surface projections involved in motility, phagocytosis, and macropinocytosis, and $CorA^-$ cells exhibit defects in cytokinesis, phagocytosis, and migration (de Hostos et al., 1993, 1991; Maniak et al., 1995). In contrast to how relaxed filaments are broken down, stretched actin filaments are relatively resistant to cofilin activity and instead preferentially engage myosin II, which stabilises filaments under tension by generating contractile forces (Hayakawa et al., 2011; Uyeda et al., 2011).

In addition to cofilin, barbed end-capping proteins such as IQGAP1, gelsolin and twinfilin also contribute to actin turnover by obstructing filament growth (Goode et al., 2023). As well as being able to sever actin filaments, gelsolin binds to the barbed ends of severed fragments to halt further polymerisation (Nag et al., 2013). This dual activity allows gelsolin to rapidly disassemble existing filaments and cap new growth, making it particularly important in responses to changes in membrane tension. Twinfilin, by contrast, binds ADP-actin monomers and also inhibits filament barbed-end elongation, working at the interface between filament disassembly and monomer recycling (Hakala et al., 2021). These observations suggest that feedback mechanisms embedded within cytoskeletal dynamics serve to monitor and coordinate filament rearrangements, ensuring both functional efficiency and the preservation of plasma membrane integrity.

1.3.3 The Orchestrators of Membrane Dynamics: Small GTPases

The coordination of actin assembly and disassembly during processes that require dynamic membrane remodelling, such as macropinocytic cup formation, is tightly regulated by small GTPase and phosphoinositide signalling cascades, which localise actin remodelling effectors to defined regions of the plasma membrane (Egami et al., 2014). Ras superfamily GTPases, including Ras, Rac, and Cdc42, act in concert with $PI(4,5)P_2$ and PIP_3 to recruit cytoskeletal regulators to specific membrane domains (Araki et al., 2007; Scott et al., 2005). Downstream of various intracellular or extracellular stimuli, Ras GTPases activate key effectors such as PI3Ks (Hoeller et al., 2013). PI3K signalling supports actin remodelling through the local generation of PIP_3 domains, which attract cytoskeletal regulators while simultaneously depleting $PI(4,5)P_2$ to displace inhibitory capping proteins (Ceccarelli et al., 2007; Scott et al., 2005). In parallel and as described in Section 1.3.2, the small GTPases Rac and Cdc42 drive branched actin polymerisation by activating effectors such as the SCAR/WAVE and WASP complexes, which stimulate the Arp2/3 complex to initiate actin nucleation at the leading edge (Dawson et al., 2006).

Small GTPases function as molecular switches that cycle between inactive GDP-bound and active GTP-bound states. This cycle is controlled by three classes of regulators: guanine nucleotide exchange factors (GEFs), which activate GTPases by promoting GDP release and GTP binding; GTPase-activating proteins (GAPs), which inactivate by accelerating GTP hydrolysis; and guanine nucleotide dissociation inhibitors (GDIs), which sequester inactive GTPases in the cytosol – together these ensure that GTPase activation is both reversible and spatially confined (Bos et al., 2007; Cherfils and Zeghouf, 2013). The transition between GDP- and GTP-bound states induces conformational rearrangements in two conserved regions, known as switch I and switch II. In the active, GTP-bound state, GTPase switches

expose effector-binding surfaces, enabling interactions with proteins such as PI3Ks, WASP and SCAR/WAVE complexes, or IQGAPs. Hydrolysis of GTP relaxes the switches and disrupts effector binding, thereby returning the GTPase to its inactive state. In this way, the cycle ensures that downstream actin remodelling is both spatially restricted and temporally precise (Vetter and Wittinghofer, 2001).

1.4 *Dictyostelium discoideum*: A Model for Investigating Class I PI3K Function in Macropinocytosis

1.4.1 *Dictyostelium discoideum* as a Model Organism

The use of amoebae in the study of endocytic pathways dates back to the early 20th century (Chapman-Andresen, 1984). Wild strains of the social amoeba *Dictyostelium discoideum* feed on bacteria in soil via phagocytosis, whereas mutant laboratory strains capable of axenic growth in liquid culture rely instead on macropinocytosis (Kay et al., 2019). This axenic growth trait was traced to a disruption in the RasGAP-encoding gene *axeB*, homologous to the mammalian neurofibromatosis type 1 (NF1) tumour suppressor gene (Bloomfield et al., 2015; Ratner and Miller, 2015). The emergence of robust macropinocytic activity in *D. discoideum* has enabled the modelling of this clinically relevant process in a genetically tractable organism, offering an alternative to more complex systems such as human immune cells. A key advantage of *D. discoideum* is its haploid genome during vegetative growth, which facilitates both forward and reverse genetic manipulation, as phenotypes manifest without the need to disrupt both alleles. Additionally, the ease of culture and live-cell imaging further supports its use as a convenient and powerful model system, particularly for studying endocytosis and cytoskeletal dynamics in a simplified eukaryotic context.

1.4.2 Molecular Basis of Macropinocytosis in *Dictyostelium discoideum*

Genomic and Structural Complexity of Signalling Networks

The study of membrane dynamics driven by Rho-related GTPases and PI3K activity is greatly facilitated by the evolutionary conservation of these signalling proteins from amoebae to humans. Although *Dictyostelium discoideum* possesses plasmanylinositols in its plasma membrane rather than phosphatidylinositol-based lipids (Clark et al., 2014), the canonical PI(P)n nomenclature is retained to encompass both lipid types.

The *D. discoideum* genome encodes a large and diverse set of signalling molecules, including 20 *rac* genes – *rac1A, rac1B, rac1C, racA, racB, racC, racD, racE, racF1, racF2, racG, racH, racI, racJ, racL, racM, racN, racO, racP,* and *racQ* (Filić et al., 2021). In parallel, the UniProt database lists 11 proteins in *D. discoideum* that contain PI3K/PI4K catalytic domains, based on UniProt database searches, highlighting the functional complexity and evolutionary diversification of phosphoinositide signalling pathways in this model organism.

Their domain conservation and arrangement are illustrated in Figure 1.6, revealing both structural similarities and key divergences that may underlie the evolution of class-specific characteristics.

Regulation of Rac Activity by GEFs and GAPs

In addition to this genomic and structural complexity, several regulatory proteins act to confine small GTPase activity during macropinocytosis. As outlined in Section 1.3.3, upstream of Rac activation, GEFs play a central role. In *D. discoideum*, two Dock180-related RacGEFs, DockA and DockD, have been shown to promote Rac activation in a PI3K-dependent manner. DockD localises to the cell cortex and leading edge, where it forms a complex with DdELMO1, and its overexpression enhances F-actin assembly at pseudopods, whereas loss of DockA or DockD reduces migration speed. These findings place Dock/Elmo complexes as key intermediates linking PIP_3 production to localised Rac activation during actin-driven protrusion (Para et al., 2009).

To prevent aberrant protrusions outside defined membrane regions, Rac activity is likewise spatially confined by scaffolding proteins such as IQGAPs. In *D. discoideum*, IQGAP3 (IqgC), a RasG-GAP, restricts Ras signalling to macropinocytic cups (Marinović et al., 2019). Similarly, DGAP1 (RgaA) localises to the flanks of macropinocytic cups, where it restricts Rac1 signalling through its ability to bind Rac1-GTP (Filić et al., 2014; Šoštar et al., 2024), although it has not evolutionarily retained RhoGAP activity (Faix et al., 1998). Additional regulation may be provided by bona fide GAPs such as CARMIL-GAP, which is thought to bind Rac1-GTP and promote hydrolysis at F-actin-rich sites while simultaneously displacing actin capping protein, thereby restricting Rac activation to regions of ongoing filament elongation (Jung et al., 2022). Collectively, these interlinked signalling axes orchestrate the spatial and temporal dynamics of actin assembly and disassembly during macropinocytic cup formation.

Downstream Effectors: PAK Kinases and Class I Myosins

Rac GTPases signal through effector kinases such as p21-activated kinases (PAKs), which are conserved regulators of actin organisation. In mammalian cells, Rac1 directly activates PAKs by binding to their CRIB domains and stimulating kinase activity (Knaus et al., 1998; Shin et al., 2013). In *D. discoideum*, PAKa has been shown to transduce Rac signalling into cytoskeletal contractility by regulating myosin II assembly at the cortex. In this way, Rac-PAK signalling links upstream GTPase activity to the mechanical force of myosin II, coupling signalling events to membrane contractility and ensuring directional persistence during chemotaxis by suppressing lateral pseudopod extension (Chung and Firtel, 1999).

In parallel to this Rac-PAK-myosin II axis, actin-membrane coupling is mediated by Class I myosins. These are single-headed, membrane-associated motors that link the actin cytoskeleton to membranes and support processes such as membrane tension generation, endocytosis, and protrusion (McIntosh and Ostap, 2016). *D. discoideum* encodes multiple Class I myosin isoforms (Myo1A-Myo1F, Myo1K), several of which localise to actin-rich

structures such as macropinocytic cups and actin waves (Brzeska et al., 2016). Genetic and imaging studies have demonstrated that Class I myosins fulfil distinct roles rather than acting redundantly. For example, Myo1F and, to a lesser extent, Myo1E suppress actin wave formation, an effect that depends on their membrane lipid-binding capacity but does not require motor activity (Brzeska et al., 2020), whereas evidence from earlier mutant analyses showed that strains lacking combinations of “classic” Class I myosins (MyoA-D) display fluid uptake defects (Jung et al., 1996). More recent studies have demonstrated that MyoB localises to the base of macropinocytic cups, where it cross-links actin filaments and contributes to the inward propulsion of vesicles into the actin cortex (Novak et al., 1995). Together, these findings point to complementary roles for different Class I myosin isoforms in shaping membrane-cytoskeleton interfaces and underscore the contribution of some Class I myosins to the mechanics of macropinocytic cup formation.

PI3Ks and the Spatial Organisation of Macropinocytic Cups

During macropinocytosis in *Dictyostelium discoideum*, Class I PI3Ks (PikA, PikB, and PikF) act downstream of activated Ras to generate PIP_3-enriched domains at the plasma membrane. These PIP_3 patches are thought to direct localised actin polymerisation by recruiting the SCAR/WAVE complex and the Arp2/3 actin nucleator to its periphery (Veltman et al., 2016). This recruitment drives the formation of SCAR-enriched F-actin rings that extend outward, while the central PIP_3 patch remains anchored at the base, thereby shaping the characteristic cup-like structure. Although active branched actin polymerisation appears to be restricted to the rim of the macropinocytic cup, an underlying F-actin scaffold remains in place throughout the process, providing structural support from initiation to closure. Cup sealing has been observed to occur via two distinct mechanisms: lip closure and base closure. In lip closure, actin polymerisation is thought to drive inward-directed membrane fusion at the cup rim. In contrast, base closure is hypothesised to occur through passive mechanisms such as elevated membrane tension, which may become high enough to induce delamination – the separation of the plasma membrane from the underlying cytoskeleton (Lutton et al., 2023).

Together, these spatially organised molecular events are thought to coordinate the membrane ruffling and cytoskeletal remodelling required for macropinocytic cup formation and subsequent fluid uptake. However, *D. discoideum* Class I PI3Ks – the enzymes responsible for PIP_3 production – have been hypothesised to fulfill specialised, non-redundant roles during macropinocytic cup formation (Hoeller et al., 2013). Additionally, active Rac has been shown to co-localise with active Ras along the inner surface of the macropinocytic cup, with Rac activity extending beyond Ras-positive domains into a peripheral “annulus” region (Buckley et al., 2020). These findings suggest more complex spatial regulation than the canonical linear model. Thus, while the prevailing framework of Ras → PIP_3 → Actin captures the general sequence of events, a critical question remains: *What are we missing?*

1.5 Summary Remarks

As outlined above, the accumulation of PIP_3 at the plasma membrane provides spatial cues for the recruitment of downstream effectors involved in actin dynamics and membrane deformation. In *Dictyostelium discoideum*, Class I PI3K activity is essential for the formation and maturation of macropinocytic cups. Despite sharing a seemingly conserved catalytic function, different Class I PI3K isoforms in *D. discoideum* have been shown to play non-redundant roles during cup formation (Hoeller et al., 2013), suggesting that isoform-specific localisation and protein-protein interactions underpin their functional specialisation.

Actin dynamics in both *D. discoideum* and mammalian systems are tightly regulated by small GTPases such as Ras and Rac, which coordinate cytoskeletal assembly, disassembly, and spatial organisation. These GTPases are, in turn, modulated by guanine nucleotide exchange factors (GEFs) and GTPase-activating proteins (GAPs), forming feedback networks that integrate diverse signals to orchestrate membrane remodelling. Ras and Rac act as molecular switches that control actin nucleators such as the Arp2/3 complex and formins. Within this regulatory landscape, Class I PI3Ks serve as key integrators of upstream signals and cytoskeletal responses, potentially through isoform-specific associations with actin-regulating proteins.

Research into macropinocytosis is of increasing importance due to its implications in human health and disease, particularly in cancer metabolism and neurodegenerative disorders. Elucidating the contributions of Class I PI3Ks to macropinocytic cup formation, and clarifying the distinct activities of individual isoforms, may ultimately support the development of targeted therapeutic strategies for diseases that currently remain without effective treatment.

1.6 Project Aims and Hypothesis

Overall Aim

To define how Class I PI3K isoforms PikA and PikF differentially regulate macropinocytosis in *Dictyostelium discoideum*. By integrating genetic, biochemical, imaging and proteomic approaches, this thesis seeks to elucidate how isoform-specific activities shape membrane dynamics and cytoskeletal organisation, and to nominate putative isoform-specific regulators and effectors involved in PI3K-mediated membrane remodelling.

Specific Aims

1. Establish functional non-redundancy in macropinocytic cup formation (Chapter 3).
   Validate whether loss of PikA or PikF independently cause macropinocytosis defects (Hoeller et al., 2013), determine whether mutants display distinct, isoform-specific phenotypes, and test macropinocytosis rescue by induced cross-expression of the opposite isoform, quantified by flow cytometry.

2. Map domain contributions to isoform specificity (Chapter 3).
   Design and construct PikA-PikF chimeras to test the contribution of individual domains (N-terminus, RBD, C2, accessory/helical, catalytic) to function, assessing macropinocytosis rescue in mutant backgrounds, quantified by flow cytometry.

3. Identify isoform-specific localisation patterns within macropinocytic cups (Chapter 3).
   Quantify GFP-PikA and GFP-PikF distributions across cup cross-sections to define base-versus-rim enrichment and characterise isoform-specific localisation patterns.

4. Characterise the impact of PikA and PikF loss on membrane signalling and actin dynamics (Chapter 4).
   Use advanced fluorescence microscopy with Fiji (ImageJ) analysis to relate disturbances in Ras/Rac signalling, PIP_3 signalling, and F-actin dynamics to isoform loss in PikA/B$^-$, PikF$^-$, and PikA/B/F$^-$ strains.

5. Identify isoform-specific interaction networks (Chapter 5).
   Use Affinity-Purification Mass Spectrometry and STRING analysis to define PikA and PikF interactomes, nominating isoform-specific regulators and effectors of membrane signalling and cytoskeletal dynamics for follow-up studies.

Central Hypothesis

Class I PI3Ks operate as central hubs in cytoskeletal coordination beyond their canonical role in PIP_3 generation. In *D. discoideum* macropinocytosis, isoform specificity is established through isoform-specific protein-protein interactions embedded within a complex signalling landscape that orchestrates PI3K spatiotemporal localisation and activity.

1.7 References

Ahuja, R., Pinyol, R., Reichenbach, N., Custer, L., Klingensmith, J., Kessels, M.M., Qualmann, B., 2007. Cordon-bleu is an actin nucleation factor and controls neuronal morphology. Cell 131, 337–350. https://doi.org/10.1016/j.cell.2007.08.030

Araki, N., Egami, Y., Watanabe, Y., Hatae, T., 2007. Phosphoinositide metabolism during membrane ruffling and macropinosome formation in EGF-stimulated A431 cells. Exp. Cell Res. 313, 1496–1507. https://doi.org/10.1016/j.yexcr.2007.02.012

Araki, N., Johnson, M.T., Swanson, J.A., 1996. A role for phosphoinositide 3-kinase in the completion of macropinocytosis and phagocytosis by macrophages. J. Cell Biol. 135, 1249–1260. https://doi.org/10.1083/jcb.135.5.1249

Berg, J.S., Derfler, B.H., Pennisi, C.M., Corey, D.P., Cheney, R.E., 2000. Myosin-X, a novel myosin with pleckstrin homology domains, associates with regions of dynamic actin. J. Cell Sci. 113, 3439–3451. https://doi.org/10.1242/jcs.113.19.3439

Bilanges, B., Posor, Y., Vanhaesebroeck, B., 2019. PI3K isoforms in cell signalling and vesicle trafficking. Nat. Rev. Mol. Cell Biol. 20, 515–534. https://doi.org/10.1038/s41580-019-0129-z

Bloomfield, G., Kay, R.R., 2016. Uses and abuses of macropinocytosis. J. Cell Sci. 129, 2697–2705. https://doi.org/10.1242/jcs.176149

Bloomfield, G., Traynor, D., Sander, S.P., Veltman, D.M., Pachebat, J.A., Kay, R.R., 2015. Neurofibromin controls macropinocytosis and phagocytosis in Dictyostelium. eLife 4, e04940. https://doi.org/10.7554/eLife.04940

Bohdanowicz, M., Grinstein, S., 2013. Role of Phospholipids in Endocytosis, Phagocytosis, and Macropinocytosis. Physiol. Rev. 93, 69–106. https://doi.org/10.1152/physrev.00002.2012

Bohdanowicz, M., Schlam, D., Hermansson, M., Rizzuti, D., Fairn, G.D., Ueyama, T., Somerharju, P., Du, G., Grinstein, S., 2013. Phosphatidic acid is required for the constitutive ruffling and macropinocytosis of phagocytes. Mol. Biol. Cell 24, 1700–1712. https://doi.org/10.1091/mbc.e12-11-0789

Bohil, A.B., Robertson, B.W., Cheney, R.E., 2006. Myosin-X is a molecular motor that functions in filopodia formation. Proc. Natl. Acad. Sci. 103, 12411–12416. https://doi.org/10.1073/pnas.0602443103

Bos, J.L., Rehmann, H., Wittinghofer, A., 2007. GEFs and GAPs: critical elements in the control of small G proteins. Cell 129, 865–877. https://doi.org/10.1016/j.cell.2007.05.018

Boucrot, E., Ferreira, A.P.A., Almeida-Souza, L., Debard, S., Vallis, Y., Howard, G., Bertot, L., Sauvonnet, N., McMahon, H.T., 2015. Endophilin marks and controls a clathrin-independent endocytic pathway. Nature 517, 460–465. https://doi.org/10.1038/nature14067

Brooks, A.B.E., Humphreys, D., Singh, V., Davidson, A.C., Arden, S.D., Buss, F., Koronakis, V., 2017. MYO6 is targeted by Salmonella virulence effectors to trigger PI3-kinase signaling and pathogen invasion into host cells. Proc. Natl. Acad. Sci. U. S. A. 114, 3915–3920.

Brzeska, H., Koech, H., Pridham, K.J., Korn, E.D., Titus, M.A., 2016. Selective localization of myosin-I proteins in macropinosomes and actin waves. Cytoskeleton (Hoboken) 73, 68–82. https://doi.org/10.1002/cm.21275

Brzeska, H., Pridham, K.J., Chhabra, E.S., Bar-Segal, O., Kruth, K.A., Sitaram, P., Ghosh, M., Korn, E.D., 2020. Dictyostelium myosin 1F and myosin 1E inhibit actin waves in a lipid-binding-dependent and motor-independent manner. J. Cell Sci. 133, jcs241091. https://doi.org/10.1002/cm.21627

Buckley, C.M., Pots, H., Gueho, A., Vines, J.H., Munn, C.J., Phillips, B.A., Gilsbach, B., Traynor, D., Nikolaev, A., Soldati, T., Parnell, A.J., Kortholt, A., King, J.S., 2020. Coordinated Ras and Rac Activity Shapes Macropinocytic Cups and Enables

Phagocytosis of Geometrically Diverse Bacteria. Curr. Biol. 30, 2912-2926.e5. https://doi.org/10.1016/j.cub.2020.05.049
Canton, J., 2018. Macropinocytosis: New Insights Into Its Underappreciated Role in Innate Immune Cell Surveillance. Front. Immunol. 9.
Canton, J., Schlam, D., Breuer, C., Gütschow, M., Glogauer, M., Grinstein, S., 2016. Calcium-sensing receptors signal constitutive macropinocytosis and facilitate the uptake of NOD2 ligands in macrophages. Nat. Commun. 7, 11284. https://doi.org/10.1038/ncomms11284
Ceccarelli, D.F.J., Blasutig, I.M., Goudreault, M., Li, Z., Ruston, J., Pawson, T., Sicheri, F., 2007. Non-canonical Interaction of Phosphoinositides with Pleckstrin Homology Domains of Tiam1 and ArhGAP9 *. J. Biol. Chem. 282, 13864–13874. https://doi.org/10.1074/jbc.M700505200
Cha, I., Jeon, T.J., 2011. Dynamic Localization of the Actin-Bundling Protein Cortexillin I during Cell Migration. Mol. Cells 32, 281–287. https://doi.org/10.1007/s10059-011-0072-0
Chapman-Andresen, C., 1984. The early days of pinocytosis. Carlsberg Res. Commun. 49, 179–186. https://doi.org/10.1007/BF02913945
Charpentier, J.C., Chen, D., Lapinski, P.E., Turner, J., Grigorova, I., Swanson, J.A., King, P.D., 2020. Macropinocytosis drives T cell growth by sustaining the activation of mTORC1. Nat. Commun. 11, 180. https://doi.org/10.1038/s41467-019-13997-3
Charpentier, J.C., King, P.D., 2021. Mechanisms and functions of endocytosis in T cells. Cell Commun. Signal. 19, 92. https://doi.org/10.1186/s12964-021-00766-3
Chen, Z., Borek, D., Padrick, S.B., Gomez, T.S., Metlagel, Z., Ismail, A.M., Umetani, J., Billadeau, D.D., Otwinowski, Z., Rosen, M.K., 2010. Structure and control of the actin regulatory WAVE complex. Nature 468, 533–538. https://doi.org/10.1038/nature09623
Cherfils, J., Zeghouf, M., 2013. Regulation of small GTPases by GEFs, GAPs, and GDIs. Physiol. Rev. 93, 269–309. https://doi.org/10.1152/physrev.00003.2012
Chung, C.Y., Firtel, R.A., 1999. PAKa, a putative PAK family member, is required for cytokinesis and the regulation of the cytoskeleton in Dictyostelium discoideum cells during chemotaxis. J. Cell Biol. 147, 559–576. https://doi.org/10.1083/jcb.147.3.559
Clague, M.J., Thorpe, C., Jones, A.T., 1995. Phosphatidylinositol 3-kinase regulation of fluid phase endocytosis. FEBS Lett. 367, 272–274. https://doi.org/10.1016/0014-5793(95)00576-U
Clark, J., Kay, R.R., Kielkowska, A., Niewczas, I., Fets, L., Oxley, D., Stephens, L.R., Hawkins, P.T., 2014. Dictyostelium uses ether-linked inositol phospholipids for intracellular signalling. EMBO J. 33, 2188–2200. https://doi.org/10.15252/embj.201488677
Commisso, C., Davidson, S.M., Soydaner-Azeloglu, R.G., Parker, S.J., Kamphorst, J.J., Hackett, S., Grabocka, E., Nofal, M., Drebin, J.A., Thompson, C.B., Rabinowitz, J.D., Metallo, C.M., Vander Heiden, M.G., Bar-Sagi, D., 2013. Macropinocytosis of protein is an amino acid supply route in Ras-transformed cells. Nature 497, 633–637. https://doi.org/10.1038/nature12138
Cox, D., Berg, J.S., Cammer, M., Chinegwundoh, J.O., Dale, B.M., Cheney, R.E., Greenberg, S., 2002. Myosin X is a downstream effector of PI(3)K during phagocytosis. Nat. Cell Biol. 4, 469–477. https://doi.org/10.1038/ncb805
Cox, D., Greenberg, S., 2001. Phagocytic signaling strategies: Fcγreceptor-mediated phagocytosis as a model system. Semin. Immunol. 13, 339–345. https://doi.org/10.1006/smim.2001.0330
Crowley, M.T., Costello, P.S., Fitzer-Attas, C.J., Turner, M., Meng, F., Lowell, C., Tybulewicz, V.L.J., DeFranco, A.L., 1997. A Critical Role for Syk in Signal Transduction and Phagocytosis Mediated by Fcγ Receptors on Macrophages. J. Exp. Med. 186, 1027–1039. https://doi.org/10.1084/jem.186.7.1027
Dawson, J.C., Legg, J.A., Machesky, L.M., 2006. Bar domain proteins: a role in tubulation, scission and actin assembly in clathrin-mediated endocytosis. Trends Cell Biol. 16,

493–498. https://doi.org/10.1016/j.tcb.2006.08.004
de Carvalho, T.M.U., Barrias, E.S., de Souza, W., 2015. Macropinocytosis: a pathway to protozoan infection. Front. Physiol. 6. https://doi.org/10.3389/fphys.2015.00106
de Hostos, E.L., Bradtke, B., Lottspeich, F., Guggenheim, R., Gerisch, G., 1991. Coronin, an actin binding protein of Dictyostelium discoideum localized to cell surface projections, has sequence similarities to G protein beta subunits. EMBO J. 10, 4097–4104. https://doi.org/10.1002/j.1460-2075.1991.tb04986.x
de Hostos, E.L., Rehfuess, C., Bradtke, B., Waddell, D.R., Albrecht, R., Murphy, J., Gerisch, G., 1993. Dictyostelium mutants lacking the cytoskeletal protein coronin are defective in cytokinesis and cell motility. J. Cell Biol. 120, 163–173. https://doi.org/10.1083/jcb.120.1.163
Desale, S.E., Chidambaram, H., Chinnathambi, S., 2021. G-protein coupled receptor, PI3K and Rho signaling pathways regulate the cascades of Tau and amyloid-β in Alzheimer's disease. Mol. Biomed. 2, 17. https://doi.org/10.1186/s43556-021-00036-1
Domin, J., Gaidarov, I., Smith, M.E.K., Keen, J.H., Waterfield, M.D., 2000. The Class II Phosphoinositide 3-Kinase PI3K-C2α Is Concentrated in the Trans-Golgi Network and Present in Clathrin-coated Vesicles. J. Biol. Chem. 275, 11943–11950. https://doi.org/10.1074/jbc.275.16.11943
Dujardin, D.L., Barnhart, L.E., Stehman, S.A., Gomes, E.R., Gundersen, G.G., Vallee, R.B., 2003. A role for cytoplasmic dynein and LIS1 in directed cell movement. J. Cell Biol. 163, 1205–1211. https://doi.org/10.1083/jcb.200310097
Egami, Y., Taguchi, T., Maekawa, M., Arai, H., Araki, N., 2014. Small GTPases and phosphoinositides in the regulatory mechanisms of macropinosome formation and maturation. Front. Physiol. 5, 374. https://doi.org/10.3389/fphys.2014.00374
Erami, Z., Khalil, B.D., Salloum, G., Yao, Y., LoPiccolo, J., Shymanets, A., Nürnberg, B., Bresnick, A.R., Backer, J.M., 2017. Rac1-stimulated macropinocytosis enhances Gβγ activation of PI3Kβ. Biochem. J. 474, 3903–3914. https://doi.org/10.1042/BCJ20170279
Etienne-Manneville, S., 2018. Cytoplasmic Intermediate Filaments in Cell Biology. Annu. Rev. Cell Dev. Biol. 34, 1–28. https://doi.org/10.1146/annurev-cellbio-100617-062534
Faix, J., Clougherty, C., Konzok, A., Mintert, U., Murphy, J., Albrecht, R., Mühlbauer, B., Kuhlmann, J., 1998. The IQGAP-related protein DGAP1 interacts with Rac and is involved in the modulation of the F-actin cytoskeleton and control of cell motility.
Faix, J., Rottner, K., 2022. Ena/VASP proteins in cell edge protrusion, migration and adhesion. J. Cell Sci. 135, jcs259226. https://doi.org/10.1242/jcs.259226
Faix, J., Steinmetz, M., Boves, H., Kammerer, R.A., Lottspeich, F., Mintert, U., Murphy, J., Stock, A., Aebi, U., Gerisch, G., 1996. Cortexillins, Major Determinants of Cell Shape and Size, Are Actin-Bundling Proteins with a Parallel Coiled-Coil Tail. Cell 86, 631–642. https://doi.org/10.1016/S0092-8674(00)80136-1
Ferguson, S., Raimondi, A., Paradise, S., Shen, H., Mesaki, K., Ferguson, A., Destaing, O., Ko, G., Takasaki, J., Cremona, O., Toole, E.O., Camilli, P.D., 2009. Coordinated Actions of Actin and BAR Proteins Upstream of Dynamin at Endocytic Clathrin-Coated Pits. Dev. Cell 17, 811–822. https://doi.org/10.1016/j.devcel.2009.11.005
Filić, V., Marinović, M., Faix, J., Weber, I., 2014. The IQGAP-related protein DGAP1 mediates signaling to the actin cytoskeleton as an effector and a sequestrator of Rac1 GTPases. Cell. Mol. Life Sci. 71, 2775–2785. https://doi.org/10.1007/s00018-014-1606-3
Filić, V., Mijanović, L., Putar, D., Talajić, A., Ćetković, H., Weber, I., 2021. Regulation of the Actin Cytoskeleton via Rho GTPase Signalling in Dictyostelium and Mammalian Cells: A Parallel Slalom. Cells 10, 1592. https://doi.org/10.3390/cells10071592
Flannagan, R.S., Jaumouillé, V., Grinstein, S., 2012. The Cell Biology of Phagocytosis. Annu. Rev. Pathol. Mech. Dis. 7, 61–98. https://doi.org/10.1146/annurev-pathol-011811-132445

Fletcher, D.A., Mullins, R.D., 2010. Cell mechanics and the cytoskeleton. Nature 463, 485–492. https://doi.org/10.1038/nature08908
Fletcher, L.M., Welsh, G.I., Oatey, P.B., Tavare, J.M., 2000. Role for the microtubule cytoskeleton in GLUT4 vesicle trafficking and in the regulation of insulin-stimulated glucose uptake.
Fritsch, R., de Krijger, I., Fritsch, K., George, R., Reason, B., Kumar, M.S., Diefenbacher, M., Stamp, G., Downward, J., 2013. RAS and RHO Families of GTPases Directly Regulate Distinct Phosphoinositide 3-Kinase Isoforms. Cell 153, 1050–1063. https://doi.org/10.1016/j.cell.2013.04.031
Fritsch, R., Downward, J., 2013. SnapShot: Class I PI3K Isoform Signaling. Cell 154, 940-940.e1. https://doi.org/10.1016/j.cell.2013.07.045
Fruman, D.A., Meyers, R.E., Cantley, L.C., 1998. PHOSPHOINOSITIDE KINASES.
Fujii, M., Kawai, K., Egami, Y., Araki, N., 2013. Dissecting the roles of Rac1 activation and deactivation in macropinocytosis using microscopic photo-manipulation. Sci. Rep. 3, 2385. https://doi.org/10.1038/srep02385
Goode, B.L., Eskin, J., Shekhar, S., 2023. Mechanisms of actin disassembly and turnover. J. Cell Biol. 222, e202309021. https://doi.org/10.1083/jcb.202309021
Gozzelino, L., De Santis, M.C., Gulluni, F., Hirsch, E., Martini, M., 2020. PI(3,4)P2 Signaling in Cancer and Metabolism. Front. Oncol. 10. https://doi.org/10.3389/fonc.2020.00360
Grimmer, S., van Deurs, B., Sandvig, K., 2002. Membrane ruffling and macropinocytosis in A431 cells require cholesterol. J. Cell Sci. 115, 2953–2962. https://doi.org/10.1242/jcs.115.14.2953
Gulluni, F., De Santis, M.C., Margaria, J.P., Martini, M., Hirsch, E., 2019. Class II PI3K Functions in Cell Biology and Disease. Trends Cell Biol. 29, 339–359. https://doi.org/10.1016/j.tcb.2019.01.001
Haag, N., Kessels, M.M., Qualmann, B., 2012. The actin nucleator Cobl is crucial for Purkinje cell development and works in close conjunction with the F-actin binding protein Abp1. J. Neurosci. 32, 17842–17856. https://doi.org/10.1523/JNEUROSCI.0843-12.2012
Hakala, M., Wioland, H., Tolonen, M., Kotila, T., Jegou, A., Romet-Lemonne, G., Lappalainen, P., 2021. Twinfilin uncaps filament barbed ends to promote turnover of lamellipodial actin networks. Nat. Cell Biol. 23, 147–159. https://doi.org/10.1038/s41556-020-00629-y
Hayakawa, K., Tatsumi, H., Sokabe, M., 2011. Actin filaments function as a tension sensor by tension-dependent binding of cofilin to the filament. J. Cell Biol. 195, 721–727. https://doi.org/10.1083/jcb.201102039
Hirokawa, N., Noda, Y., Tanaka, Y., Niwa, S., 2009. Kinesin superfamily motor proteins and intracellular transport. Nat. Rev. Mol. Cell Biol. 10, 682–696. https://doi.org/10.1038/nrm2774
Hirsch, E., Braccini, L., Ciraolo, E., Morello, F., Perino, A., 2009. Twice upon a time: PI3K's secret double life exposed. Trends Biochem. Sci. 34, 244–248. https://doi.org/10.1016/j.tibs.2009.02.003
Hoeller, O., Bolourani, P., Clark, J., Stephens, L.R., Hawkins, P.T., Weiner, O.D., Weeks, G., Kay, R.R., 2013. Two distinct functions for PI3-kinases in macropinocytosis. J. Cell Sci. jcs.134015. https://doi.org/10.1242/jcs.134015
Hoepfner, S., Severin, F., Cabezas, A., Habermann, B., Runge, A., Gillooly, D., Stenmark, H., Zerial, M., 2005. Modulation of Receptor Recycling and Degradation by the Endosomal Kinesin KIF16B. Cell 121, 437–450. https://doi.org/10.1016/j.cell.2005.02.017
Hohmann, T., Dehghani, F., 2019. The Cytoskeleton—A Complex Interacting Meshwork. Cells 8, 362. https://doi.org/10.3390/cells8040362
Innocenti, M., Zucconi, A., Disanza, A., Frittoli, E., Areces, L.B., Steffen, A., Stradal, T.E., Di Fiore, P.P., Carlier, M.-F., Scita, G., 2004. Abi1 is essential for the formation and activation of a WAVE2 signalling complex. Nat. Cell Biol. 6, 319–327. https://doi.org/10.1038/ncb1105

Insall, R.H., Machesky, L.M., 2009. Actin Dynamics at the Leading Edge: From Simple Machinery to Complex Networks. Dev. Cell 17, 310–322. https://doi.org/10.1016/j.devcel.2009.08.012
Jefferson, J.J., Leung, C.L., Liem, R.K.H., 2004. Plakins: Goliaths that link cell junctions and the cytoskeleton. Nat. Rev. Mol. Cell Biol. 5, 542–553. https://doi.org/10.1038/nrm1425
Jung, G., Wu, X., Hammer, J.A., 1996. Dictyostelium mutants lacking multiple classic myosin I isoforms exhibit defects in fluid-phase pinocytosis. J. Cell Biol. 133, 305–323. https://doi.org/10.1083/jcb.133.2.305
Jung, G., Pan, M., Alexander, C.J., Jin, T., Hammer, J.A., 2022. Dual regulation of the actin cytoskeleton by CARMIL-GAP. J. Cell Sci. 135, jcs258704. https://doi.org/10.1242/jcs.258704
Kage, F., Winterhoff, M., Dimchev, V., Mueller, J., Thalheim, T., Freise, A., Brühmann, S., Kollasser, J., Block, J., Dimchev, G., Geyer, M., Schnittler, H.-J., Brakebusch, C., Stradal, T.E.B., Carlier, M.-F., Sixt, M., Käs, J., Faix, J., Rottner, K., 2017. FMNL formins boost lamellipodial force generation. Nat. Commun. 8, 14832. https://doi.org/10.1038/ncomms14832
Kay, R.R., 2021. Macropinocytosis: Biology and mechanisms. Cells Dev., Quantitative Cell and Developmental Biology 168, 203713. https://doi.org/10.1016/j.cdev.2021.203713
Kay, R.R., Williams, T.D., Manton, J.D., Traynor, D., Paschke, P., 2019. Living on soup: macropinocytic feeding in amoebae. Int. J. Dev. Biol. 63, 473–483. https://doi.org/10.1387/ijdb.190220rk
Kendrick-Jones, J., Buss, F., 2016. Editorial Overview: Myosins in Review. Traffic 17, 819–821. https://doi.org/10.1111/tra.12405
Kerr, M.C., Teasdale, R.D., 2009. Defining Macropinocytosis. Traffic 10, 364–371. https://doi.org/10.1111/j.1600-0854.2009.00878.x
Kim, S.M., Nguyen, T.T., Ravi, A., Kubiniok, P., Finicle, B.T., Jayashankar, V., Malacrida, L., Hou, J., Robertson, J., Gao, D., Chernoff, J., Digman, M.A., Potma, E.O., Tromberg, B.J., Thibault, P., Edinger, A.L., 2018. PTEN Deficiency and AMPK Activation Promote Nutrient Scavenging and Anabolism in Prostate Cancer Cells. Cancer Discov. 8, 866–883. https://doi.org/10.1158/2159-8290.CD-17-1215
Kirkham, M., Nixon, S.J., Howes, M.T., Abi-Rached, L., Wakeham, D.E., Hanzal-Bayer, M., Ferguson, C., Hill, M.M., Fernandez-Rojo, M., Brown, D.A., Hancock, J.F., Brodsky, F.M., Parton, R.G., 2008. Evolutionary analysis and molecular dissection of caveola biogenesis. J. Cell Sci. 121, 2075–2086. https://doi.org/10.1242/jcs.024588
Kirkham, M., Parton, R.G., 2005. Clathrin-independent endocytosis: New insights into caveolae and non-caveolar lipid raft carriers. Biochim. Biophys. Acta BBA - Mol. Cell Res. 1745, 273–286. https://doi.org/10.1016/j.bbamcr.2005.06.002
Klopfenstein, D.R., Tomishige, M., Stuurman, N., Vale, R.D., 2002. Role of Phosphatidylinositol(4,5)bisphosphate Organization in Membrane Transport by the Unc104 Kinesin Motor. Cell 109, 347–358. https://doi.org/10.1016/S0092-8674(02)00708-0
Knaus, U.G., Morris, S., Dong, H.-J., Chernoff, J., Bokoch, G.M., 1998. Structural requirements for PAK activation by Rac GTPases. J. Biol. Chem. 273, 13905–13908. https://www.jbc.org/article/S0021-9258%2818%2948815-1/pdf
Kovar, D.R., 2006. Molecular details of formin-mediated actin assembly. Curr. Opin. Cell Biol. 18, 11–17. https://doi.org/10.1016/j.ceb.2005.12.011
Kumari, S., Mg, S., Mayor, S., 2010. Endocytosis unplugged: multiple ways to enter the cell. Cell Res. 20, 256–275. https://doi.org/10.1038/cr.2010.19
Lacruz, R.S., Brookes, S.J., Wen, X., Jimenez, J.M., Vikman, S., Hu, P., White, S.N., Lyngstadaas, S.P., Okamoto, C.T., Smith, C.E., Paine, M.L., 2013. Adaptor Protein Complex 2 (AP-2) Mediated, Clathrin Dependent Endocytosis, And Related Gene Activities, Are A Prominent Feature During Maturation Stage Amelogenesis. J. Bone Miner. Res. Off. J. Am. Soc. Bone Miner. Res. 28, 672. https://doi.org/10.1002/jbmr.1779

Laplante, M., Sabatini, D.M., 2009. mTOR signaling at a glance. J. Cell Sci. 122, 3589–3594. https://doi.org/10.1242/jcs.051011
Lappalainen, P., 2016. Actin-binding proteins: the long road to understanding the dynamic landscape of cellular actin networks. Mol. Biol. Cell 27, 2519–2522. https://doi.org/10.1091/mbc.e15-10-0728
Lappalainen, P., Kotila, T., Jégou, A., Romet-Lemonne, G., 2022. Biochemical and mechanical regulation of actin dynamics. Nat. Rev. Mol. Cell Biol. 23, 836–852. https://doi.org/10.1038/s41580-022-00508-4
Lee, Yuree, Kim, E.-S., Choi, Y., Hwang, I., Staiger, C.J., Chung, Y.-Y., Lee, Youngsook, 2008. The Arabidopsis Phosphatidylinositol 3-Kinase Is Important for Pollen Development. Plant Physiol. 147, 1886–1897. https://doi.org/10.1104/pp.108.121590
Leevers, S.J., Vanhaesebroeck, B., Waterfield, M.D., 1999. Signalling through phosphoinositide 3-kinases: the lipids take centre stage. Curr. Opin. Cell Biol. 11, 219–225. https://doi.org/10.1016/S0955-0674(99)80029-5
Levy, J.R., Holzbaur, E.L.F., 2008. Dynein drives nuclear rotation during forward progression of motile fibroblasts. J. Cell Sci. 121, 3187–3195. https://doi.org/10.1242/jcs.033878
Lewis, W.H., 1937. Pinocytosis by Malignant Cells. Am. J. Cancer 29, 666–679. https://doi.org/10.1158/ajc.1937.666
Li, J., Zou, Y., Li, Z., Jiu, Y., 2019. Joining actions: crosstalk between intermediate filaments and actin orchestrates cellular physical dynamics and signaling. Sci. China Life Sci. 62, 1368–1374. https://doi.org/10.1007/s11427-018-9488-1
Liberali, P., Kakkonen, E., Turacchio, G., Valente, C., Spaar, A., Perinetti, G., Böckmann, R.A., Corda, D., Colanzi, A., Marjomaki, V., Luini, A., 2008. The closure of Pak1-dependent macropinosomes requires the phosphorylation of CtBP1/BARS. EMBO J. 27, 970–981. https://doi.org/10.1038/emboj.2008.59
Lim, J.P., Gleeson, P.A., 2011. Macropinocytosis: an endocytic pathway for internalising large gulps. Immunol. Cell Biol. 89, 836–843. https://doi.org/10.1038/icb.2011.20
Lo, W.-T., Zhang, Y., Vadas, O., Roske, Y., Gulluni, F., De Santis, M.C., Zagar, A.V., Stephanowitz, H., Hirsch, E., Liu, F., Daumke, O., Kudryashev, M., Haucke, V., 2022. Structural basis of phosphatidylinositol 3-kinase C2α function. Nat. Struct. Mol. Biol. 29, 218–228. https://doi.org/10.1038/s41594-022-00730-w
Loh, L.N., McCarthy, E.M.C., Narang, P., Khan, N.A., Ward, T.H., 2017. Escherichia coli K1 utilizes host macropinocytic pathways for invasion of brain microvascular endothelial cells. Traffic 18, 733–746. https://doi.org/10.1111/tra.12508
Lu, Q., Yu, J., Yan, J., Wei, Z., Zhang, M., 2011. Structural basis of the myosin X PH1N-PH2-PH1C tandem as a specific and acute cellular PI(3,4,5)P3 sensor. Mol. Biol. Cell 22, 4268–4278. https://doi.org/10.1091/mbc.e11-04-0354
Lutton, J.E., Coker, H.L.E., Paschke, P., Munn, C.J., King, J.S., Bretschneider, T., Kay, R.R., 2023. Formation and closure of macropinocytic cups in Dictyostelium. Curr. Biol. 33, 3083-3096.e6. https://doi.org/10.1016/j.cub.2023.06.017
McIntosh, B.B., Ostap, E.M., 2016. Myosin-I molecular motors at a glance. J. Cell Sci. 129, 2689–2695. https://doi.org/10.1242/jcs.186403
Maekawa, M., Terasaka, S., Mochizuki, Y., Kawai, K., Ikeda, Y., Araki, N., Skolnik, E.Y., Taguchi, T., Arai, H., 2014. Sequential breakdown of 3-phosphorylated phosphoinositides is essential for the completion of macropinocytosis. Proc. Natl. Acad. Sci. 111, E978–E987. https://doi.org/10.1073/pnas.1311029111
Maniak, M., Rauchenberger, R., Albrecht, R., Murphy, J., Gerisch, G., 1995. Coronin involved in phagocytosis: Dynamics of particle-induced relocalization visualized by a green fluorescent protein tag. Cell 83, 915–924. https://doi.org/10.1016/0092-8674(95)90207-4
Manning, B.D., Toker, A., 2017. AKT/PKB Signaling: Navigating the Network. Cell 169, 381–405. https://doi.org/10.1016/j.cell.2017.04.001
Marinović, M., Mijanović, L., Šoštar, M., Vizovišek, M., Junemann, A., Fonović, M., Turk, B., Weber, I., Faix, J., Filić, V., 2019. IQGAP-related protein IqgC suppresses Ras signaling during large-scale endocytosis. Proc. Natl. Acad. Sci. 116, 1289–1298.

https://doi.org/10.1073/pnas.1810268116
Mayor, S., Pagano, R.E., 2007. Pathways of clathrin-independent endocytosis. Nat. Rev. Mol. Cell Biol. 8, 603–612. https://doi.org/10.1038/nrm2216
Mechanobiology Institute, National University of Singapore, 2023. What is the CLIC/GEEC Endocytosis pathway? URL https://www.mbi.nus.edu.sg/mbinfo/what-is-the-clic-geec-endocytosis-pathway/ (accessed 4.16.25).
Merlot, S., Firtel, R.A., 2003. Leading the way: directional sensing through phosphatidylinositol 3-kinase and other signaling pathways. J. Cell Sci. 116, 3471–3478. https://doi.org/10.1242/jcs.00703
Mikati, M.A., Breitsprecher, D., Jansen, S., Reisler, E., Goode, B.L., 2015. Coronin Enhances Actin Filament Severing by Recruiting Cofilin to Filament Sides and Altering F-Actin Conformation. J. Mol. Biol. 427, 3137–3147. https://doi.org/10.1016/j.jmb.2015.08.011
Montaño-Rendón, F., Walpole, G.F.W., Krause, M., Hammond, G.R.V., Grinstein, S., Fairn, G.D., 2022. PtdIns(3,4)P2, Lamellipodin, and VASP coordinate actin dynamics during phagocytosis in macrophages. J. Cell Biol. 221, e202207042. https://doi.org/10.1083/jcb.202207042
Mousavi, S.A., Malerød, L., Berg, T., Kjeken, R., 2004. Clathrin-dependent endocytosis. Biochem. J. 377, 1–16. https://doi.org/10.1042/bj20031000
Mullins, R.D., Heuser, J.A., Pollard, T.D., 1998. The interaction of Arp2/3 complex with actin: Nucleation, high affinity pointed end capping, and formation of branching networks of filaments. Proc. Natl. Acad. Sci. 95, 6181–6186. https://doi.org/10.1073/pnas.95.11.6181
Nag, S., Larsson, M., Robinson, R.C., Burtnick, L.D., 2013. Gelsolin: The tail of a molecular gymnast. Cytoskeleton 70, 360–384. https://doi.org/10.1002/cm.21117
Nikolaou, S., Juin, A., Whitelaw, J.A., Paul, N.R., Fort, L., Nixon, C., Spence, H.J., Bryson, S., Machesky, L.M., 2024. CYRI-B-mediated macropinocytosis drives metastasis via lysophosphatidic acid receptor uptake. eLife 13, e83712. https://doi.org/10.7554/eLife.83712
Ninomiya, N., Hazeki, K., Fukui, Y., Seya, T., Okada, T., Hazeki, O., Ui, M., 1994. Involvement of phosphatidylinositol 3-kinase in Fc gamma receptor signaling.
Novak, K.D., Peterson, M.D., Reedy, M.C., Titus, M.A., 1995. Dictyostelium myosin I double mutants exhibit conditional defects in pinocytosis. J. Cell Biol. 131, 1205–1221. https://doi.org/10.1083/jcb.131.5.1205
O'Reilly, P.J., Hickman-Davis, J.M., Davis, I.C., Matalon, S., 2003. Hyperoxia Impairs Antibacterial Function of Macrophages Through Effects on Actin. Am. J. Respir. Cell Mol. Biol. 28, 443–450. https://doi.org/10.1165/rcmb.2002-0153OC
Palm, W., 2019. Metabolic functions of macropinocytosis. Philos. Trans. R. Soc. B Biol. Sci. 374, 20180285. https://doi.org/10.1098/rstb.2018.0285
Para, A., Krischke, M., Merlot, S., Shen, Z., Oberholzer, M., Lee, S., Briggs, S., De Lozanne, A., Schleicher, M., Williams, J.G., Noegel, A.A., Firtel, R.A., 2009. Dictyostelium Dock180-related RacGEFs regulate the actin cytoskeleton. Mol. Biol. Cell 20, 699–707. https://doi.org/10.1091/mbc.E08-09-0899
Park, W.S., Heo, W.D., Whalen, J.H., O'Rourke, N.A., Bryan, H.M., Meyer, T., Teruel, M.N., 2008. Comprehensive Identification of PIP3-Regulated PH Domains from C. elegans to H. sapiens by Model Prediction and Live Imaging. Mol. Cell 30, 381–392. https://doi.org/10.1016/j.molcel.2008.04.008
Parton, R.G., Kozlov, M.M., Ariotti, N., 2020. Caveolae and lipid sorting: Shaping the cellular response to stress. J. Cell Biol. 219, e201905071. https://doi.org/10.1083/jcb.201905071
Pollard, T.D., Borisy, G.G., 2003. Cellular Motility Driven by Assembly and Disassembly of Actin Filaments. Cell 112, 453–465. https://doi.org/10.1016/S0092-8674(03)00120-X
Portes, J., Barrias, E., Travassos, R., Attias, M., De Souza, W., 2020. Toxoplasma gondii Mechanisms of Entry Into Host Cells. Front. Cell. Infect. Microbiol. 10, 294.

https://doi.org/10.3389/fcimb.2020.00294
Powers, R.M., Daza, R., Koehler, A.E., Courchet, J., Calabrese, B., Hevner, R.F., Halpain, S., 2022. Growth cone macropinocytosis of neurotrophin receptor and neuritogenesis are regulated by neuron navigator 1. Mol. Biol. Cell 33, ar64. https://doi.org/10.1091/mbc.E21-12-0623
Qiu, Z., Liu, W., Zhu, Qianru, Ke, K., Zhu, Qicong, Jin, W., Yu, S., Yang, Z., Li, L., Sun, X., Ren, S., Liu, Y., Zhu, Z., Zeng, J., Huang, X., Huang, Y., Wei, L., Ma, M., Lu, J., Chen, X., Mou, Y., Xie, T., Sui, X., 2022. The Role and Therapeutic Potential of Macropinocytosis in Cancer. Front. Pharmacol. 13. https://doi.org/10.3389/fphar.2022.919819
Quinlan, M.E., Heuser, J.E., Kerkhoff, E., Mullins, R.D., 2005. Drosophila Spire is an actin nucleation factor. Nature 433, 382–388. https://doi.org/10.1038/nature03241
Ratner, N., Miller, S.J., 2015. A RASopathy gene commonly mutated in cancer: the neurofibromatosis type 1 tumour suppressor. Nat. Rev. Cancer 15, 290–301. https://doi.org/10.1038/nrc3911
Rennick, J.J., Johnston, A.P.R., Parton, R.G., 2021. Key principles and methods for studying the endocytosis of biological and nanoparticle therapeutics. Nat. Nanotechnol. 16, 266–276. https://doi.org/10.1038/s41565-021-00858-8
Renault, L., Bugyi, B., Carlier, M.-F., 2008. Spire and Cordon-bleu: multifunctional regulators of actin dynamics. Trends Cell Biol. 18, 494–504. https://doi.org/10.1016/j.tcb.2008.07.008
Río-Bergé, C., Cong, Y., Reggiori, F., 2023. Getting on the right track: Interactions between viruses and the cytoskeletal motor proteins. Traffic 24, 114–130. https://doi.org/10.1111/tra.12835
Risca, V.I., Wang, E.B., Chaudhuri, O., Chia, J.J., Geissler, P.L., Fletcher, D.A., 2012. Actin filament curvature biases branching direction. Proc. Natl. Acad. Sci. 109, 2913–2918. https://doi.org/10.1073/pnas.1114292109
Roberts, A.J., Kon, T., Knight, P.J., Sutoh, K., Burgess, S.A., 2013. Functions and mechanics of dynein motor proteins. Nat. Rev. Mol. Cell Biol. 14, 713–726. https://doi.org/10.1038/nrm3667
Royle, S.J., Lagnado, L., 2003. Endocytosis at the synaptic terminal. J. Physiol. 553, 345–355. https://doi.org/10.1113/jphysiol.2003.049221
Saeed, M.F., Kolokoltsov, A.A., Albrecht, T., Davey, R.A., 2010. Cellular Entry of Ebola Virus Involves Uptake by a Macropinocytosis-Like Mechanism and Subsequent Trafficking through Early and Late Endosomes. PLOS Pathog. 6, e1001110. https://doi.org/10.1371/journal.ppat.1001110
Salamon, R.S., Dbouk, H.A., Collado, D., Lopiccolo, J., Bresnick, A.R., Backer, J.M., 2015. Identification of the Rab5 Binding Site in p110β - Assays for PI3Kβ binding to Rab5. Methods Mol. Biol. Clifton NJ 1298, 271–281. https://doi.org/10.1007/978-1-4939-2569-8_23
Salloum, G., Bresnick, A.R., Backer, J.M., 2023. Macropinocytosis: mechanisms and regulation. Biochem. J. 480, 335–362. https://doi.org/10.1042/BCJ20210584
Salloum, G., Jakubik, C.T., Erami, Z., Heitz, S.D., Bresnick, A.R., Backer, J.M., 2019. PI3Kβ is selectively required for growth factor-stimulated macropinocytosis. J. Cell Sci. 132, jcs231639. https://doi.org/10.1242/jcs.231639
Sathe, M., Muthukrishnan, G., Rae, J., Disanza, A., Thattai, M., Scita, G., Parton, R.G., Mayor, S., 2018. Small GTPases and BAR domain proteins regulate branched actin polymerisation for clathrin and dynamin-independent endocytosis. Nat. Commun. 9, 1835. https://doi.org/10.1038/s41467-018-03955-w
Schlam, D., Bagshaw, R.D., Freeman, S.A., Collins, R.F., Pawson, T., Fairn, G.D., Grinstein, S., 2015. Phosphoinositide 3-kinase enables phagocytosis of large particles by terminating actin assembly through Rac/Cdc42 GTPase-activating proteins. Nat. Commun. 6, 8623. https://doi.org/10.1038/ncomms9623
Scott, C.C., Dobson, W., Botelho, R.J., Coady-Osberg, N., Chavrier, P., Knecht, D.A., Heath, C., Stahl, P., Grinstein, S., 2005. Phosphatidylinositol-4,5-bisphosphate hydrolysis

directs actin remodeling during phagocytosis. J. Cell Biol. 169, 139–149. https://doi.org/10.1083/jcb.200412162
Sept, D., McCammon, J.A., 2001. Thermodynamics and kinetics of actin filament nucleation. Biophys. J. 81, 667–674.
Shimoyama, M., Nakada-Tsukui, K., Nozaki, T., 2024. EhRacM differentially regulates macropinocytosis and motility in the enteric protozoan parasite Entamoeba histolytica. PLoS Pathog. 20, e1012364. https://doi.org/10.1371/journal.ppat.1012364
Shin, E.Y., Woo, K.N., Lee, C.S., Koo, S.H., Kim, Y.G., Kim, W.J., Park, D., Kim, E.G., 2013. Phosphorylation of p21-activated kinase 4 (PAK4) at Ser99 by Polo-like kinase 1 (Plk1) is required for mitotic progression. PLoS ONE 8, e71495. https://doi.org/10.1371/journal.pone.0071495
Skau, C.T., Courson, D.S., Bestul, A.J., Winkelman, J.D., Rock, R.S., Sirotkin, V., Kovar, D.R., 2011. Actin Filament Bundling by Fimbrin Is Important for Endocytosis, Cytokinesis, and Polarization in Fission Yeast. J. Biol. Chem. 286, 26964–26977. https://doi.org/10.1074/jbc.M111.239004
Šoštar, M., Marinović, M., Filić, V., Pavin, N., Weber, I., 2024. Oscillatory dynamics of Rac1 activity in Dictyostelium discoideum amoebae. PLOS Comput. Biol. 20, e1012025. https://doi.org/10.1371/journal.pcbi.1012025
Sotodosos-Alonso, L., Pulgarín-Alfaro, M., del Pozo, M.A., 2023. Caveolae Mechanotransduction at the Interface between Cytoskeleton and Extracellular Matrix. Cells 12, 942. https://doi.org/10.3390/cells12060942
Stow, J.L., Hung, Y., Wall, A.A., 2020. Macropinocytosis: Insights from immunology and cancer. Curr. Opin. Cell Biol., Membrane Trafficking 65, 131–140. https://doi.org/10.1016/j.ceb.2020.06.005
Svitkina, T.M., 2012. Actin bends over backward for directional branching. Proc. Natl. Acad. Sci. 109, 2693–2694. https://doi.org/10.1073/pnas.1121360109
Swanson, J.A., Johnson, M.T., Beningo, K., Post, P., Mooseker, M., Araki, N., 1999. A contractile activity that closes phagosomes in macrophages. J. Cell Sci. 112, 307–316. https://doi.org/10.1242/jcs.112.3.307
Swanson, J.A., Watts, C., 1995. Macropinocytosis. Trends Cell Biol. 5, 424–428. https://doi.org/10.1016/S0962-8924(00)89101-1
Takeda, K., Sasaki, A.T., Ha, H., Seung, H.-A., Firtel, R.A., 2007. Role of Phosphatidylinositol 3-Kinases in Chemotaxis in Dictyostelium. J. Biol. Chem. 282, 11874–11884. https://doi.org/10.1074/jbc.M610984200
Takei, K., Haucke, V., 2001. Clathrin-mediated endocytosis: membrane factors pull the trigger. Trends Cell Biol. 11, 385–391. https://doi.org/10.1016/S0962-8924(01)02082-7
Takenawa, T., Suetsugu, S., 2007. The WASP–WAVE protein network: connecting the membrane to the cytoskeleton. Nat. Rev. Mol. Cell Biol. 8, 37–48. https://doi.org/10.1038/nrm2069
Thorpe, L.M., Yuzugullu, H., Zhao, J.J., 2015. PI3K in cancer: divergent roles of isoforms, modes of activation, and therapeutic targeting. Nat. Rev. Cancer 15, 7–24. https://doi.org/10.1038/nrc3860
Toker, A., Cantley, L.C., 1997. Signalling through the lipid products of phosphoinositide-3-OH kinase. Nature 387, 673–676. https://doi.org/10.1038/42648
Tong, Y., Tempel, W., Wang, H., Yamada, K., Shen, L., Senisterra, G.A., MacKenzie, F., Chishti, A.H., Park, H.-W., 2010. Phosphorylation-independent dual-site binding of the FHA domain of KIF13 mediates phosphoinositide transport via centaurin α1. Proc. Natl. Acad. Sci. 107, 20346–20351. https://doi.org/10.1073/pnas.1009008107
Torrino, S., Shen, W.-W., Blouin, C.M., Mani, S.K., Lesegno, C.V. de, Bost, P., Grassart, A., Köster, D., Valades-Cruz, C.A., Chambon, V., Johannes, L., Pierobon, P., Soumelis, V., Coirault, C., Vassilopoulos, S., Lamaze, C., 2018. EHD2 is a mechanotransducer connecting caveolae dynamics with gene transcription. J. Cell Biol. 217, 4092. https://doi.org/10.1083/jcb.201801122
Trösch, R., 2025. How villin subclasses coordinate actin remodelling. Nat. Plants 11, 6–6.

https://doi.org/10.1038/s41477-024-01887-6
Uyeda, T.Q.P., Iwadate, Y., Umeki, N., Nagasaki, A., Yumura, S., 2011. Stretching actin filaments within cells enhances their affinity for the myosin II motor domain. PloS One 6, e26200. https://doi.org/10.1371/journal.pone.0026200
Vanhaesebroeck, B., Leevers, S.J., Panayotou, G., Waterfield, M.D., 1997. Phosphoinositide 3-kinases: A conserved family of signal transducers. Trends Biochem. Sci. 22, 267–272. https://doi.org/10.1016/S0968-0004(97)01061-X
Vanhaesebroeck, B., Whitehead, M.A., Piñeiro, R., 2016. Molecules in medicine mini-review: isoforms of PI3K in biology and disease. J. Mol. Med. 94, 5–11. https://doi.org/10.1007/s00109-015-1352-5
Veltman, D.M., Williams, T.D., Bloomfield, G., Chen, B.-C., Betzig, E., Insall, R.H., Kay, R.R., 2016. A plasma membrane template for macropinocytic cups. eLife 5, e20085. https://doi.org/10.7554/eLife.20085
Vetter, I.R., Wittinghofer, A., 2001. The guanine nucleotide-binding switch in three dimensions. Science 294, 1299–1304. https://doi.org/10.1126/science.1062023
Vines, J.H., King, J.S., 2019. The endocytic pathways of Dictyostelium discoideum. Int. J. Dev. Biol. 63, 461–471. https://doi.org/10.1387/ijdb.190236jk
Wang, Y., Huynh, W., Skokan, T.D., Lu, W., Weiss, A., Vale, R.D., 2019. CRACR2a is a calcium-activated dynein adaptor protein that regulates endocytic traffic. J. Cell Biol. 218, 1619–1633. https://doi.org/10.1083/jcb.201806097
Yerbury, J.J., 2016. Protein aggregates stimulate macropinocytosis facilitating their propagation. Prion 10, 119–126. https://doi.org/10.1080/19336896.2016.1141860
Yu, M., Chen, J., Xu, Z., Yang, B., He, Q., Luo, P., Yan, H., Yang, X., 2023. Development and safety of PI3K inhibitors in cancer. Arch. Toxicol. 97, 635–650. https://doi.org/10.1007/s00204-023-03440-4
Zeineddine, R., Pundavela, J.F., Corcoran, L., Stewart, E.M., Do-Ha, D., Bax, M., Guillemin, G., Vine, K.L., Hatters, D.M., Ecroyd, H., Dobson, C.M., Turner, B.J., Ooi, L., Wilson, M.R., Cashman, N.R., Yerbury, J.J., 2015. SOD1 protein aggregates stimulate macropinocytosis in neurons to facilitate their propagation. Mol. Neurodegener. 10, 57. https://doi.org/10.1186/s13024-015-0053-4
Zeineddine, R., Yerbury, J.J., 2015. The role of macropinocytosis in the propagation of protein aggregation associated with neurodegenerative diseases. Front. Physiol. 6. https://doi.org/10.3389/fphys.2015.00277

Chapter 2: Methods

2.1 Bioinformatics and Cloning

2.1.1 *Dictyostelium discoideum* PI3K Isoform Sequence Analysis

A UniProt search was performed with the aim to identify all PI3K domain-containing proteins in the *Dictyostelium discoideum* proteome. 11 proteins containing the *Dictyostelium discoideum* 'PI3K/PI4K catalytic domain', as annotated on UniProt, were identified: PikA (P54673), PikB (P54674), PikC (P54675), PikD (P54677), PikE (P54676), PikF (Q55FX5), PikG (Q54S78), PikH (Q54F55), Q54UU9, Q54ES0, and Q54LR9. All amino acid sequences and domain annotations were obtained from UniProt (uniprot.org), and these were aligned using the Clustal Omega Multiple Sequence Alignment (MSA) tool (ebi.ac.uk/jdispatcher/msa/clustalo). The alignment results were visualised and analysed using Jalview software (jalview.org). To gain an understanding of the evolutionary relationships between the 11 *Dictyostelium discoideum* PI3K domain-containing proteins, a Neighbour Joining phylogenetic tree was calculated using the BLOSUM62 substitution matrix. The domain annotations obtained from UniProt were also used to draw a schematic diagram of the 11 potential *Dictyostelium discoideum* PI3K isoforms to visualise the similarities and differences in their sequence lengths and domain arrangements. Inkscape (inkscape.org) was used to create this graphic.

2.1.2 PikA and PikF Protein Structure Prediction and Visualisation

To visualise structural differences between the *Dictyostelium discoideum* Class I PI3K isoforms PikA (P54673) and PikF (Q55FX5), protein structure predictions were downloaded from AlphaFold (alphafold.ebi.ac.uk). PyMOL software (pymol.org) was used to visualise, annotate and superimpose the two protein structures to make full-lenght and domain-specific comparisons.

2.1.3 Construction of Extrachromosomal Expression Vectors

pDMs were used to construct all extrachromosomal expression vectors in this study. As described by Dr Douwe M. Veltman and colleagues, the pDM vector series comprises engineered plasmids specifically optimised for tagged-protein expression in *D. discoideum* (Veltman et al., 2009). pDM1043 was specifically used to tag proteins with GFP at the N-terminus. Following Polymerase Chain Reaction (PCR) amplification and construct engineering, as detailed below, inserts were ligated into Blunt II-TOPO vectors (Invitrogen, Cat. #K2800-20SC) and transformed into ultracompetent *E. coli*, such as XL10-Gold cells. Following miniprep, Blunt II-TOPO vectors were digested with the appropriate restriction enzymes to facilitate insert transfer into pDM1043 by sticky-end ligation. For full-length PikA and PikF integration (Sections 2.1.4 and 2.1.6), pDM1043 was pre-digested with BglII and SpeI (BcuI). For integration of the chimera constructs (Section 2.1.5), pDM1043 was digested with SpeI alone, with Calf Intestinal Alkaline Phosphatase (CIP) added to prevent vector re-ligation. Hence, for plasmid integration, all flanking primers used in this study

included BglII or BamHI sites at the 5′ end and SpeI or XbaI sites at the 3′ end, compatible with the insertion sites of the pDM vector. All pDM1043 ligations were performed in 5µl reactions using T4 DNA Ligase (Thermo Scientific, Cat. #EL0011). Following ligation, pDM1043 constructs were transformed into ultracompetent *E. coli* and selected on Ampicillin-containing LB agar. Successful colonies were cultured, miniprepped, and plasmids were screened by diagnostic restriction digests. SnapGene (snapgene.com) was used to simulate all PCR reactions and ligations for the generation of accurate vector sequence files and to predict expected digest electrophoresis patterns.

2.1.4 Tagging PikA and PikF with N-terminal GFP

To insert the pikA and pikF genes into pDM1043, their full-length sequences were amplified using *D. discoideum* genomic DNA as a template. PikA was amplified with oligos oAP1 and oAP2, and PikF was amplified with oligos oAP5 and oAP7 (Table 2.1). PCRs were performed in 20 µL reactions using Takara Bio PrimeSTAR Max DNA Polymerase (Cat. #R045A/B), with 35 cycles under the following conditions: 10 s at 98 °C, 15 s at 50 °C, and 40 s at 68 °C (5 s per 1 kb), followed by a final hold at 4 °C.

Name	Sequence	Oligo
oAP1	agatctATGAATAGTATTGAAAGTTCTTCTAATGATAGC	pikA_5'fwBglII
oAP2	tctagaCTAAGCATGTGCAAGATGATGAAAAA	pikA_3'rvXbaI
oAP5	ggatccATGTTATTGGAAGATGAGGAATTAACATAC	pikF_5'fwBamHI
oAP6	actagtATCATCAGAACTTGTTCCTGAATGAG	pikF_3'rvSpeI

Table 2.1: Oligos used for the amplification of PikA and PikF from *D. discoideum* gDNA.

2.1.5 Protein Design: PikA/PikF Chimeras

To test whether PI3K isoform specificity is determined by a particular domain in the *Dictyostelium discoideum* Class I PI3K isoforms PikA and PikF, we designed eight PikA/PikF chimeras, each intended to sequentially convert one isoform into the other, one domain at a time (Figure 2.1). The construction of the chimeras involved a two-step PCR strategy: the first to amplify individual fragments, and the to join the respective fragments together via overlap extension. Each domain swap was intended to occur at the first nucleotide position as per domain annotations. PikA (P54673) and PikF (Q55FX5) DNA sequences and domain annotations were obtained from UniProt. The primers used to amplify individual fragments are listed in Table 2.2. The 5′ and 3′ primers used to stitch PikA and PikF fragments together were identical to those used for the amplification of full-length PikA and PikF from *D. discoideum* genomic DNA (Section 2.1.4), except that all restriction sites were replaced with XbaI sites (Table 2.3). This modification was necessary because undesired restriction sites were introduced into the protein coding sequences during the construction of the chimera constructs. All PCRs were performed in 50 µL reactions using Takara Bio PrimeSTAR Max DNA Polymerase (Cat. #R045A/B), with 35 cycles under the following conditions: 10 s at 98 °C, 15 s at 53 °C, and 40 s at 72 °C (5 s per 1 kb), followed by a final hold at 4 °C.

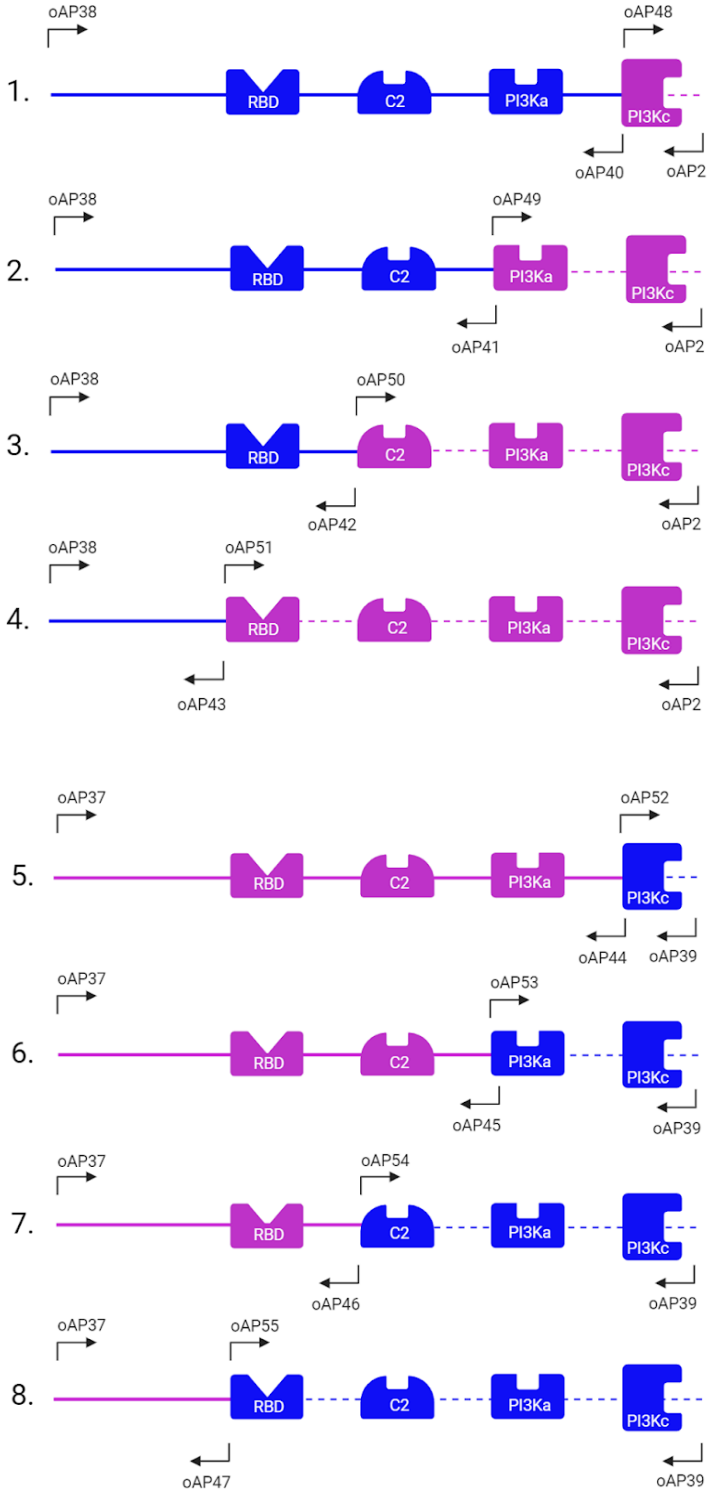

Figure 2.1: Design of PikA/PikF Chimeras 1-8. Magenta: PikA; Blue: PikF.

Name	Sequence	Oligo
oAP40	CACCAGCTTTGAAAATCACTTCTATTGGTTCACCAACGGGG	pikF_ch1_3'rv
oAP41	CATTTGAATTTATATTGGTTGGTGGTTGAATTTCTGTACGTTCCATCATCTC	pikF_ch2_3'rv
oAP42	GGTTTTTTAATTTCTCTAATAGAAATATGTGTAATTTCAAATGGTCTATTAATT TCATATAATAAAATTGATC	pikF_ch3_3'rv
oAP43	GTATTGGTAATGGTGATAATCTAACCAAAATTGTAATTTTAACACGATCTCTTT CATCC	pikF_ch4_3'rv
oAP44	CATCACCATTCTTAAAGATTACTGCAATAGGGTCAGCGTTCATATCG	pikA_ch5_3'rv
oAP45	CTTTACGAGACTCTACGTAATCTCTTTCAATAACTGAGACACTTGTAGAG	pikA_ch6_3'rv
oAP46	GGTAAAACTAAATTCTCTAAACAAATTATTCTAATTGATCCCAATTATCAAAA TTTATATTATTATTATTTGTAC	pikA_ch7_3'rv
oAP47	GAGCATTGGTTACAGGTGCTAGAGTAGACTGAATTGATCCTTTAATC	pikA_ch8_3'rv
oAP48	CCCCGTTGGTGAACCAATAGAAGTGATTTTCAAAGCTGGTG	pikA_PI3Kc_5'fw
oAP49	GAGATGATGGAACGTACAGAAATTCAACCACCAACCAATATAAATTCAAATG	pikA_PI3Ka_5'fw
oAP50	GATCAATTTTATTATATGAAATTAATAGACCATTTGAAATTACACATATTTCTAT TAGAGAAATTAAAAAACC	pikA_C2_5'fw
oAP51	GGATGAAAGAGATCGTGTTAAAATTACAATTTTGGTTAGATTATCACCATTAC CAATAC	pikA_RBD_5'fw
oAP52	CGATATGAACGCTGACCCTATTGCAGTAATCTTTAAGAATGGTGATG	pikF_PI3Kc_5'fw
oAP53	CTCTACAAGTGTCTCAGTTATTGAAAGAGATTACGTAGAGTCTCGTAAAG	pikF_PI3Ka_5'fw
oAP54	GTACAAATAATAATAATATAAATTTTGATAATTGGGATCAAATTAGAATAATTT GTTTAGAGAATTTAGTTTTACC	pikF_C2_5'fw
oAP55	GATTAAAGGATCAATTCAGTCTACTCTAGCACCTGTAACCAATGCTC	pikF_RBD_5'fw

Table 2.2: Oligos used for fragment amplification in the construction of Chimeras 1-8.

Name	Sequence	Oligo
oAP2	tctagaCTAAGCATGTGCAAGATGATGAAAAA	pikA_3'rvXbaI
oAP37	tctagaATGAATAGTATTGAAAGTTCTTCTAATGATAGC	pikA_5'fwXbaI
oAP38	tctagaATGTTATTGGAAGATGAGGAATTAACATAC	pikF_5'fwXbaI
oAP39	tctagaTTAATCATCAGAACTTGTTCCTGAATGAG	pikF_3'rvXbaI

Table 2.3: Oligos used to join fragments together in the construction of Chimeras 1-8.

2.1.6 Protein Design: Kinase-inactive PikF

The vector construct pDM1043-pikF, generated as described in Section 2.1.4, was used to introduce a debilitating point mutation at a conserved lysine residue in the PikF kinase domain (Yart et al., 2002) via insertion of an eBlock gene fragment synthesised by Integrated DNA Technologies (IDT, eu.idtdna.com). This eBlock was designed to replace an adenine (A) with a guanine (G) within the codon spanning nucleotide positions 3355–3357 of the *pikF* coding sequence, resulting in a codon change from AAG (lysine, K) to AGG (arginine, R). The resulting kinase-inactive PikF mutant is therefore referred to as K3356R in Chapter 3.

pDM1043-pikF (pAP11) and the 1,150 bp eBlock were digested with BglII and SpeI (BcuI), and ligated using T4 DNA Ligase (Thermo Scientific, Cat. #EL0011). The mutation in pDM1043-K3356R (pAP73) was confirmed by whole-plasmid sequencing by Plasmidsaurus (plasmidsaurus.com) (Figure 2.2).

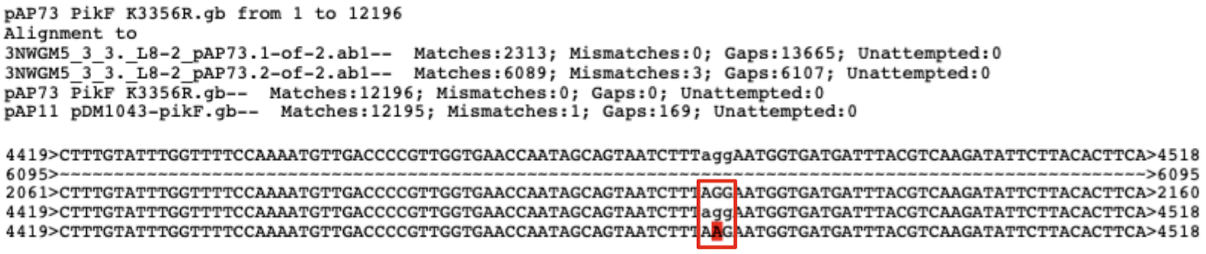

Figure 2.2: Confirmation of A to G mutation in pDM1043-K3356R (pAP73).

2.2 *Dictyostelium discoideum* Strains and Cell Culture

Ax2 (Ax2-MRC) is the standard wild-type *D. discoideum* strain used in this study. The PI3K mutant strains HM141 (PikA/B$^-$), HM1149 (PikF$^-$), and HM1159 (PikA/B/F$^-$) of the Ax2-MRC parent background were kindly provided by Dr Robert Kay (MRC Laboratory of Molecular Biology, Cambridge) (Hoeller et al., 2013).

2.2.1 Growth of *D. discoideum* in Axenic and Non-Axenic Culture

D. discoideum cells were cultivated axenically at 22 °C in 9 cm plastic petri dishes (Thermo Fisher, Cat. #100315Z) using Formedium HL5 medium supplemented with glucose (composition: peptone 14 g/L, yeast extract 7 g/L, glucose 13.5 g/L, KH_2PO_4 0.5 g/L, Na_2HPO_4 0.5 g/L). To prevent the accumulation of secondary mutations that could obscure macropinocytic phenotypes in PI3K mutant strains, cells were not maintained in liquid culture. Instead, following plasmid transformation (as described below), cells were kept in

SorMC buffer 15 mM KH_2PO_4, 2 mM Na_2HPO_4, 50 µM $MgCl_2$, 50 µM $CaCl_2$, pH ~6.0) supplemented with *Klebsiella aerogenes*, and only transferred to liquid culture for acclimatisation prior to experimental procedures.

Non-axenic *D. discoideum* cells were grown at 22 °C on Formedium SM agar plates (composition: peptone 10 g/L, yeast extract 1 g/L, glucose 10 g/L, KH_2PO_4 1.9 g/L, $K_2HPO_4 \cdot 3H_2O$ 1.3 g/L, $MgSO_4$ anhydrous 0.49 g/L, 1.7% agar) seeded with *Klebsiella aerogenes* lawns.

2.2.2 *D. discoideum* Transformations with Plasmid DNA

As described by Dr Peggy Paschke and colleagues, all protein expression vectors detailed in Sections 2.1.3-2.1.6 were transformed into *D. discoideum* cells using a square wave electroporation protocol consisting of two 345 V pulses of 8 ms duration separated by a 0.9 s interval (Paschke et al., 2018), delivered with a BTX Harvard Apparatus ECM 630 Electro Cell Manipulator. *D. discoideum* cells were cultured on *K. aerogenes* lawns prior to transformation, and approximately 3 cm of cells were collected from fresh growth zones using a disposable inoculation loop, yielding ~2×10^6 cells. The cells were washed twice in 1ml SorMC buffer (15 mM KH_2PO_4, 2 mM Na_2HPO_4, 50 µM $MgCl_2$, 50 µM $CaCl_2$, pH ~6.0), and following the second flash spin at 10,000 x g, cells were resuspended in ice-cold H40 buffer (40 mM HEPES, 1 mM $MgCl_2$, pH 7.0). Aliquots of 100 µl cell suspension were transferred to pre-chilled 2 mm-gap electroporation cuvettes (Geneflow, Cat. #E6-0062) along with 10µl of plasmid DNA minipreps (~40 µg). Following electroporation, the 110µl cell suspensions were transferred to 10ml SorMC in Nunclon Delta-treated petri dishes (Thermo Fisher, Cat. #110508921), and these were supplemented with 200µl of live *K. aerogenes* (OD_{600} = 100). The *K. aerogenes* suspension was prepared by inoculating 250ml of LB broth and incubating overnight at 37 °C. Bacterial cells were harvested and washed three times by centrifugation (20 min at 6,000 x g), then resuspended in SorMC buffer to an optical density (OD_{600}) of 100. This bacterial suspension was stored at 4 °C for a maximum of three months. All extrachromosomal expression vectors used in this study are listed in (Table 2.4). pAPs were constructed by the author of this study (Ana Paula Guevara-Cerdán); pJSK696 was constructed by the project supervisor, Professor Jason King; and the two pPIs were constructed by Dr Peggy Paschke (MRC Laboratory of Molecular Biology, Cambridge) and kindly gifted to the King Laboratory.

Plasmid name	Insert 1	Insert 2	Function
pAP7	GFP-PikA	None	PikA expression
pAP11	GFP-PikF	None	PikF expression
pAP27	GFP-Chimera 1	None	Chimera 1 expression
pAP28	GFP-Chimera 2	None	Chimera 2 expression

pAP29	GFP-Chimera 3	None	Chimera 3 expression
pA30	GFP-Chimera 4	None	Chimera 4 expression
pA73	GFP-K3356R	None	K3356R expression
pJSK696	RFP-PH-PkgE	GFP-TAPP1	PIP_3/$PI(3,4)P_2$ reporters
pPI304	LifeAct-mCherry	PkgE-PH-GFP	F-actin/PIP_3 reporters
pPI587	PakB-CRIB-mCherry	GFP-Raf1-RBD	Rac/Ras activity reporters

Table 2.4: *D. discoideum* expression vectors used in this study.

2.3 Cellular Uptake Assays

2.3.1 Macropinocytosis Assay

Macropinocytosis was measured by flow cytometry using a Thermo Fisher Attune NxT Flow Cytometer. 48 hours prior to the experiment, transformed cells were washed by centrifugation in sterile SorMC buffer and transferred from SorMC plates supplemented with *K. aerogenes* into axenic HL5 medium. On the day of the experiment, cells were seeded into 96-well plates in HL5 medium at a density of 1-2 × 10^6 cells/ml, with 50µl of cell suspension added to each well. After seeding, the cells were allowed to settle for 1-2 hours at 22 °C. To initiate the experiment, 50µl of 1 mg/ml TRITC-Dextran (see Section 2.3.3 for preparation) diluted in HL5 was added to the first set of wells to achieve a final concentration of 0.5 mg/ml TRITC-Dextran. Additional wells received 1 mg/ml TRITC-Dextran at 30, 45, 55, and 60 minutes after the start of the experiment to create a time-course. Immediately after the final addition at 60 minutes, the 96-well plate was inverted into the sink, submerged in ice-cold KK_2 buffer (16.6 mM KH_2PO_4, 3.8 mM K_2HPO_4, pH ~6.1), and inverted again to discard as much buffer as possible. Immediately thereafter, 110 µl of ice-cold 5 mM NaN_3 was added to each well, and cells were resuspended by gently vortexing the bottom of the plate. After initiating the flow cytometer and completing laser calibration between time points, the plate was immediately transferred to the autosampler. *D. discoideum* cells were identified using forward scatter (FSC) and side scatter (SSC) parameters, and subsequently analysed for the median fluorescence intensity in the YG-582/15 channel. Background signal - measured from wells where TRITC-Dextran was added at the 60 min time point immediately prior to plate inversion - was subtracted from all readings. Results were then normalised to total uptake in the positive control (Ax2) cells, defined as 100%. GraphPad Prism (graphpad.com) was used to plot macropinocytosis data and to perform statistical analysis.

2.3.2 Phagocytosis Assay

Phagocytosis was measured by live-cell imaging using a widefield fluorescence microscope, following a 30-minute exposure of *D. discoideum* cells to Alexa594-labelled yeast (see Section 2.3.3 for preparation). For each strain tested, 3ml of cell suspension at a concentration of 1×10^4 cells/ml was added to a 15ml Falcon tube, which was then placed on a benchtop roller for 30 minutes without disturbance. With a staggered start to allow sufficient time for imaging between samples, 7.5µl of 1×10^9 cells/ml Alexa594-labelled yeast stock was added to each Falcon tube, which was then returned to the benchtop roller. After 30 minutes of exposure, samples were transferred to glass-bottom microscopy dishes (VWR, Cat. #734-2904) and allowed to settle for 5 minutes. Subsequently, 100 µl of 0.4% Trypan Blue solution was added to each dish and mixed by gentle swirling. Imaging was performed using a 63x oil-immersion DIC objective with both the RFP and brightfield channels. Images were viewed using Fiji (imagej.net), and the yeast-to-cell ratio was calculated by manually counting individual cells, taking into account that only ingested yeast fluoresce. GraphPad Prism was used to plot phagocytosis data and to perform statistical analysis.

2.3.3 Preparation of TRITC-Dextran and Alexa405/594-Labelled Yeast

For macropinocytosis assays, Texas Red-conjugated 70kDa dextran (Life Technologies) was dissolved in water, diluted to 2 mg/ml, and aliquoted for storage.

For yeast preparation, *Saccharomyces cerevisiae* were cultured at 37 °C in YPD medium (Formedium). To obtain a budded population, cells were harvested during logarithmic growth, pelleted at 1,000 x g for 5 minutes, and resuspended in PBS (pH 7) at 1×10^9 cells/ml before storage at -20 °C. For fluorescent labelling, 0.5×10^9 yeast were resuspended in 200 µl PBS (pH 8.5) and incubated with 10 µl Alexa Fluor 405 or Alexa Fluor 594 succinimidyl ester (final concentration 2.5 mM; Life Technologies) for 30 min at 37 °C with gentle agitation. Yeast labelled with Alexa405 were used for Spinning Disk Confocal Microscopy, while those labelled with Alexa594 were used for quantitative phagocytosis assays as described in Section 2.3.2. After incubation, cells were pelleted and washed sequentially with 1 ml PBS (pH 8.5), 1 ml 25 mM Tris-HCl (pH 8.5), and a final 1 ml PBS (pH 8.5). The labelled yeast were resuspended in 500 µl KK2 buffer (pH 6.1), diluted in SIH medium to 1×10^9 cells/ml, and stored at -20 °C.

2.3.4 Statistical Analysis

Quantitative macropinocytosis and phagocytosis data were plotted as mean ± standard deviation (SD), and statistical analyses were performed using GraphPad Prism version 10. Group comparisons were made with one-way ANOVA, while pairwise differences were tested with unpaired t-tests. A p value < 0.05 was considered statistically significant.

2.4 Protein-Based Assays

2.4.1 Western Blotting

After preparation in Laemmli sample buffer, samples were run on a 4–15% Bio-Rad precast gel (Cat. #4561085) at a constant voltage of 300 V for 15 minutes. The gel was then equilibrated in 1x Western blot transfer buffer (25ml 1M Tris pH 8.3, 14.4g Glycine, 150ml Methanol, distilled water to 1L), and proteins were transferred to a PVDF membrane at 75 V for 45 minutes. Following transfer, the membrane was air-dried for 30 minutes, reactivated in methanol, and rehydrated in Tris-buffered saline (TBS; 20 mM Tris-HCl, pH 7.4–7.6, 150 mM NaCl) for 15 minutes on a benchtop shaker. The TBS was then replaced, and the membrane was transferred to a shaker in the cold room overnight at 4 °C. The following morning, the membrane was blocked at room temperature for 30 minutes in 5% nonfat dry milk prepared in TBS. It was then incubated with primary antibody diluted 1:500 in TBST and gently shaken at room temperature for 1-2 hours. The membrane was rinsed in TBST for 1 minute before incubation with secondary antibody (800nm) diluted 1:10,000 in TBST, along with streptavidin control antibody (680nm) diluted 1:25,000. To conclude, the membrane was rinsed five times for 1 minute in TBST, and imaged using a LI-COR Odyssey 9260 Fluorescence Imager. Image processing was performed using Image Studio software (licorbio.com/image-studio), and band quantification was conducted in Fiji.

2.4.2 Rac1 Pull-Down and Detection

The Rac1 pull-down assay was performed according to the manufacturer's instructions provided with the Rac1 Activation Assay Biochem Kit (Cytoskeleton, Inc., Cat. #BK035). However, no Rac1 activator was added, as the aim was to assess the basal (unstimulated) Rac1 activity in Ax2, HM141 (PikA/B^{-}), and HM1149 (PikF^{-}) cells. 48 hours prior to the experiment, cells from all three strains were transferred from SM agar to HL5 medium in 150 mm polystyrene petri dishes (Sarstedt Ltd, Cat. #82.1184.500). On the day of the experiment, confluent 150 mm dishes were rinsed twice with ice-cold SorMC buffer supplemented with 120 mM Sorbitol. After the second rinse, the buffer was aspirated at a steep angle while the dishes were kept on ice for 1 minute. 1ml of the kit's Cell Lysis Buffer, supplemented with 20µl of the provided 100x Protease Inhibitor Cocktail, was then added to each dish. Cells were carefully scraped using a standard tissue culture cell scraper while the plates were kept on ice at an incline. The lysates were then transferred to Eppendorf tubes and kept on ice until lysates from all three cell strains were collected. Immediately afterwards, the lysates were clarified by centrifugation at 10,000 x g for 1 minute at 4 °C. At this stage, 20µl of each lysate was transferred into a cuvette containing 1ml of Precision Red for protein quantification. The remaining lysate samples were either processed immediately or snap-frozen in liquid nitrogen for bead pull-down at a later time. If frozen and stored at −70 °C, lysates were thawed in a room-temperature water bath, equalised with ice-cold Cell Lysis Buffer, and immediately transferred to ice. For each sample, approximately 50 µg of protein was reserved for total Rac1 quantification by Western blot, and ~300 µg of protein was added to 15 µl of the provided PAK-PBD beads for the pull-down assay. This volume of beads was selected based on results from a bead titration assay. The lysate-bead mixtures

were then incubated on a rotator in the cold room for 1 hour. These were then pelleted by centrifugation at 5,000 x g for 1 minute at 4 °C. 90% of the supernatant was removed, and the pellets were resuspended in 500µl of the kit's Wash Buffer. The beads were then pelleted again by centrifugation at 5,000 g for 3 minutes at 4 °C. At this stage, the supernatant was completely removed, and the beads were resuspended in 10µl of 2x Laemmeli sample buffer. To complete the preparation, the samples were boiled on a heat block at 100 °C for 5 minutes.

For positive and negative controls, protein amounts equal to those used in the bead pull-down were mixed with 200 µM GTPγS or 1 mM GDP and incubated for 15 minutes at room temperature with gentle rotation. The control samples were then mixed with 15µl of the provided PAK-PBD beads and processed as described above.

All samples were then analysed by Western blot, as described in Section 2.4.1, using an anti-DdRac1 primary monoclonal antibody kindly provided to the King Lab by Professor Jan Faix (University of Hannover).

2.4.3 Affinity Purification Mass Spectrometry (AP-MS)

GFP-PikA and GFP-PikF interactor samples were obtained from HM141 (PikA/B$^-$) and HM1149 (PikF$^-$) cells expressing these constructs, respectively. GFP-expressing Ax2 cells were used as a GFP-only control. GFP-trapping was performed with GFP-Trap Agarose beads according to the manufacturer's instructions (ChromoTek, Cat. #gta). Samples were then processed by Dr Khoa Pham at the University of Sheffield's Faculty of Science Mass Spectrometry Centre. The resulting mass spectrometry data were analysed using STRING version 12 (string-db.org), based on relevant enrichment parameters.

2.5 Live-Cell Microscopy

2.5.1 General Sample Preparation and Image Analysis

If cells had been previously maintained on SM agar or SorMC plates supplemented with *Klebsiella aerogenes*, they were transferred to liquid HL5 medium 48 hours prior to all live-cell microscopy experiments. The night before imaging, cells were seeded at appropriate densities into glass-bottom confocal microscopy dishes. One to two hours before imaging, the medium was replaced with SIH or SUM to prepare cells for acquisition.

Spinning Disk Confocal and Total Internal Reflection Fluorescence (TIRF) imaging were performed on Nikon systems controlled by NIS-Elements software. A Nikon W1 Spinning Disk Confocal Microscope and a Nikon N-STORM system were used, respectively, both equipped with a 100×/1.49 NA oil immersion objective. Lattice Light Sheet Microscopy (LLSM) was performed on a 3i Lattice LightSheet Microscope (University of Warwick), and images were deconvoluted by collaborators (Dr Till Bretschneider and Dr Judith Lutton). All image datasets were processed, and where appropriate, quantified in Fiji (ImageJ).

2.6 References

Hoeller, O., Bolourani, P., Clark, J., Stephens, L.R., Hawkins, P.T., Weiner, O.D., Weeks, G., Kay, R.R., 2013. Two distinct functions for PI3-kinases in macropinocytosis. J. Cell Sci. jcs.134015. https://doi.org/10.1242/jcs.134015

Paschke, P., Knecht, D.A., Silale, A., Traynor, D., Williams, T.D., Thomason, P.A., Insall, R.H., Chubb, J.R., Kay, R.R., Veltman, D.M., 2018. Rapid and efficient genetic engineering of both wild type and axenic strains of Dictyostelium discoideum. PLOS ONE 13, e0196809. https://doi.org/10.1371/journal.pone.0196809

Veltman, D.M., Akar, G., Bosgraaf, L., Van Haastert, P.J.M., 2009. A new set of small, extrachromosomal expression vectors for *Dictyostelium discoideum*. Plasmid 61, 110–118. https://doi.org/10.1016/j.plasmid.2008.11.003

Yart, A., Roche, S., Wetzker, R., Laffargue, M., Tonks, N., Mayeux, P., Chap, H., Raynal, P., 2002. A Function for Phosphoinositide 3-Kinase β Lipid Products in Coupling βγ to Ras Activation in Response to Lysophosphatidic Acid*. J. Biol. Chem. 277, 21167–21178. https://doi.org/10.1074/jbc.M110411200

Chapter 3: Class I PI3K Isoform Specificity in *Dictyostelium discoideum* Macropinocytosis

3.1 Introduction

This chapter examines *Dictyostelium discoideum* Class I PI3K isoforms and their individual roles in macropinocytic cup formation. A long-standing model proposes that distinct PI3K activities are required at two successive stages (Egami et al., 2014; Hoeller et al., 2013): membrane ruffling (Araki et al., 2007; Wennström et al., 1994) and macropinocytic cup closure (Araki et al., 1996; Rupper et al., 2001). Consistent with this framework, Hoeller *et al*. (2013) reported that PikA and PikB act partly redundantly to generate PIP_3 at F-actin-driven membrane ruffles that mature into cups and fuse to form macropinosomes. By contrast, $PikF^-$ cells retain the ability to form PIP_3 patches, implicating PikF in a later stage – facilitating the transition from PIP_3-positive, F-actin-rich ruffles to sealed macropinosomes. Building on these findings, this chapter aims to characterise the isoform-specific activities of PikA (formerly PI3K1) and PikF (formerly PI3K4), and to identify structural differences that may underlie their distinct functions (Figure 3.1).

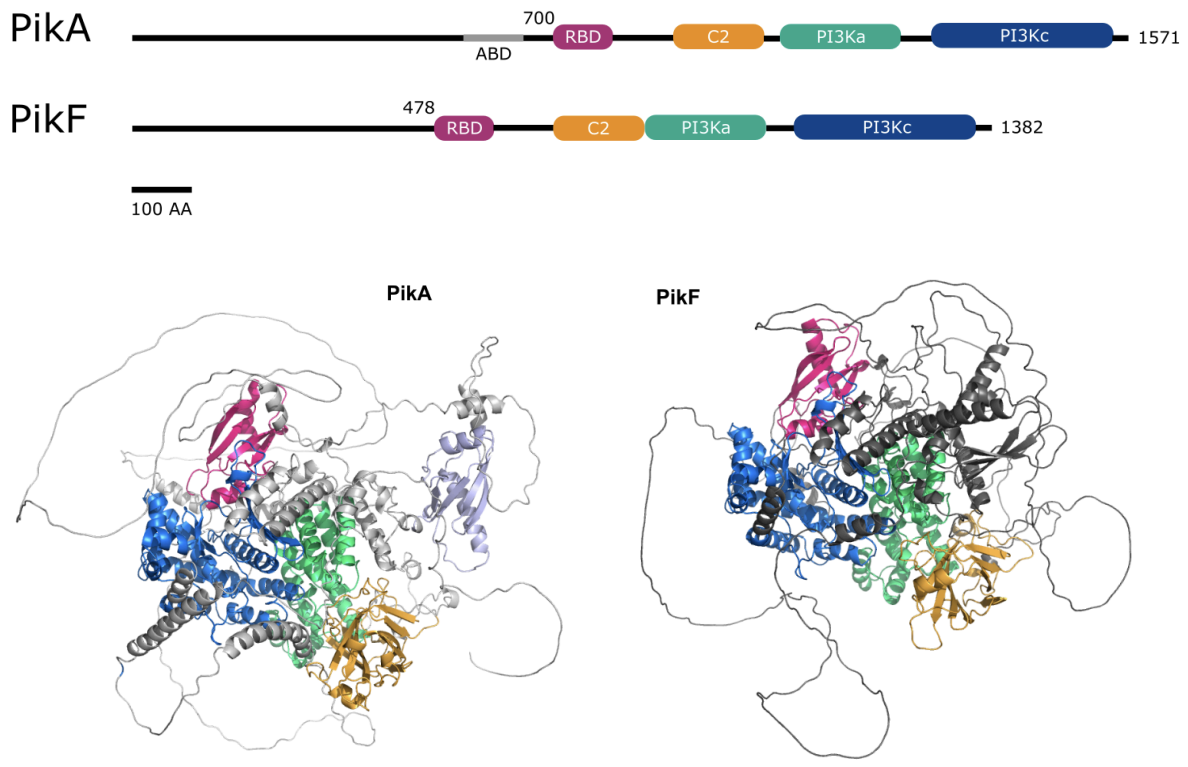

Figure 3.1: Domain arrangements and tertiary structures of PikA and PikF. Sequence information was obtained from UniProt, and domain arrangement illustrations were created using Inkscape. Predicted protein structures were obtained from AlphaFold, and PyMOL was used to visualise, annotate, and colour individual domains. RBD: Ras-binding domain (pink); C2: C2 domain (orange); PI3Ka: accessory/helical domain (green); PI3Kc: catalytic domain (blue); ABD: PikA adapter-binding domain (grey/lilac).

In this chapter we confirm the macropinocytosis defects of PikA/B^{-} and PikF^{-} strains (Hoeller *et al*., 2013), show that PikA and PikF perform non-redundant functions, and begin to map the structural basis of isoform specificity. As outlined in Section 1.2.2, Class I/II PI3Ks share a conserved catalytic core comprising the Ras-binding (RBD), C2, helical, and catalytic domains. Figure 3.1 presents the PikA and PikF tertiary structures side by side, highlighting the conservation of this catalytic core with a notable divergence in their N-terminal regions – particularly the positioning of a PikA-specific adaptor-binding domain (lilac in Figure 3.1). To dissect domain contributions, we generated PikA/PikF chimeras and performed macropinocytosis rescue experiments to determine how the N-terminal regions and elements of the conserved catalytic core drive isoform-specific activity during cup formation.

Using Spinning Disk Confocal Microscopy, we characterise the subcellular localisation patterns of GFP-PikA and GFP-PikF within macropinocytic cups – representing, to our knowledge, the first visualisation of GFP-tagged Class I PI3Ks at this resolution during macropinocytic events. We also, for the first time to our knowledge, quantitatively validate differences in cell size and morphology between PikA/B^{-} and PikF^{-} mutants, providing insight into how these mutations dysregulate membrane dynamics in *D. discoideum* cells.

Research Questions Addressed in this Chapter

1. Are the macropinocytic defects previously reported in PikA/B^{-} and PikF^{-} cells reproducible under our experimental conditions?

2. If so, can GFP-PikA and GFP-PikF rescue macropinocytosis defects interchangeably across the two mutant backgrounds?

3. If not, in which domain(s) does isoform specificity reside?

4. Do PikA and PikF localise differently within macropinocytic cups?

5. Can differences in phosphoinositide dynamics be observed on the plasma membrane of PikA/B^{-} and PikF^{-} cells?

6. Can observed differences in cell size and morphology between PikA/B^{-} and PikF^{-} mutants be quantified and statistically validated?

3.2 Results

3.2.1 PikA and PikF Mutants Display Impaired Macropinocytosis

Hoeller et al. (2013) reported that the only *D. discoideum* PI3K mutant strains with macropinocytosis defects as severe as the quintuple mutant – lacking all identified Class I PI3Ks (PikA, PikB, PikC, PikF, PikG) – were PikA/B$^-$ and PikF$^-$ (Hoeller et al., 2013). The current study began by confirming these phenotypes through dextran uptake measurements in PikA$^-$, PikA/B$^-$ and PikF$^-$ cells. Macropinocytosis defects in PikA/B$^-$ cells were confirmed to be more severe than in PikA$^-$ cells, indicating that the additional deletion of *pikB* further exacerbates the fluid uptake deficiency, possibly because PikA and PikB play partially redundant canonical roles in PIP_3 synthesis during macropinocytic cup formation. While PikA$^-$ cells exhibited a macropinocytic defect corresponding to 59.4% of wild-type levels, macropinocytosis in PikA/B$^-$ cells was further reduced to just 7.4% (Figure 3.2). Additionally, our findings confirm that the sole deletion of *pikF* is sufficient to cause a severe fluid uptake deficiency. Two PikF$^-$ strains (HM1149 and HM1241) were tested for comparison, both exhibiting macropinocytosis defects of 27-28% relative to wild-type levels (Figure 3.2). These results confirm the observations reported by Hoeller et al. (2013), demonstrating that PikA/B$^-$ and PikF$^-$ strains exhibit severe macropinocytosis defects.

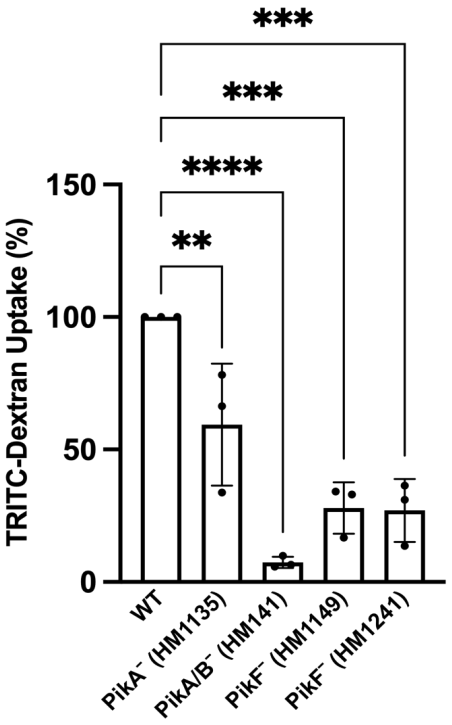

Figure 3.2: Macropinocytosis defects in PikA$^-$, PikA/B$^-$, and PikF$^-$ cells.
Fluid uptake was measured by flow cytometry following a 60-minute exposure to 0.5 mg/ml TRITC-dextran. Each point represents a biological replicate (n = 2 per genotype), with 3 technical measurements per replicate (10,000 events/measurement). Bars show the mean; error bars represent standard deviation (SD). Statistical analysis was performed using ordinary one-way ANOVA, comparing the mean of each mutant strain to the wild-type (WT) control. $P = 0.0083$ (**); $P = 0.0001$ (***); $P < 0.0001$ (****).

3.2.2 PikA and PikF Perform Distinct, Non-Redundant Functions

Based on the results presented above, strains HM141 (PikA/B$^-$) and HM1149 (PikF$^-$) were selected for further study. To test for functional redundancy, GFP-PikA and GFP-PikF constructs were generated and introduced into both mutant backgrounds. The PikA/B$^-$ macropinocytosis defect was exclusively rescued by GFP-PikA, and the PikF$^-$ phenotype was exclusively rescued by GFP-PikF (Figure 3.3), indicating isoform-specific roles during macropinocytic cup formation, consistent with a two-stage, PI3K-driven model (Araki et al., 2007, 1996; Egami et al., 2014; Hoeller et al., 2013; Rupper et al., 2001; Wennström et al., 1994). However, interpretation is constrained by expression concerns: while fluorescence microscopy confirmed GFP-PikA and GFP-PikF expression in their respective mutant backgrounds, we could not visually detect expression of either construct in the opposite genotype (data not shown), raising the possibility of differential expression, instability, or proteasomal degradation (see Section 3.2.4). Thus, the failure of cross-rescue may, in part, reflect insufficient abundance or stability rather than strict functional non-interchangeability. Within these limits, the data support isoform specificity, but definitive tests would require expression-normalised cross-rescue and direct quantification of protein levels.

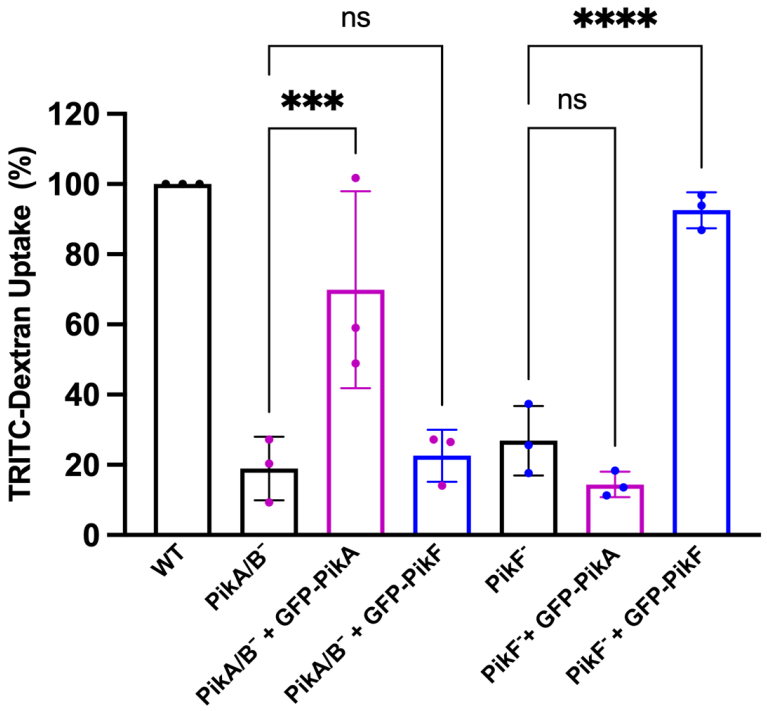

Figure 3.3: Rescue of PikA/B$^-$ and PikF$^-$ macropinocytosis defects by GFP-PikA and GFP-PikF. Fluid uptake was measured by flow cytometry following a 60-minute exposure to 0.5 mg/ml TRITC-dextran. Each point represents a biological replicate (n = 2 per genotype), with 3 technical measurements per replicate (10,000 events/measurement). Bars show the mean; error bars represent standard deviation (SD). Statistical analysis was performed using ordinary one-way ANOVA, comparing the means of GFP-PikA and GFP-PikF rescue conditions to their respective PikA/B$^-$ and PikF$^-$ parent strains. $P = 0.0007$ (***); $P < 0.0001$ (****).

3.2.3 Isoform-Specific Function Is Independent of the Catalytic Domain

To dissect the contribution of individual domains to PikA and PikF isoform specificity, eight chimeric proteins were designed to convert PikA into PikF, and vice versa, one domain at a time (Figure 3.4). Expression vectors for Chimeras 1-4, each N-terminally fused to GFP, were generated and introduced into both PikA/B^{-} and PikF^{-} strains, but Chimeras 5-8 could not be constructed despite repeated attempts – including unsuccessful outsourced synthesis (GenScript Biotech) – owing to persistent cloning difficulties. Nevertheless, fluid uptake rescue assays with Chimeras 1-4 yielded informative results: none rescued the PikA/B^{-} phenotype (Figure 3.5), including GFP-Chimera 4, which conserves most of the PikA structure while retaining only the PikF N-terminal tail; whereas GFP-Chimera 1 rescued the PikF^{-} phenotype but Chimeras 2-4 did not (Figure 3.6), suggesting that PikF retains isoform-specific function when carrying the PikA catalytic domain (Chimera 1), and that replacement of the helical domain (PI3Ka) in Chimera 2 is sufficient to impair activity. Critically, interpretation is constrained by expression and stability concerns, as PI3K levels appear subject to proteasomal regulation (Section 3.2.4). Therefore, failures to rescue may reflect insufficient expression or misfolding rather than true loss of domain function. Within these limitations, the data are most consistent with the N-terminal domain of PikA being essential for its role in macropinocytic cup formation (ABD, Figure 3.1), while the catalytic domain appears to be functionally interchangeable between the two isoforms, as evidenced by the successful rescue of the PikF^{-} defect with GFP-Chimera 1.

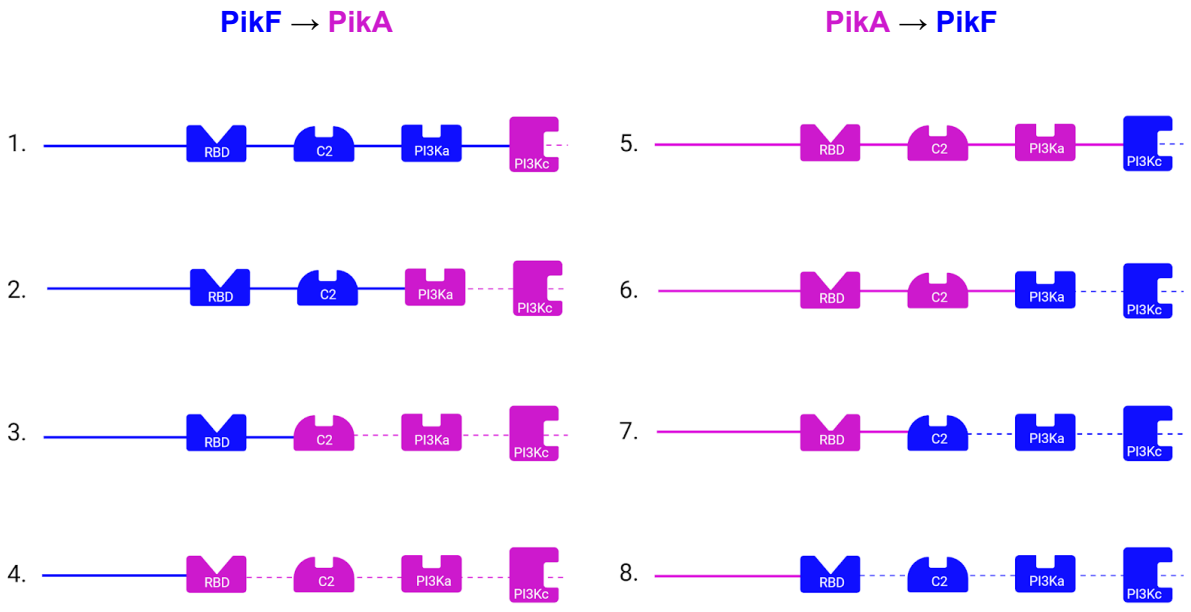

Figure 3.4: Schematic representation of PikA/PikF chimeras (Chimeras 1–8). PikA-derived domains are shown in magenta, and PikF-derived domains in blue. Chimeras 1-4 progressively convert PikF into PikA, one domain at a time, until only the PikF N-terminal 'tail' remains. Conversely, Chimeras 5-8 convert PikA into PikF in the same stepwise manner, culminating in a construct retaining only the PikA N-terminal 'tail'. RBD: Ras-binding domain; C2: C2 domain; PI3Ka: accessory/helical domain; PI3Kc: catalytic domain. Created with BioRender.

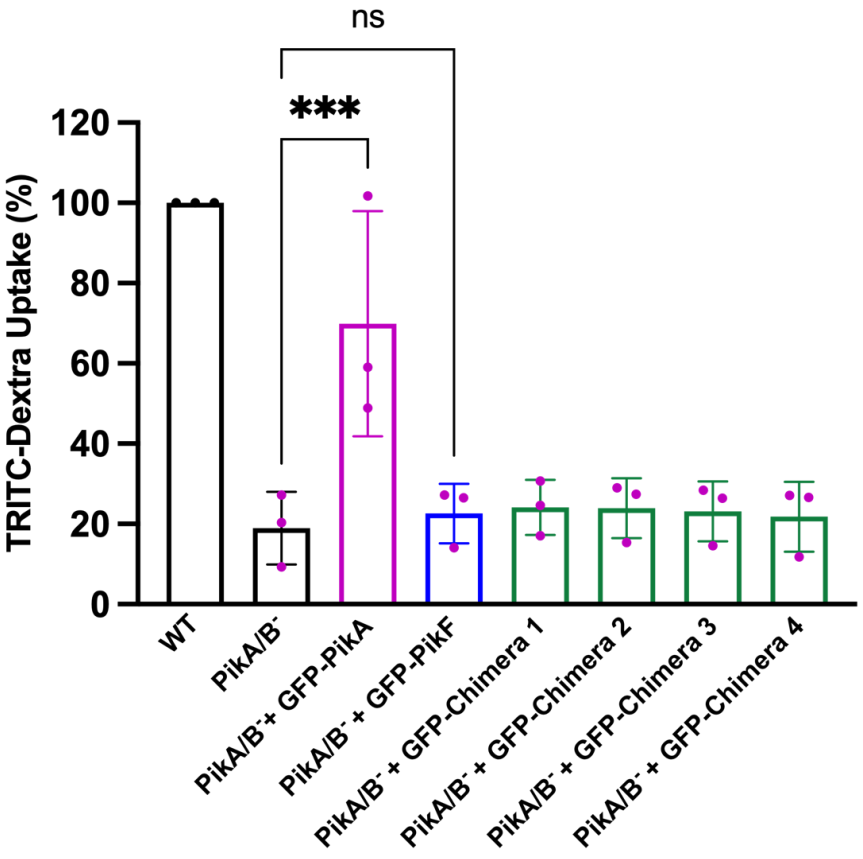

Figure 3.5: Rescue of PikA/B$^-$ macropinocytosis defect by GFP-PikA, GFP-PikF and GFP-tagged Chimeras 1 to 4. Fluid uptake was measured by flow cytometry following a 60-minute exposure to 0.5 mg/ml TRITC-dextran. Each point represents a biological replicate (n = 2 per genotype), with 3 technical measurements per replicate (10,000 events/measurement). Bars show the mean; error bars represent standard deviation (SD). Statistical comparisons were made using ordinary one-way ANOVA, comparing each condition to the PikA/B$^-$ parent strain. Only GFP-PikA significantly rescued the macropinocytosis defect. P=0.0005 (***)

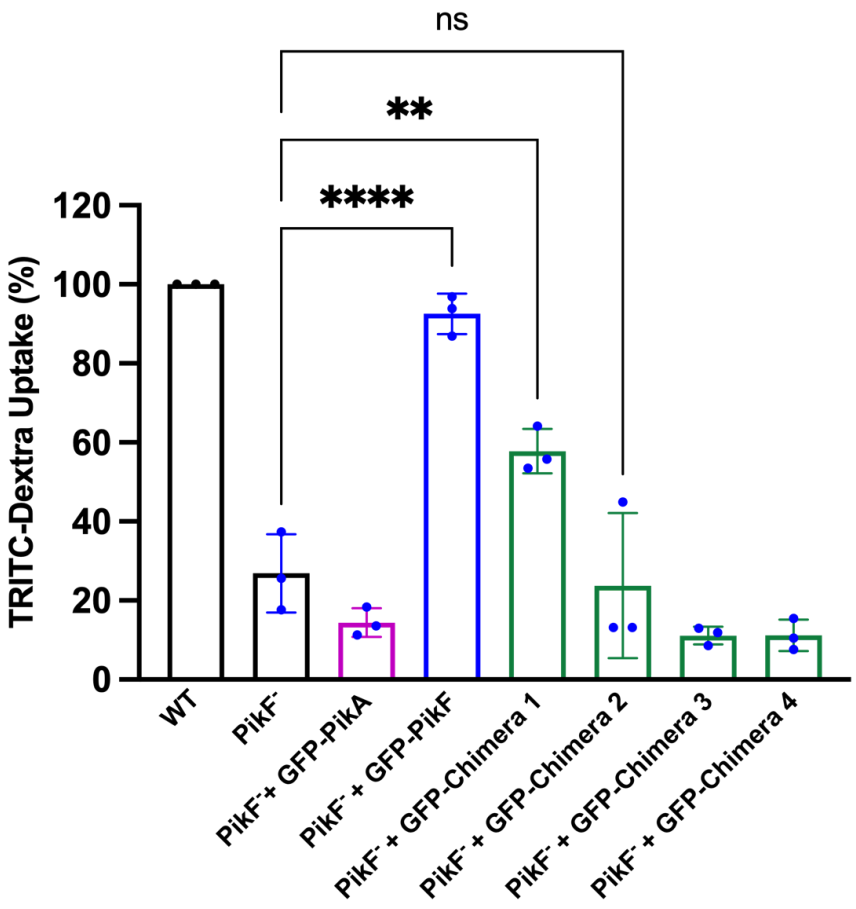

Figure 3.6: Rescue of PikF$^-$ macropinocytosis defect by GFP-PikA, GFP-PikF and GFP-tagged Chimeras 1 to 4. Fluid uptake was measured by flow cytometry following a 60-minute exposure to 0.5 mg/ml TRITC-dextran. Each point represents a biological replicate (n = 2 per genotype), with 3 technical measurements per replicate (10,000 events/measurement). Bars show the mean; error bars represent standard deviation (SD). Statistical comparisons were made using ordinary one-way ANOVA, comparing each condition to the PikF$^-$ parent strain. Only GFP-PikF and GFP-Chimera 1 significantly rescued the macropinocytosis defect. P=0.0015 (**); P<0.0001 (****)

The ability of Chimera 1 to rescue the PikF$^-$ macropinocytosis defect prompted further investigation into whether PikF catalytic activity is essential for macropinocytic cup formation. This question is also supported by previous findings showing that PikF$^-$ cells retain 50-126% of wild-type PIP_3 levels (Hoeller et al., 2013).

A catalytically inactive form of PikF was generated via point mutation of an evolutionarily conserved lysine within the ATP-binding loop of the PikF catalytic domain, located at position 1119 of the PikF amino acid sequence. This lysine residue is conserved across species from amoebae to humans and has been previously mutated in human Class I PI3K isoforms to create kinase-dead variants (Yart et al., 2002). Figure 3.7 shows a sequence alignment of two conserved regions within the PikA, PikB, and PikF catalytic domains, highlighting the invariant lysine in relation to the ATP-binding site and three conserved loop structures characteristic of the PI3K catalytic domain. Using a synthesised eBlock gene fragment, this lysine (K) residue was successfully substituted with an arginine (R) (See Section 2.1.6). As the mutation was introduced at nucleotide position 3356 of the *pikF* coding sequence – changing an adenine (A) to a guanine (G) – the resulting kinase-inactive variant was designated K3356R.

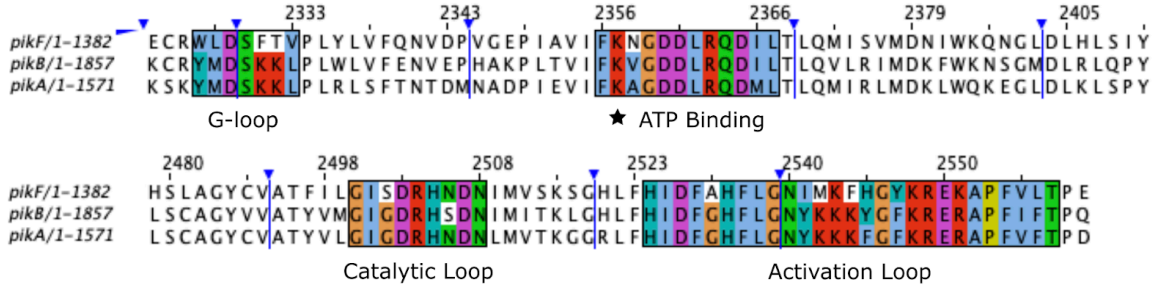

Figure 3.7: Amino acid sequence alignment of conserved regions within the PI3K catalytic domains of PikA, PikB, and PikF. The catalytic domain alignment includes two regions containing three conserved loop structures — G-loop, catalytic loop, and activation loop — as well as the ATP-binding site. Residue numbers correspond to the alignment of all 11 PI3K/PI4K catalytic domain-containing proteins in the *D. discoideum* proteome. Conserved features are highlighted using the Clustal X colour scheme. The lysine residue mutated in the K3356R variant is indicated with a star. Protein sequences were obtained from UniProt, aligned using Clustal Omega (MSA), and visualised with Jalview.

Following its construction, the kinase-inactive PikF variant (K3356) was fused to an N-terminal GFP tag, and its ability to rescue the PikF$^-$ macropinocytosis defect was assessed. The results show that GFP-K3356R partially rescues TRITC-dextran uptake in PikF$^-$ cells, increasing macropinocytosis from 20.3% to 38.5% of wild-type levels (Figure 3.8). This partial rescue indicates that PikF catalytic activity is required for its full function. However, the observed improvement also suggests that PikF contributes to macropinocytic cup formation through an additional, non-catalytic structural role.

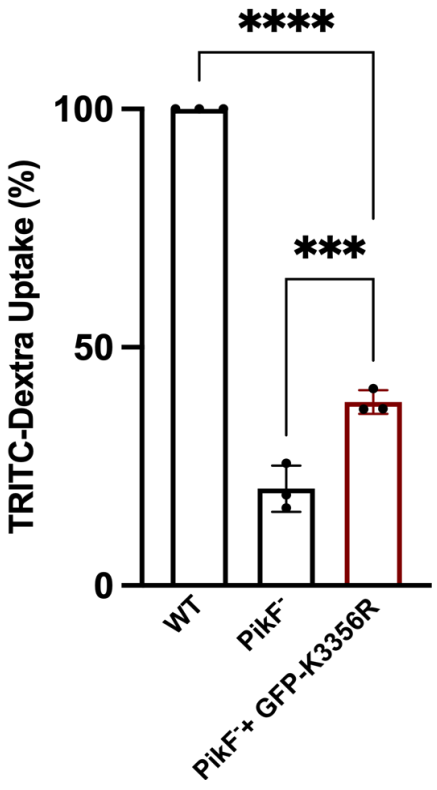

Figure 3.8: Rescue of PikF$^-$ macropinocytosis defect by GFP-tagged kinase-inactive PikF (GFP-K3356R). Fluid uptake was measured by flow cytometry following a 60-minute exposure to 0.5 mg/ml TRITC-dextran. Each point represents a biological replicate (n = 2 per genotype), with 3 technical measurements per replicate (10,000 events/measurement). Bars show the mean; error bars represent standard deviation (SD). Statistical analysis was performed using ordinary one-way ANOVA, comparing both conditions to the wild-type (WT) control. GFP-K3356R rescued the PikF$^-$ macropinocytosis defect from an average of 20.3% to an average of 38.5% in relation to WT levels. P=0.0008 (***); P<0.0001 (****)

3.2.4 Proteasomal Regulation of PI3K Isoform Expression

Because Chimeras 2-4 failed to rescue macropinocytosis in both PikA/B^{-} and PikF^{-} mutants, we assessed whether lack of rescue reflected absent/low expression. Western blots were performed on lysates from PikF^{-} cells – untransformed and expressing GFP-PikA, GFP-PikF, or GFP-tagged Chimeras 1-4 – using a monoclonal anti-GFP (from Prof. Andrew Peden, University of Sheffield). Strikingly, only the constructs that rescued the PikF^{-} phenotype (GFP-PikF and GFP-Chimera 1) were detectable by immunoblot in PikF^{-} cells (Figure 3.9A), and this was consistent with fluorescence microscopy observations (data not shown). To investigate whether non-rescuing constructs were degraded, PikF^{-} cells transformed with GFP-PikA were treated with the general protease inhibitor HALT, the proteasome inhibitor MG132, and the PI3K inhibitor LY294002. Of these, only MG132 (≥0.1 mM) restored a detectable GFP-PikA band by Western blot (Figures 3.9B and 3.9C), implicating proteasomal degradation in limiting overexpression of exogenous PikA in this background. These findings indicate that expression and stability are major confounders of rescue outcomes; accordingly, the apparent failure of GFP-PikA and Chimeras 2-4 to rescue PikF^{-} macropinocytosis may at least partly reflect insufficient steady-state abundance rather than true loss of function.

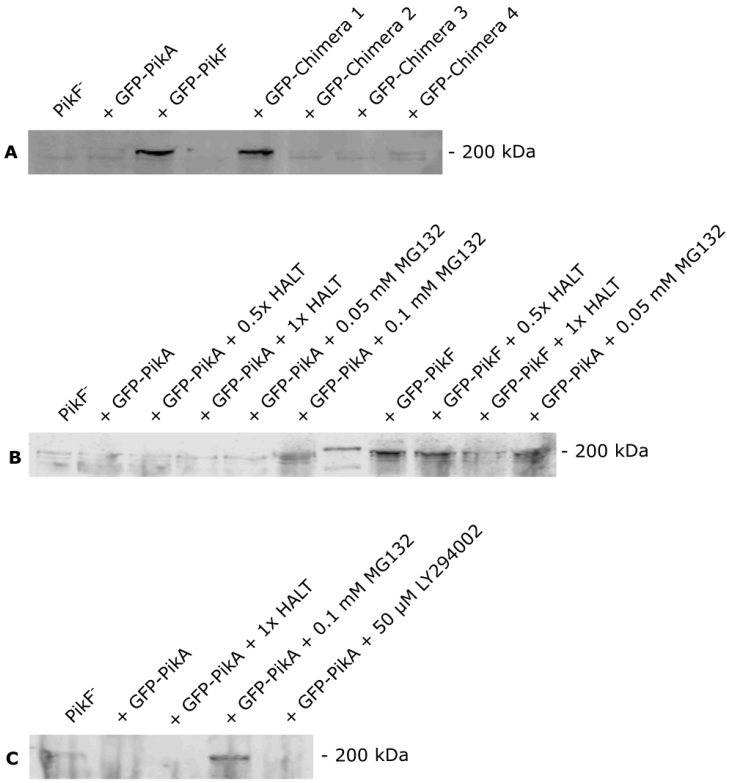

Figure 3.9: Western blot analysis of PikF^{-} cells expressing GFP-PikA, GFP-PikF and GFP-tagged Chimeras 1 to 4. (A) Untreated PikF^{-} cells expressing GFP-PikA, GFP-PikF and GFP-Chimeras 1 to 4. Only GFP-PikF and GFP-Chimera 1 were expressed. (B) PikF^{-} cells expressing GFP-PikA and GFP-PikF, treated with 0.5x/1x HALT (protease inhibitor), and 0.05/0.1 mM MG132 (proteasome inhibitor). Only 0.1 mM MG132 treatment restored detectable GFP-PikA. (C) PikF^{-} cells expressing GFP-PikA, treated with 1x HALT, 0.1 mM MG132, and 50 µM LY294002 (PI3K inhibitor). Again, only 0.1 mM MG132 treatment restored detectable GFP-PikA. Bands were detected at ~200 kDa.

3.2.5 Differential Localisation of PikA and PikF in Macropinocytic Cups

Following the findings presented above, where we concluded that isoform-specificity is not conferred by the PI3K catalytic domain, we next investigated whether PikA and PikF localise to distinct regions within the macropinocytic cup, potentially enabling isoform-specific functions. Ideally, this would have been visualised via live-cell imaging of co-expressed GFP-PikA/RFP-PikF or RFP-PikA/GFP-PikF constructs. However, co-expression in PikA/B/F$^-$ cells, as well as all PI3K overexpression attempts in wild-type (Ax2), was unsuccessful (data not shown). To address this limitation, using Spinning Disk Confocal Microscopy, we first examined isoform-specific localisation during macropinocytic cup formation by individually expressing GFP-tagged PikA and PikF in PikA/B$^-$ and PikF$^-$ cells, respectively. Representative cross-sections of imaged macropinocytic cups are shown in Figure 3.10. Signal intensities across these structures were quantified using tip-to-tip line scans, with cup lengths normalised for comparison. The resulting intensity plots revealed two distinct localisation profiles: PikA predominantly accumulates at the base of the cup, whereas PikF exhibits a more uniform distribution that spans the base and extends into the cup rim (Figure 3.11). A notable difference was observed in the background cytoplasmic signal between GFP-PikA and GFP-PikF, requiring a secondary axis for direct comparison of normalised line scan data. This disparity may indicate differences in cytoplasmic dynamics between the isoforms, warranting further investigation.

To investigate spatiotemporal localisation, we co-expressed the PIP_3 probe PkgE-PH-mCherry with either GFP-PikA or GFP-PikF in PikA/B$^-$ and PikF$^-$ cells, respectively. The probe was intended to function as a temporal marker for macropinocytic cup formation. However, in PikF$^-$ cells, expression of PkgE-PH-mCherry almost completely inhibited GFP-PikF localisation, thereby limiting the probe's usefulness for spatiotemporal analysis in this context. Interestingly, GFP-PikA localisation remained unaffected, suggesting that PikF operates downstream of PikA. This observation supports the hypothesis proposed by Hoeller *et al*. (2013), which theorises that two temporally distinct PI3K activities occur during macropinocytic cup formation.

In PikA/B$^-$ cells, dual-expression movies confirmed the preferential localisation of GFP-PikA at the cup base (Figures 3.12 and 3.13) and revealed vesicular trafficking patterns suggesting that PikA is recycled from closing macropinocytic cups into newly forming ones (Figure 3.14; see also Supplementary Movie 2). Notably, strong PIP_3 signals detected on internalised vesicles raise questions about the specificity of PkgE-PH-mCherry as a gold-standard probe for monitoring PIP_3 dynamics in *D. discoideum*, given that PIP_3 is thought to be rapidly converted to $PI(3,4)P_2$ following cup closure.

In PikF$^-$ cells, PkgE-PH-mCherry appeared to interfere with GFP-PikF recruitment to the plasma membrane (Figures 3.15 and 3.16), in contrast to the clear membrane localisation observed with GFP-PikF alone (Figure 3.10). This interference, manifesting as a diffuse cytoplasmic GFP-PikF signal, was consistently observed (Figure 3.17 shows three additional examples). These findings suggest that the lipid bound by PkgE-PH-mCherry – presumed to be PIP_3 – is essential for PikF recruitment to nascent macropinocytic cups.

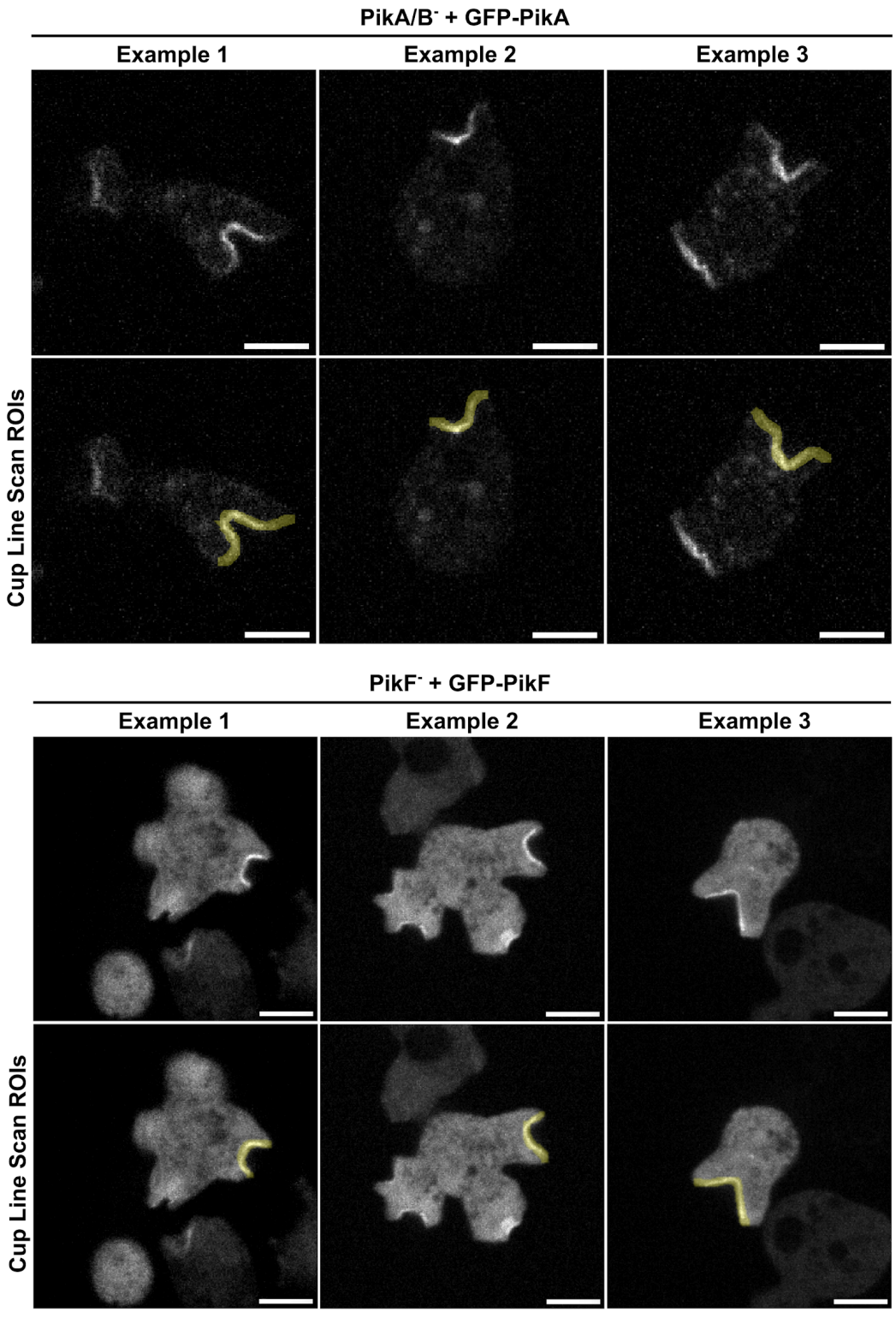

Figure 3.10: Representative images of macropinocytic cups in PikA/B$^-$ and PikF$^-$ cells expressing GFP-PikA and GFP-PikF, respectively, used for quantitative analysis. Images were acquired using a Nikon W1 Spinning Disk Confocal Microscope. Maximum intensity projections of three Z-slices per cell are shown and were used for measurements. Line scans were 6 pixels wide. The scale bar represents 5 µm and is 4 pixels thick.

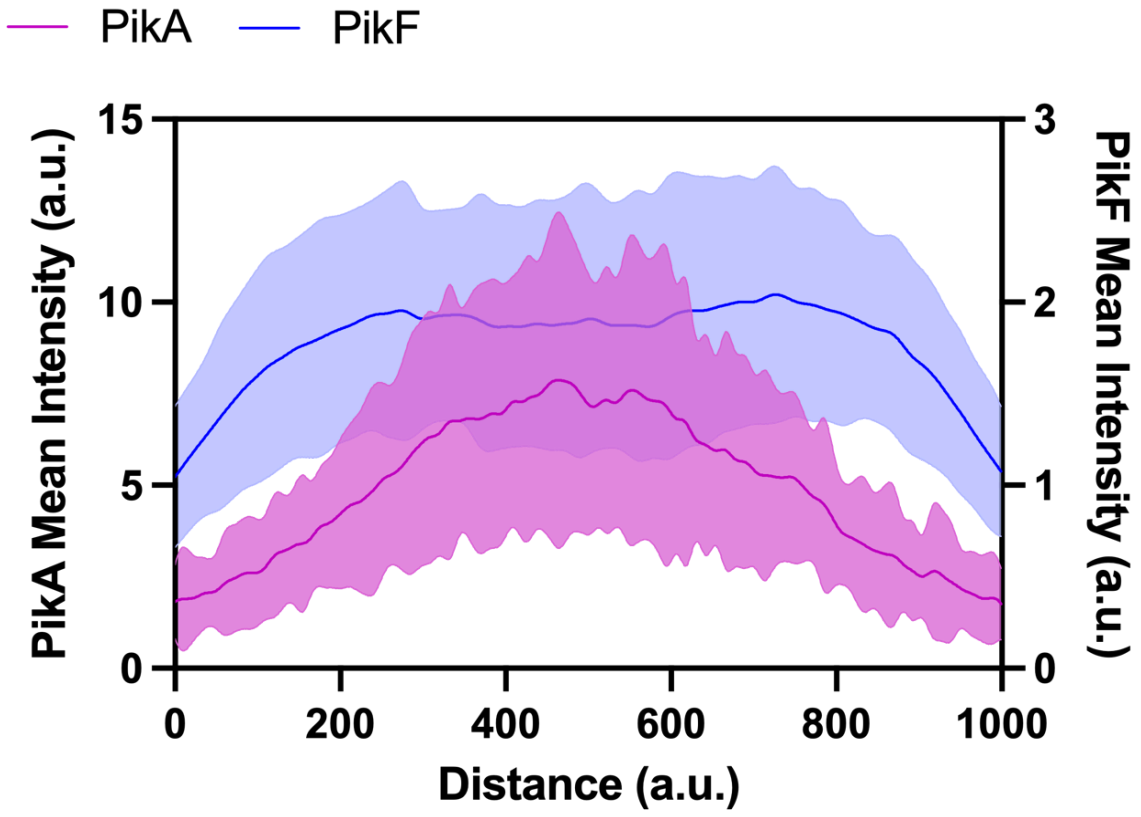

Figure 3.11: Localisation patterns of PikA and PikF throughout macropinocytic cups. The plot shows measurements from PikA/B^{-} and PikF^{-} cells expressing GFP-PikA and GFP-PikF, respectively, as depicted in Figure 3.10. PikA is represented in pink and PikF in blue. N = 30 cups per condition. Lines show the mean; shaded error regions represent standard deviation (SD).

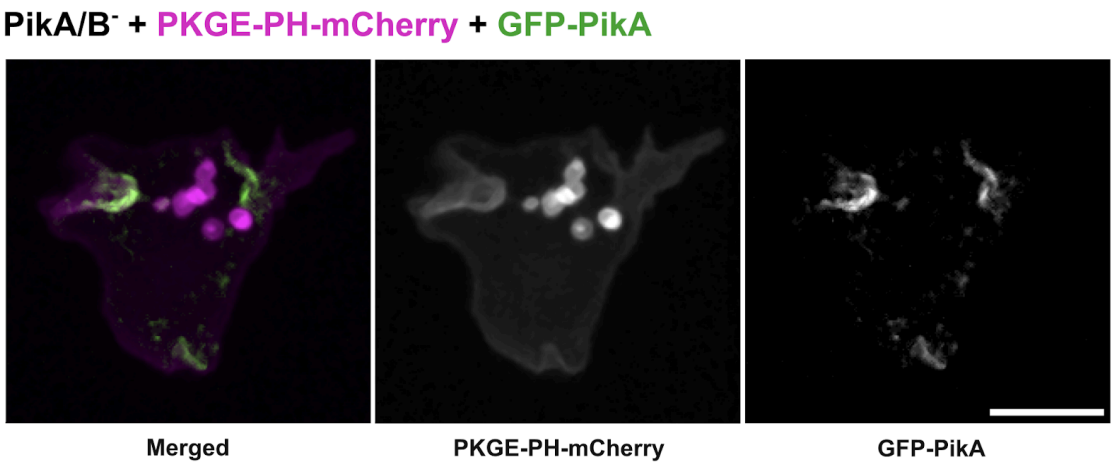

Figure 3.12: Co-localisation of GFP-PikA with the PIP_3 probe PkgE-PH-mCherry at macropinocytic cups in PikA/B$^-$ cells. GFP-PikA is shown in green; PkgE-PH-mCherry, which binds PIP_3, is shown in magenta. Images were acquired using a Nikon W1 Spinning Disk Confocal Microscope. Maximum intensity projections of three Z-slices per cell are shown and were used for measurements. The scale bar represents 5 µm and is 4 pixels thick.

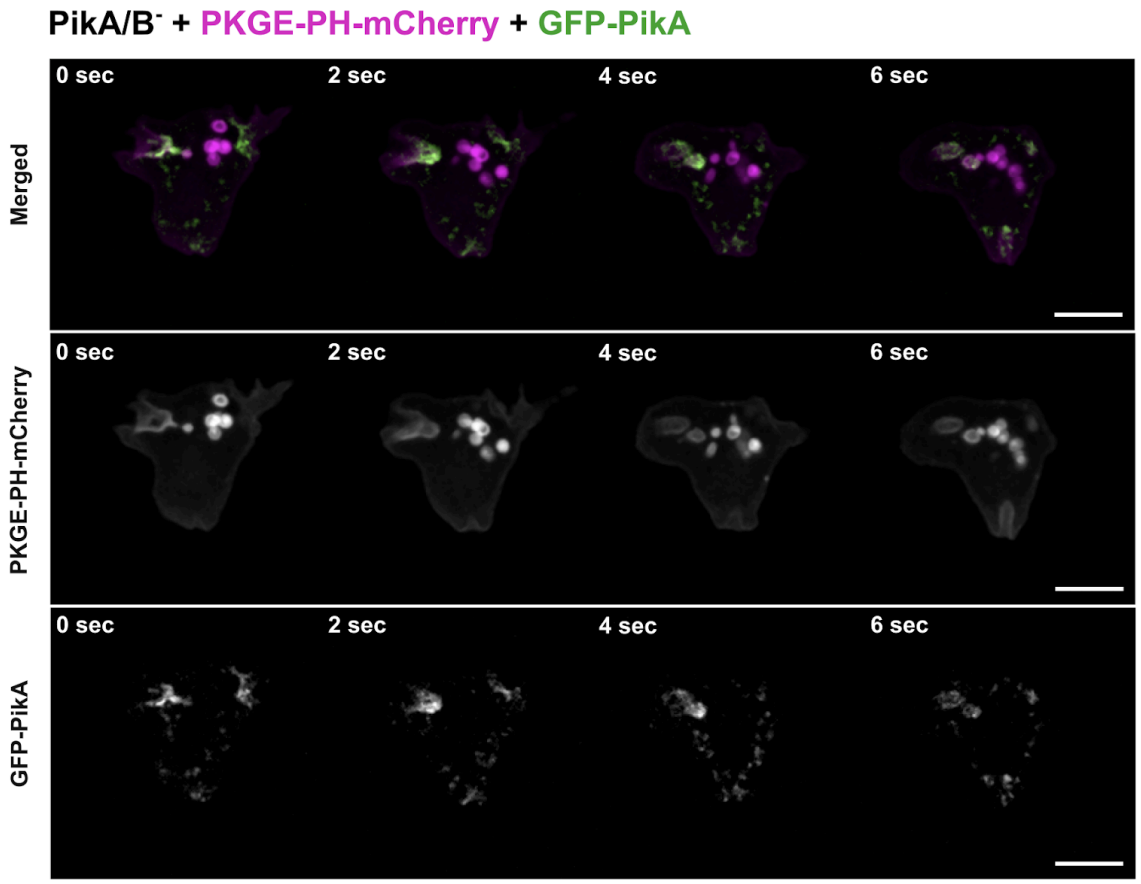

Figure 3.13: Time-lapse filmstrip (6 seconds) showing co-localisation of GFP-PikA with the PIP_3 probe PkgE-PH-mCherry at the macropinocytic cup in PikA/B$^-$ cells. GFP-PikA is shown in green; PkgE-PH-mCherry, which binds PIP_3, is shown in magenta. Images were acquired using a Nikon W1 Spinning Disk Confocal Microscope. Maximum intensity projections of three Z-slices are shown. The scale bar represents 5 µm and is 4 pixels thick. See also Supplementary Movie 1 (SM1).

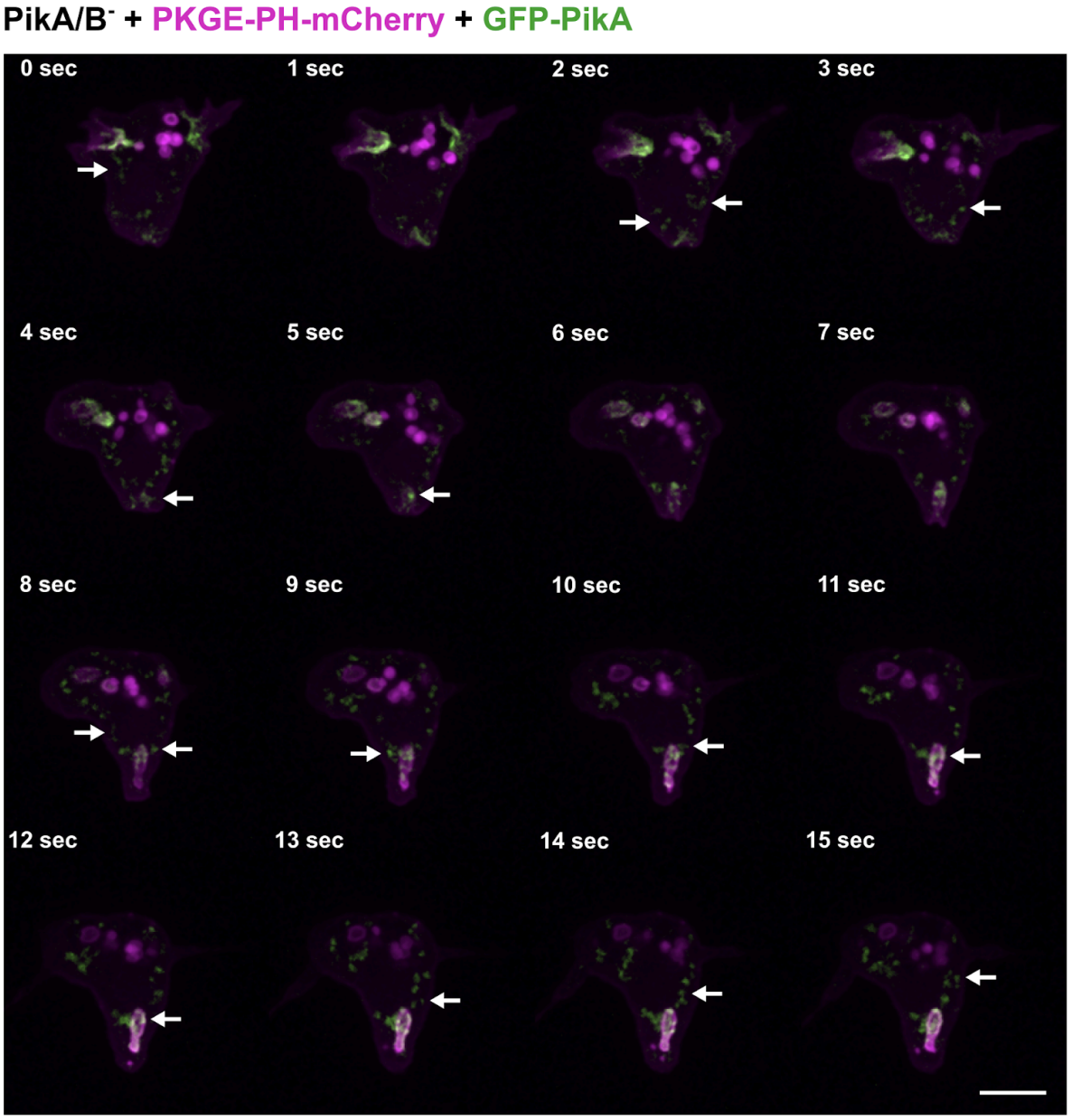

Figure 3.14: Time-lapse filmstrip (15 seconds) showing co-localisation of GFP-PikA with the PIP_3 probe PkgE-PH-mCherry at the macropinocytic cup in PikA/B$^-$ cells. GFP-PikA is shown in green; PkgE-PH-mCherry, which binds PIP_3, is shown in magenta. Images were acquired using a Nikon W1 Spinning Disk Confocal Microscope. Maximum intensity projections of three Z-slices are shown. The scale bar represents 5 µm and is 4 pixels thick. See also Supplementary Movie 2 (SM2).

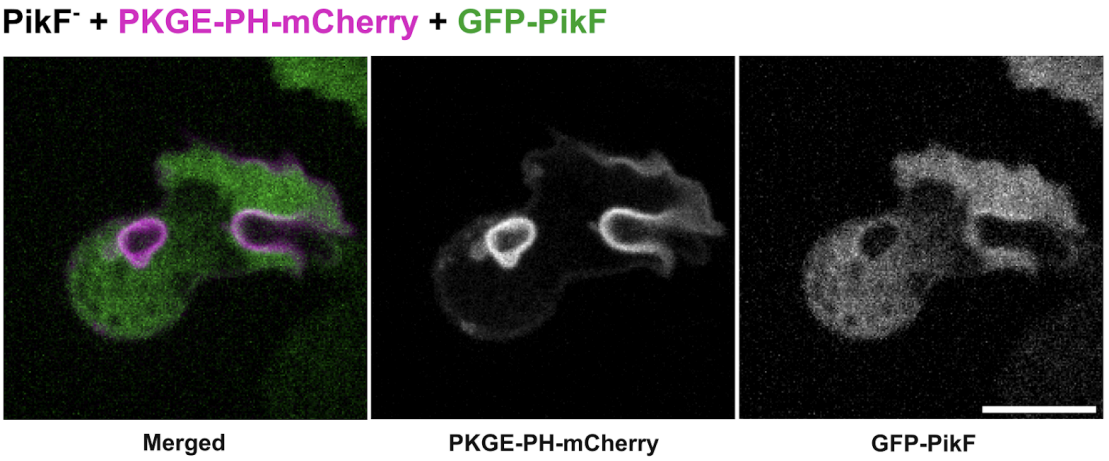

Figure 3.15: Co-localisation of GFP-PikF with the PIP_3 probe PkgE-PH-mCherry at macropinocytic cups in PikF$^-$ cells. GFP-PikF is shown in green; PkgE-PH-mCherry, which binds PIP_3, is shown in magenta. Images were acquired using a Nikon W1 Spinning Disk Confocal Microscope. Maximum intensity projections of three Z-slices per cell are shown and were used for measurements. The scale bar represents 5 µm and is 4 pixels thick.

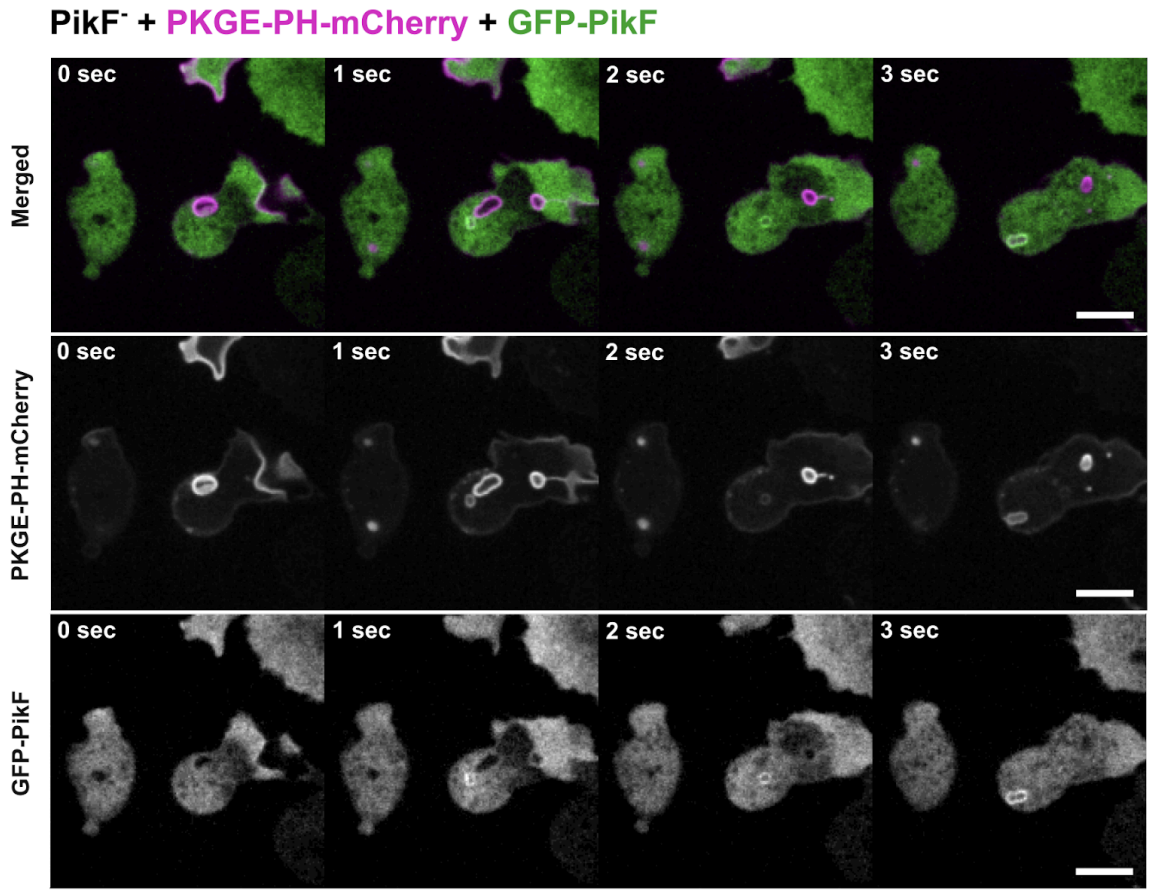

Figure 3.16: Time-lapse filmstrip (3 seconds) showing co-localisation of GFP-PikF with the PIP_3 probe PkgE-PH-mCherry at the macropinocytic cup in PikF$^-$ cells. GFP-PikF is shown in green; PkgE-PH-mCherry, which binds PIP_3, is shown in magenta. Images were acquired using a Nikon W1 Spinning Disk Confocal Microscope. Maximum intensity projections of three Z-slices are shown. The scale bar represents 5 µm and is 4 pixels thick. See also Supplementary Movie 3 (SM3).

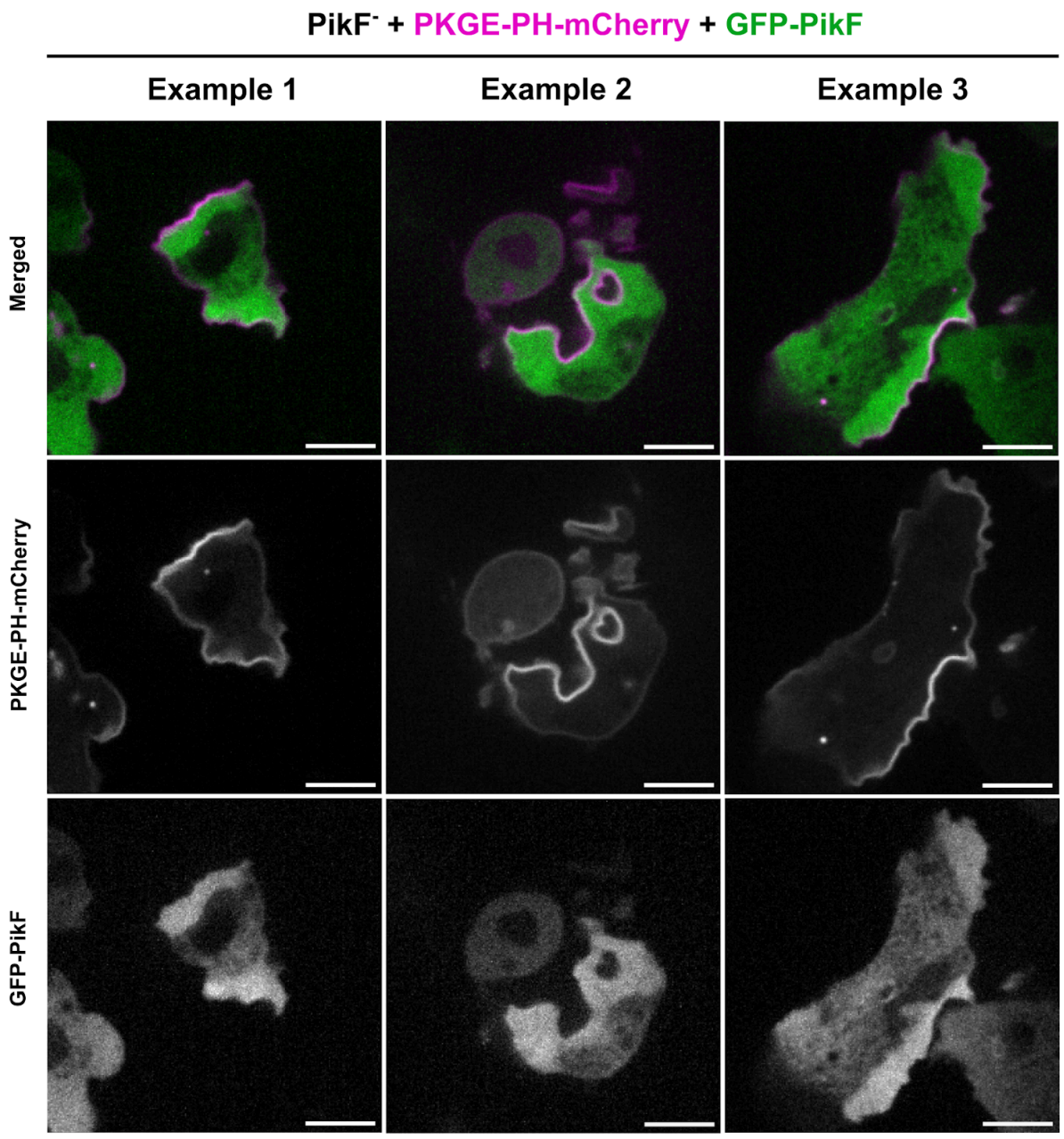

Figure 3.17: Representative examples of GFP-PikF co-localisation with the PIP_3 probe PkgE-PH-mCherry in PikF$^-$ cells. GFP-PikF is shown in green; PkgE-PH-mCherry, which binds PIP_3, is shown in magenta. Images were acquired using a Nikon W1 Spinning Disk Confocal Microscope. Maximum intensity projections of three Z-slices are shown. The scale bar represents 5 µm and is 4 pixels thick.

3.2.6 Challenges in Visualising Phosphoinositide Dynamics

To investigate isoform-specific catalytic activities of PikA and PikF, the $PI(3,4)P_2$ and PIP_3 probes – GFP-TAPP1 and RFP-PH-PKGE, respectively – were expressed in Ax2, PikA/B$^-$, and PikF$^-$ cells. Supporting a hypothesis personally communicated to the King Laboratory by Marc Edwards (Amherst College), which proposes that PikF activity may drive $PI(3,4)P_2$ production rather than PIP_3, preliminary observations (Figure 3.18) suggest a reduction in the number of $PI(3,4)P_2$-coated vesicles in PikF$^-$ cells. However, these levels cannot be reliably quantified due to morphological abnormalities observed in both Ax2 and PikF$^-$ cells upon expression of these probes, which appear to disrupt membrane integrity and fluid uptake.

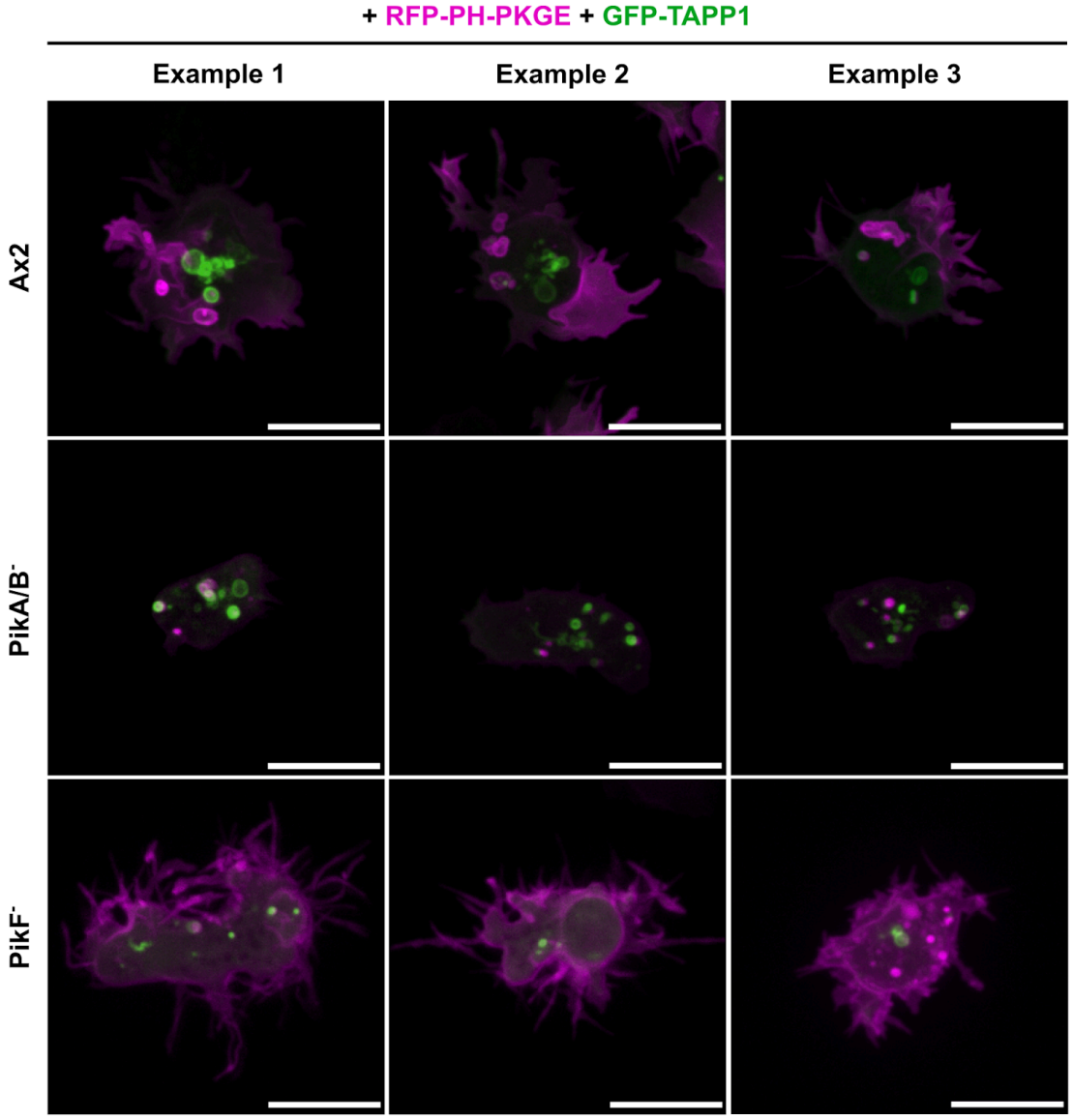

Figure 3.18: 3D projections of wild-type (Ax2), PikA/B$^-$ and PikF$^-$ cells expressing $PI(3,4)P_2$ and PIP_3 probes. RFP-PH-PkgE (magenta) binds PIP_3, and GFP-TAPP1 (green) binds $PI(3,4)P_2$. Images were acquired using a Nikon W1 Spinning Disk Confocal Microscope. Shown are cell-wide 3D maximum intensity projections. Scale bar: 10 µm.

3.2.7 Morphological Differences Between PikA/B$^-$ and PikF$^-$ Cells

Notable differences in cell morphology were observed in untransformed PikA/B$^-$ and PikF$^-$ cells. PikA/B$^-$ cells appeared smaller than wild-type (Ax2), whereas PikF$^-$ cells appeared larger. Although the reduced size of PikA/B$^-$ cells has been noted since the first genetic characterisation of *D. discoideum* PI3K homologues (Zhou et al., 1995), to our knowledge, the increased size of PikF$^-$ cells has not been previously quantified or reported. To assess these observations, cell area and perimeter were quantified using Fiji (ImageJ) from polygonal selections manually traced along the outlines of maximum intensity projections. Measurements were obtained from Ax2, PikA/B$^-$, and PikF$^-$ cells co-expressing the Rac and Ras activity probes PakB-CRIB-mCherry and GFP-Raf1-RBD as fluorescent membrane markers. PikA/B$^-$ cells exhibited a significantly smaller mean area than Ax2 (84.35 µm^2 vs 116.2 µm^2), whereas PikF$^-$ cells showed a significantly larger mean area (160.40 µm^2) (Figure 3.19A). Perimeter did not differ between Ax2 and PikA/B$^-$ (62.87 µm vs 64.29 µm), but was markedly greater in PikF$^-$ cells (152.20 µm) (Figure 3.19B).

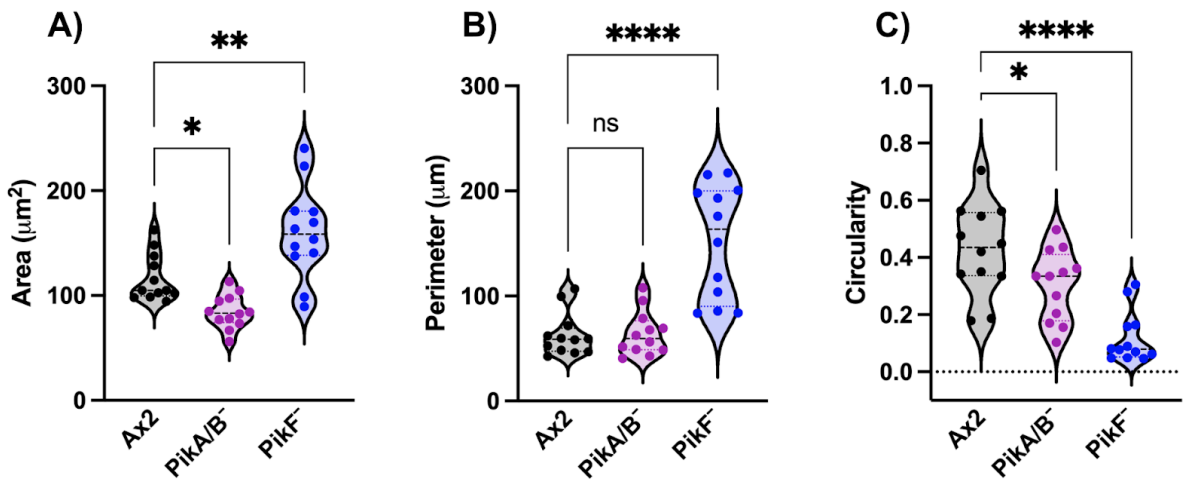

Figure 3.19: Cell area, perimeter, and circularity measurements in wild-type (Ax2), PikA/B$^-$, and PikF$^-$. Measurements were obtained from maximum intensity projections of cells expressing the Rac and Ras probes PakB-CRIB-mCherry and GFP-Raf1-RBD. Statistical analysis was performed using one-way ANOVA, comparing the mean values of PikA/B$^-$ and PikF$^-$ cells to wild-type (WT) controls. (A) Cell area: WT vs. PikA/B$^-$, P = 0.0257 (*); WT vs. PikF$^-$, P = 0.0019 (**). (B) Cell perimeter: WT vs. PikA/B$^-$, P = 0.9930 (ns); WT vs. PikF$^-$, P < 0.0001 (****). (C) Cell circularity: WT vs. PikA/B$^-$, P = 0.0434 (*); WT vs. PikF$^-$, P < 0.0001 (****). N = 12 cells per strain.

PikF$^-$ cells were also noted to frequently exhibit a ‘spiky’ morphology (Figure 3.20). This phenotype closely resembles that of cells overexpressing Rac1 isoforms (Rac1A, Rac1B, Rac1C) (Dumontier et al., 2000), as well as that of DGAP1$^-$ mutants (Faix et al., 1998; Filić et al., 2014). To quantify the effect of the spike-like structures on overall cell morphology, circularity was calculated for each strain using the same polygon selections used for area

and perimeter measurements (Figure 3.19C). A circularity value of 1 indicates a perfect circle (Rasband, 2000). Ax2 cells exhibited an average circularity of 0.4260, which was significantly higher than that of PikF$^-$ cells – 0.1192 – consistent with the more irregular and protrusion-rich morphology of the mutants.

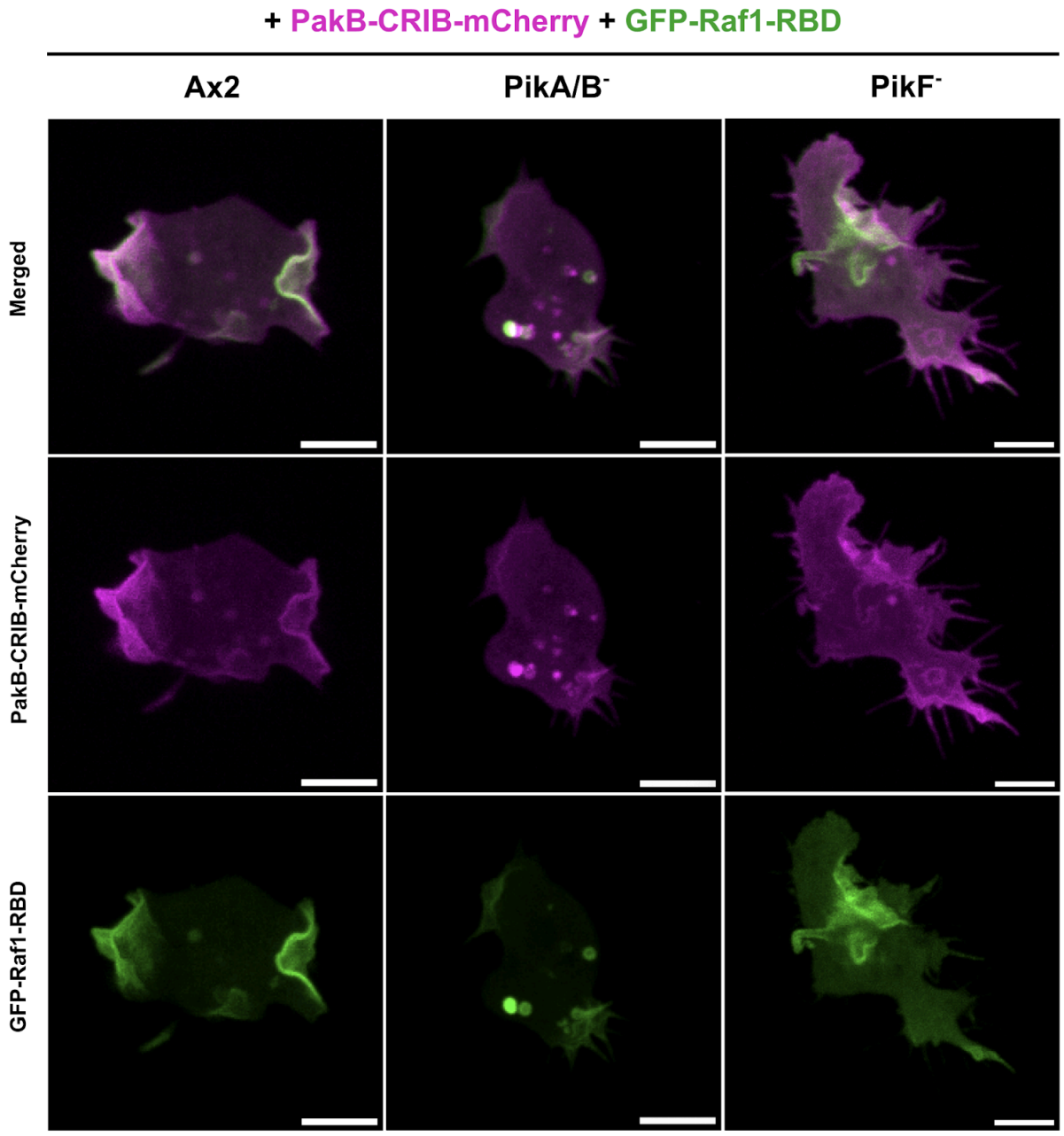

Figure 3.20: Representative images of spike-like membrane protrusions in wild-type (Ax2), PikA/B$^-$, and PikF$^-$ cells expressing Rac and Ras activity probes. Cells were transformed with PakB-CRIB-mCherry (magenta), which binds active Rac, and GFP-Raf1-RBD (green), which binds active Ras. Images were acquired using a Nikon W1 Spinning Disk Confocal Microscope. Maximum intensity projections are shown. Scale bar: 5 µm (width: 4 pixels).

Rotational 3D projections of wild-type (Ax2), PikA/B^{-}, and PikF^{-} cells co-expressing the Rac and Ras activity probes PakB-CRIB-mCherry and GFP-Raf1-RBD were generated to enhance visualisation, and spike-like protrusions were manually counted in 360° in 30 cells per strain (10 cells per biological replicate). PikF^{-} cells exhibited a strikingly large number of these protrusions, with an average of 265 spikes per cell, compared to 67 and 78 spikes in Ax2 and PikA/B^{-} cells, respectively (Figure 3.21). Although spike length was not quantitatively measured, protrusions in PikF^{-} cells appeared noticeably longer than those in the other strains (Figure 3.20), consistent with previous reports of filopodia extending up to 6 µm in Rac1-overexpressing cells (Dumontier et al., 2000). Notably, these longer protrusions in PikF^{-} cells predominantly contained active Rac, whereas short spikes in Ax2 and PikA/B^{-} exhibited both active Rac and Ras signals (Figure 3.20). Interestingly, PikA/B^{-} cells showed a prominent accumulation of vesicular structures coated with active Ras and Rac, which may reflect compensatory signalling or altered trafficking dynamics in the absence of PikA and PikB (Figure 3.20).

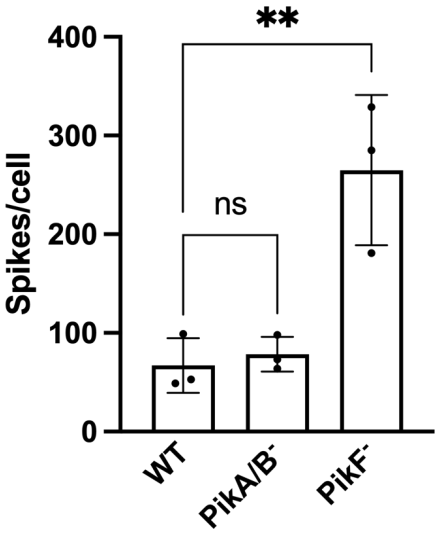

Figure 3.21: Quantification of spike-like membrane protrusions in wild-type (Ax2), PikA/B^{-}, and PikF^{-} cells. Spike-like membrane protrusions were manually counted in 3D MIPs of cells expressing the Rac and Ras activity probes PakB-CRIB-mCherry and GFP-Raf1-RBD. Bars show the mean; error bars represent standard deviation (SD). Statistical analysis was performed using a one-way ANOVA, comparing the means of PikA/B^{-} and PikF^{-} to wild-type (WT). WT vs. PikA/B^{-}: P = 0.9410 (ns). WT vs. PikF^{-}: P = 0.0041 (**). N = 30 cells per strain.

3.3 Discussion

Beyond catalysis: structural basis of PikA and PikF functional divergence

This chapter provides evidence supporting the long-standing hypothesis that PikA and PikF perform distinct roles during macropinocytic cup formation (Hoeller et al., 2013). Furthermore, the data demonstrate that these roles are non-redundant and that their functional divergence lies outside of the catalytic domains (Figure 3.22). Notably, the catalytic domains of PikA and PikF are highly conserved and closely related evolutionarily (Figure 3.23), and they appear to be functionally interchangeable based on the ability of GFP-Chimera 1 to rescue PikF^{-} macropinocytosis defects. Additionally, the ability of GFP-K3356R to partially rescue the PikF^{-} macropinocytosis defect suggests that PikF may play an important non-catalytic, structural role in macropinocytic cup formation, which could underlie its isoform-specific function. It is possible that subtle structural differences mediate distinct protein-protein interactions, leading to divergent spatial or temporal localisations of PI3K isoforms within the forming cup. Given that some PI3Ks are reported to exhibit scaffolding roles and protein kinase activity in addition to their canonical lipid kinase functions (Bilanges et al., 2019; Hirsch et al., 2009; Leevers et al., 1999), it is worth considering whether such alternative activities contribute to the distinct functions of Class I PI3K isoforms in *D. discoideum*.

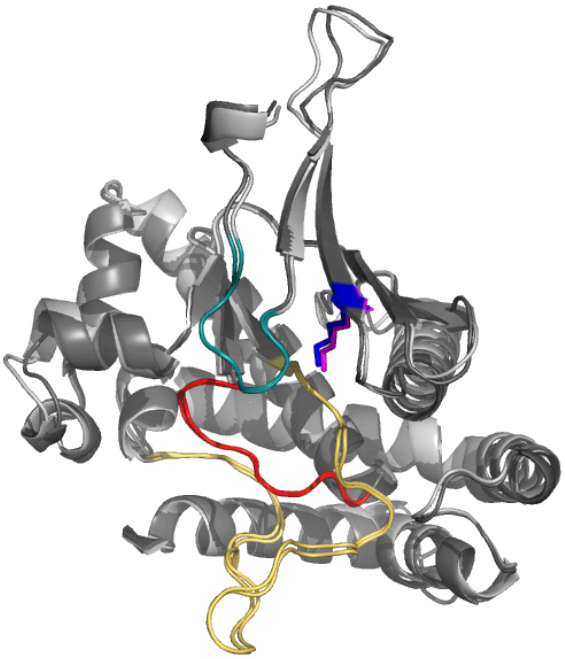

Figure 3.22: Structural superimposition of PikA and PikF catalytic domains highlighting conserved features. PikA is shown in light grey and PikF in dark grey to emphasise the colour-highlighted conserved structures. Coloured features include – Teal: G-loop; Red: Catalytic loop; Yellow: Activation loop; Blue: Conserved lysine residue in PikF; Magenta: Conserved lysine residue in PikA. Predicted protein structures were obtained from AlphaFold. Domain visualisation, annotation, and superimposition were performed using PyMOL.

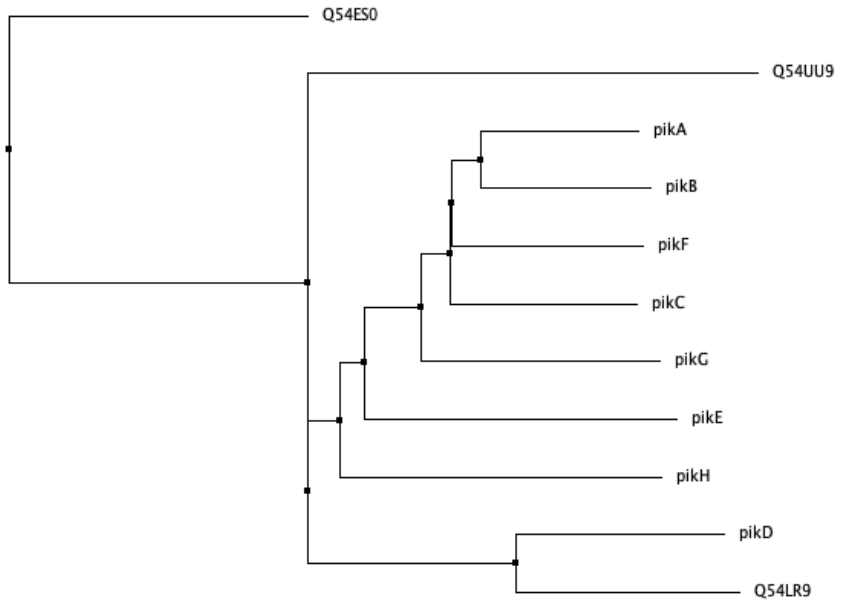

Figure 3.23: Phylogram of the 11 PI3K/PI4K catalytic domains in the *Dictyostelium discoideum* proteome. Catalytic domain sequences were obtained from UniProt and aligned using the Clustal Omega Multiple Sequence Alignment (MSA) tool. The alignment results were visualised and analysed in Jalview. A Neighbour-joining phylogenetic tree was constructed using the BLOSUM62 substitution matrix.

The inability of GFP-Chimera 4 to rescue the PikA/B^{-} macropinocytosis defect highlights the N-terminal domain of PikA as a strong candidate for mediating isoform-specific protein-protein interactions. Since the design and construction of the Chimeras in 2021, updated UniProt annotations have identified an adapter-binding domain (ABD) within the PikA N-terminal tail – previously considered a largely unstructured region – which appears to be absent from the PikF N-terminus. This 97-residue segment is shown in grey in Figure 3.24A, where its tertiary structure and spatial orientation relative to the PikF N-terminal domain can be appreciated. Notably, no canonical PI3K adapter proteins – such as the mammalian Class I PI3K regulatory subunits p85, p84/p87, or p101 – have been identified in *D. discoideum*. This raises important questions: what protein(s) interact with the PikA ABD, and are these interactions critical for mediating PikA's isoform-specific function during macropinocytic cup formation?

Additionally, the inability of GFP-Chimera 2 to rescue the PikF^{-} macropinocytosis defect raises further questions about how domains within the structurally conserved PI3K catalytic core may also contribute to isoform-specific activities during macropinocytic cup formation. It remains unclear whether the disruption of PikF function in Chimera 2 results from the replacement of its helical domain – following the catalytic domain substitution in Chimera 1 – or from issues related to protein expression or the misfolding of chimeric proteins. However, structural comparison of the PikA and PikF helical domains reveals no major differences, aside from a minor angular shift in an α-helix at the lower right edge of the domain superimposition (Figure 3.24D).

Crucially, the loss of function observed from Chimera 2 onward may obscure the contributions of upstream PikF domains to isoform specificity, such as the Ras-binding and C2 domains. To address this, future investigations involving individual domain swaps between PikA and PikF would be valuable for delineating the role of each domain in isoform-specific activities. Structural alignments reveal that the PikA and PikF RBDs are highly similar (Figure 3.24B), whereas more pronounced, yet subtle differences are evident in the alignment of their C2 domains (Figure 3.24C).

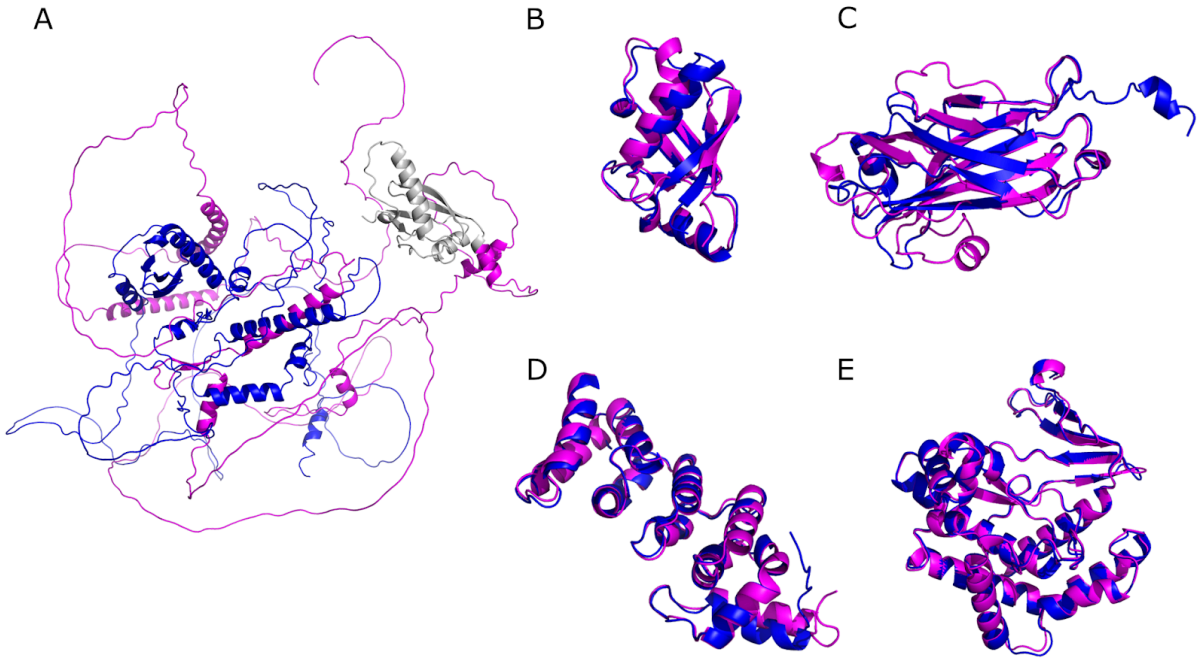

Figure 3.24: Structural superimposition of individual PikA and PikF domains. PikA is shown in magenta and PikF in blue. (A) N-terminal tail, with the PikA adapter-binding domain (ABD) highlighted in light grey. (B) Ras-binding domain (RBD). (C) C2 domain. (D) Accessory/helical domain (PI3Ka). (E) Catalytic domain (PI3Kc). Predicted protein structures were obtained from AlphaFold, and domain visualisation, annotation, and superimposition were performed using PyMOL.

Regrettably, persistent cloning difficulties hindered the completion of macropinocytosis rescue assays for the full set of chimeric proteins designed in this study (Chimeras 1-8, Figure 3.4). For example, Chimera 5 would have enabled us to test whether the PikA catalytic domain is also dispensable for its activity, while Chimera 8 would have allowed us to assess whether the PikF N-terminal domain is also essential for its function.
Although the successful construction of Chimeras 5-8 remains a desirable goal for future investigations, continued cloning challenges may call for the use of alternative strategies. In this context, the new chimera designs (Chimeras 9-12, Figure 3.25) represent a promising next step, offering insight into the interchangeability of the accessory/helical domain and further investigating the contribution of N-terminal domains to PikA and PikF isoform-specific functions.

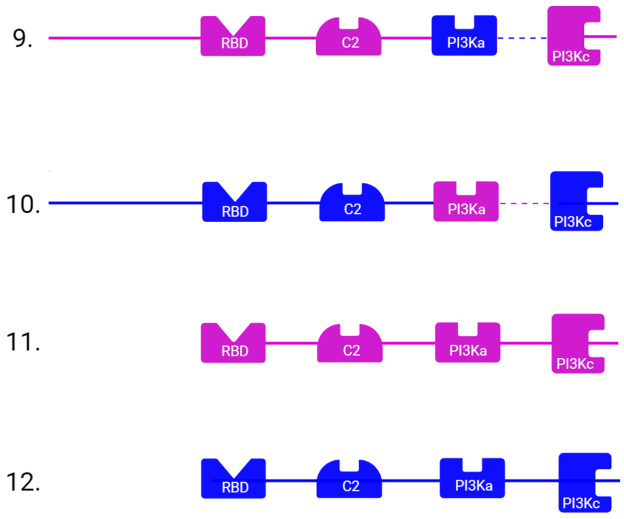

Figure 3.25: Schematic representation of PikA/PikF Chimeras 9-12.
PikA domains are shown in magenta and PikF domains in blue. Chimeras 9 and 10 feature individual substitutions of the accessory/helical domain (PI3Ka) between PikA and PikF. Constructs 11 and 12 are N-terminal truncations of PikA and PikF, respectively, lacking their N-terminal tails. RBD: Ras-binding domain; C2: C2 domain; PI3Ka: accessory/helical domain; PI3Kc: catalytic domain. Created with BioRender.

It is important to acknowledge the limitations of the macropinocytosis rescue experiments presented in this chapter, particularly concerning the regulation of PI3K overexpression via proteasomal degradation. This remains an area requiring further investigation, but the restored detection of GFP-PikA in PikF$^-$ cells following treatment with 0.1 mM MG132 confirmed that the lack of rescue in this context was not due to insufficient background expression of the construct. Similar experiments should now be conducted in PikA/B$^-$ cells expressing GFP-PikF, as well as in both mutant strains expressing GFP-tagged Chimeras 1-4, to determine whether proteasomal degradation similarly affects their expression and functional assessment.

Isoform-specific localisation patterns during macropinocytic cup formation

To our knowledge, this is the first report of GFP-tagged PI3K isoform localisation within macropinocytic cups. As noted by Professor Bart Vanhaesebroeck (University College London, personal communication), overexpressing and visualising PI3Ks in mammalian systems is very challenging. Consequently, most insights into PI3K signalling during macropinocytosis have come from phosphoinositide probes – such as Akt-PH-mSc in mammalian cells (Quinn et al., 2021) and PH-CRAC-mRFP (Veltman et al., 2016) or PkgE-PH-GFP in *D. discoideum* (Lutton et al., 2023). Moreover, the roles of individual PI3K isoforms have received limited attention since Hoeller *et al*. (2013) proposed functional specificity. This chapter extends that work by directly visualising isoform-specific localisation patterns and assessing their cytoskeletal impact.

Quantitative analysis of GFP-PikA and GFP-PikF signal intensities across macropinocytic cups revealed distinct localisation patterns: PikA is enriched at the base of the cup, whereas PikF distributes more uniformly and extends into the rim (Figure 3.11). This suggests functional differentiation, with PikA acting earlier in cup formation and PikF contributing to later stages and/or closure, consistent with Hoeller *et al*. (2013). Notably, PikA's base localisation resembles that of the PIP_3 reporter PH-CRAC when co-expressed with the SCAR complex marker HSPC300-GFP, which localises to the rim (Veltman et al., 2016) hinting – pending validation – at preferential SCAR complex engagement with PikF. Live-cell imaging also suggests divergent trafficking mechanisms of PI3K isoforms: PikA exhibits vesicular recycling, budding from cup bases and relocating to newly forming cups, whereas PikF shows no such behaviour.

Additionally, disruption of GFP-PikF localisation in the presence of the PIP_3 probe PkgE-PH-mCherry suggests that PikF recruitment depends on upstream PikA activity and may be competitively inhibited by phosphoinositide probes (Figure 3.17). Such interference is well-documented: PH domains can compete with native protein-lipid interactions (Idevall-Hagren and De Camilli, 2015; Mousavi et al., 2004). While this complicates spatiotemporal interpretation, it simultaneously offers mechanistic insight into the sequential recruitment of PI3K isoforms to nascent macropinocytic cups.

Interpreting phosphoinositide probe specificity

In PikA/B$^-$ cells co-expressing PkgE-PH-mCherry and GFP-PikA, the prolonged PIP_3 signal on internalised vesicles raises concerns about probe specificity (Figures 3.13 and 3.14). Although some degree of overlap between PIP_3 and $PI(3,4)P_2$ signals is expected – because PIP_3 is progressively dephosphorylated to $PI(3,4)P_2$ by inositol polyphosphate 5-phosphatases after macropinosome internalisation (Ooms et al., 2009) – it is possible that PkgE-PH-mCherry binds $PI(3,4)P_2$ during this sequential breakdown following cup closure (Maekawa et al., 2014), a recognised limitation of PH domain-based reporters (Montaño-Rendón et al., 2022).

To further investigate $PI(3,4)P_2$ and PIP_3 production in wild-type (Ax2), PikA/B$^-$, and PikF$^-$ cells, we co-expressed GFP-TAPP1 ($PI(3,4)P_2$) and RFP-PH-PkgE (PIP_3). However, the expression of these probes induced marked morphological abnormalities in both Ax2 and PikF$^-$ cells, preventing reliable interpretation (Figure 3.18). Moreover, we observed minimal spatial overlap between the putative $PI(3,4)P_2$ and PIP_3 signals, further calling probe specificity into question.

The differing effects of RFP-PH-PkgE and PkgE-PH-mCherry in wild-type and mutant cells suggest that fluorophore orientation (N- versus C-terminal tagging) can interfere with essential protein-protein or protein-lipid interactions at the cell surface. This observation underscores the need for caution when inferring lipid dynamics from PH-domain probes and emphasises the importance of complementary, independent strategies to validate phosphoinositide dynamics during macropinocytic cup formation.

Comparative morphology of PikA/B^{-} and PikF^{-} cells

Live-cell microscopy revealed two phenotypic differences that warranted further investigation: PikA/B^{-} cells appeared smaller than wild-type, whereas PikF^{-} cells appeared larger and displayed prominent spike-like membrane protrusions. Although reduced size in PikA/B^{-} cells have been reported since the earliest genetic analyses (Zhou et al., 1995), PikF^{-} cells had not, to our knowledge, been morphologically characterised. Our measurements show that PikF^{-} cells are significantly larger than Ax2 and PikA/B^{-} cells, while PikA/B^{-} cells are significantly smaller than Ax2; however, the mechanisms underlying these size differences remain unclear. Intriguingly, PikF^{-} cells also exhibit a ‘spiky’ phenotype resembling that of Rac1-overexpressing cells (Dumontier et al., 2000), raising the possibility of Rac signalling dysregulation in the absence of PikF.

The following chapters examine the interplay between Class I PI3K signalling and Ras/Rac dynamics, characterise PIP_3 and F-actin behaviour in PikA/B^{-}, PikF^{-}, and PikA/B/F^{-} cells, and map isoform-specific protein-protein interactions by proteomics, to further elucidate how PikA and PikF differentially contribute to macropinocytosis in *D. discoideum*.

3.4 References

Araki, N., Egami, Y., Watanabe, Y., Hatae, T., 2007. Phosphoinositide metabolism during membrane ruffling and macropinosome formation in EGF-stimulated A431 cells. Exp. Cell Res. 313, 1496–1507. https://doi.org/10.1016/j.yexcr.2007.02.012

Araki, N., Johnson, M.T., Swanson, J.A., 1996. A role for phosphoinositide 3-kinase in the completion of macropinocytosis and phagocytosis by macrophages. J. Cell Biol. 135, 1249–1260. https://doi.org/10.1083/jcb.135.5.1249

Bilanges, B., Posor, Y., Vanhaesebroeck, B., 2019. PI3K isoforms in cell signalling and vesicle trafficking. Nat. Rev. Mol. Cell Biol. 20, 515–534. https://doi.org/10.1038/s41580-019-0129-z

Dumontier, M., Höcht, P., Mintert, U., Faix, J., 2000. Rac1 GTPases control filopodia formation, cell motility, endocytosis, cytokinesis and development in Dictyostelium. J. Cell Sci. 113, 2253–2265. https://doi.org/10.1242/jcs.113.12.2253

Egami, Y., Taguchi, T., Maekawa, M., Arai, H., Araki, N., 2014. Small GTPases and phosphoinositides in the regulatory mechanisms of macropinosome formation and maturation. Front. Physiol. 5.

Faix, J., Clougherty, C., Konzok, A., Mintert, U., Murphy, J., Albrecht, R., Mühlbauer, B., Kuhlmann, J., 1998. The IQGAP-related protein DGAP1 interacts with Rac and is involved in the modulation of the F-actin cytoskeleton and control of cell motility.

Filić, V., Marinović, M., Faix, J., Weber, I., 2014. The IQGAP-related protein DGAP1 mediates signaling to the actin cytoskeleton as an effector and a sequestrator of Rac1 GTPases. Cell. Mol. Life Sci. 71, 2775–2785. https://doi.org/10.1007/s00018-014-1606-3

Hirsch, E., Braccini, L., Ciraolo, E., Morello, F., Perino, A., 2009. Twice upon a time: PI3K's secret double life exposed. Trends Biochem. Sci. 34, 244–248. https://doi.org/10.1016/j.tibs.2009.02.003

Hoeller, O., Bolourani, P., Clark, J., Stephens, L.R., Hawkins, P.T., Weiner, O.D., Weeks, G., Kay, R.R., 2013. Two distinct functions for PI3-kinases in macropinocytosis. J. Cell Sci. jcs.134015. https://doi.org/10.1242/jcs.134015

Idevall-Hagren, O., De Camilli, P., 2015. Detection and manipulation of phosphoinositides. Biochim. Biophys. Acta BBA - Mol. Cell Biol. Lipids 1851, 736–745. https://doi.org/10.1016/j.bbalip.2014.12.008

Leevers, S.J., Vanhaesebroeck, B., Waterfield, M.D., 1999. Signalling through phosphoinositide 3-kinases: the lipids take centre stage. Curr. Opin. Cell Biol. 11, 219–225. https://doi.org/10.1016/S0955-0674(99)80029-5

Lutton, J.E., Coker, H.L.E., Paschke, P., Munn, C.J., King, J.S., Bretschneider, T., Kay, R.R., 2023. Formation and closure of macropinocytic cups in Dictyostelium. Curr. Biol. 33, 3083-3096.e6. https://doi.org/10.1016/j.cub.2023.06.017

Maekawa, M., Terasaka, S., Mochizuki, Y., Kawai, K., Ikeda, Y., Araki, N., Skolnik, E.Y., Taguchi, T., Arai, H., 2014. Sequential breakdown of 3-phosphorylated phosphoinositides is essential for the completion of macropinocytosis. Proc. Natl. Acad. Sci. 111, E978–E987. https://doi.org/10.1073/pnas.1311029111

Montaño-Rendón, F., Walpole, G.F.W., Krause, M., Hammond, G.R.V., Grinstein, S., Fairn, G.D., 2022. PtdIns(3,4)P2, Lamellipodin, and VASP coordinate actin dynamics during phagocytosis in macrophages. J. Cell Biol. 221, e202207042. https://doi.org/10.1083/jcb.202207042

Mousavi, S.A., Malerød, L., Berg, T., Kjeken, R., 2004. Clathrin-dependent endocytosis. Biochem. J. 377, 1–16. https://doi.org/10.1042/bj20031000

Ooms, L.M., Horan, K.A., Rahman, P., Seaton, G., Gurung, R., Kethesparan, D.S., Mitchell, C.A., 2009. The role of the inositol polyphosphate 5-phosphatases in cellular function and human disease. Biochem. J. 419, 29–49. https://doi.org/10.1042/BJ20081673

Quinn, S.E., Huang, L., Kerkvliet, J.G., Swanson, J.A., Smith, S., Hoppe, A.D., Anderson,

R.B., Thiex, N.W., Scott, B.L., 2021. The structural dynamics of macropinosome formation and PI3-kinase-mediated sealing revealed by lattice light sheet microscopy. Nat. Commun. 12, 4838. https://doi.org/10.1038/s41467-021-25187-1

Rasband, W., 2000. Circularity [WWW Document]. URL https://imagej.net/ij/plugins/circularity.html (accessed 4.1.25).

Rupper, A., Lee, K., Knecht, D., Cardelli, J., 2001. Sequential Activities of Phosphoinositide 3-Kinase, PKB/Akt, and Rab7 during Macropinosome Formation inDictyostelium. Mol. Biol. Cell 12, 2813–2824. https://doi.org/10.1091/mbc.12.9.2813

Veltman, D.M., Williams, T.D., Bloomfield, G., Chen, B.-C., Betzig, E., Insall, R.H., Kay, R.R., 2016. A plasma membrane template for macropinocytic cups. eLife 5, e20085. https://doi.org/10.7554/eLife.20085

Wennström, S., Hawkins, P., Cooke, F., Hara, K., Yonezawa, K., Kasuga, M., Jackson, T., Claesson-Welsh, L., Stephens, L., 1994. Activation of phosphoinositide 3-kinase is required for PDGF-stimulated membrane ruffling. Curr. Biol. 4, 385–393. https://doi.org/10.1016/S0960-9822(00)00087-7

Yart, A., Roche, S., Wetzker, R., Laffargue, M., Tonks, N., Mayeux, P., Chap, H., Raynal, P., 2002. A Function for Phosphoinositide 3-Kinase β Lipid Products in Coupling βγ to Ras Activation in Response to Lysophosphatidic Acid*. J. Biol. Chem. 277, 21167–21178. https://doi.org/10.1074/jbc.M110411200

Zhou, K., Takegawa, K., Emr, S.D., Firtel, R.A., 1995. A Phosphatidylinositol (PI) Kinase Gene Family in Dictyostelium discoideum: Biological Roles of Putative Mammalian p110 and Yeast Vps34p PI 3-Kinase Homologs during Growth and Development. Mol. Cell. Biol. 15, 5645–5656. https://doi.org/10.1128/MCB.15.10.5645

Chapter 4: Isoform-Specific Regulation of GTPase Signalling and Actin Dynamics by Class I PI3Ks in *Dictyostelium discoideum*

4.1 Introduction

As outlined in Chapter 1, dynamic remodelling of the actin cytoskeleton is the principal mechanical driver of processes that require coordinated deformation of the plasma membrane, such as macropinocytosis. This remodelling is orchestrated by small GTPases – particularly Ras and Rac – that act as molecular switches to organise the spatial and temporal assembly of actin filaments. Phosphoinositide signalling further modulates membrane dynamics by recruiting cytoskeletal effectors to defined membrane regions, with Class I PI3Ks traditionally viewed as generators of localised PIP_3 domains at the plasma membrane. However, Chapter 3 showed that the *Dictyostelium discoideum* Class I PI3K isoforms PikA and PikF fulfil non-redundant, partly non-catalytic roles during macropinocytic cup formation, and highlighted important caveats related to expression control and phosphoinositide probe specificity.

Building on that framework, this chapter investigates how Ras, Rac, PIP_3 and F-actin activities are organised in space and time, and how this organisation is perturbed in PI3K isoform mutants. Using live-cell imaging and fluorescent reporters for active Ras and Rac, we examine how PikA and PikF differentially modulate GTPase signalling during macropinocytic cup formation and basal wave propagation. In parallel, we examine cytoskeletal dynamics in PikA/B$^-$, PikF$^-$, and PikA/B/F$^-$ strains through a combination of Spinning Disk Confocal and Lattice Light Sheet Microscopy. By co-expressing fluorescent reporters for PIP_3 and F-actin, we capture the real-time dynamics of macropinocytic and phagocytic cup formation, as well as basal wave propagation. Comparing these features across mutant backgrounds, we aim to define how PikA and PikF contribute to the spatial and temporal regulation of actin-driven membrane processes, with a primary focus on macropinocytosis. This analysis extends Chapter 3 by linking isoform-specific localisation to the way GTPase and phosphoinositide signals organise the actin cytoskeleton, and how this coordination is perturbed in PikA and PikF mutant strains.

Research Questions Addressed in this Chapter

1. Does the morphological resemblance of PikF$^-$ cells to Rac1-overexpressing strains reflect mislocalised Rac activity in the absence of PikF?

2. Do PikA/B$^-$, PikF$^-$, and PikA/B/F$^-$ cells show aberrant PIP_3 production and F-actin dynamics during macropinocytic cup formation and basal wave propagation?

3. If so, does each mutant display a distinct spatiotemporal pattern of Ras, Rac, PIP_3 and F-actin disruption indicative of isoform-specific function (base vs rim control)?

4. Given that large-scale phagocytosis in mammalian cells depends on tightly regulated actin dynamics and PI3K-driven actin turnover (Schlam et al., 2015), are Class I PI3Ks similarly required for the engulfment of large particles in *D. discoideum*? If required, do PikA and PikF play non-redundant roles in phagocytosis comparable to those defined for macropinocytosis?

4.2 Results

4.2.1 Class I PI3Ks Influence Ras and Rac Signalling Pathways

Ras and Rac Signalling in Macropinocytic Cups

The interplay between Ras and Rac signalling at macropinocytic and phagocytic cups was first described by Buckley *et al*. (2020). Using active Ras and Rac probes – GFP-RBD and RFP-PakB-CRIB, respectively – they observed that in macropinocytic cups, active Ras is confined within the cup rim, while active Rac extends approximately 2 µm beyond the active Ras signal (Buckley et al., 2020). Using a similar approach, we quantified active Ras and Rac distribution in Ax2, PikA/B^{-}, and PikF^{-} cells using the probes GFP-Raf1-RBD and PakB-CRIB-mCherry, respectively. Line scans were drawn across 30 macropinocytic cup cross-sections per strain to measure signal distribution (Figure 4.1), and intensity values were normalised relative to the average of the 10 highest signal peaks (set as 1.0). The point where active Ras signal declined at the cup rim was defined as the zero point (0 µm), such that negative values represent positions inside the cup, and positive values represent positions extending outward along the protruding membrane.

In Ax2 cells, the active Ras signal intensity dropped to 0.25 at 2.5 µm from the cup rim, while the active Rac signal dropped to 0.50 at 3.5 µm, showing a 1 µm outward extension of active Rac over active Ras (Figure 4.2B). In PikA/B^{-} cells, the active Ras distribution remained consistent with Ax2, dropping to 0.25 at 2.5 µm. However, the active Rac signal declined more gradually, reaching 0.50 intensity at 5.5 µm from the rim, suggesting a 2 µm increase in the active Rac-Ras differential (Figure 4.3B). Notably, inside PikA/B^{-} macropinocytic cups, active Ras and Rac signals exhibit a coordinated, gradually declining slope from the centre toward the rim – a pattern not observed in Ax2 cells. This correlation between the two signals is particularly evident when the line scans are normalised to cytoplasmic intensity rather than peak values (Figures 4.2A and 4.3A).

In PikF^{-} cells, the active Ras signal extended 1µm further than in either Ax2 or PikA/B^{-}, cells, dropping to 0.25 intensity at 3.5 µm past the rim. Even more striking was the Rac signal: it began rising before the cup rim (at -1 µm), peaked at 5.5 µm beyond the rim, and showed greater variability across the measured range (Figure 4.4B). These findings suggest that while Ras localisation remains relatively conserved across Class I PI3K mutant strains, Rac signalling is moderately dysregulated in PikA/B^{-} cells and dramatically altered in PikF^{-} cells, potentially reflecting a failure to spatially confine Rac activity during macropinocytic cup formation. This confirms that the morphological similarities between PikF^{-} and Rac1-overexpressing cells might be indicative of a mechanistic relationship.

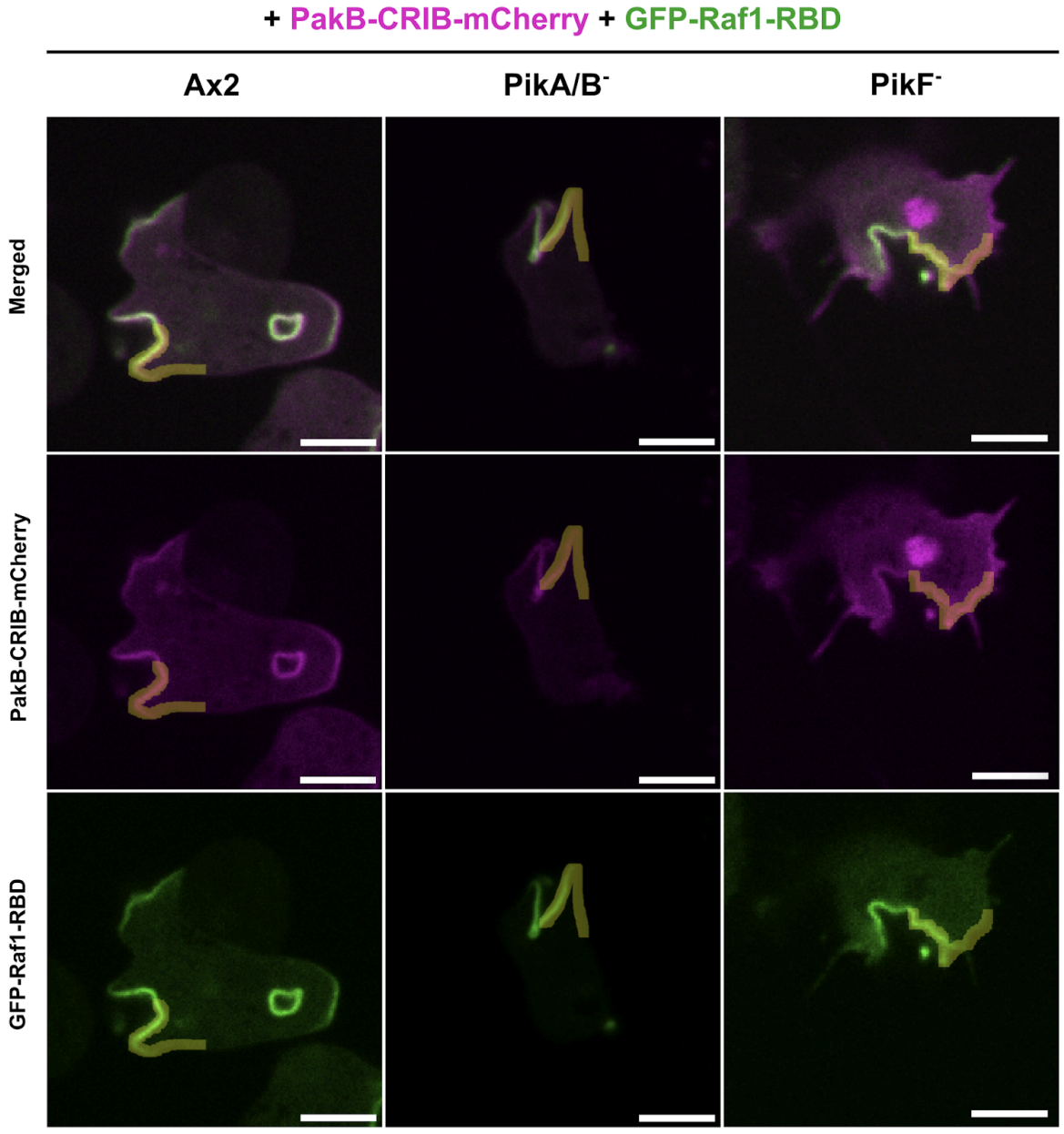

Figure 4.1: Representative line scans used to measure Rac and Ras signal distribution across macropinocytic cups in wild-type (Ax2), PikA/B$^-$, and PikF$^-$ cells. Cells were co-transformed with PakB-CRIB-mCherry (magenta), which binds active Rac, and GFP-Raf1-RBD (green), which binds active Ras. Line scans (6 pixels wide, ~12 µm in length) were drawn across macropinocytic cups to quantify signal intensity from the interior to the exterior of the cup. Images are maximum intensity projections of three Z-slices per cell, acquired using a Nikon W1 Spinning Disk Confocal Microscope. Scale bar: 5 µm (4 pixels wide).

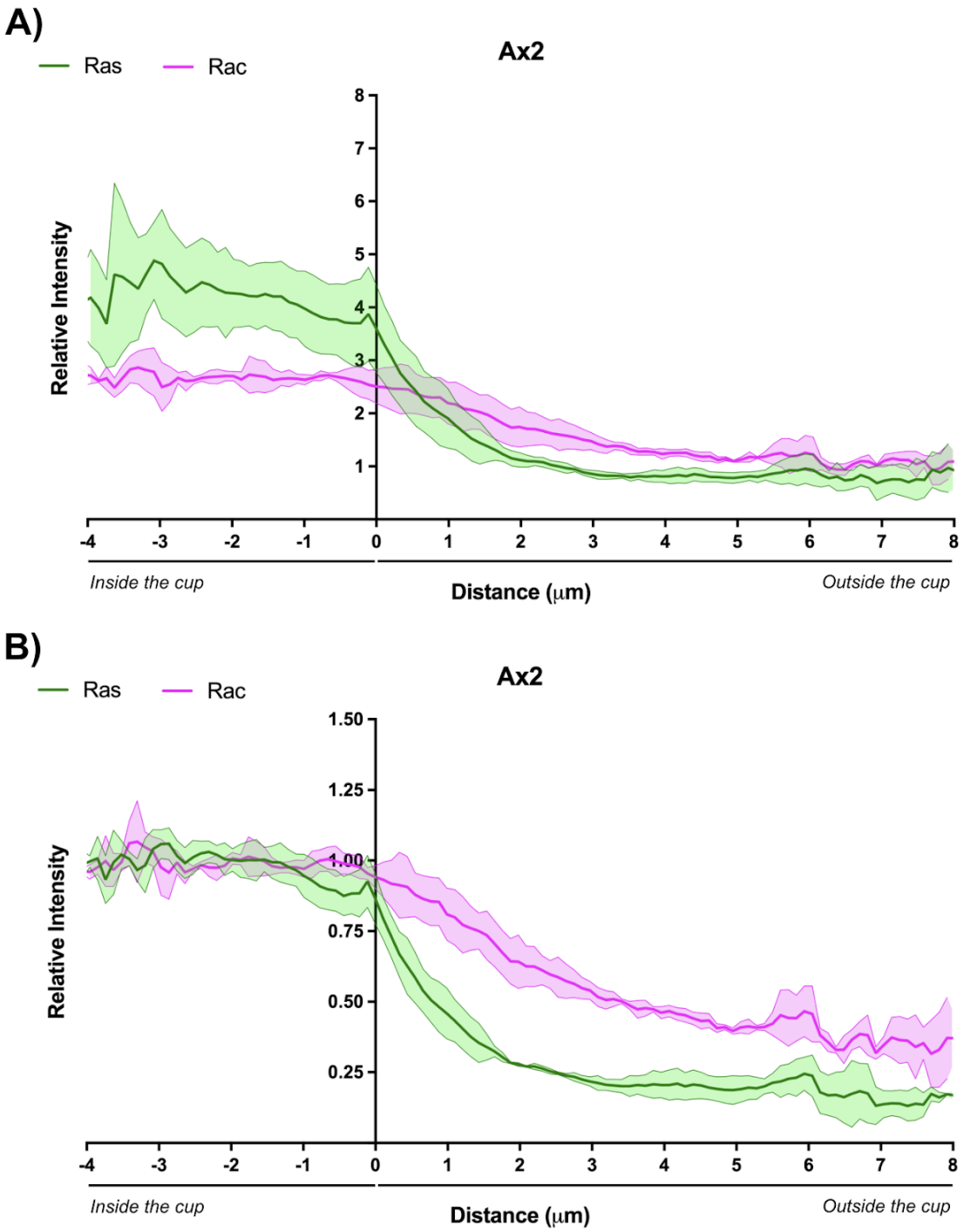

Figure 4.2: Relative intensity profiles of Ras and Rac signals across macropinocytic cups in wild-type (Ax2) cells. Line scan analysis was performed on Ax2 cells expressing GFP-Raf1-RBD (active Ras) and PakB-CRIB-mCherry (active Rac). Signal intensity was measured across macropinocytic cups from the interior to the exterior rim. (A) Signal intensities normalised to cytoplasmic fluorescence (1 = mean cytoplasmic intensity). (B) Signal intensities normalised to the average of the 10 highest values per scan (set as 1.0). Sample size (N) = 30 macropinocytic cups.

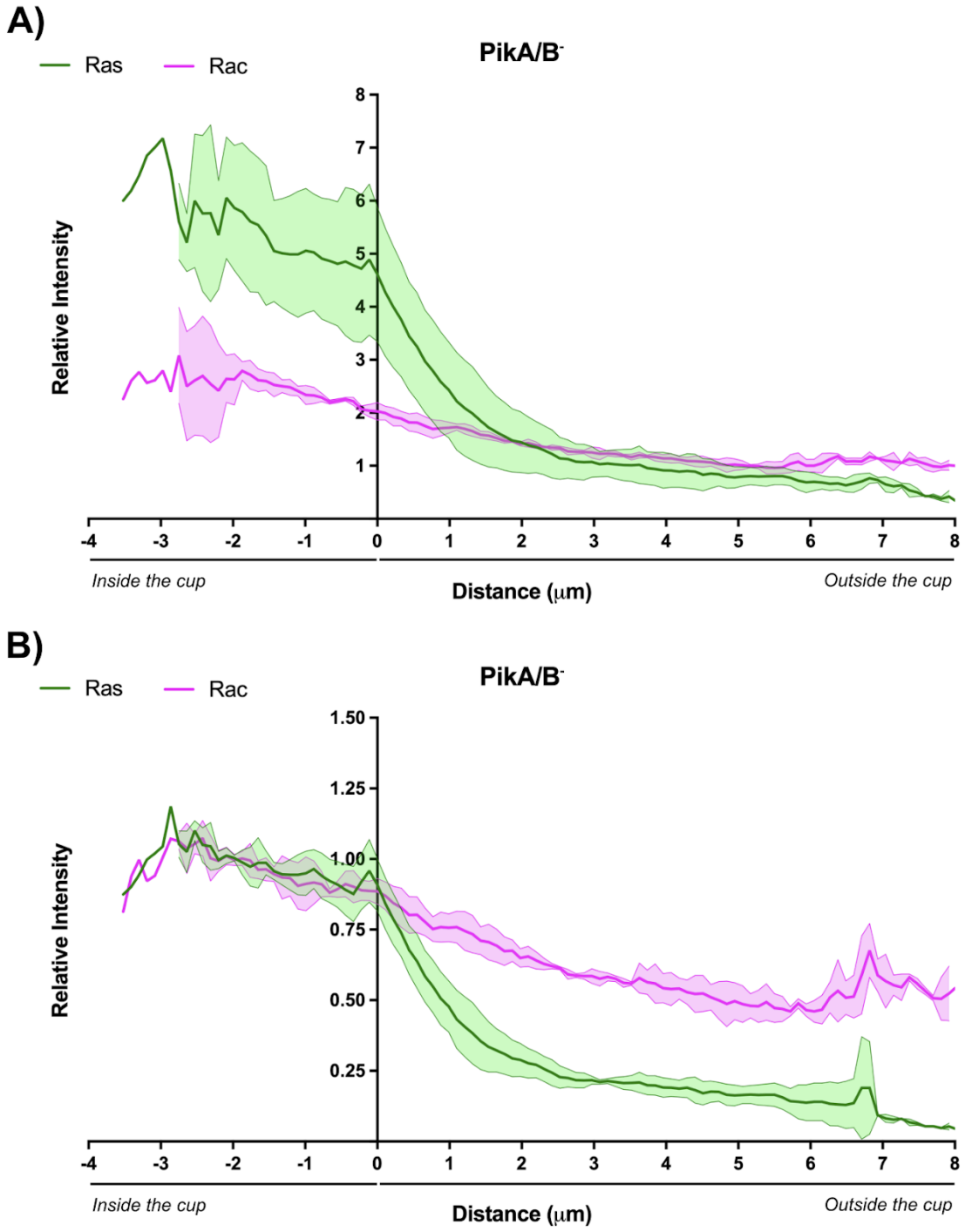

Figure 4.3: Relative intensity profiles of Ras and Rac signals across macropinocytic cups in PikA/B$^-$ cells. Line scan analysis was performed on Ax2 cells expressing GFP-Raf1-RBD (active Ras) and PakB-CRIB-mCherry (active Rac). Signal intensity was measured across macropinocytic cups from the interior to the exterior rim. (A) Signal intensities normalised to cytoplasmic fluorescence (1 = mean cytoplasmic intensity). (B) Signal intensities normalised to the average of the 10 highest values per scan (set as 1.0). Sample size (N) = 30 macropinocytic cups.

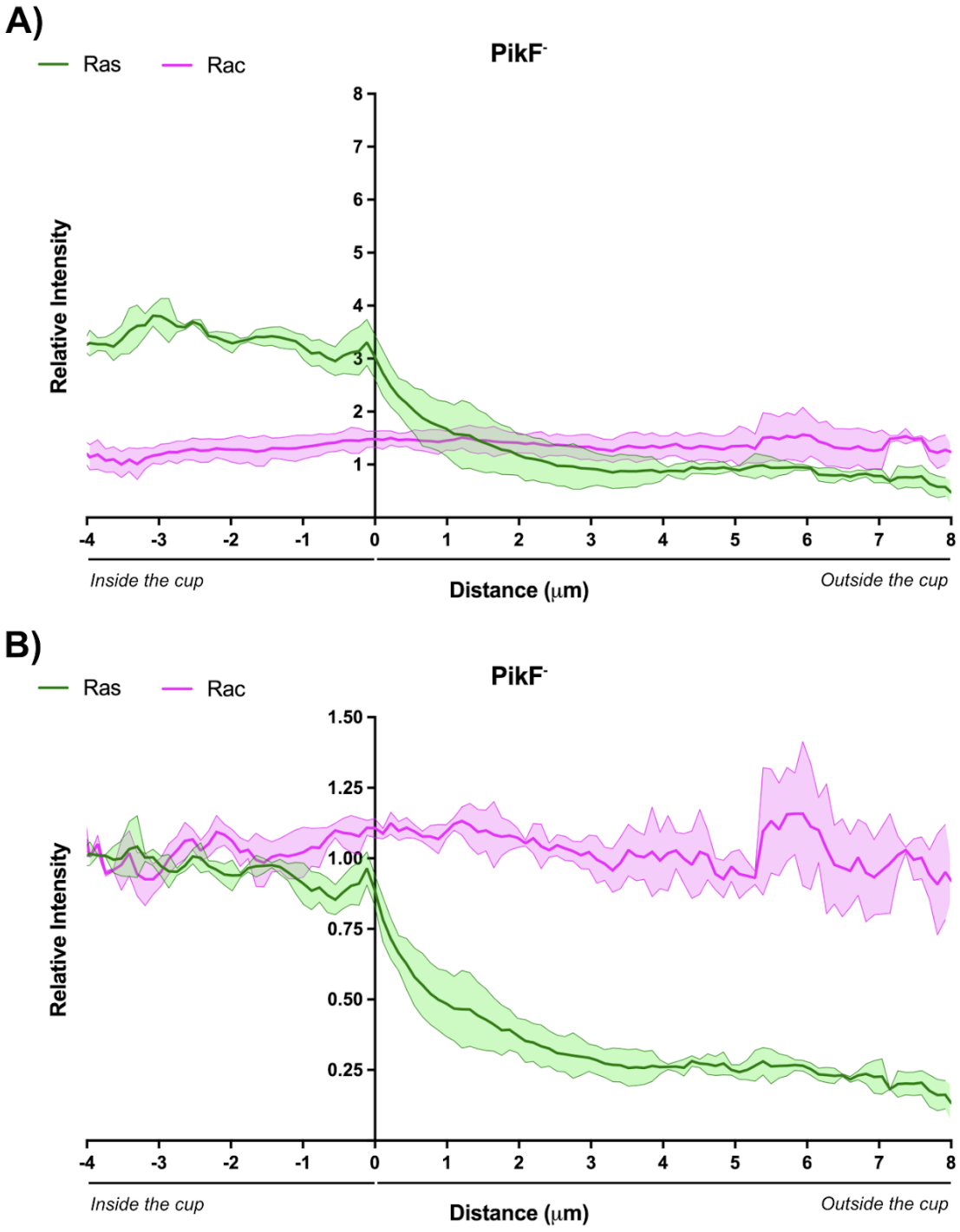

Figure 4.4: Relative intensity profiles of Ras and Rac signals across macropinocytic cups in PikF$^-$ cells. Line scan analysis was performed on Ax2 cells expressing GFP-Raf1-RBD (active Ras) and PakB-CRIB-mCherry (active Rac). Signal intensity was measured across macropinocytic cups from the interior to the exterior rim. (A) Signal intensities normalised to cytoplasmic fluorescence (1 = mean cytoplasmic intensity). (B) Signal intensities normalised to the average of the 10 highest values per scan (set as 1.0). Sample size (N) = 30 macropinocytic cups.

Ras and Rac Signalling in Basal Waves

Cytoskeletal dynamics underlying the formation and propagation of planar actin waves have long been debated as models for either macropinocytic or phagocytic cups (Gerisch et al., 2009; Masters et al., 2016; Veltman et al., 2016). To further explore this question, we investigated whether the disturbances in active Ras and Rac signalling observed in macropinocytic cups are also reflected in basal actin waves. Using the same Ax2, PikA/B$^-$ and PikF$^-$ cell lines co-expressing GFP-Raf1-RBD and PakB-CRIB-mCherry, line scans were taken across images of basal signalling patches captured by Total Internal Reflection Fluorescence (TIRF) microscopy (Figure 4.5).

When signal intensity was normalised to the average cytoplasmic level (set to 1), no consistent spatial offset between active Ras and Rac signals was observed in any of the three strains. However, when intensities were instead normalised to the average of the 10 highest values – an approach that improved spatial resolution of the signal distributions – differences became more apparent. In Ax2 cells, a ~2 µm differential was detected between the extents of active Rac over active Ras signals: from left to right, the active Ras signal declined to 0.4 relative intensity at 4 µm into the patch, while the active Rac signal did not fall to that level until 6 µm (Figure 4.6B). In PikA/B$^-$ cells, this differential decreased to just 0.4 µm (Figure 4.7B), although interpretation is complicated by the smaller size of PikA/B$^-$ cells and, consequently, their basal patches. In PikF$^-$ cells, most of the active Rac signal appeared uniformly distributed across the basal membrane, with no clearly defined patches. From left to right, while a transient decline in active Rac signal intensity was observed at the same location as an active Ras signal drop, the Rac signal then rebounded and extended up to 6 µm beyond the Ras signal (Figure 4.8B).

These results are inconclusive, primarily due to cell size differences and the inherently variable nature of basal patch formation. However, they suggest that the spatial offset between active Rac and Ras seen in Ax2 may be diminished in PikA/B$^-$ basal patches, in contrast to the enhanced active Rac extension seen in PikA/B$^-$ macropinocytic cups. Importantly, Rac signalling in PikF$^-$ cells appears profoundly dysregulated. Whether this reflects an aberrant spread of active Rac across the basal surface or a failure to form discrete active Rac basal patches altogether remains unclear.

Together, these results highlight that the spatial regulation of Ras and Rac signalling is more consistently disrupted in macropinocytic cups than in basal patches, particularly in PikF$^-$ cells, making the former more amenable to quantification and interpretation. While Ax2 cells exhibit a clear and reproducible spatial differential between active Rac and Ras signals in both contexts, this appears compressed in PikA/B$^-$ basal patches and is difficult to interpret due to their reduced cell size. In contrast, PikF$^-$ cells display a pronounced loss of Rac activity confinement across both macropinocytic cups and basal membranes; however, direct quantitative comparison remains challenging. As a result, it remains uncertain whether basal patches can serve as a reliable, simplified proxy for studying macropinocytic cup signalling. These findings reinforce the notion that PikF plays a key role in constraining Rac signalling spatially, and suggest that its absence compromises the maintenance of defined Rac signalling domains, potentially contributing to the aberrant morphology and dysregulated protrusive activity observed in PikF$^-$ cells.

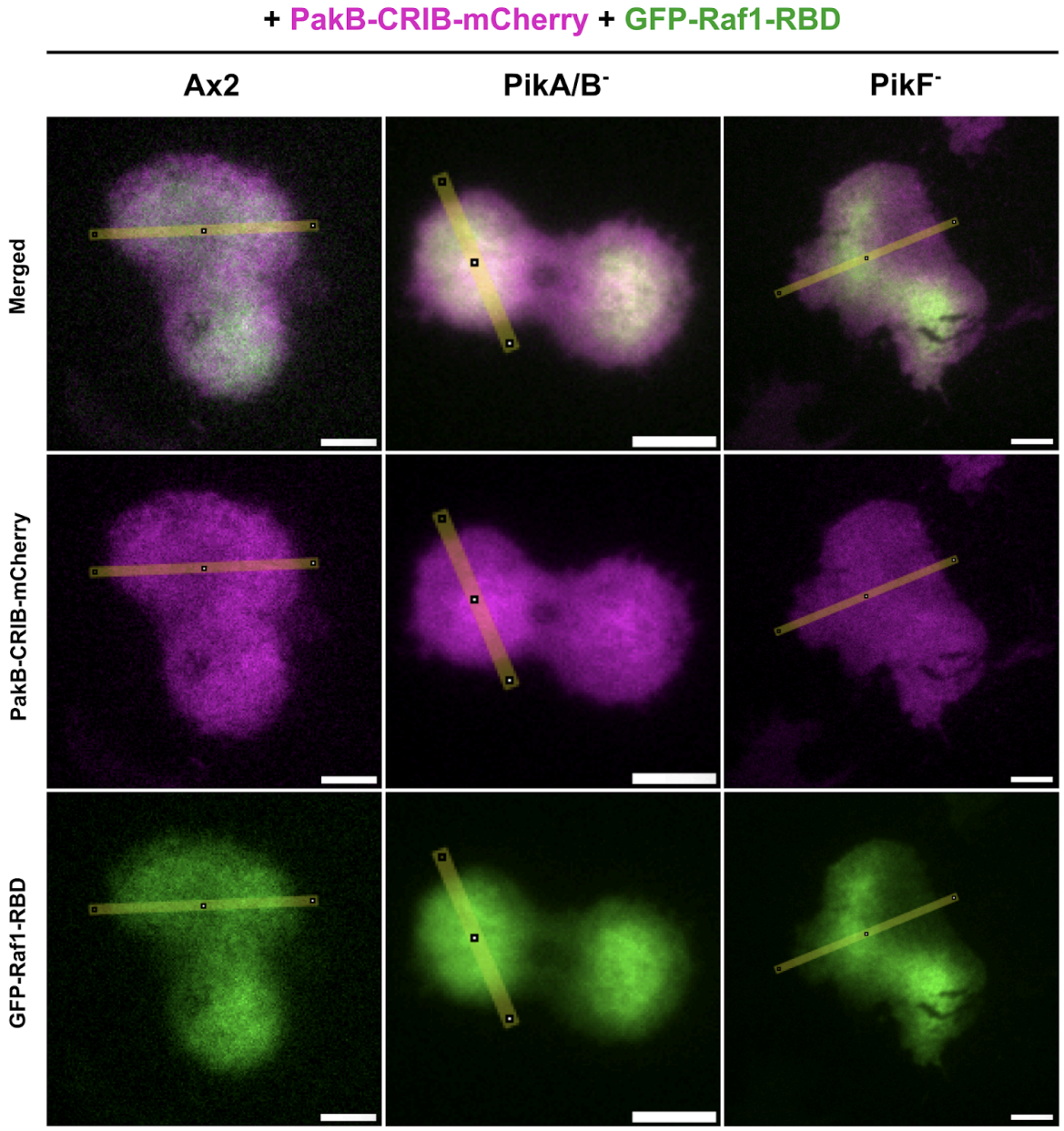

Figure 4.5: Representative line scans used to measure Rac and Ras signal distribution across basal patches in wild-type (Ax2), PikA/B$^-$, and PikF$^-$ cells. Cells co-expressing PakB-CRIB-mCherry (magenta, active Rac) and GFP-Raf1-RBD (green, active Ras) were imaged using Total Internal Reflection Fluorescence (TIRF) microscopy on a Nikon N-STORM system. Line scans (6 pixels wide, 10–22 µm in length) were drawn across basal membrane patches to quantify spatial signal distribution. Scale bar: 5 µm (4 pixels wide).

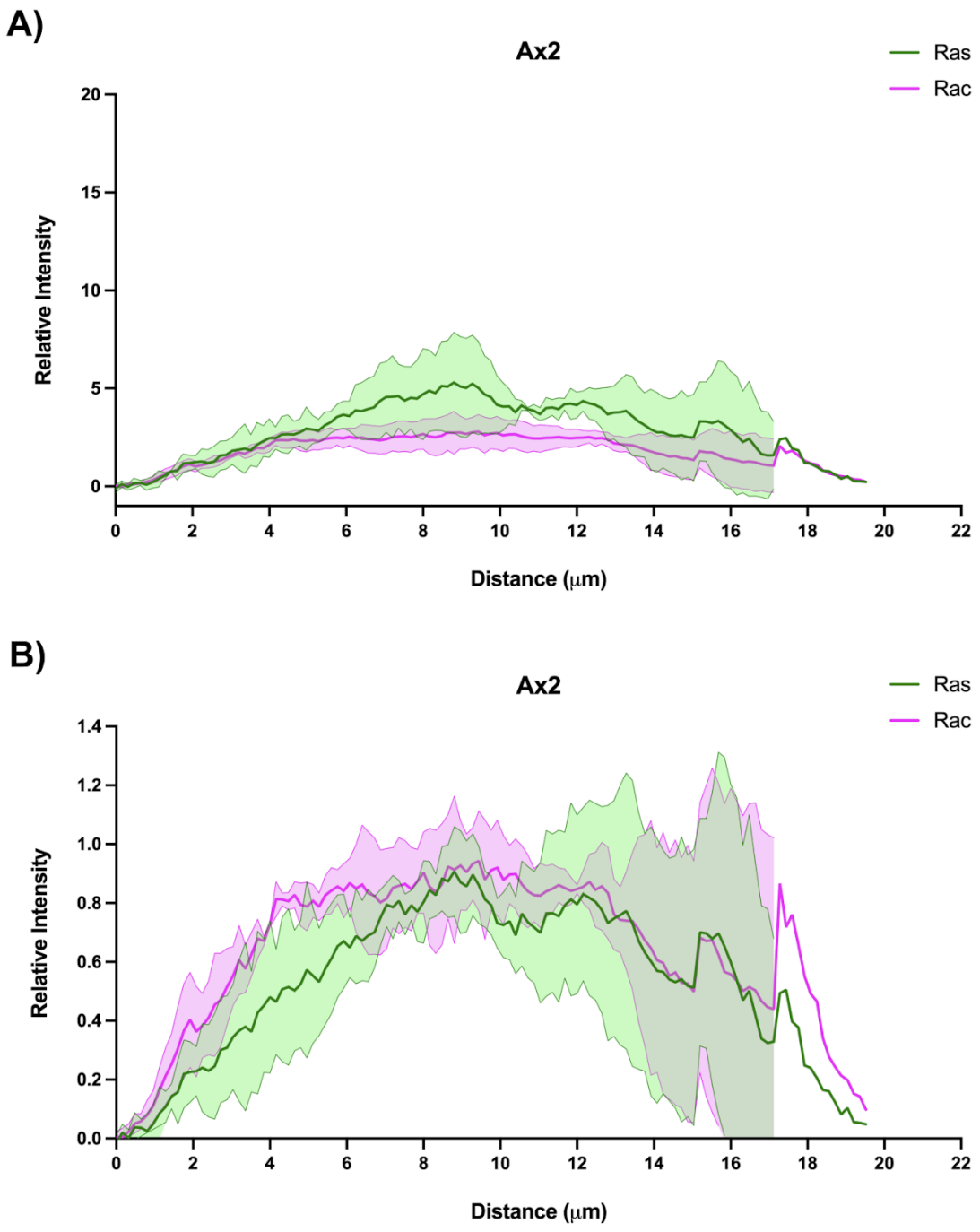

Figure 4.6: Relative intensity profiles of Ras and Rac signals across basal membrane patches in wild-type (Ax2) cells. Signal intensities of GFP-Raf1-RBD (active Ras) and PakB-CRIB-mCherry (active Rac) were measured from line scans drawn across basal patches imaged by TIRF microscopy. (A) Intensities normalised to the mean cytoplasmic fluorescence (1 = average cytoplasmic signal). (B) Intensities normalised to the average of the 10 highest values per scan (set as 1.0). Sample size (N) = 3 biological replicates.

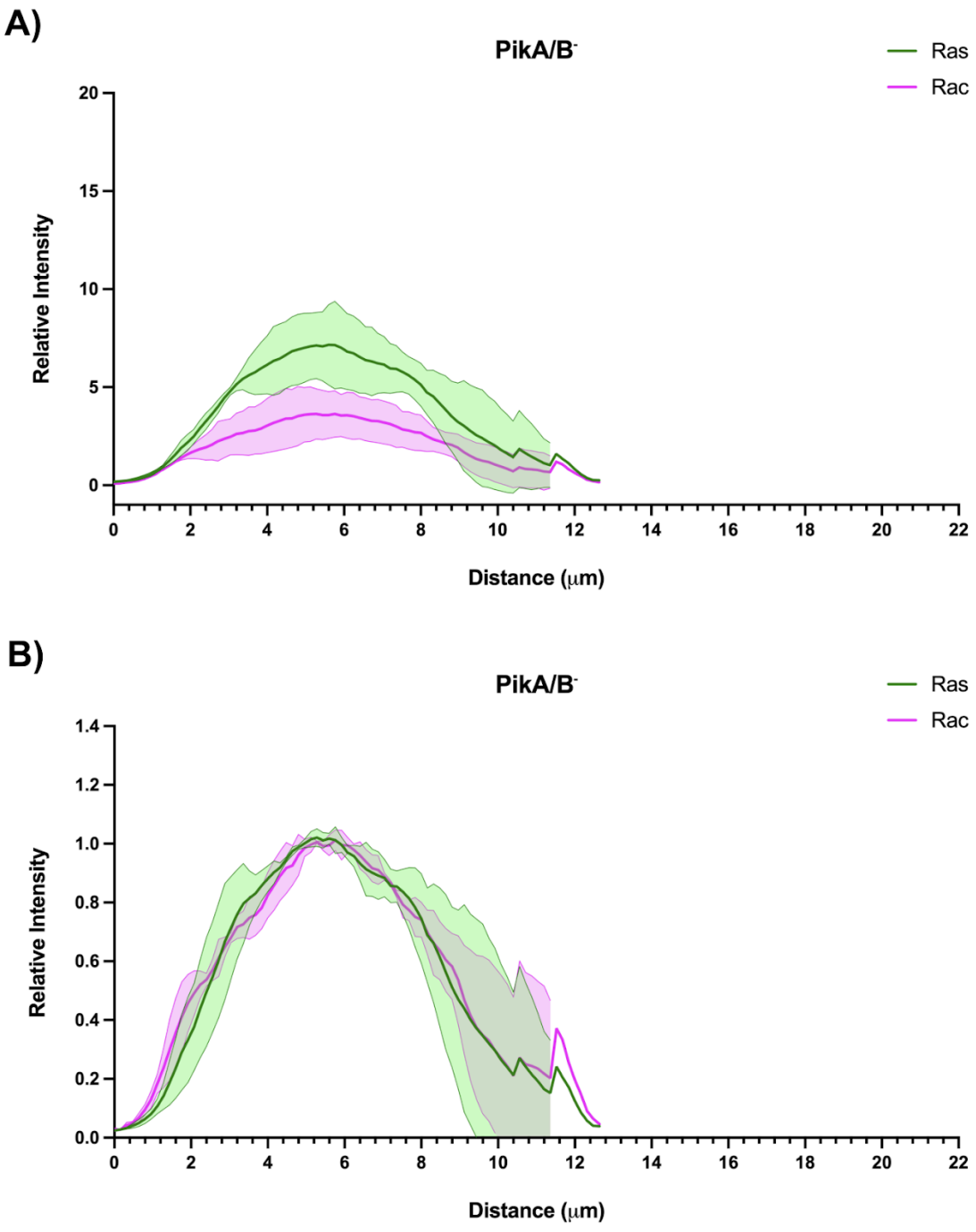

Figure 4.7: Relative intensity profiles of Ras and Rac signals across basal membrane patches in PikA/B$^-$ cells. Signal intensities of GFP-Raf1-RBD (active Ras) and PakB-CRIB-mCherry (active Rac) were measured from line scans drawn across basal patches imaged by TIRF microscopy. (A) Intensities normalised to the mean cytoplasmic fluorescence (1 = average cytoplasmic signal). (B) Intensities normalised to the average of the 10 highest values per scan (set as 1.0). Sample size (N) = 3 biological replicates.

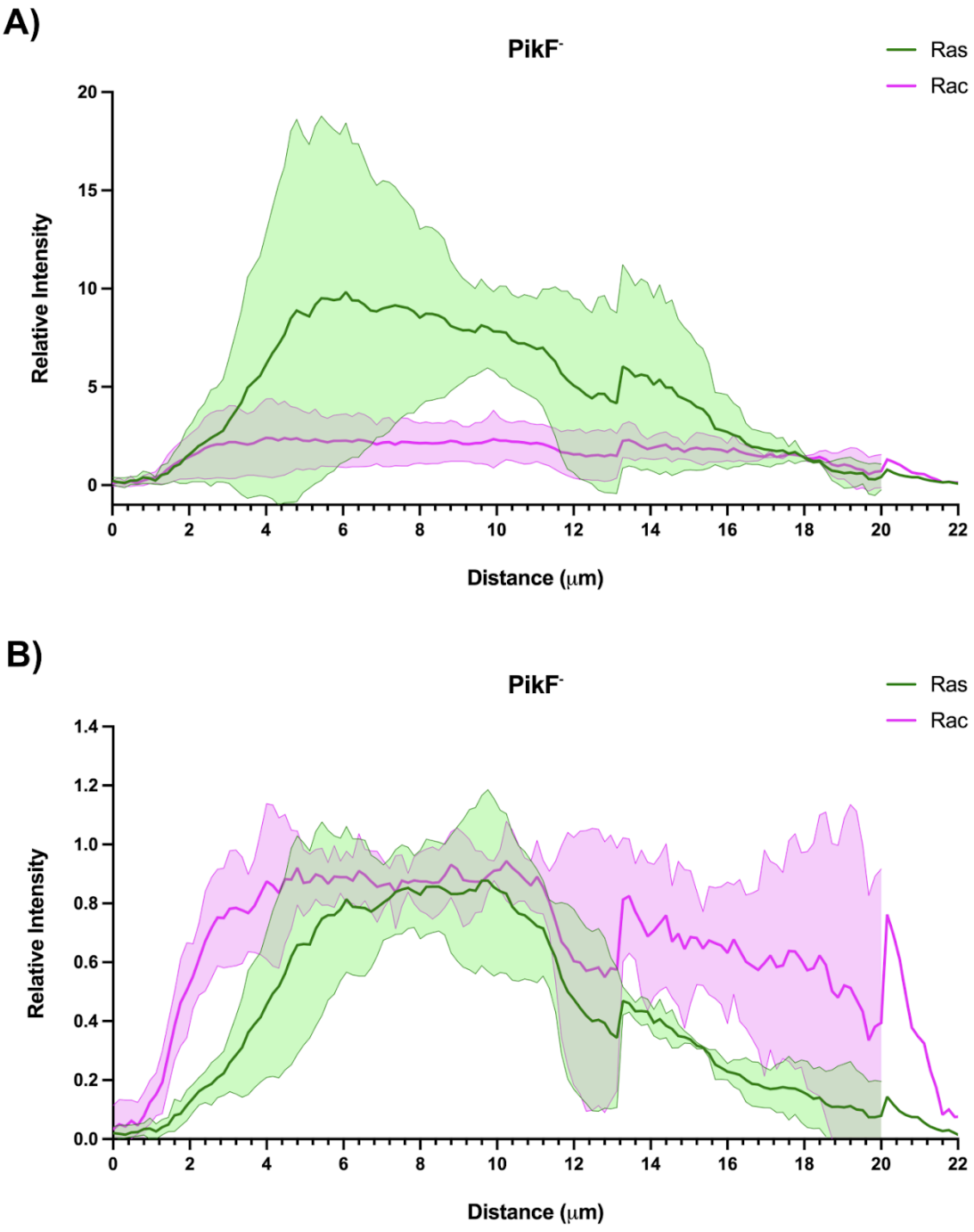

Figure 4.8: Relative intensity profiles of Ras and Rac signals across basal membrane patches in PikF$^-$ cells. Signal intensities of GFP-Raf1-RBD (active Ras) and PakB-CRIB-mCherry (active Rac) were measured from line scans drawn across basal patches imaged by TIRF microscopy. (A) Intensities normalised to the mean cytoplasmic fluorescence (1 = average cytoplasmic signal). (B) Intensities normalised to the average of the 10 highest values per scan (set as 1.0). Sample size (N) = 3 biological replicates.

Rac1 Pull-Down Assays

To assess whether the Rac signalling dysregulation described above correlates with increased levels of active Rac1 in PikF$^-$ cells, Rac1 Pull-Down assays were performed using lysates from wild-type (Ax2), PikA/B$^-$, and PikF$^-$ cells. Western blots from three biological replicates are shown in Figure 4.9, alongside their respective band intensity measurements relative to Ax2. Active Rac levels in PikA/B$^-$ cells ranged from 0.82 to 1.70 relative to Ax2, while PikF$^-$ cells displayed a range from 0.72 to 1.60. Due to this variation across replicates, it remains inconclusive whether significant differences in active Rac1 levels exist among the three strains. It is important to note that the Rac1 Pull-Down kit used (Cytoskeleton, Inc.) is optimised for detecting GTP-bound human Rac and Cdc42 proteins. The kit's positive (GTPγS) and negative (GDP) controls failed to function reliably with *D. discoideum* lysates, suggesting that further protocol optimisation is necessary. Additionally, the anti-DdRac1A monoclonal antibody used, produced a band at ~35 kDa, while the predicted molecular weight for *D. discoideum* Rac1A/B/C is ~22 kDa. This discrepancy raises concerns about antibody specificity and whether the detected signal corresponds to the expected Rac isoforms.

Taken together, while Rac dysregulation is clearly evident in microscopy-based spatial analyses of PikF$^-$ cells, the biochemical data from Rac1 Pull-Down assays remain inconclusive. It is possible that the observed signalling defects stem from purely mislocalised Rac1 activity, and total activity is not increased. Alternatively, unidentified over-activated small GTPases could be responsible for the disruption in Rac signalling observed in PikF$^-$ cells. Further validation of antibody specificity and the development of *D. discoideum*-specific assay conditions will be essential for drawing firm conclusions.

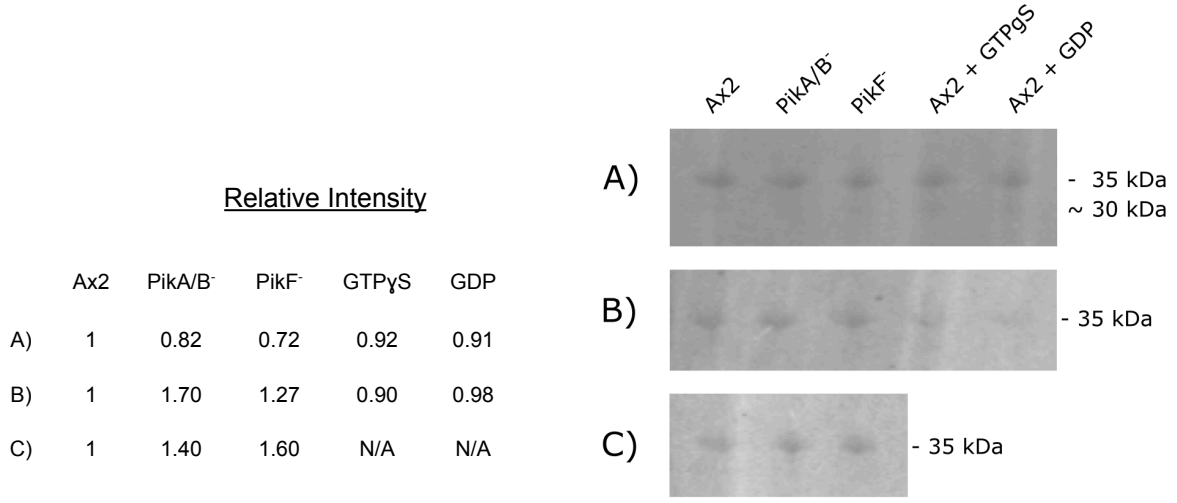

Relative Intensity

	Ax2	PikA/B$^-$	PikF$^-$	GTPγS	GDP
A)	1	0.82	0.72	0.92	0.91
B)	1	1.70	1.27	0.90	0.98
C)	1	1.40	1.60	N/A	N/A

Figure 4.9: Western blot analysis of Rac1 Pull-Down samples from wild-type (Ax2), PikA/B$^-$ and PikF$^-$ cells. Blots were probed using a monoclonal anti-DdRac1A antibody kindly provided by Professor Jan Faix (University of Hannover). Relative band intensities were quantified using the Gel Analysis tool in Fiji (ImageJ) and normalised to the corresponding Ax2 control for each replicate.

4.2.2 Altered F-actin and PIP_3 Dynamics in PikA and PikF Mutant Cells

To investigate the effects of PikA and PikF loss on cytoskeletal dynamics, the F-actin and PIP_3 probes RFP-LifeAct and GFP-PH-PkgE, respectively, were co-expressed in WT (Ax2), PikA/B$^-$, PikF$^-$ and PikA/B/F$^-$ cells for live cell imaging. Macropinocytic cup formation was visualised using Lattice Light Sheet Microscopy, and to examine F-actin and PIP_3 dynamics in a simpler, planar context, basal waves were imaged using Spinning Disk Confocal Microscopy. Across both processes, the mutant cell lines displayed distinct and genotype-specific aberrant F-actin and PIP_3 dynamics.

A comparison of pinocytic activity across genotypes is shown in Figure 4.10. Ax2 cells form large, F-actin-driven macropinocytic cups (Figure 4.11), whereas PikA/B$^-$, PikF$^-$ and PikA/B/F$^-$ cells generate smaller, F-actin-dependent pinocytic structures. In PikA/B$^-$ and PikA/B/F$^-$ cells, these small vesicles – difficult to classify definitively as macropinosomes due to their size – originate from non-protruding actin assemblies and gradually acquire GFP-PH-PkgE signal upon internalisation (Figures 4.12 and 4.13). Whether this delayed labelling reflects probe binding to PIP_3 or to $PI(3,4)P_2$ remains unclear. However, the data suggest that some fluid-phase uptake resembling clathrin-independent, microscale endocytosis occurs in the absence of large macropinocytic cup formation. Similarly, PikF$^-$ cells can internalise small volumes of extracellular fluid through invaginations formed by actin and PIP_3 domains at the base of what appear to be large, structurally compromised macropinocytic cups (Figure 4.14). Notably, the PikF$^-$ cell in Figure 4.14 exhibits prominent F-actin and PIP_3 structures that are entirely uncoupled. Moreover, the PikA/B/F$^-$ cell in Figure 4.13 shows extensive protruding F-actin structures lacking PIP_3 association – features absent in the PikA/B$^-$ cell (Figure 4.12). These observations support a disruption in the coupling between cytoskeletal activity and phosphoinositide signalling in the absence of PikF.

Striking differences in F-actin and PIP_3 dynamics are also evident in basal waves of Ax2, PikA/B$^-$, PikF$^-$ and PikA/B/F$^-$ cells (Figure 4.15). In Ax2 cells, F-actin polymerisation is organised around a central patch of PIP_3. As the wave propagates, the entire F-actin/PIP_3 structure moves unidirectionally, with F-actin polymerisation shifting from the front to the rear of the PIP_3 patch – indicating coordinated zones of F-actin polymerisation and depolymerisation (Figure 4.16). In PikA/B$^-$ cells, where the central PIP_3 patch is absent, this directional coordination is lost. As a result, the basal wave's travelling motion is impaired, leading to the collapse of the F-actin structure toward its centre (Figure 4.17). This may result from the rear zone of F-actin polymerisation catching up with the front before effective disassembly occurs, causing the structure to implode in the absence of spatial cues provided by PIP_3. In contrast, PikF$^-$ cells exhibit a different disruption: the F-actin/PIP_3 structure fails to move unidirectionally and instead expands outward in multiple directions. This lack of coordinated propagation results in fragmentation of the wave into multiple independent structures (Figure 4.18). These observations suggest that in the absence of PikF, there is neither a feedback mechanism to constrain PIP_3 domain expansion nor a means to spatially organise F-actin polymerisation and depolymerisation within the basal wave. In PikA/B/F$^-$ cells, F-actin structures appear entirely uncoupled, and discrete patches of F-actin flash sporadically across the basal surface (Figure 4.19). This further highlights the need for PI3K activity in the coordination of highly structured cytoskeletal dynamics.

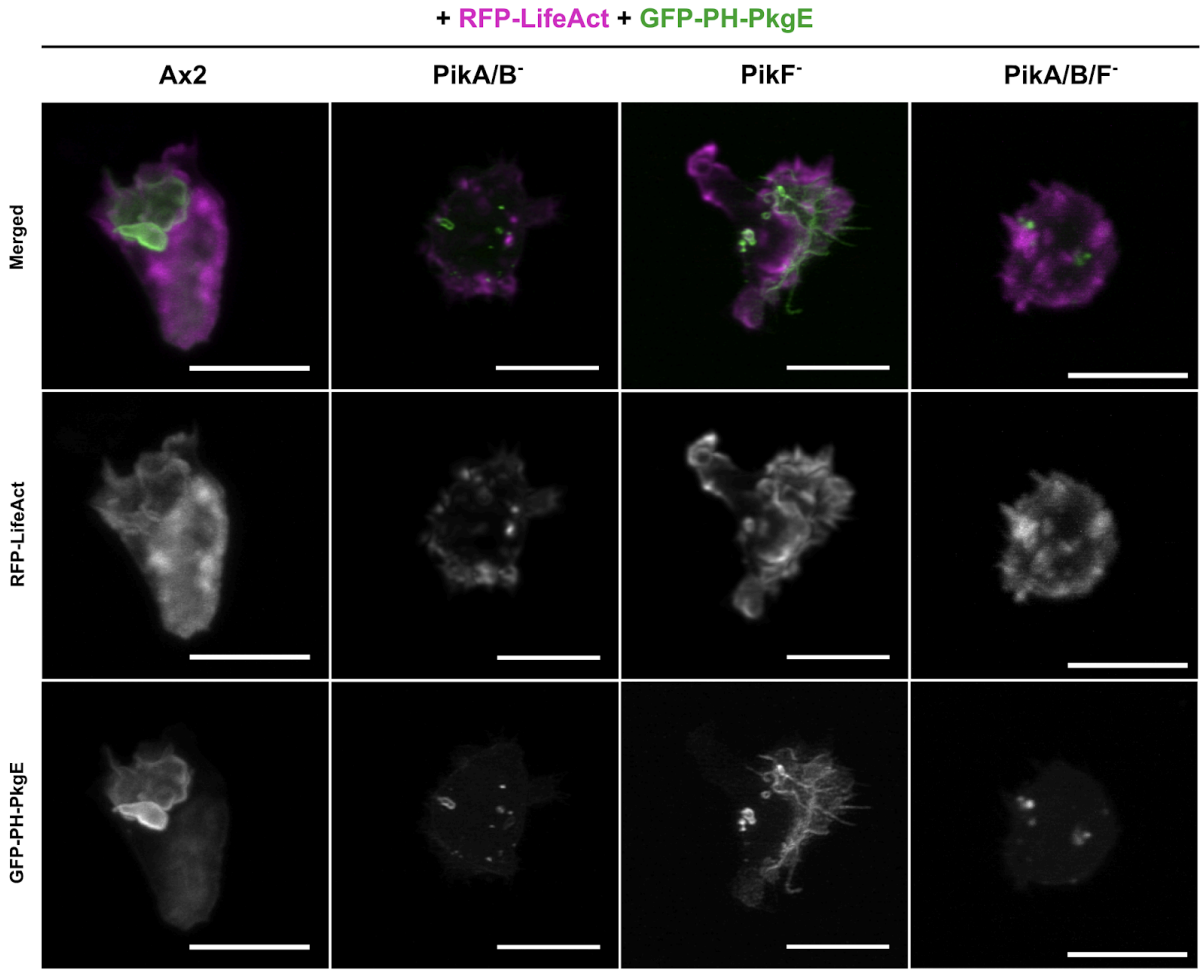

Figure 4.10: Representative pinocytic events in wild-type (Ax2), PikA/B$^-$, PikF$^-$ and PikA/B/F$^-$ cells. RFP-LifeAct (magenta) labels filamentous actin (F-actin), and GFP-PH-PkgE (green) binds PIP_3. Images were acquired using Lattice Light Sheet Microscopy. Deconvoluted maximum intensity projections are shown for Ax2, PikA/B$^-$, and PikF$^-$ cells, while a raw maximum intensity projection is shown for PikA/B/F$^-$. The scale bar represents 10 µm and is 4 pixels thick.

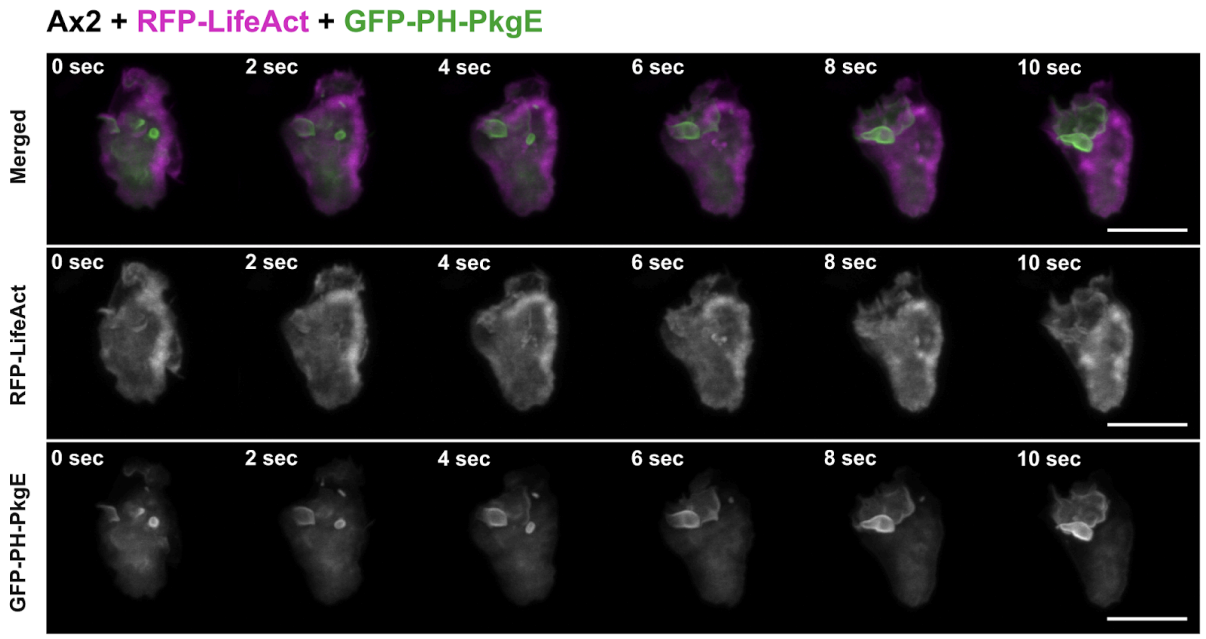

Figure 4.11: Macropinocytic cup formation in wild-type (Ax2) cells. RFP-LifeAct (magenta) labels filamentous actin (F-actin), and GFP-PH-PkgE (green) binds PIP_3. Images were acquired using Lattice Light Sheet Microscopy. Maximum intensity projections are shown. The scale bar represents 10 µm and is 4 pixels thick. See also Supplementary Movie 4 (SM4). This Ax2 control movie was kindly provided by Dr Judith Lutton (University of Warwick).

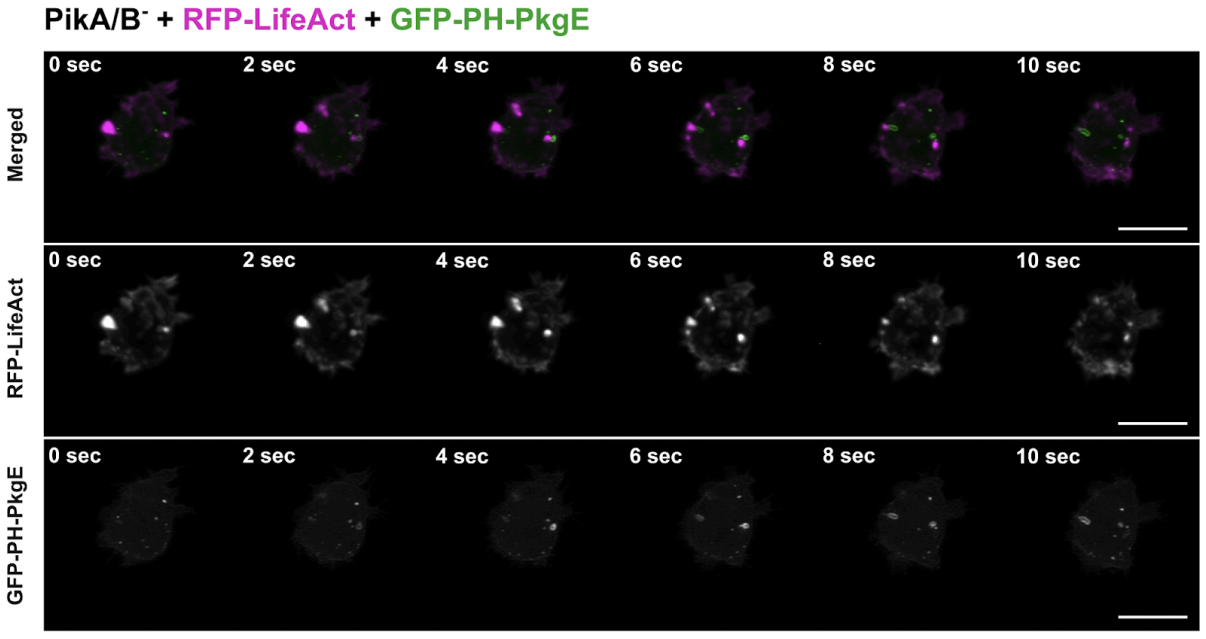

Figure 4.12: Pinocytic events in PikA/B$^-$ cells. RFP-LifeAct (magenta) labels filamentous actin (F-actin), and GFP-PH-PkgE (green) binds PIP_3. Images were acquired using Lattice Light Sheet Microscopy. Maximum intensity projections are shown. The scale bar represents 10 µm and is 4 pixels thick. See also Supplementary Movie 5 (SM5).

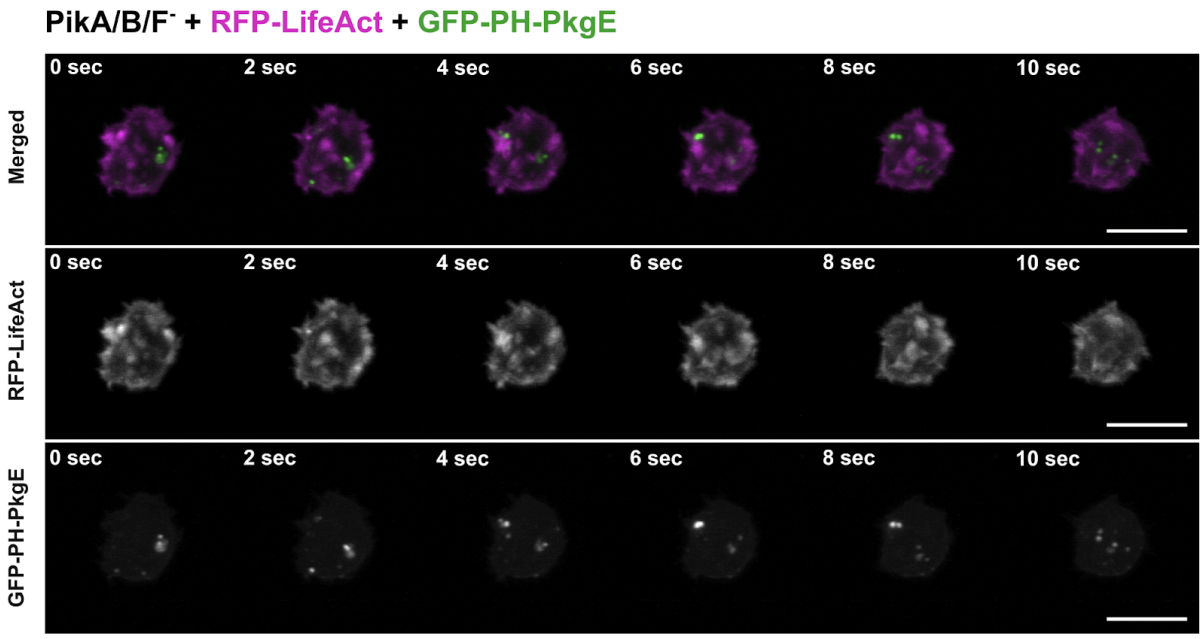

Figure 4.13: Pinocytic events in PikA/BF$^-$ cells. RFP-LifeAct (magenta) labels filamentous actin (F-actin), and GFP-PH-PkgE (green) binds PIP_3. Images were acquired using Lattice Light Sheet Microscopy. Maximum intensity projections are shown. The scale bar represents 10 µm and is 4 pixels thick. See also Supplementary Movie 7 (SM7).

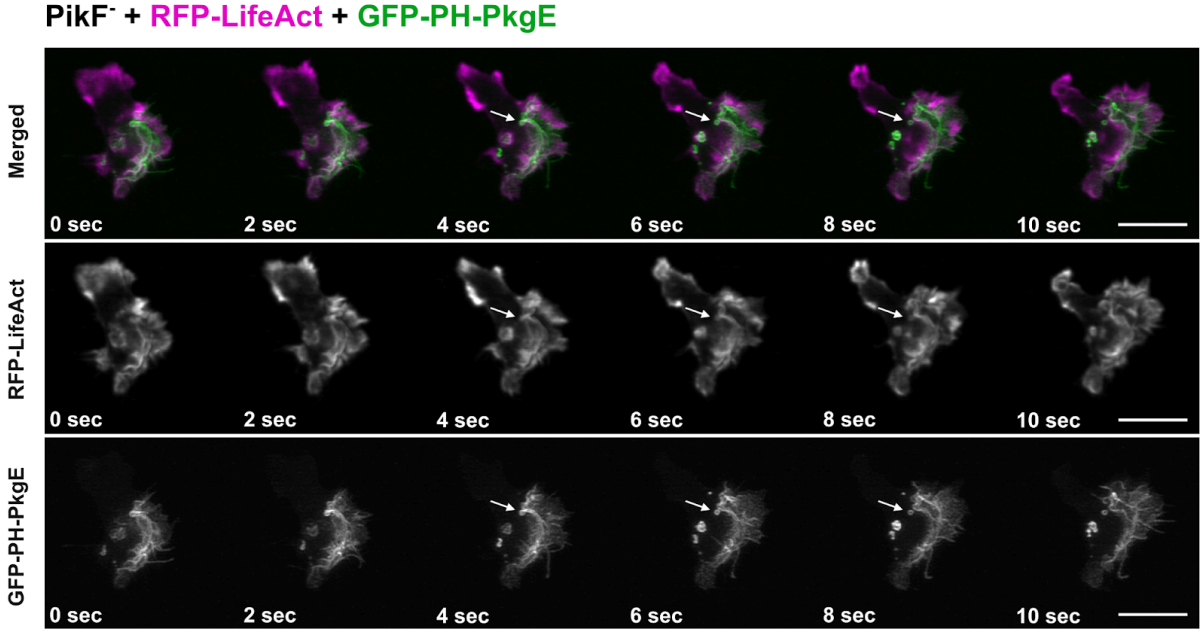

Figure 4.14: Pinocytic events in PikF$^-$ cells. RFP-LifeAct (magenta) labels filamentous actin (F-actin), and GFP-PH-PkgE (green) binds PIP_3. Images were acquired using Lattice Light Sheet Microscopy. Maximum intensity projections are shown. The scale bar represents 10 µm and is 4 pixels thick. See also Supplementary Movie 6 (SM6).

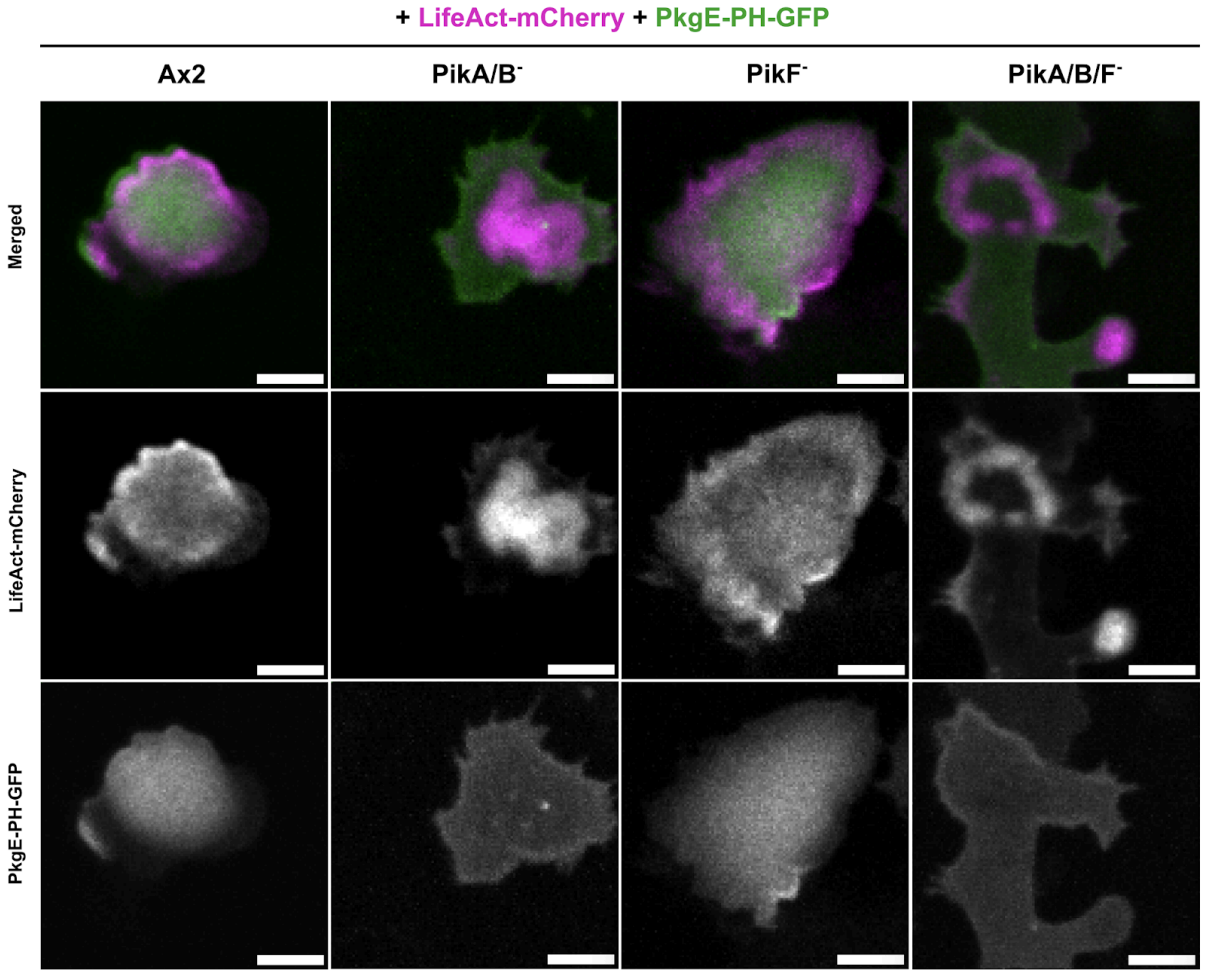

Figure 4.15: Localisation of F-actin and PIP_3 at basal waves in wild-type (Ax2), PikA/B$^-$, PikF$^-$ and PikA/B/F$^-$ cells. LifeAct-mCherry (magenta) labels filamentous actin (F-actin), and PkgE-PH-GFP (green) binds PIP_3. Images were acquired using a Nikon W1 Spinning Disk Confocal Microscope. Maximum intensity projections of three Z-slices are shown. The scale bar represents 5 µm and is 4 pixels thick.

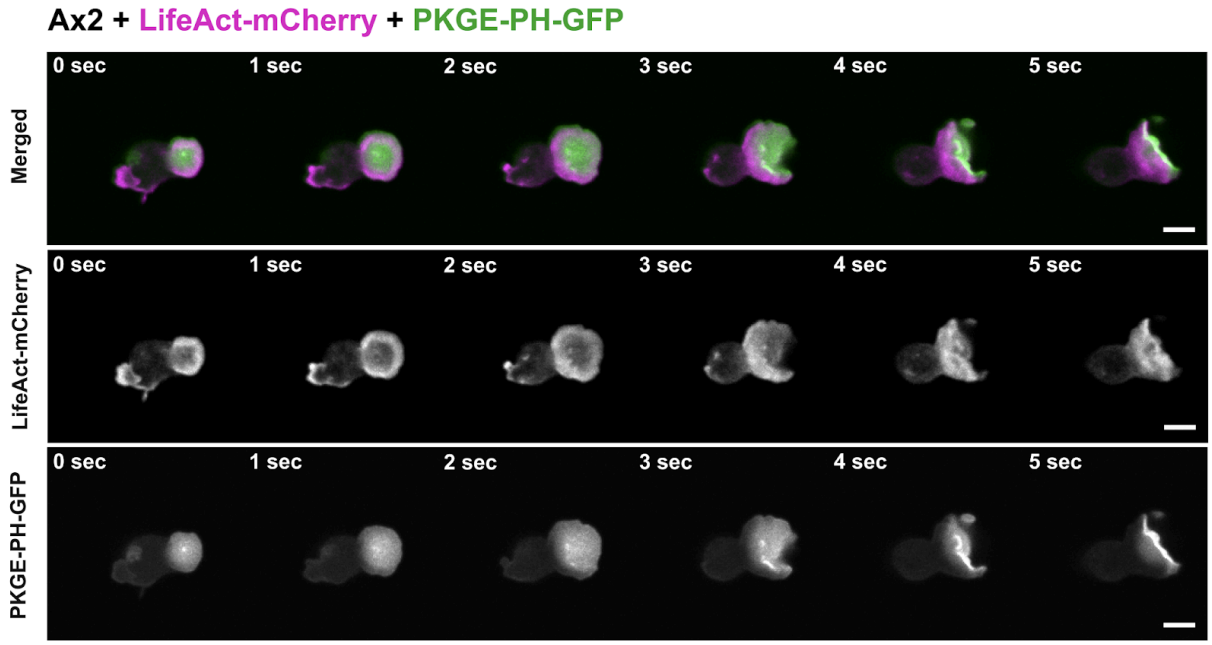

Figure 4.16: Localisation of F-actin and PIP_3 at basal waves in wild-type (Ax2) cells. LifeAct-mCherry (magenta) labels filamentous actin (F-actin), and PkgE-PH-GFP (green) binds PIP_3. Images were acquired using a Nikon W1 Spinning Disk Confocal Microscope. Maximum intensity projections of three Z-slices are shown. The scale bar represents 5 µm and is 4 pixels thick. See also Supplementary Movie 8 (SM8).

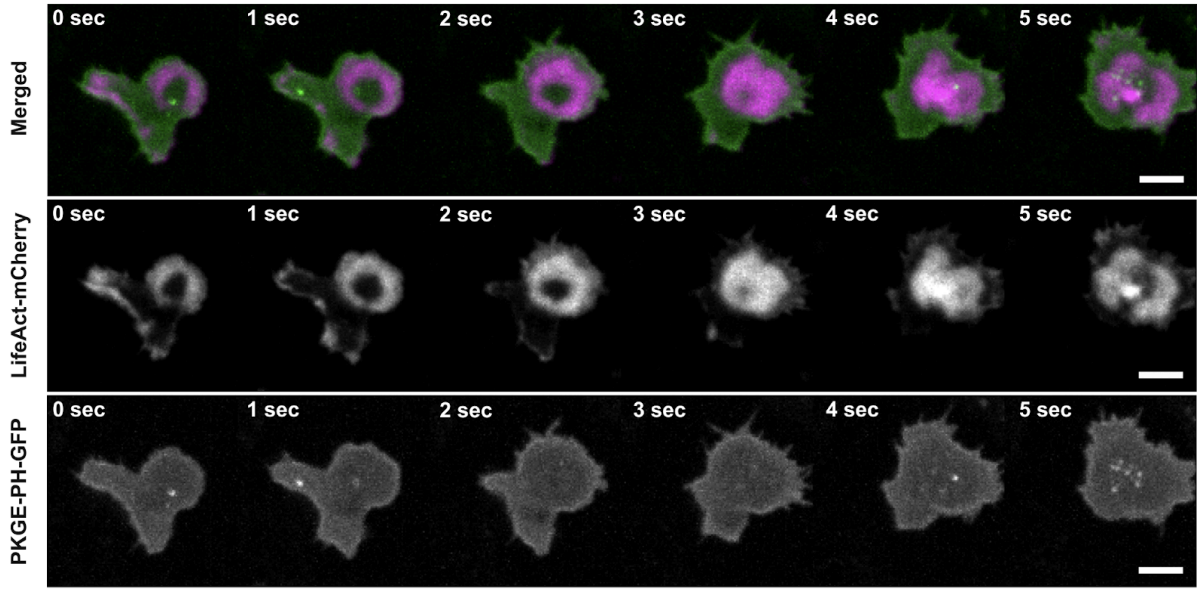

Figure 4.17: Localisation of F-actin and PIP_3 at basal waves in PikA/B$^-$ cells. LifeAct-mCherry (magenta) labels filamentous actin (F-actin), and PkgE-PH-GFP (green) binds PIP_3. Images were acquired using a Nikon W1 Spinning Disk Confocal Microscope. Maximum intensity projections of three Z-slices are shown. The scale bar represents 5 µm and is 4 pixels thick. See also Supplementary Movie 9 (SM9).

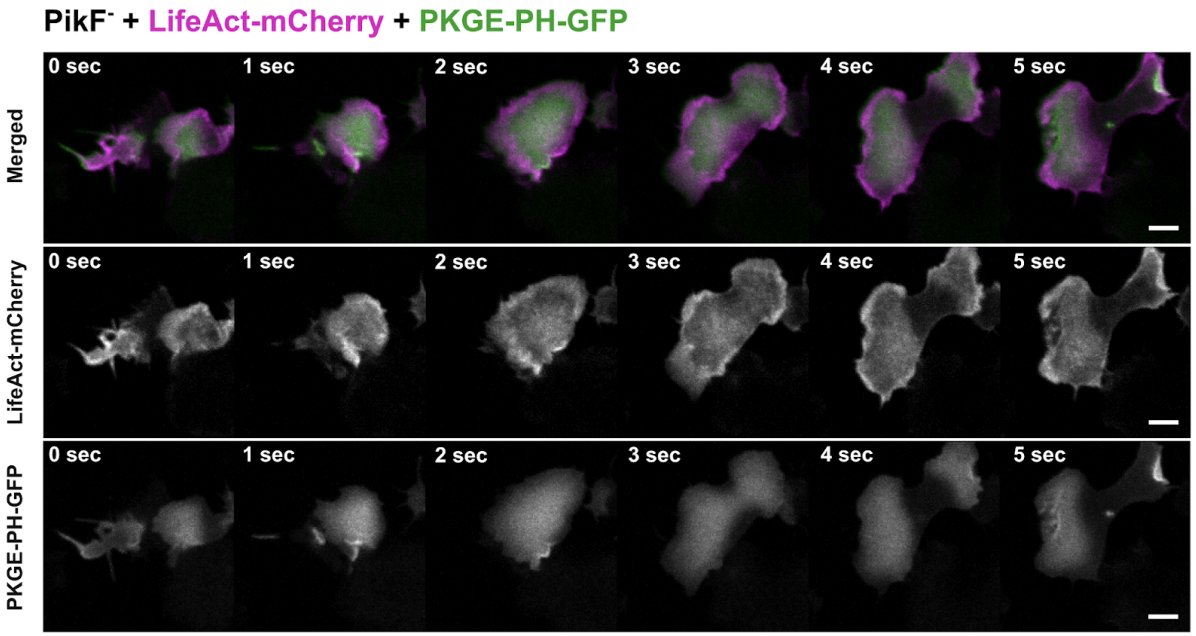

Figure 4.18: Localisation of F-actin and PIP_3 at basal waves in PikF$^-$ cells.
LifeAct-mCherry (magenta) labels filamentous actin (F-actin), and PkgE-PH-GFP (green) binds PIP_3. Images were acquired using a Nikon W1 Spinning Disk Confocal Microscope. Maximum intensity projections of three Z-slices are shown. The scale bar represents 5 µm and is 4 pixels thick. See also Supplementary Movie 10 (SM10).

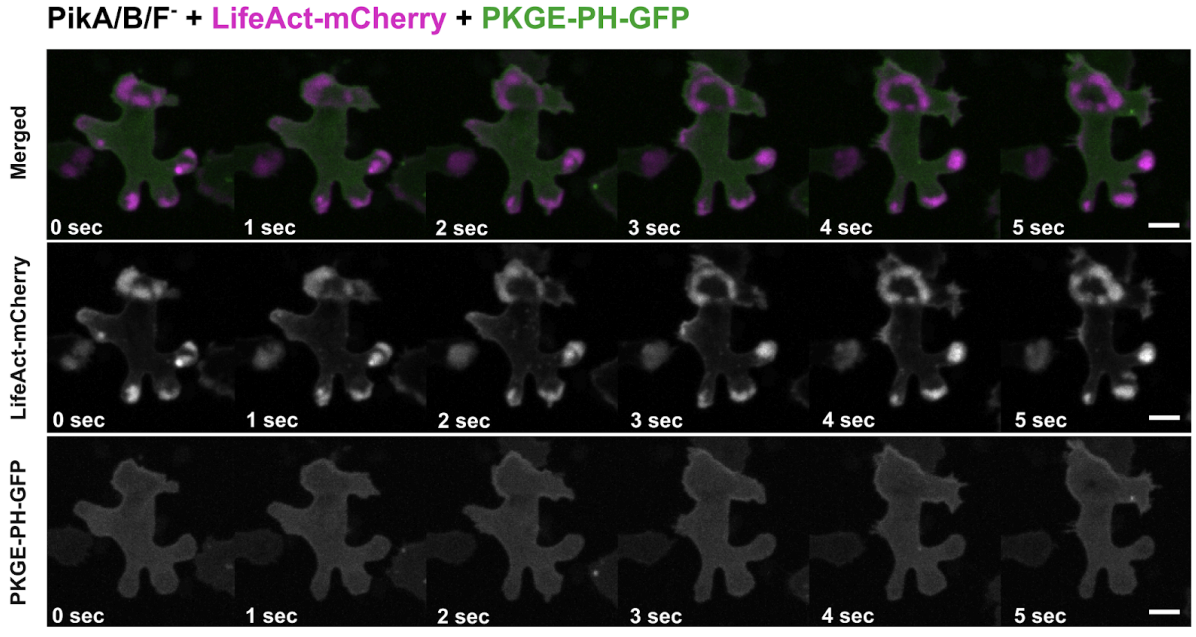

Figure 4.19: Localisation of F-actin and PIP_3 at basal waves in PikA/B/F$^-$ cells.
LifeAct-mCherry (magenta) labels filamentous actin (F-actin), and PkgE-PH-GFP (green) binds PIP_3. Images were acquired using a Nikon W1 Spinning Disk Confocal Microscope. Maximum intensity projections of three Z-slices are shown. The scale bar represents 5 µm and is 4 pixels thick. See also Supplementary Movie 11 (SM11).

4.2.3 F-actin and PIP_3 Dynamics in Phagocytic Cup Formation

To explore whether the disrupted cytoskeletal dynamics in PikA/B$^-$ and PikF$^-$ cells also impair their ability to phagocytose large particles, cells were imaged after a 30-minute exposure to Alexa594-labelled yeast. The number of ingested yeast particles per cell was quantified for each strain. While there were no significant differences in yeast uptake between wild-type (0.46 yeast/cell) and PikF$^-$ cells (0.42 yeast/cell), PikA/B$^-$ cells exhibited a markedly reduced phagocytic capacity, averaging just 0.08 yeast per cell (Figure 4.20).

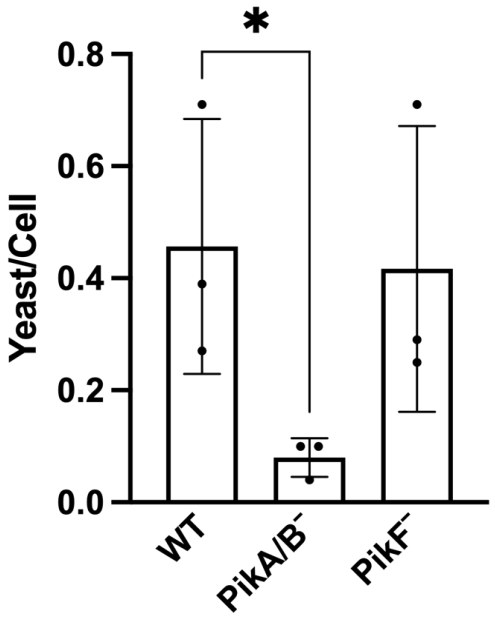

Figure 4.20: Phagocytosis defects in PikA/B$^-$ compared to wild-type (Ax2) and PikF$^-$ cells. Cells were exposed to Alexa594-labelled yeast for 30 minutes, and phagocytic uptake was quantified by live-cell microscopy. The number of yeast particles internalised per cell was manually counted, and the average yeast-to-cell ratio was calculated. An ordinary one-way ANOVA across all three strains detected no significant differences due to sample variability. However, a targeted unpaired t-test comparing PikA/B$^-$ to WT cells revealed a statistically significant reduction in phagocytic uptake (P = 0.0471), as shown in the chart.

To further investigate this phenotype, wild-type (Ax2), PikA/B$^-$, PikF$^-$, and PikA/B/F$^-$ cells co-expressing F-actin and PIP_3 probes were incubated with Alexa405-labelled budding yeast for live-cell imaging via Spinning Disk Confocal Microscopy. This allowed real-time visualisation of phagocytic cup formation, and the frequency of successful cup closure events was quantified. Due to experimental constraints, three biological replicates were obtained for PikA/B$^-$ and PikF$^-$ cells, but only two replicates were obtained for PikA/B/F$^-$, and a single replicate was obtained for Ax2. As a result, statistical comparison was only possible between PikA/B$^-$ and PikF$^-$ cells, where a significant difference in phagocytic cup closure

success was observed (0.20 vs. 0.74, P = 0.0005). Although not statistically tested, PikA/B/F^{-} cells exhibited an even more severe phagocytosis impairment, with an average success rate of 0.05 across the two replicates (Figure 4.21). Interestingly, the single replicate of Ax2 cells yielded a phagocytic cup closure success rate of only 41%, suggesting that successful phagocytosis in wild-type cells may be less frequent than in PikF^{-} cells. This may reflect their capacity for efficient macropinocytosis, reducing reliance on phagocytosis for nutrient uptake. Indeed, we observed several instances in which attempted phagocytosis was aborted in favour of macropinocytic cup formation in Ax2 cells (Figures 4.22A and 4.22B). These observations raise the possibility that phagocytosis and macropinocytosis in *D. discoideum* rely on shared cytoskeletal machinery, yet are governed by distinct regulatory pathways that prevent them from occurring simultaneously or transitioning seamlessly between modes.

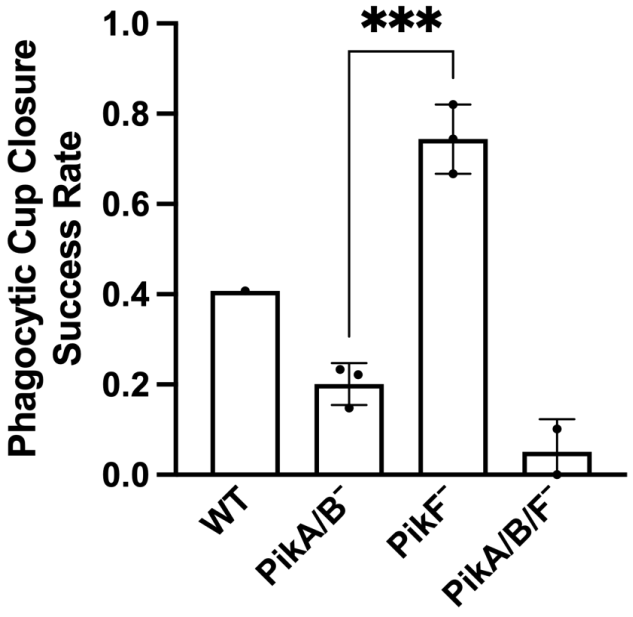

Figure 4.21: Rate of successful phagocytic cup closure events in wild-type (Ax2), PikA/B^{-}, PikF^{-}, and PikA/B/F^{-} cells. Cells co-expressing F-actin and PIP_3 probes were imaged in suspension with Alexa405-labelled budding yeast using a Nikon W1 Spinning Disk Confocal Microscope. Phagocytic cup closure success rates were quantified across strains. Owing to limited biological replication, formal statistical testing was restricted to a comparison between PikA/B^{-} and PikF^{-}, using an unpaired t-test, which indicated a significant difference in closure rates (P = 0.0005). N denotes the number of successful phagocytic events scored: Ax2 N = 11; PikA/B^{-} N = 27; PikF^{-} N = 70; PikA/B/F^{-} N = 11.

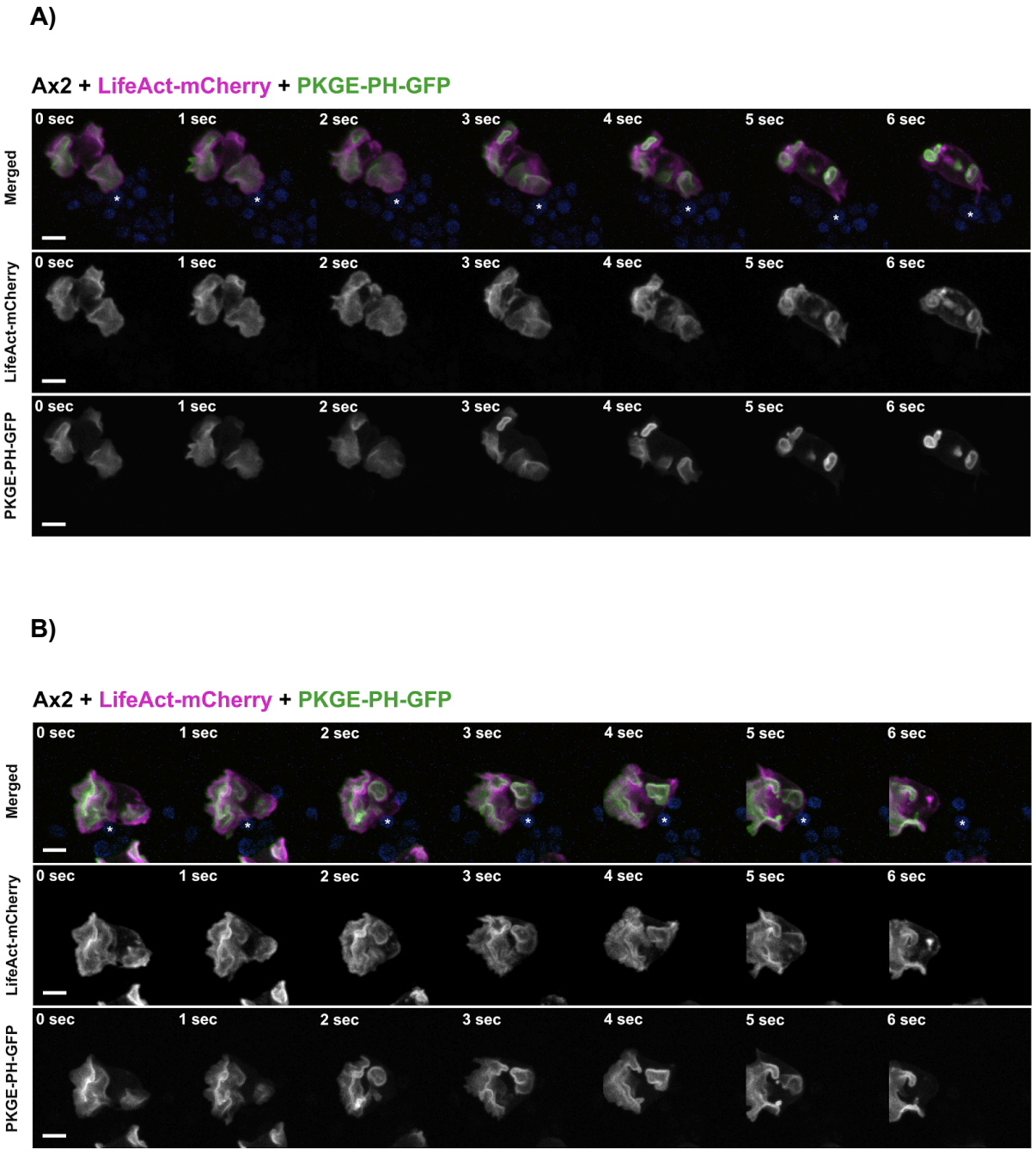

Figure 4.22: Failure of phagocytic cup formation in favour of macropinocytic cup closure in wild-type (Ax2) cells. A) Example 1. B) Example 2. Cells were imaged in suspension with Alexa405-labelled budding yeast using a Nikon W1 Spinning Disk Confocal Microscope. LifeAct-mCherry (magenta) labels filamentous actin (F-actin), and PkgE-PH-GFP (green) binds PIP_3. Maximum intensity projections are shown. Asterisks (*) indicate the yeast particles of interest. The scale bar represents 5 µm and is 4 pixels thick. See also Supplementary Movies 12 (SM12) and 13 (SM13).

Live imaging movies of phagocytosis in wild-type (Ax2), PikA/B$^-$, PikF$^-$, and PikA/B/F$^-$ cells revealed the cytoskeletal behaviours underlying successful and failed phagocytic cup formation in each strain. In Ax2 cells, Figure 4.23A illustrates a successful event where F-actin and PIP_3 initially co-localise at the site of yeast engagement. F-actin polymerisation drives membrane extension around the particle, with a stronger actin signal accumulating at the cup rim, and a similar PIP_3 gradient is observed. Upon cup closure, PkgE-PH-GFP redistributes evenly around the phagosome before gradually dissociating, while F-actin disassembles unevenly (Figure 4.24). In contrast, Figure 4.23B shows a failed phagocytosis event in Ax2 cells where cup extension is aborted as a competing macropinocytic cup closes elsewhere. In this case, F-actin and PIP_3 signals fade from the yeast-binding site without engulfment.

In PikA/B$^-$ cells, successful phagocytosis (Figure 4.25A) is driven by F-actin polymerisation in the absence of early PIP_3 signalling. PkgE-PH-GFP is recruited to the phagosome only after cup closure, at which point F-actin gradually disassembles. Unsuccessful events, such as the one in Figure 4.25B, feature early recruitment of the PIP_3 probe to the base of the extending cup, followed by premature F-actin disassembly before the cup closes. This raises the possibility that premature PIP_3 signalling may trigger actin destabilisation and abort phagocytosis.

In PikF$^-$ cells, there appears to be no regulatory interference between macropinocytosis and phagocytosis. As shown in Figure 4.26A, successful engulfment occurs when yeast particles enter the large, dynamic membrane ruffles described above as structurally compromised macropinocytic cups (see Figure 4.14; Section 4.2.2). In these instances, F-actin and PIP_3 uniformly surround the particle from initial contact through to closure. In contrast, failed phagocytic events are typically associated with particle engagement at non-ruffling regions of the membrane, where PIP_3 recruitment is weak or absent and F-actin assembly cannot progress, preventing cup completion (Figure 4.26B). These findings suggest that phagocytosis in PikF$^-$ cells may depend on the passive capture of particles by pre-existing ruffles, rather than on active membrane extension initiated at the site of contact.

Interestingly, successful phagocytosis in PikA/B/F$^-$ cells resembles that of PikA/B$^-$ cells. As shown in Figure 4.27A, yeast particles are engulfed by F-actin-driven protrusions in the absence of early PIP_3 production, and PkgE-PH-GFP is recruited only after cup closure. Unlike PikA/B$^-$ cells, however, F-actin disassembly is slower after cup closure, and PIP_3 signal intensifies briefly before declining, at which point actin is re-assembled around the internalised particle. Conversely, failed phagocytic events in PikA/B/F$^-$ cells mirror those in PikA/B$^-$ cells: early PIP_3 generation coincides with premature F-actin disassembly and stalled cup progression (Figure 4.27B). Figure 4.28 presents six examples of forming phagosomes in PikA/B/F$^-$ cells, highlighting several patterns:

1. F-actin-driven phagocytic cups can progress independently of early PIP_3 signalling;

2. PkgE-PH-GFP is often recruited only after successful engulfment;

3. Early PIP_3 recruitment may correlate with failure to complete engulfment.

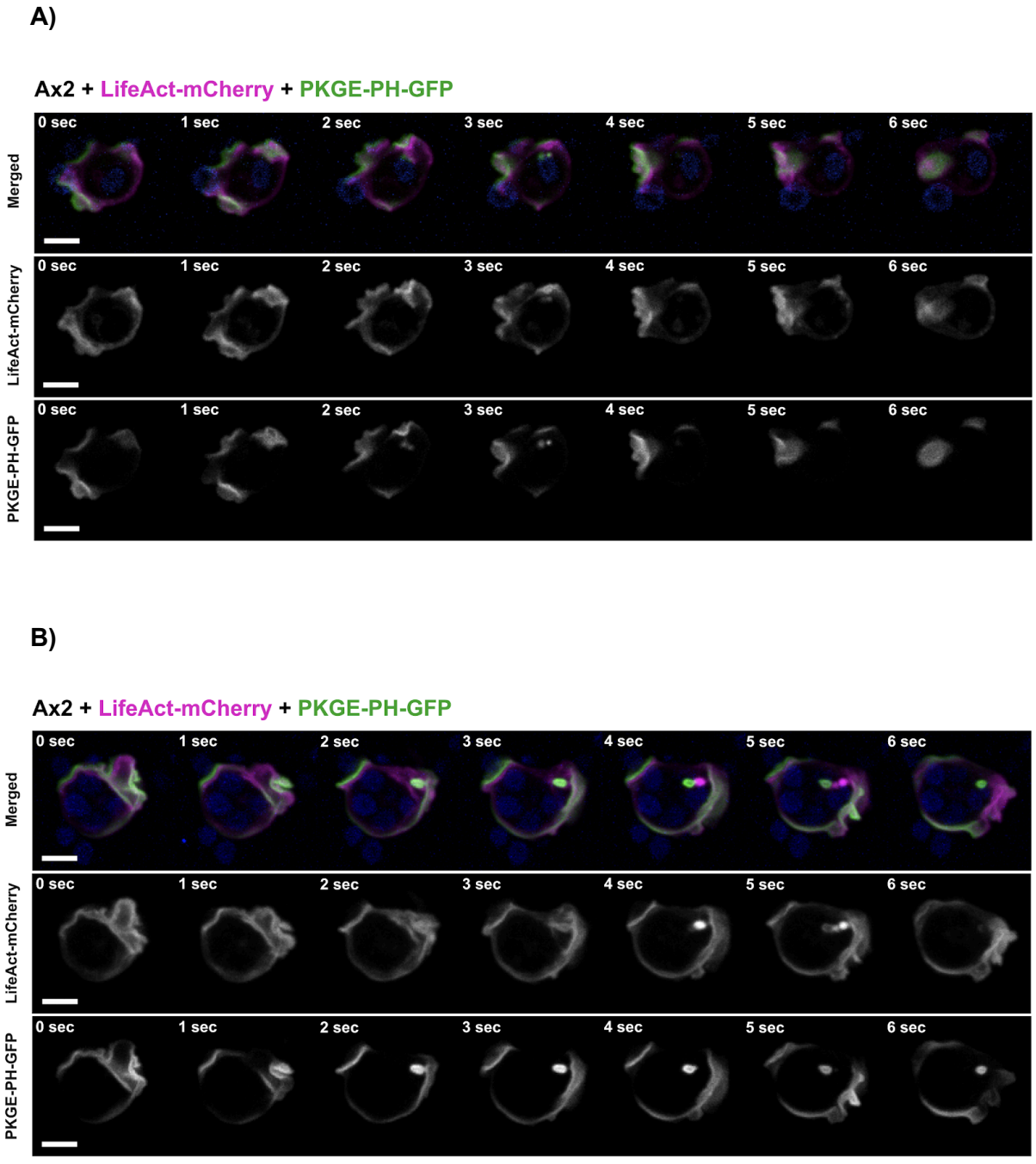

Figure 4.23: Successful (A) and unsuccessful (B) phagocytic cup formation in wild-type (Ax2) cells. Cells were imaged in suspension with Alexa405-labelled budding yeast using a Nikon W1 Spinning Disk Confocal Microscope. LifeAct-mCherry (magenta) labels filamentous actin (F-actin), and PkgE-PH-GFP (green) binds PIP_3. Maximum intensity projections of three Z-slices are shown. The scale bar represents 5 µm and is 4 pixels thick. See also Supplementary Movies 14 (SM14) and 15 (SM15).

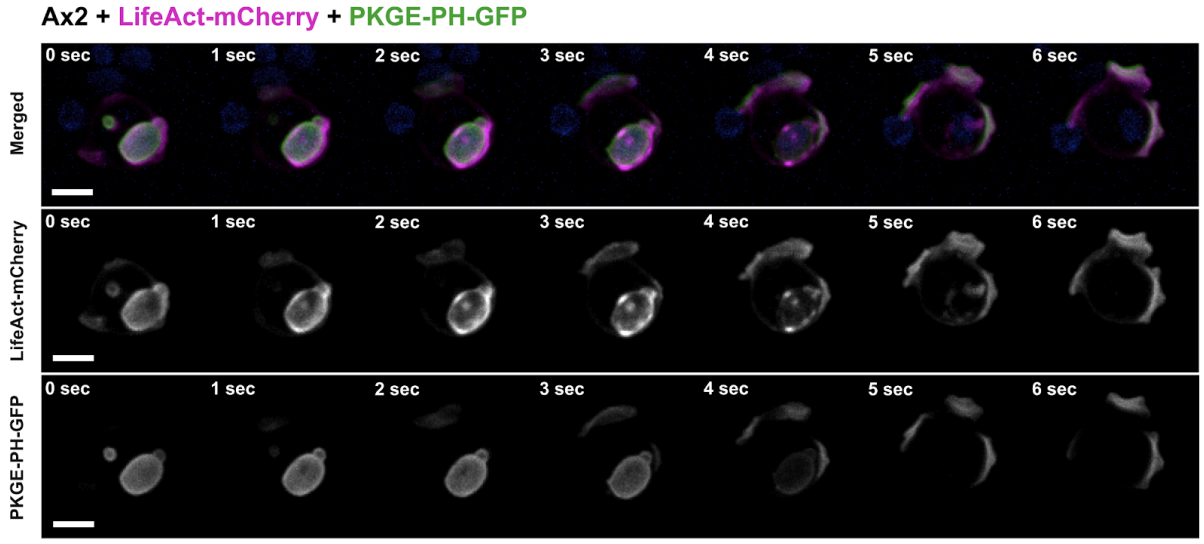

Figure 4.24: Post-engulfment disassembly of F-actin around a budding yeast particle in a wild-type (Ax2) cell. Cells were imaged in suspension with Alexa405-labelled budding yeast using a Nikon W1 Spinning Disk Confocal Microscope. LifeAct-mCherry (magenta) labels filamentous actin (F-actin), and PkgE-PH-GFP (green) binds PIP_3. Maximum intensity projections of three Z-slices are shown. The scale bar represents 5 µm and is 4 pixels thick. See also Supplementary Movie 16 (SM16).

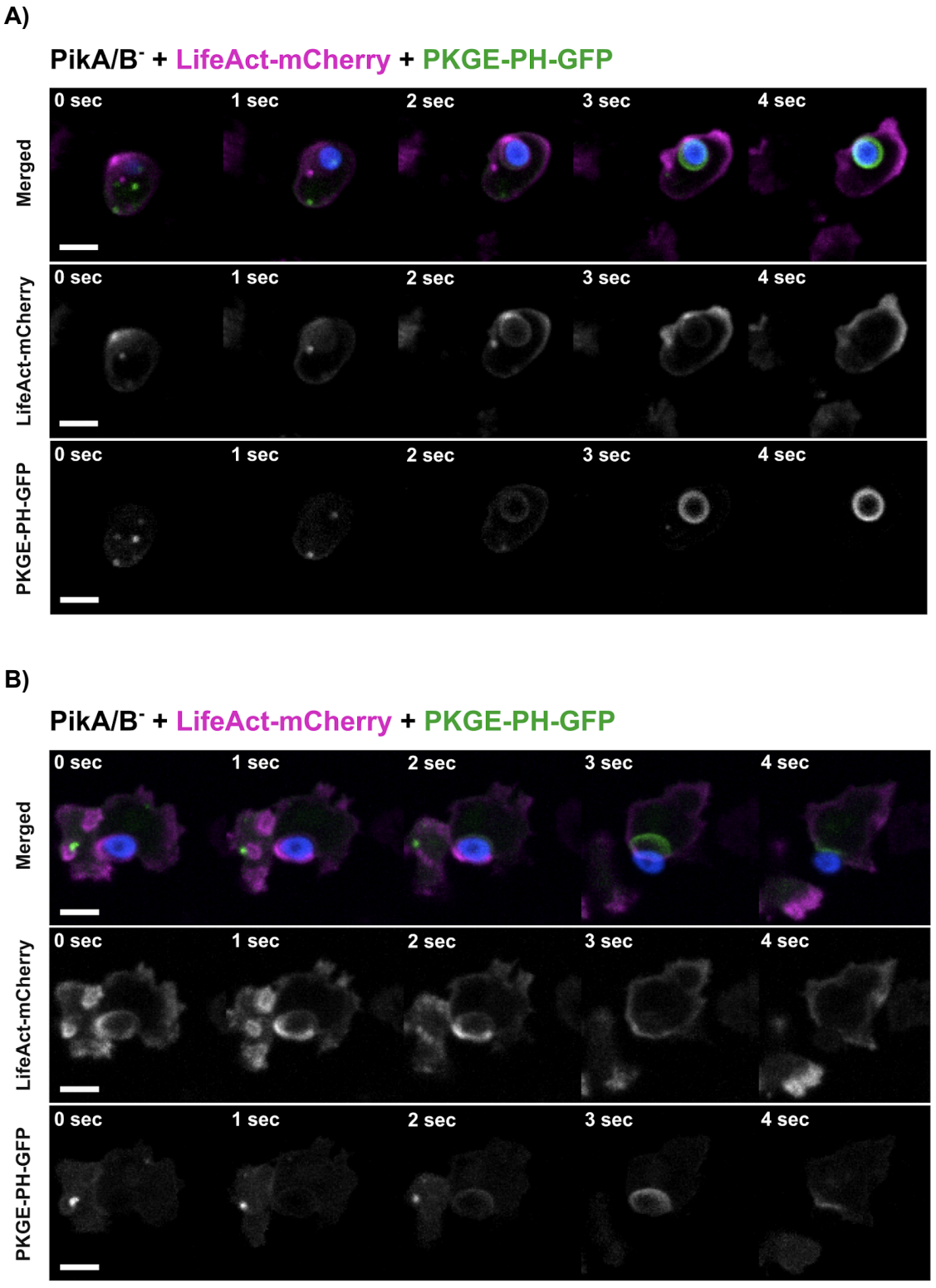

Figure 4.25: Successful (A) and unsuccessful (B) phagocytic cup formation in PikA/B⁻ cells. Cells were imaged in suspension with Alexa405-labelled budding yeast using a Nikon W1 Spinning Disk Confocal Microscope. LifeAct-mCherry (magenta) labels filamentous actin (F-actin), and PkgE-PH-GFP (green) binds PIP_3. Maximum intensity projections of three Z-slices are shown. The scale bar represents 5 µm and is 4 pixels thick. See also Supplementary Movies 17 (SM17) and 18 (SM18).

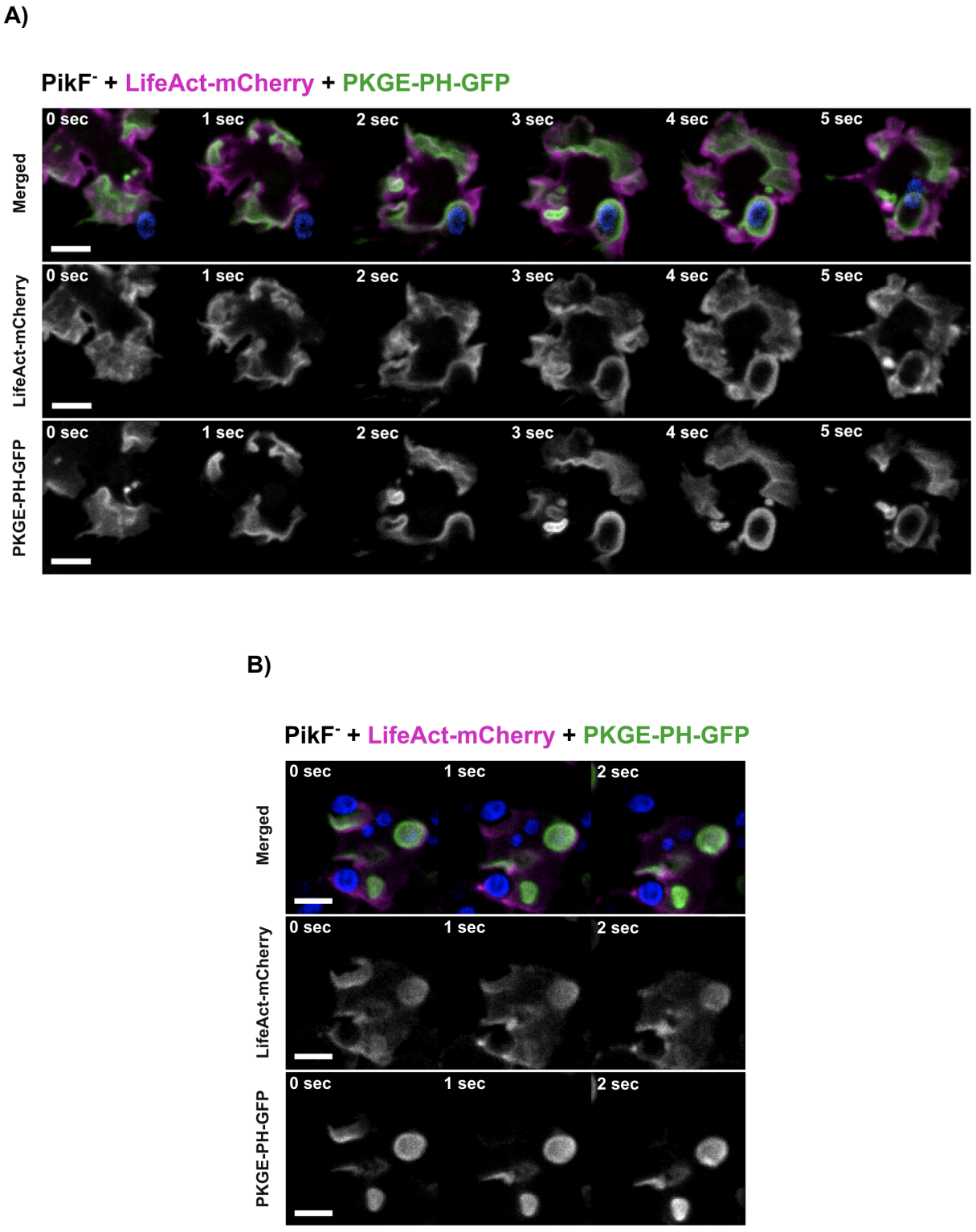

Figure 4.26: Successful (A) and unsuccessful (B) phagocytic cup formation in PikF$^-$ cells. Cells were imaged in suspension with Alexa405-labelled budding yeast using a Nikon W1 Spinning Disk Confocal Microscope. LifeAct-mCherry (magenta) labels filamentous actin (F-actin), and PkgE-PH-GFP (green) binds PIP_3. Maximum intensity projections of three Z-slices are shown. The scale bar represents 5 µm and is 4 pixels thick. See also Supplementary Movies 19 (SM19) and 20 (SM20).

A)

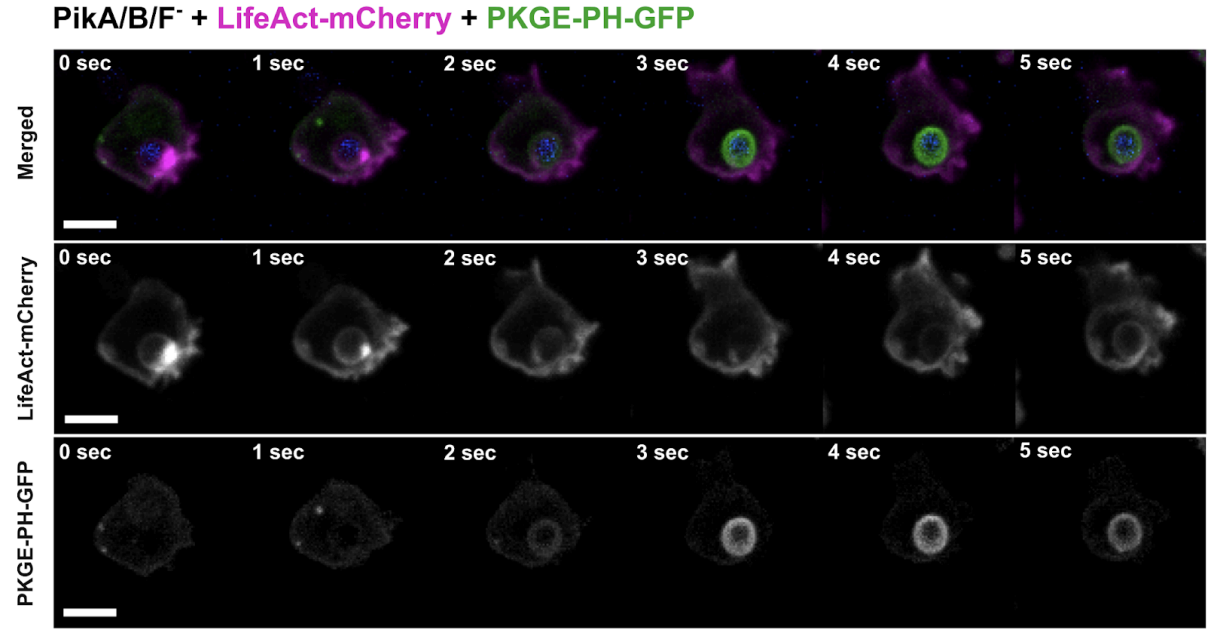

B)

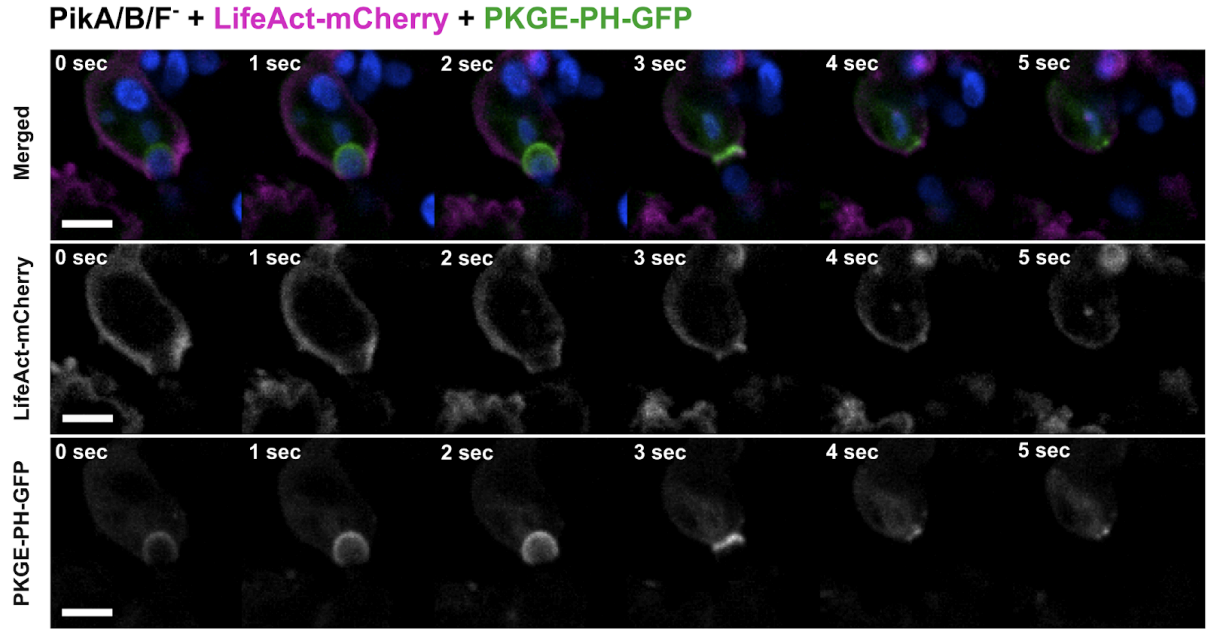

Figure 4.27: Successful (A) and unsuccessful (B) phagocytic cup formation in PikA/B/F⁻ cells. Cells were imaged in suspension with Alexa405-labelled budding yeast using a Nikon W1 Spinning Disk Confocal Microscope. LifeAct-mCherry (magenta) labels filamentous actin (F-actin), and PkgE-PH-GFP (green) binds PIP_3. Maximum intensity projections of three Z-slices are shown. The scale bar represents 5 µm and is 4 pixels thick. See also Supplementary Movies 21 (SM21) and 22 (SM22).

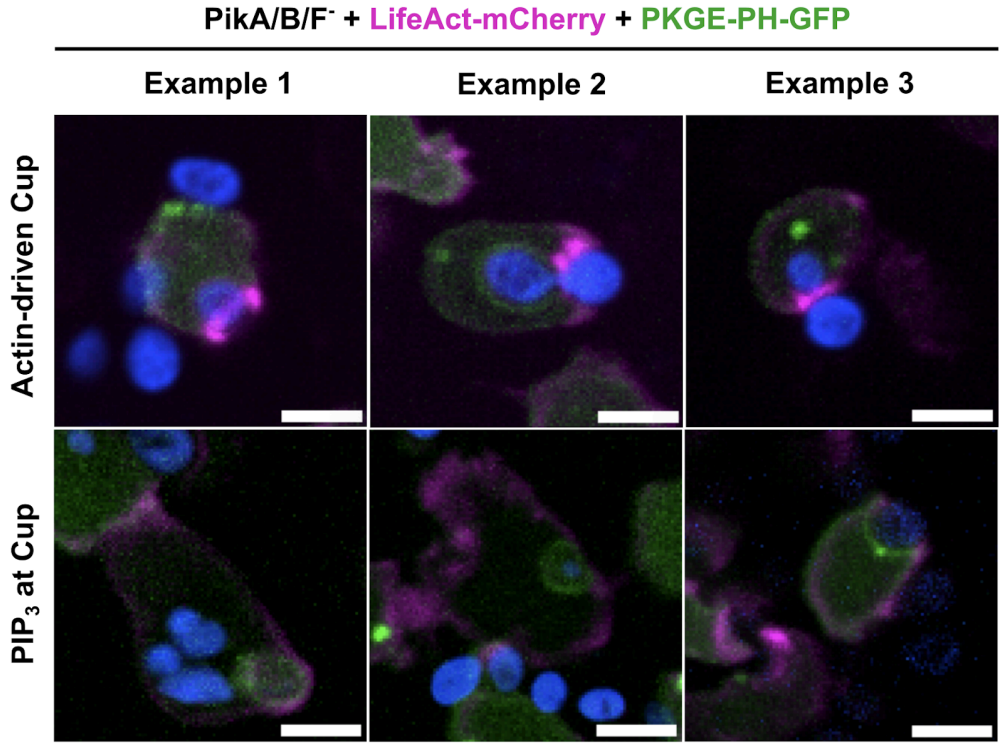

Figure 4.28: Examples of F-actin and PIP_3 localisation at phagocytic cups in PikA/B/F$^-$ cells. Cells were imaged in suspension with Alexa405-labelled budding yeast using a Nikon W1 Spinning Disk Confocal Microscope. LifeAct-mCherry (magenta) labels filamentous actin (F-actin), and PkgE-PH-GFP (green) binds PIP_3. Maximum intensity projections of three Z-slices are shown. The scale bar represents 5 µm and is 4 pixels thick.

4.3 Discussion

Rim feedback fails in PikF$^-$ cells, expanding Rac activity beyond the cup rim

Our findings reveal that PikA/B$^-$ and PikF$^-$ cells exhibit distinct Rac signalling defects at macropinocytic cups. Quantitative mapping of active Ras (GFP-Raf1-RBD) and active Rac (PakB-CRIB-mCherry) across cups showed isoform-specific perturbations. In contrast to RGBARG$^-$ cells (Buckley *et al.* 2020), which lose the distance differential between active Ras and Rac across macropinocytic cup cross-sections, PikA/B$^-$ cells display an increase in this distance, with active Rac extending approximately 2 µm beyond active Ras relative to wild-type (Ax2). More strikingly, in PikF$^-$ cells the localisation of active Rac is profoundly disrupted: rather than declining beyond the rim, active Rac rises from the cup interior, peaks at 5.5 µm outside the rim, and remains elevated. Although less dramatically, Ras signalling is also altered in both PI3K mutant strains, with a gradual signal decline inside the cup in PikA/B$^-$ cells, and a modest outward extension in PikF$^-$. These spatial shifts suggest that loss of PikF compromises the rim-based feedback required to confine Rac activity and maintain the geometry of actin-driven protrusions – consistent with the ‘spiky’ PikF$^-$ morphology quantified in Chapter 3 and its resemblance to Rac1 overexpression (Dumontier et al., 2000). In keeping with the PikF localisation patterns observed in macropinocytic cups (Chapter 3), these findings place PikF at the core of a rim-centred Rac-restriction mechanism, whereas PikA underpins basal cup organisation during the initiation stage of macropinocytosis.

Rac1 pull-down assays: technical challenges and interpretative caution

To assess whether Rac dysregulation stems from increased activation or broader membrane dispersion of Rac-GTP, we performed ‘Rac1/Cdc42’ pull-down assays. We detected no consistent increase in pull-down signal in PikF$^-$ relative to Ax2 or PikA/B$^-$, suggesting that the live-cell phenotypes likely reflect spatiotemporal mislocalisation rather than a bulk rise in Rac1 activity. However, these results are inconclusive: the commercial kit (Cytoskeleton Inc.) is mammalian-optimised and showed compatibility issues with *D. discoideum* lysates. Additionally, the anti-Rac1A antibody detected a ~35 kDa band rather than the expected ~22 kDa for *D. discoideum* Rac1A/B/C, indicating detection specificity problems. Both the pull-down workflow and immunoblot conditions therefore require further optimisation.

Basal waves may not be a reliable proxy for cup dynamics

To test whether basal actin waves could model macropinocytic cup signalling, we quantified active Ras and Rac within basal patches. Substantial variability in patch size and orientation impeded standardisation, and, critically, the spatial profiles did not recapitulate those seen in macropinocytic cups. This suggests that basal waves represent a related but distinct mode of actin regulation rather than a simplified proxy for cup signalling. This conclusion is consistent with prior reports that differentiate wave- and cup-associated behaviours of formins such as ForG and ForB (Ecke et al., 2020; Körber et al., 2023), and with the

proposal that waves may instead represent frustrated phagocytic cups (Gerisch et al., 2009). Further characterisation using orientation-controlled sampling and geometry-matched analyses will be required to clarify these distinctions.

PikA/B loss impairs cup initiation, whereas PikF loss disrupts rim confinement

Lattice Light Sheet Microscopy enabled the visualisation of 3D fluid uptake in Ax2, PikA/B$^-$, PikF$^-$, and PikA/B/F$^-$ strains expressing the F-actin (RFP-LifeAct) and PIP_3 (GFP-PH-PkgE) probes. Ax2 cells formed large, well-defined macropinocytic cups, whereas mutants displayed distinct compensatory behaviours. PikA/B$^-$ and PikA/B/F$^-$ cells appeared to rely on forms of clathrin-independent microscale endocytosis, consistent with a failure to initiate protrusive cups. By contrast, PikF$^-$ cells internalised fluid via invaginations arising at the base of disfigured cup-like structures that lacked a defined rim and instead extended into spike-like protrusions. These large, structurally compromised protrusions support a failure of rim-based negative feedback, suggesting that PikF activity is required to spatially confine cytoskeletal protrusions during cup growth and closure. Conversely, the absence of prominent cups in PikA/B$^-$ and PikA/B/F$^-$ confirms that PikA/B activity is essential for cup initiation, as proposed by Hoeller *et al*. (2013).

Basal-wave behaviour exposes isoform-specific defects in initiation and confinement

Basal wave imaging provided further insight into isoform-specific control of actin dynamics. In Ax2 cells, waves propagated unidirectionally and remained organised around a central PIP_3 patch. In PikA/B$^-$ cells, loss of this central PIP_3 domain resulted in uncoordinated F-actin turnover and inward wave collapse. By contrast, PikF$^-$ cells retained the central PIP_3 patch but exhibited outward wave expansion, again indicating defective feedback restraint. In PikA/B/F$^-$ cells, coherent wave-like motion was abolished altogether and replaced by sporadic, uncoupled F-actin flashes. Taken together, these behaviours support a model in which PikA promotes coordinated actin polymerisation-depolymerisation (wave coherence), whereas PikF spatially constrains expansion (rim confinement); both functions are required to sustain stable basal-wave propagation.

Phagocytosis reveals isoform-specific roles and competition with macropinocytosis

We examined large-scale cytoskeletal rearrangements during phagocytosis across Ax2, PikA/B$^-$, PikF$^-$, and PikA/B/F$^-$ strains. Although previous studies reported normal uptake of 1 µm beads and unaltered growth on bacterial lawns across all Class I PI3K mutants (Buczynski et al., 1997; Hoeller et al., 2013), our results reveal that PikA/B$^-$ cells are severely impaired in engulfing larger, 5 µm yeast particles, whereas PikF$^-$ cells retain this capacity. Confocal imaging showed that PikA/B$^-$ and PikA/B/F$^-$ cells could initiate F-actin-driven cups around yeast but typically without early PIP_3 production, and attempts frequently failed due to premature actin disassembly. This mirrors findings in Dd5P4$^-$ cells, where cups form around yeast but fail to close when Dd5P4's RhoGAP and inositol 5-phosphatase catalytic activities are lost (Loovers et al., 2007). In the rare successful phagocytic events observed in PikA/B$^-$

and PikA/B/F$^-$ cells, F-actin fully encircled the particle and the PIP_3 signal (PkgE-PH-GFP) appeared only after closure; given PH-probe cross-reactivity (see Chapter 3), this late signal likely reports $PI(3,4)P_2$ rather than PIP_3. The seemingly intact uptake in PikF$^-$, by contrast, may reflect passive capture by broad, dynamic ruffles rather than fully regulated, PI3K-coordinated engulfment, potentially obscuring a feedback role for PikF during phagocytic cup maturation. Overall, these observations indicate that PikA is essential for efficient phagocytosis of large particles, stabilising the actin architecture needed for cup progression – likely via both catalytic and scaffolding functions – whereas PikF is not strictly required for engulfment but likely fine-tunes membrane dynamics and spatial feedback during closure.

Strikingly, Ax2 cells completed phagocytic cup formation in fewer than half of observed events; many were aborted in favour of macropinocytic cup formation. This points to competition between phagocytosis and macropinocytosis, potentially owing to their reliance on shared machinery such as SCAR/WAVE and Arp2/3. To our knowledge, this phenomenon has not been previously reported, although similar competition has been observed between macropinocytosis and cell motility (Veltman, 2015). How cytoskeletal coordination is balanced between competing endocytic processes, and which molecular players mediate the decision-making that grants one process priority over another, remains an open and intriguing question.

The next chapter builds on these mechanistic insights, mapping PikA- and PikF-specific interactomes by AP-MS and STRING analysis to identify the protein networks that underpin their distinct contributions to cytoskeletal regulation.

4.4 References

Buckley, C.M., Pots, H., Gueho, A., Vines, J.H., Munn, C.J., Phillips, B.A., Gilsbach, B., Traynor, D., Nikolaev, A., Soldati, T., Parnell, A.J., Kortholt, A., King, J.S., 2020. Coordinated Ras and Rac Activity Shapes Macropinocytic Cups and Enables Phagocytosis of Geometrically Diverse Bacteria. Curr. Biol. 30, 2912-2926.e5. https://doi.org/10.1016/j.cub.2020.05.049

Buczynski, G., Grove, B., Nomura, A., Kleve, M., Bush, J., Firtel, R.A., Cardelli, J., 1997. Inactivation of Two Dictyostelium discoideum Genes, DdPIK1 and DdPIK2, Encoding Proteins Related to Mammalian Phosphatidylinositide 3-kinases, Results in Defects in Endocytosis, Lysosome to Postlysosome Transport, and Actin Cytoskeleton Organization. J. Cell Biol. 136, 1271–1286. https://doi.org/10.1083/jcb.136.6.1271

Dumontier, M., Höcht, P., Mintert, U., Faix, J., 2000. Rac1 GTPases control filopodia formation, cell motility, endocytosis, cytokinesis and development in Dictyostelium. J. Cell Sci. 113, 2253–2265. https://doi.org/10.1242/jcs.113.12.2253

Ecke, M., Prassler, J., Tanribil, P., Müller-Taubenberger, A., Körber, S., Faix, J., Gerisch, G., 2020. Formins specify membrane patterns generated by propagating actin waves. Mol. Biol. Cell 31, 373–385. https://doi.org/10.1091/mbc.E19-08-0460

Gerisch, G., Ecke, M., Schroth-Diez, B., Gerwig, S., Engel, U., Maddera, L., Clarke, M., 2009. Self-organizing actin waves as planar phagocytic cup structures. Cell Adhes. Migr. https://doi.org/10.4161/cam.3.4.9708

Hoeller, O., Bolourani, P., Clark, J., Stephens, L.R., Hawkins, P.T., Weiner, O.D., Weeks, G., Kay, R.R., 2013. Two distinct functions for PI3-kinases in macropinocytosis. J. Cell Sci. jcs.134015. https://doi.org/10.1242/jcs.134015

Körber, S., Junemann, A., Litschko, C., Winterhoff, M., Faix, J., 2023. Convergence of Ras- and Rac-regulated formin pathways is pivotal for phagosome formation and particle uptake in Dictyostelium. Proc. Natl. Acad. Sci. 120, e2220825120. https://doi.org/10.1073/pnas.2220825120

Loovers, H.M., Kortholt, A., de Groote, H., Whitty, L., Nussbaum, R.L., van Haastert, P.J.M., 2007. Regulation of Phagocytosis in Dictyostelium by the Inositol 5-Phosphatase OCRL Homolog Dd5P4. Traffic 8, 618–628. https://doi.org/10.1111/j.1600-0854.2007.00546.x

Masters, T.A., Sheetz, M.P., Gauthier, N.C., 2016. F-actin waves, actin cortex disassembly and focal exocytosis driven by actin-phosphoinositide positive feedback. Cytoskeleton 73, 180–196. https://doi.org/10.1002/cm.21287

Schlam, D., Bagshaw, R.D., Freeman, S.A., Collins, R.F., Pawson, T., Fairn, G.D., Grinstein, S., 2015. Phosphoinositide 3-kinase enables phagocytosis of large particles by terminating actin assembly through Rac/Cdc42 GTPase-activating proteins. Nat. Commun. 6, 8623. https://doi.org/10.1038/ncomms9623

Veltman, D.M., 2015. Drink or drive: competition between macropinocytosis and cell migration. Biochem. Soc. Trans. 43, 129–132. https://doi.org/10.1042/BST20140251

Veltman, D.M., Williams, T.D., Bloomfield, G., Chen, B.-C., Betzig, E., Insall, R.H., Kay, R.R., 2016. A plasma membrane template for macropinocytic cups. eLife 5, e20085. https://doi.org/10.7554/eLife.20085

Chapter 5: Proteomic Dissection of PikA and PikF Isoform-Specific Interactors in *Dictyostelium discoideum* Macropinocytosis

5.1 Introduction

Class I PI3Ks are traditionally viewed as lipid kinases that generate local pools of PIP_3 to direct actin polymerisation by recruiting the SCAR/WAVE complex and the Arp2/3 actin nucleator to the periphery of PIP_3 patches (Veltman et al., 2016). However, data in Chapters 3 and 4 indicate that, in *Dictyostelium discoideum*, PikA and PikF perform non-redundant, partly non-catalytic roles during macropinocytosis: PikA supports cup initiation at the base, whereas PikF constrains rim dynamics by restricting Rac activity during maturation and closure. These spatially segregated functions imply that each isoform engages distinct protein networks that position, stabilise, and tune PI3K outputs in space and time.

Proteomics offers a direct route from phenotype to mechanism. Here, we use Affinity Purification-Mass Spectrometry (AP-MS) to define isoform-specific interactomes for PikA and PikF. Our design contrasts GFP-PikA (expressed in PikA/B$^-$ cells) and GFP-PikF (expressed in PikF$^-$ cells) against a GFP-only wild-type (Ax2) control, enabling subtraction of background binders. Based on the imaging-derived model (Chapter 4), we predicted that PikA would associate with transport/motor machinery and actin nucleators consistent with basal recruitment and recycling, whereas PikF would associate with Rac regulators, IQGAP-like scaffolds, and actin-turnover/capping factors that enforce rim confinement.

Methodologically, AP-MS complements the structural and imaging approaches used earlier by capturing native multi-protein assemblies for identification by Mass Spectrometry. However, it also carries caveats: bait expression is subject to proteasomal control (Chapter 3), weak or transient interactions may be under-sampled, and preliminary discovery runs have limited statistical power. Accordingly, we pair AP-MS with STRING v12 network analysis to identify functional binding partners, prioritising shared interactors present in both PI3K samples (and absent from the GFP control) alongside isoform-specific candidates.

Together, the findings in this chapter provide mechanistic insight into how distinct Class I PI3K isoforms orchestrate cytoskeletal dynamics across macropinocytic cup initiation, maturation and closure, embedded within – and dependent on – broader protein interaction networks.

Research Questions Addressed in this Chapter

1. Do PikA and PikF engage distinct protein-protein interactions that underpin their isoform-specific functions during macropinocytic cup formation?

2. If so, which classes of interactors are preferentially associated with each isoform, and what do these suggest about PI3K-mediated control of cytoskeletal and membrane dynamics?

5.2 Results

To identify isoform-specific interaction partners of PikA and PikF, we performed Affinity Purification-Mass Spectrometry (AP-MS) (Morris et al., 2014). GFP-trap pull-downs were carried out on lysates from wild-type (Ax2) cells expressing GFP (control), PikA/B^{-} cells expressing GFP-PikA, and PikF^{-} cells expressing GFP-PikF. During method development, the chosen resin (GFP-Trap Agarose; ChromoTek, #gta) yielded variable protein recoveries across three technical repeats (Figure 5.1). To minimise this technical variability in the discovery phase, we submitted a single preliminary MS run using the pull-down set with the most consistent protein concentrations across strains (Trap 2, Figure 5.1). Identified proteins were analysed using STRING version 12 (Szklarczyk et al., 2025, 2023).

The output of this preliminary run is summarised in Table 5.1. In the absence of biological replicates at this stage, all enrichment estimates are provisional. Accordingly, the data presented in this chapter focuses on shared interactors detected in both PI3K samples but absent from the GFP-only Ax2 control (Section 5.2.1), and on isoform-specific interactors uniquely associated with GFP-PikA or GFP-PikF (Sections 5.2.2 and 5.2.3).

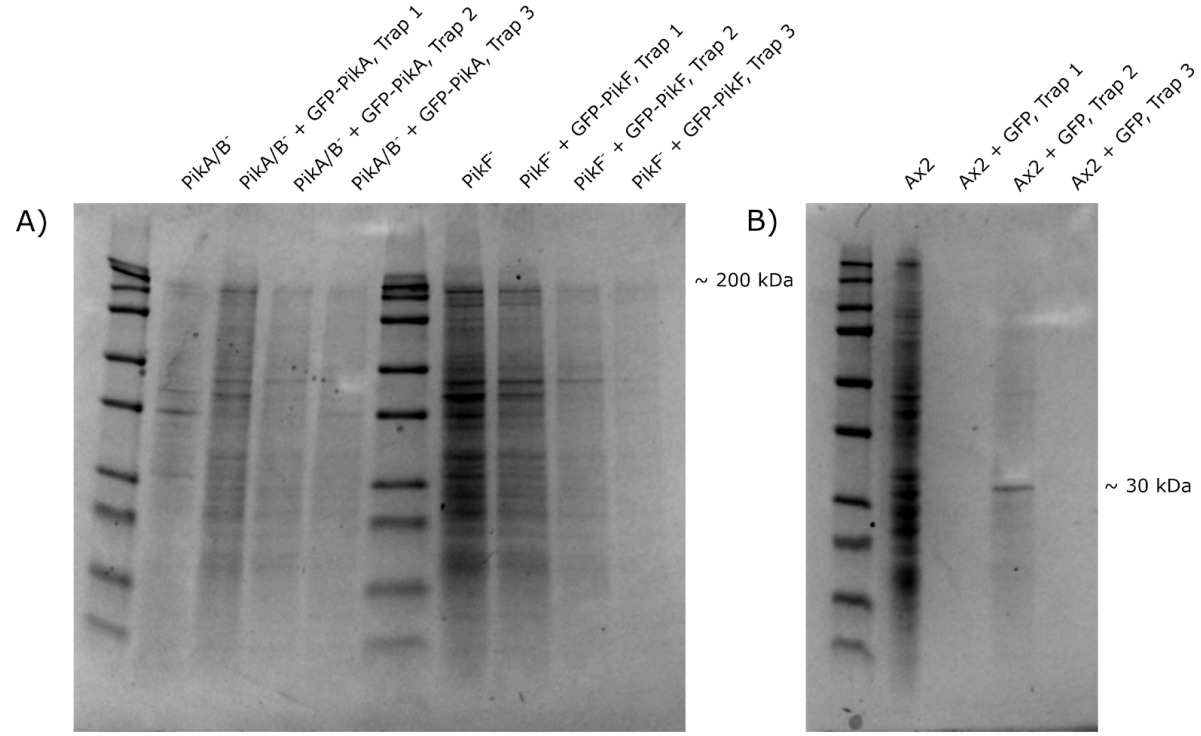

Figure 5.1: Variability in GFP-trap pull-down yields across technical repeats. Total protein recovered in GFP eluates from Ax2 + GFP (control), PikA/B^{-} + GFP-PikA, and PikF^{-} + GFP-PikF across three technical repeats (Trap 1-3). Due to variability between repeats, Trap 2 – exhibiting the most consistent cross-strain yields – was chosen for preliminary MS analysis. Signal quantification was performed in Fiji (ImageJ). Assay details are described in Methods.

Output	Number of Genes
Total	4,168
Exclusively detected in GFP-PikA sample	659
Exclusively detected in GFP-PikF sample	398
Detected in both GFP-PikA and GFP-PikF samples but not in the GFP control	203
PikA/PikF enrichment > 2 fold	142
PikF/PikA enrichment > 2 fold	37

Table 5.1: Summary of Affinity Purification-Mass Spectrometry (AP-MS) output for GFP-PikA and GFP-PikF interactors. A total of 4,168 protein-coding genes were detected across all samples. Of these, 659 were exclusively identified in the GFP-PikA sample, and 398 in the GFP-PikF sample. An additional 203 proteins were detected in both GFP-PikA and GFP-PikF samples but not in the GFP-only control. Of the 4,168 proteins detected in total, 142 were enriched more than twofold in the GFP-PikA sample relative to both GFP-PikF and the GFP-only control, while 37 were enriched more than twofold in the GFP-PikF sample relative to both GFP-PikA and the GFP-only control.

5.2.1 Shared PikA and PikF Interactors

AP-MS identified 203 proteins that interact with both GFP-PikA and GFP-PikF but not with GFP alone, with bidirectional enrichment ranging between 0.7- and 1.3-fold (Table 5.1). Reactome Pathway enrichment analysis of these shared interactors revealed significant associations with pathways including the ‘RHO GTPase cycle’, ‘RAC1 GTPase cycle’, ‘Signaling by Rho GTPases, Miro GTPases and RHOBTB3’, and ‘Signal Transduction’ (Figure 5.2). Notably, the genes identified in association with the Rho GTPase cycle included Rho GTPase **RacP**, the RhoGAP **GacEE**, and the RasGEF **GefV**. Additionally, **AbiA**, a component of the SCAR/WAVE complex (Pollitt and Insall, 2008; Singh et al., 2021), and **Dd5p4**, an inositol 5-phosphatase with RhoGAP activity (Loovers et al., 2007) were also identified (Figure 5.3). While most proteins involved in the Rho GTPase cycle overlapped with the RAC1 GTPase cycle, Dd5p4 and RacP appeared to be uniquely associated with the broader Rho GTPase signaling category (Figure 5.4).

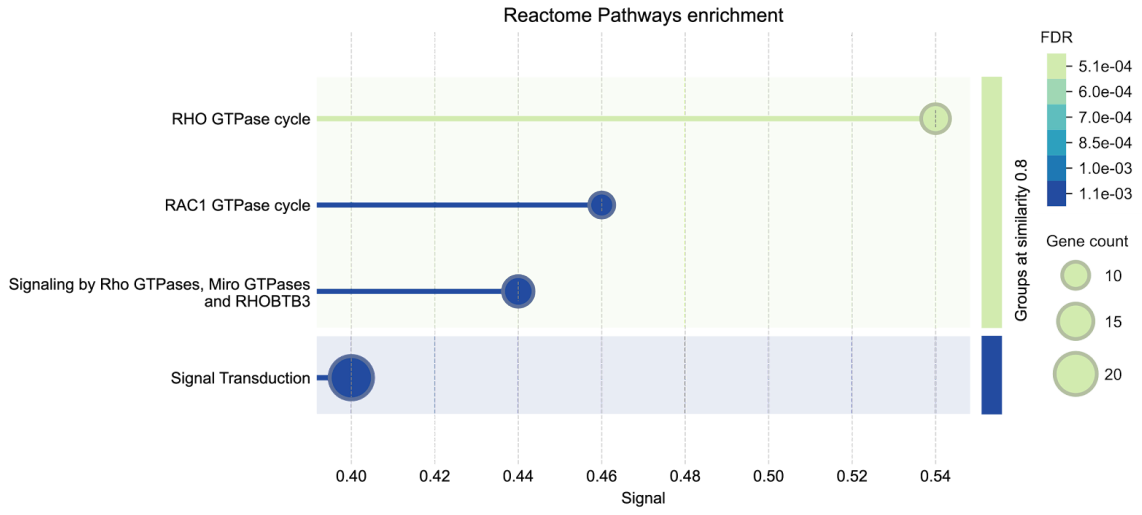

Figure 5.2: Reactome Pathway enrichment analysis of the 203 interactors shared between GFP-PikA and GFP-PikF. ‘Signal’ refers to the weighted harmonic mean of the observed-to-expected gene occurrence ratio and the corresponding -log(FDR) value. FDR: False Discovery Rate. ‘Groups at similarity 0.8’ indicates clustering based on the Jaccard index, where a value of 1 denotes complete (100%) overlap between gene sets.

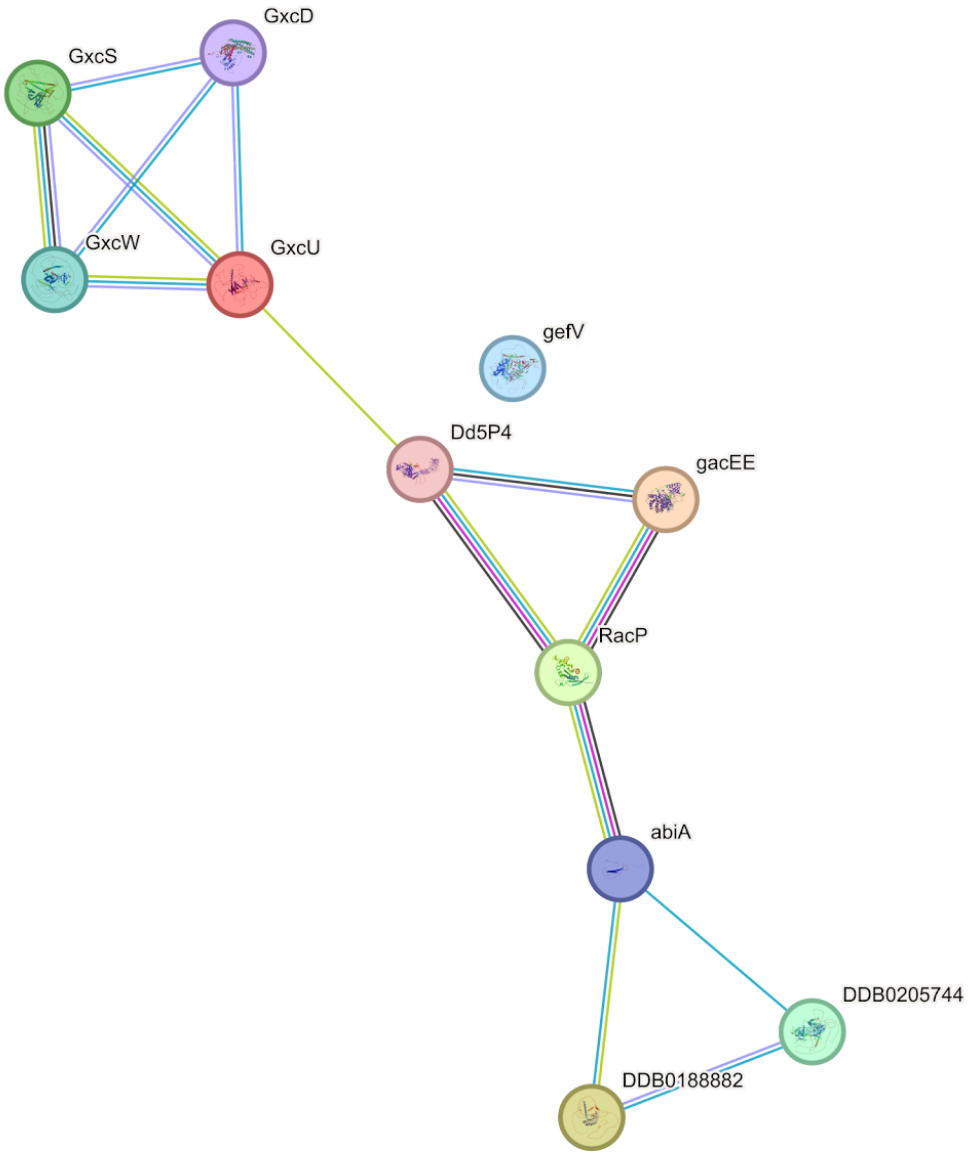

Figure 5.3: Protein-protein interaction network of interactors shared between GFP-PikA and GFP-PikF associated with the 'RHO GTPase Cycle' pathway.
The network was identified through AP-MS and analysed using STRING (v12). Nodes represent proteins and edges indicate known or predicted functional associations. Edge colours: curated databases (blue), experimentally determined (magenta), co-expression (grey), text-mining (green), and protein homology (lilac).

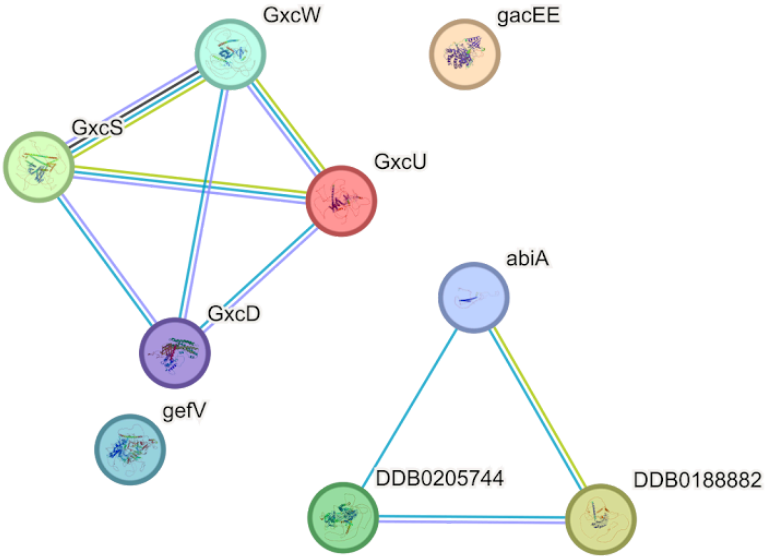

Figure 5.4: Protein-protein interaction network of interactors shared between GFP-PikA and GFP-PikF associated with the 'RAC1 GTPase Cycle'. The network was identified through AP-MS and analysed using STRING (v12). Nodes represent proteins and edges indicate known or predicted functional associations. Edge colours: curated databases (blue), co-expression (grey), text-mining (green), and protein homology (lilac).

Although the list of interactors associated with 'Signaling by Rho GTPases, Miro GTPases and RHOBTB3' is nearly identical to that of the 'Rho GTPase cycle' – differing only by the inclusion of DDB0229988, an uncharacterised **Rab** family member (Q552H0, ADP-ribosylation factor-related) (data not shown) – a broader interaction network emerges in the context of the 'Signal Transduction' pathway. This expanded network includes RasGEF **GefM**, the ELMO domain-containing protein **ElmoE**, and MOB kinase activator-like protein **Mob2** (Figure 5.5). Notably, a group of uncharacterised proteins – DDB0205744 (Q54WW0), DDB0188882 (Q54G40; **leucine-rich repeat**-containing protein), **GxcD** (Q55G27; **RhoGEF** domain-containing), **GxcS** (Q54VX2; **Pleckstrin homology** domain-containing), **GxcU** (Q54DW7; **Pleckstrin homology** domain-containing), and **GxcW** (Q54YP1; **Pleckstrin homology** domain-containing) – were detected across all four major pathway groups.

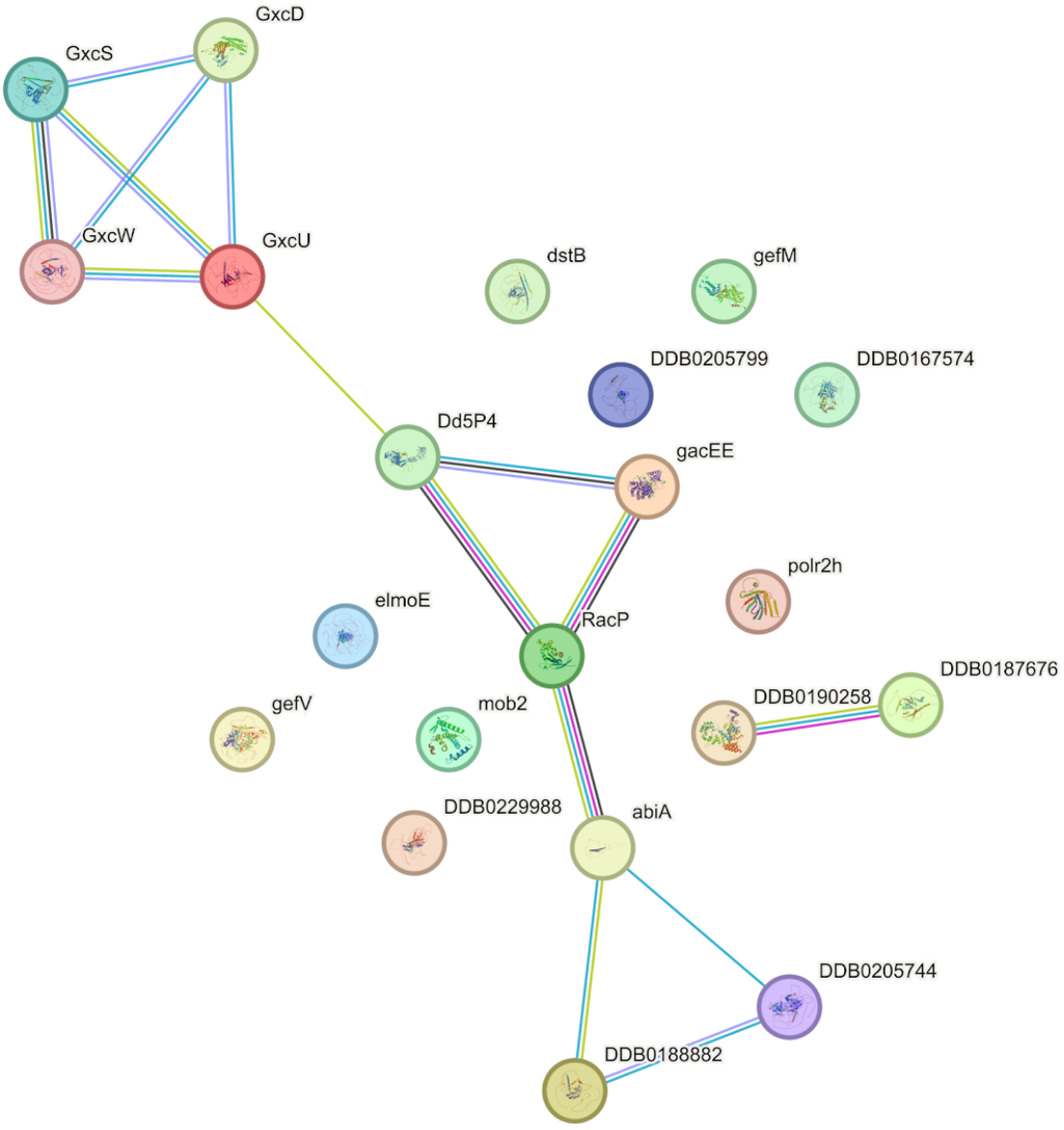

Figure 5.5: Protein-protein interaction network of interactors shared between GFP-PikA and GFP-PikF associated with 'Signal Transduction'. The network was identified through AP-MS and analysed using STRING (v12). Nodes represent proteins and edges indicate known or predicted functional associations. Edge colours: curated databases (blue), experimentally determined (magenta), co-expression (grey), text-mining (green), and protein homology (lilac).

Table 5.2 summarises five genes from the 203 shared interactors associated with the ‘Cytoskeleton’ Reactome pathway, including the scaffolding LIM domain-containing proteins **LimB** and **LimE** (Sala and Oakes, 2023), the **SCAR** complex member **ScrA**, the actin-binding protein **FimC** (Bañuelos et al., 1998), and the Rho GTPase **RacP**. A corresponding Cellular Component enrichment analysis highlights their localisation to structures such as the cell cortex, cell projections, filopodia, pseudopodia, and the leading edge (Figure 5.6). Complementary Biological Process enrichment analysis links these proteins to actin cytoskeleton organisation, actin filament bundling, cortical cytoskeleton assembly, and bleb formation (Figure 5.7).

Table 5.3 lists ten genes associated with ‘Cytoskeleton Organisation’ among the shared GFP-PikA and GFP-PikF interactors. In addition to LimE, RacP, ElmoE, FimC, GefV, and GxcD described above, the set includes **VASP**-interacting guanylyl cyclase **SgcA** (Zhou et al., 2008), and three uncharacterised proteins: the **WASP**-interacting DDB_G0271676 (Q75JD4; **SH3** and **F-BAR** domain-containing) (Chen et al., 2013), DDB0218209 (Q54W22, **Pleckstrin homology** domain-containing protein), and **GxcZ** (Q1ZX99, **RhoGEF** domain-containing protein).

limE	*LIM domain-containing protein E; Associates with the actin cytoskeleton and may regulate actin polymerization in lamellipodia, through a rac1-dependent signaling pathway. May play a role in cell motility. Involved in cytokinesis by regulating the microtubule system and linking it to the cortical actin network. (199 aa)*
RacP	*Rho GTPase. (376 aa)*
scrA	*Protein SCAR; Involved in regulation of actin and microtubule organization. Regulates phagocytosis and macropinocytosis. Belongs to the SCAR/WAVE family. (443 aa)*
limB	*LIM domain-containing protein B; Regulates and controls rearrangements of the actin cytoskeleton. Required for tip formation, morphogenesis, cell adhesion and motility, chemotaxis and aggregates formation. May function downstream of paxB. (553 aa)*
FimC	*Uncharacterized protein. (1213 aa)*

Table 5.2: GFP-PikA and GFP-PikF shared interactors associated with ‘Cytoskeleton’. Interactors were identified through STRING (v12) analysis of AP-MS data. The geneset analysed includes proteins with a relative enrichment between 0.7 and 1.3 in both GFP-PikA and GFP-PikF samples, which were absent from the GFP-only. Interactor descriptions are reproduced directly from the STRING database interface, incorporating annotations from UniProt, EnsemblProtists, and KEGG: Kyoto Encyclopedia of Genes and Genomes.

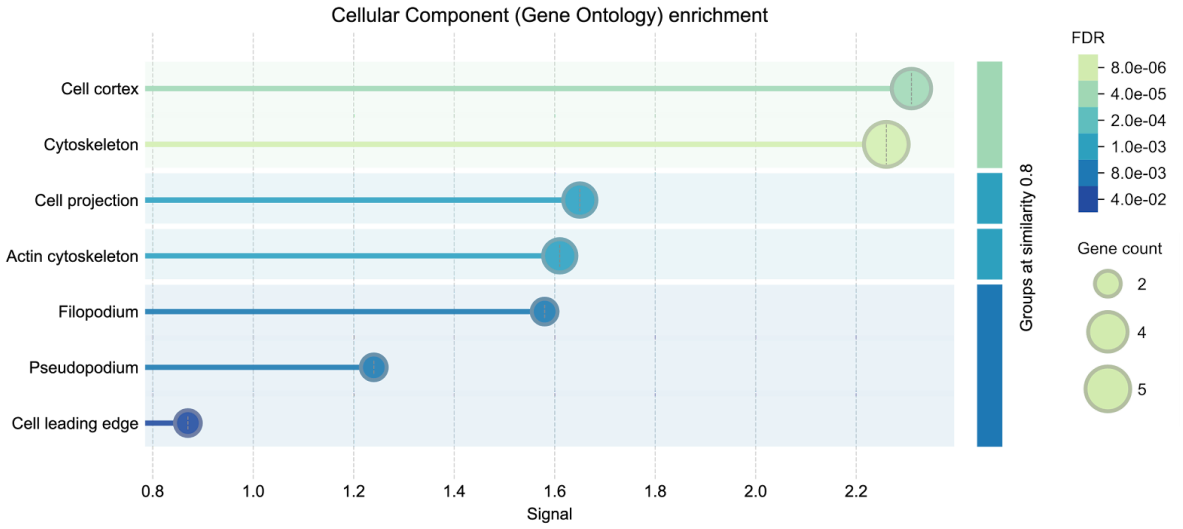

Figure 5.6: Cellular Component enrichment analysis of interactors shared between GFP-PikA and GFP-PikF associated with 'Cytoskeleton'. Terms such as *cell cortex*, *filopodium*, *pseudopodium*, and *leading edge* highlight the spatial association of these proteins with actin-rich cellular protrusions. Enrichment was calculated using STRING (v12) Reactome annotations. 'Signal' refers to the weighted harmonic mean of the observed-to-expected gene occurrence ratio and the corresponding -log(FDR) value. FDR: False Discovery Rate. 'Groups at similarity 0.8' indicates clustering based on the Jaccard index, where a value of 1 denotes complete (100%) overlap between gene sets.

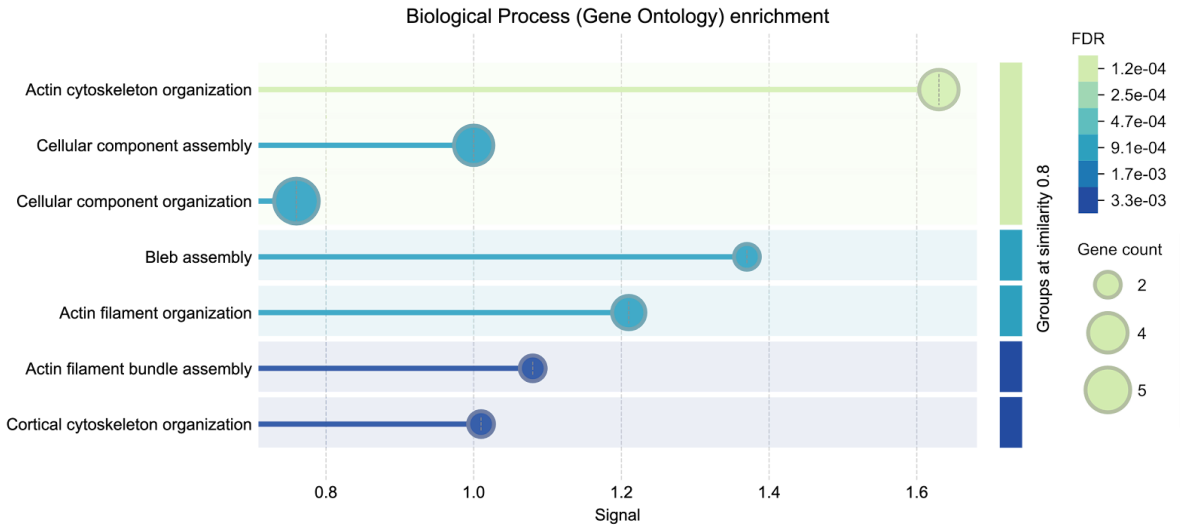

Figure 5.7: Biological Process enrichment analysis of interactors shared between GFP-PikA and GFP-PikF associated with 'Cytoskeleton'. Enriched processes include actin cytoskeleton organisation, cortical cytoskeleton organisation, and bleb assembly. Enrichment was calculated using STRING (v12) Reactome annotations. 'Signal' refers to the weighted harmonic mean of the observed-to-expected gene occurrence ratio and the corresponding -log(FDR) value. FDR: False Discovery Rate. 'Groups at similarity 0.8' indicates clustering based on the Jaccard index, where a value of 1 denotes complete (100%) overlap between gene sets.

limE	*LIM domain-containing protein E; Associates with the actin cytoskeleton and may regulate actin polymerization in lamellipodia, through a rac1-dependent signaling pathway. May play a role in cell motility. Involved in cytokinesis by regulating the microtubule system and linking it to the cortical actin network. (199 aa)*
RacP	*Rho GTPase. (376 aa)*
elmoE	*ELMO domain-containing protein E. (1677 aa)*
FimC	*Uncharacterized protein. (1213 aa)*
sgcA	*Guanylyl cyclase. (2843 aa)*
gefV	*Ras guanine nucleotide exchange factor V; Promotes the exchange of Ras-bound GDP by GTP. (1982 aa)*
GxcD	*Uncharacterized protein. (1063 aa)*
GxcZ	*RhoGEF domain-containing protein. (1028 aa)*
DDB_G0271676	*SH3 and F-BAR domain-containing protein DDB_G0271676. (533 aa)*
DDB0218209	*PH domain-containing protein. (741 aa)*

Table 5.3: GFP-PikA and GFP-PikF shared interactors associated with 'Cytoskeleton Organisation'. Interactors were identified through STRING (v12) analysis of AP-MS data. The geneset analysed includes proteins with a relative enrichment between 0.7 and 1.3 in both GFP-PikA and GFP-PikF samples, which were absent from the GFP-only. Interactor descriptions are reproduced directly from the STRING database interface, incorporating annotations from UniProt, EnsemblProtists, and KEGG: Kyoto Encyclopedia of Genes and Genomes.

Table 5.4 lists 13 genes identified in association with the Reactome pathway term “Endosome” among the 203 interactors shared between GFP-PikA and GFP-PikF. Notably, **ElmoE** – highlighted previously – and **Dd5P4**, which was also associated with the Rho GTPase cycle, reappear in this group. In addition, several other interactors linked to endosomal processes were identified, including Pip5k3 (**PIKfyve**), the protein tyrosine phosphatase **PtpC**, and **Chmp2a2** (**Vps2B**), a member of the charged multivesicular body protein (CHMP) family. Other components include the trafficking protein particle complex subunit **Trappc5**, vacuolar protein sorting-associated protein **Vps51**, vesicle-associated membrane protein **Vamp7A**, and **Washc2** (**Fam21**), a subunit of the Arp2/3-activating WASH complex (Wang et al., 2014). Additional interactors comprise **Wdr91**, a negative regulator of Class III PI3K signalling and Rab7 interactor negative regulator of Class III PI3K signalling and Rab7 interactor **Wdr91** (Ma et al., 2024), **IvsB**, a sorting-associated BEACH domain-containing protein involved in transmembrane trafficking (Pankiv et al., 2024), and DDB0229988 (Q552H0), an uncharacterised ADP-ribosylation factor (**Arf**)-related Rab GTPase. Cellular Component and Biological Process enrichment analyses of these proteins indicate their involvement across multiple stages of the endocytic pathway – from early to late endosomes – as well as roles in exocytosis, lysosomal transport, and vacuolar trafficking (Figures 5.8 and 5.9).

pip5k3	*1-phosphatidylinositol 3-phosphate 5-kinase; Catalyzes the phosphorylation of phosphatidylinositol 3- phosphate on the fifth hydroxyl of the myo-inositol ring, to form phosphatidylinositol 3,5-bisphosphate. (2656 aa)*
ptpC	*Tyrosine-protein phosphatase 3; Seems to dephosphorylate a protein of 130 kDa (p130). (990 aa)*
chmp2a2	*Charged multivesicular body protein 2a homolog 2; Probable core component of the endosomal sorting required for transport complex III (ESCRT-III) which is involved in multivesicular bodies (MVBs) formation and sorting of endosomal cargo proteins into MVBs. MVBs contain intraluminal vesicles (ILVs) that are generated by invagination and scission from the limiting membrane of the endosome and are delivered to lysosomes enabling degradation of membrane proteins (By similarity). (198 aa)*
DDB0188326	*Uncharacterized protein. (801 aa)*
vps51	*Vacuolar protein sorting-associated protein 51 homolog; May act as component of the GARP complex that is involved in retrograde transport from early and late endosomes to the trans-Golgi network (TGN); Belongs to the VPS51 family. (917 aa)*
vamp7A	*Vesicle-associated membrane protein 7A; Involved in the targeting and/or fusion of transport vesicles to their target membrane during transport of proteins from the early endosome to the lysosome. Required for heterotypic fusion of late endosomes with lysosomes and*

	homotypic lysosomal fusion. Required for calcium regulated lysosomal exocytosis; Belongs to the synaptobrevin family. (216 aa)
elmoE	*ELMO domain-containing protein E. (1677 aa)*
trappc5	*Trafficking protein particle complex subunit 5; May play a role in vesicular transport from endoplasmic reticulum to Golgi. (186 aa)*
washc2	*WASH complex subunit 2. (1479 aa)*
DDB0229988	*ADP-ribosylation factor-related. (837 aa)*
wdr91	*WD repeat-containing protein 91 homolog; Functions as a negative regulator of the PI3 kinase/PI3K activity associated with endosomal membranes. By modifying the phosphatidylinositol 3-phosphate/PtdInsP3 content of endosomal membranes may regulate endosome fusion, recycling, sorting and early to late endosome transport; Belongs to the WD repeat WDR91 family. (766 aa)*
lvsB	*BEACH domain-containing protein lvsB; Involved in negative regulation of lysosome biogenesis, by limiting the heterotypic fusion of early endosomes and postlysosomal compartments. (4118 aa)*
Dd5P4	*Inositol 5-phosphatase 4. (787 aa)*

Table 5.4: GFP-PikA and GFP-PikF shared interactors associated with 'Endosome'. Interactors were identified through STRING (v12) analysis of AP-MS data. The geneset analysed includes proteins with a relative enrichment between 0.7 and 1.3 in both GFP-PikA and GFP-PikF samples, which were absent from the GFP-only. Interactor descriptions are reproduced directly from the STRING database interface, incorporating annotations from UniProt, EnsemblProtists, and KEGG: Kyoto Encyclopedia of Genes and Genomes.

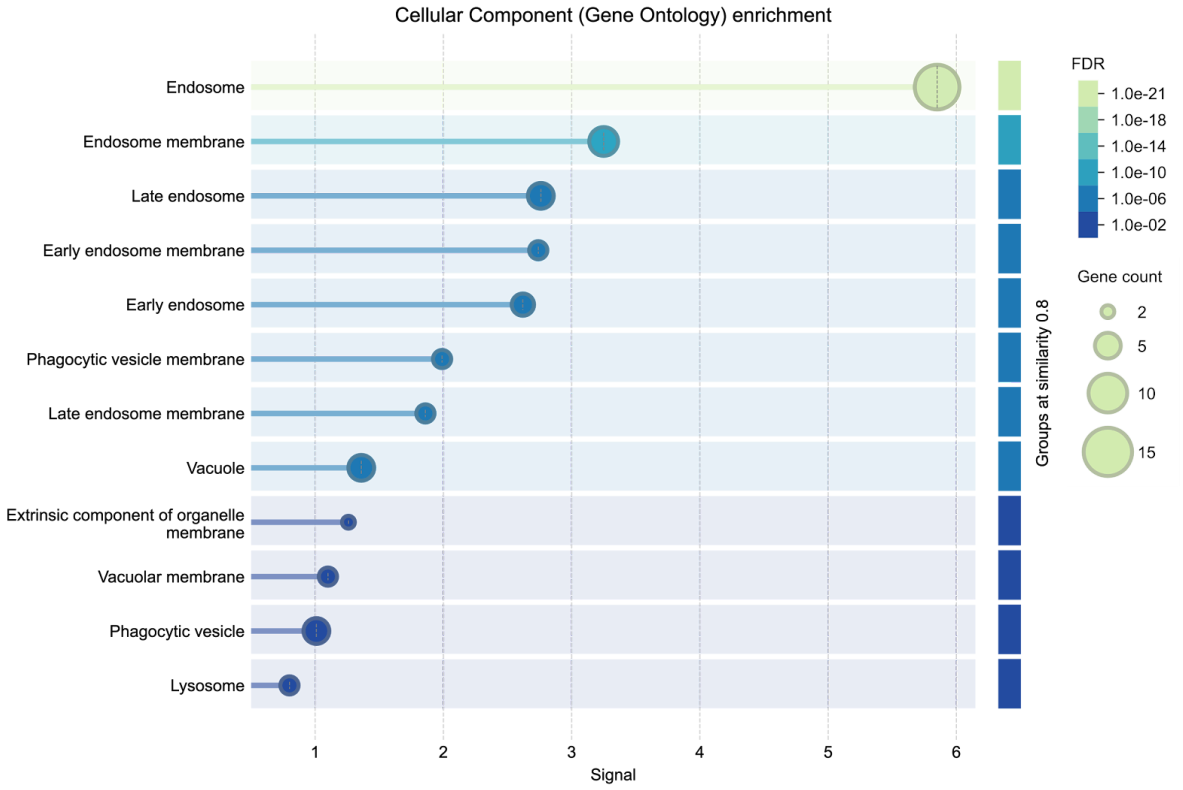

Figure 5.8: Cellular Component enrichment analysis of interactors shared between GFP-PikA and GFP-PikF associated with 'Endosome'. Enriched processes include actin cytoskeleton organisation, cortical cytoskeleton organisation, and bleb assembly. Enrichment was calculated using STRING (v12) Reactome annotations. 'Signal' refers to the weighted harmonic mean of the observed-to-expected gene occurrence ratio and the corresponding -log(FDR) value. FDR: False Discovery Rate. 'Groups at similarity 0.8' indicates clustering based on the Jaccard index, where a value of 1 denotes complete (100%) overlap between gene sets.

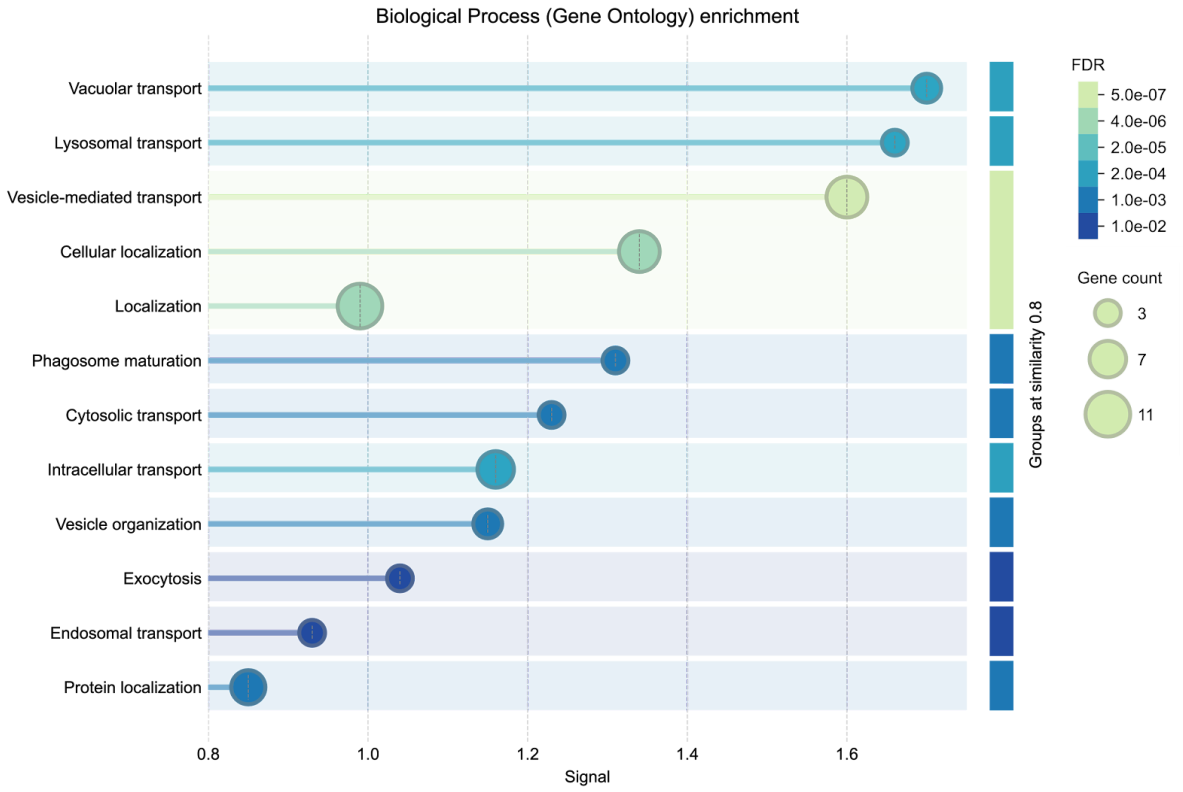

Figure 5.9: Biological Process enrichment analysis of interactors shared between GFP-PikA and GFP-PikF associated with 'Endosome'. Enriched processes include actin cytoskeleton organisation, cortical cytoskeleton organisation, and bleb assembly. Enrichment was calculated using STRING (v12) Reactome annotations. 'Signal' refers to the weighted harmonic mean of the observed-to-expected gene occurrence ratio and the corresponding -log(FDR) value. FDR: False Discovery Rate. 'Groups at similarity 0.8' indicates clustering based on the Jaccard index, where a value of 1 denotes complete (100%) overlap between gene sets.

5.2.2 PikA-Specific Interactors

AP-MS identified 659 interactors unique to GFP-PikA (Table 5.1). Among these, 17 were associated with the term ‘Cytoskeleton’ according to STRING analysis (Table 5.5). This group includes members of the myosin (**MlcR**, **MyoJ**, **MyoG**), dynactin (**DynF**, **DynB**, **DynE**), kinesin (**Kif2**, **Kif3**, **Kif7**, **Kif9**, **Kif11**), and tubulin (**TubC**) complexes, along with the dynein regulator **NudE** (Reck-Peterson et al., 2018). Subcellular localisation enrichment analysis indicates a nearly twofold stronger association of PikA-specific interactors with the microtubule cytoskeleton compared to the actin cytoskeleton (Figure 5.10). This trend is supported by biological process enrichment data, which highlights key roles in microtubule-based transport, organisation, and dynamics, including microtubule polymerisation and depolymerisation (Figure 5.11). Consistently, molecular function enrichment reveals a predominance of microtubule motor activities among these PikA interactors, with an enrichment in microfilament motor activity and calmodulin binding – both relevant to myosin regulation (Walsh, 1983) (Figure 5.12); and a local network cluster enrichment analysis further reinforces their with myosin, calmodulin, kinesin, tubulin, and dynactin complexes (Figure 5.13).

A more focused subset of five PikA-specific interactors – MlcR, MyoG, MyoJ, Kif9, and TubC – was linked specifically to ‘Cytoskeleton Organisation’ by STRING (Table 5.6). These proteins, all present in the broader cytoskeletal category above, feature key structural domains, including kinesin motor domains, myosin head domains, and calmodulin-interacting motifs such as IQ and EF-hand domains (Bähler and Rhoads, 2002) (Figure 5.14). These features support a model in which PikA engages with a network of cytoskeletal motor proteins to regulate microtubule and actin dynamics during macropinocytosis.

mlcR	*Myosin regulatory light chain. (161 aa)*
myoJ	*Myosin-J heavy chain; Processive motor protein that can move over long distances along F-actin without disassociating; processiveness depends on high physiological Mg(2+) concentrations. Presents a high actin affinity in the presence of ADP, fast ATP hydrolysis, and a high steady-state ATPase activity in the presence of actin that is rate limited by ADP release. Physiological decrease of free Mg(2+) ions leads to an increased rate of ADP release and shortening of the fraction of time it spends in the strong acting binding states. (2245 aa)*
dynF	*Dynactin subunit 6; Belongs to the dynactin subunits 5/6 family. Dynactin subunit 6 subfamily. (189 aa)*
dynB	*Dynactin subunit 2; Modulates cytoplasmic dynein binding to an organelle, and plays a role in prometaphase chromosome alignment and spindle organization during mitosis. (430 aa)*

kif7	*Kinesin-related protein 7; Microtubule-associated force-producing protein that plays a role in organelle transport. Its motor activity is directed toward the microtubule's plus end. May be involved in cell motility or cell differentiation during prestalk formation. Belongs to the TRAFAC class myosin-kinesin ATPase superfamily. Kinesin family. (1255 aa)*
kif3	*Kinesin-related protein 3; Microtubule-associated force-producing protein that plays a role in organelle transport. Its motor activity is directed toward the microtubule's plus end. The maximal velocity in an inverted motility assay (moving microtubules on fixed motors) was 1.96 um/s. Belongs to the TRAFAC class myosin-kinesin ATPase superfamily. Kinesin family. Kinesin subfamily. (1193 aa)*
DDB0205745	*Uncharacterized protein. (560 aa)*
dynE	*Dynactin subunit 5; Belongs to the dynactin subunits 5/6 family. Dynactin subunit 5 subfamily. (198 aa)*
kif9	*Kinesin-related protein 9; Microtubule-associated force-producing protein that plays a role in organelle transport. Its motor activity is directed toward the microtubule's plus end (By similarity); Belongs to the TRAFAC class myosin-kinesin ATPase superfamily. Kinesin family. (1222 aa)*
tubC	*Tubulin gamma chain; Tubulin is the major constituent of microtubules. The gamma chain is found at microtubule organizing centers (MTOC) such as the spindle poles or the centrosome, suggesting that it is involved in the minus-end nucleation of microtubule assembly (By similarity). (462 aa)*
DDB0190842	*Uncharacterized protein. (889 aa)*
kif11	*Kinesin-related protein 11; Microtubule-associated force-producing protein that plays a role in organelle transport. Its motor activity is directed toward the microtubule's plus end (By similarity); Belongs to the TRAFAC class myosin-kinesin ATPase superfamily. Kinesin family. (685 aa)*
nudE	*Lis-interacting protein. (398 aa)*
myoG	*Myosin-G heavy chain; Myosins are actin-based motor molecules with ATPase activity. (3446 aa)*
kif2	*Kinesin-related protein 2; Microtubule-dependent motor that is probably involved in microtubule organization in the mitotic spindle. (792 aa)*
numA	*Nucleomorphin. (756 aa)*

cycB	*G2/mitotic-specific cyclin-B; Essential for the control of the cell cycle at the G2/M (mitosis) transition. (436 aa)*

Table 5.5: GFP-PikA-specific interactors associated with 'Cytoskeleton'. Interactors were identified through STRING (v12) analysis of AP-MS data. The geneset analysed set includes proteins uniquely detected in GFP-PikA samples and absent from both GFP-PikF samples and the GFP-only control. Interactor descriptions are reproduced directly from the STRING database interface, incorporating annotations from UniProt, EnsemblProtists, and KEGG: Kyoto Encyclopedia of Genes and Genomes.

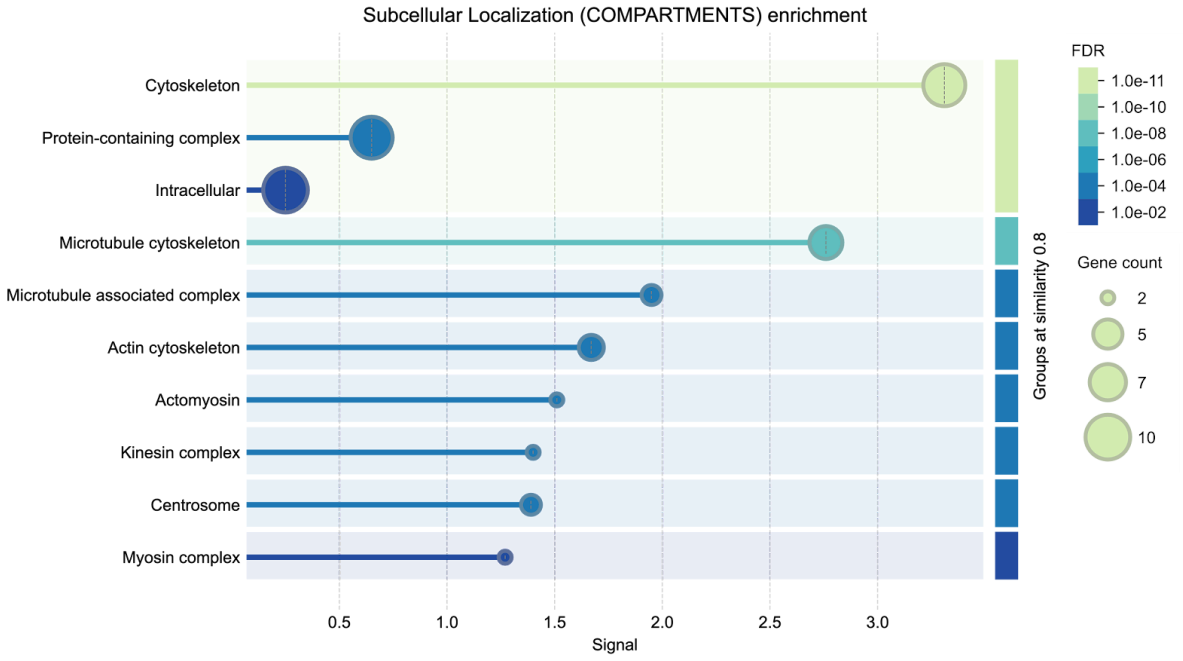

Figure 5.10: Subcellular Localisation enrichment analysis of GFP-PikA-specific interactors associated with 'Cytoskeleton'. Enrichment was calculated using STRING (v12) Reactome annotations. 'Signal' refers to the weighted harmonic mean of the observed-to-expected gene occurrence ratio and the corresponding -log(FDR) value. FDR: False Discovery Rate. 'Groups at similarity 0.8' indicates clustering based on the Jaccard index, where a value of 1 denotes complete (100%) overlap between gene sets.

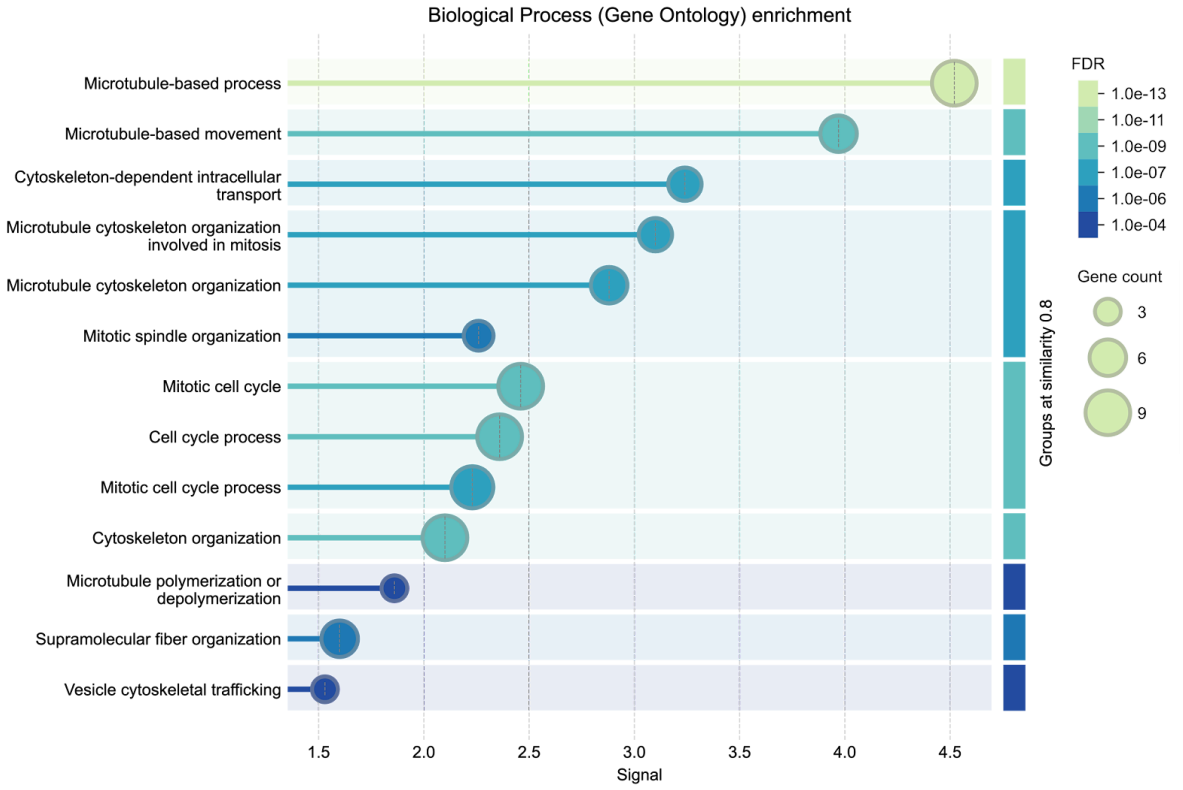

Figure 5.11: Biological Process enrichment analysis of GFP-PikA-specific interactors associated with 'Cytoskeleton'. Enrichment was calculated using STRING (v12) Reactome annotations. 'Signal' refers to the weighted harmonic mean of the observed-to-expected gene occurrence ratio and the corresponding -log(FDR) value. FDR: False Discovery Rate. 'Groups at similarity 0.8' indicates clustering based on the Jaccard index, where a value of 1 denotes complete (100%) overlap between gene sets.

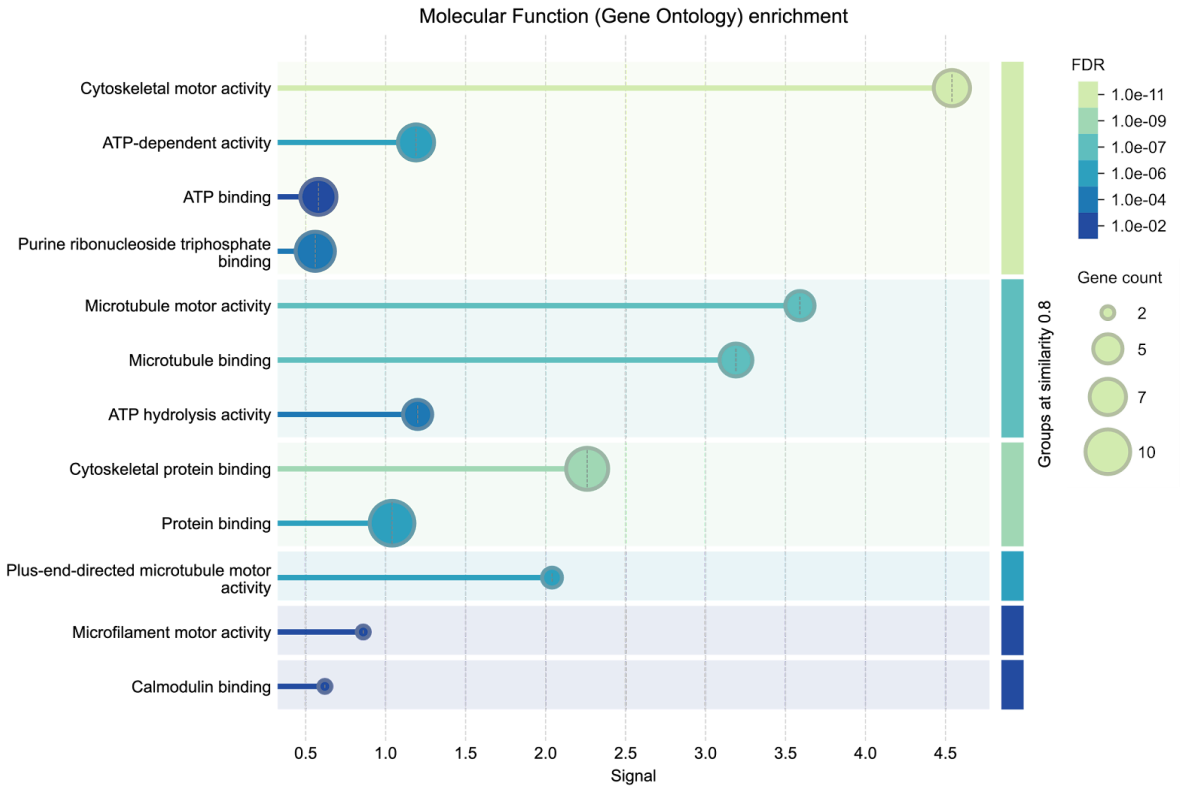

Figure 5.12: Molecular Function enrichment enrichment analysis of GFP-PikA-specific interactors associated with 'Cytoskeleton'. Enrichment was calculated using STRING (v12) Reactome annotations. 'Signal' refers to the weighted harmonic mean of the observed-to-expected gene occurrence ratio and the corresponding -log(FDR) value. FDR: False Discovery Rate. 'Groups at similarity 0.8' indicates clustering based on the Jaccard index, where a value of 1 denotes complete (100%) overlap between gene sets.

mlcR	*Myosin regulatory light chain. (161 aa)*
myoJ	*Myosin-J heavy chain; Processive motor protein that can move over long distances along F-actin without disassociating; processiveness depends on high physiological Mg(2+) concentrations. Presents a high actin affinity in the presence of ADP, fast ATP hydrolysis, and a high steady-state ATPase activity in the presence of actin that is rate limited by ADP release. Physiological decrease of free Mg(2+) ions leads to an increased rate of ADP release and shortening of the fraction of time it spends in the strong acting binding states. (2245 aa)*
kif9	*Kinesin-related protein 9; Microtubule-associated force-producing protein that plays a role in organelle transport. Its motor activity is directed toward the microtubule's plus end (By similarity); Belongs to the TRAFAC class myosin-kinesin ATPase superfamily. Kinesin family. (1222 aa)*
tubC	*Tubulin gamma chain; Tubulin is the major constituent of microtubules. The gamma chain is found at microtubule organizing centers (MTOC) such as the spindle poles or the centrosome, suggesting that it is involved in the minus-end nucleation of microtubule assembly (By similarity). (462 aa)*
myoG	*Myosin-G heavy chain; Myosins are actin-based motor molecules with ATPase activity. (3446 aa)*

Table 5.6: GFP-PikA-specific interactors associated with 'Cytoskeleton Organisation'. Interactors were identified through STRING (v12) analysis of AP-MS data. The geneset analysed set includes proteins uniquely detected in GFP-PikA samples and absent from both GFP-PikF samples and the GFP-only control. Interactor descriptions are reproduced directly from the STRING database interface, incorporating annotations from UniProt, EnsemblProtists, and KEGG: Kyoto Encyclopedia of Genes and Genomes.

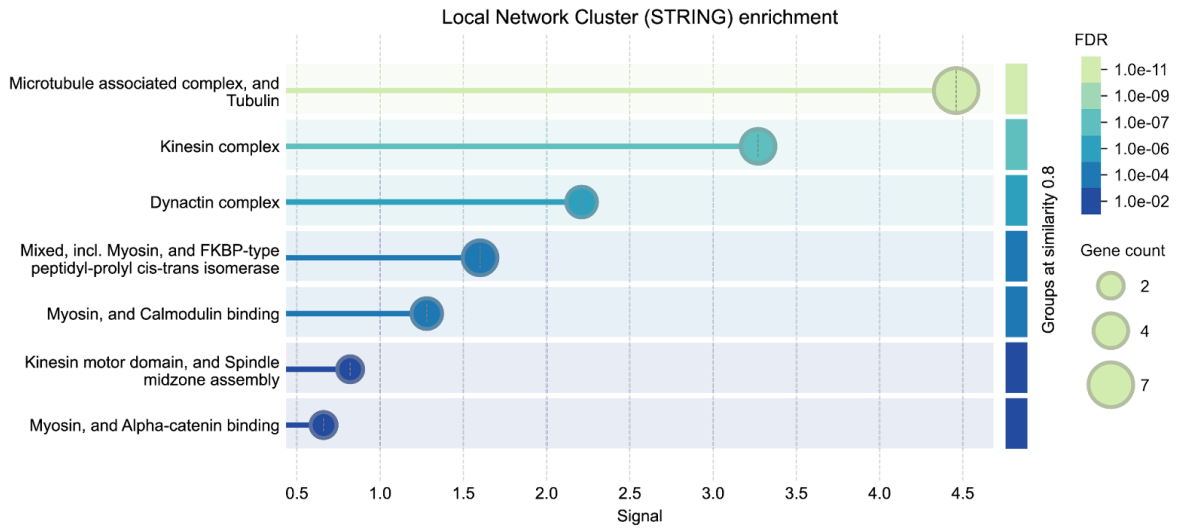

Figure 5.13: Local Network Cluster enrichment analysis of GFP-PikA-specific interactors associated with 'Cytoskeleton'. Enrichment was calculated using STRING (v12) Reactome annotations. 'Signal' refers to the weighted harmonic mean of the observed-to-expected gene occurrence ratio and the corresponding -log(FDR) value. FDR: False Discovery Rate. 'Groups at similarity 0.8' indicates clustering based on the Jaccard index, where a value of 1 denotes complete (100%) overlap between gene sets.

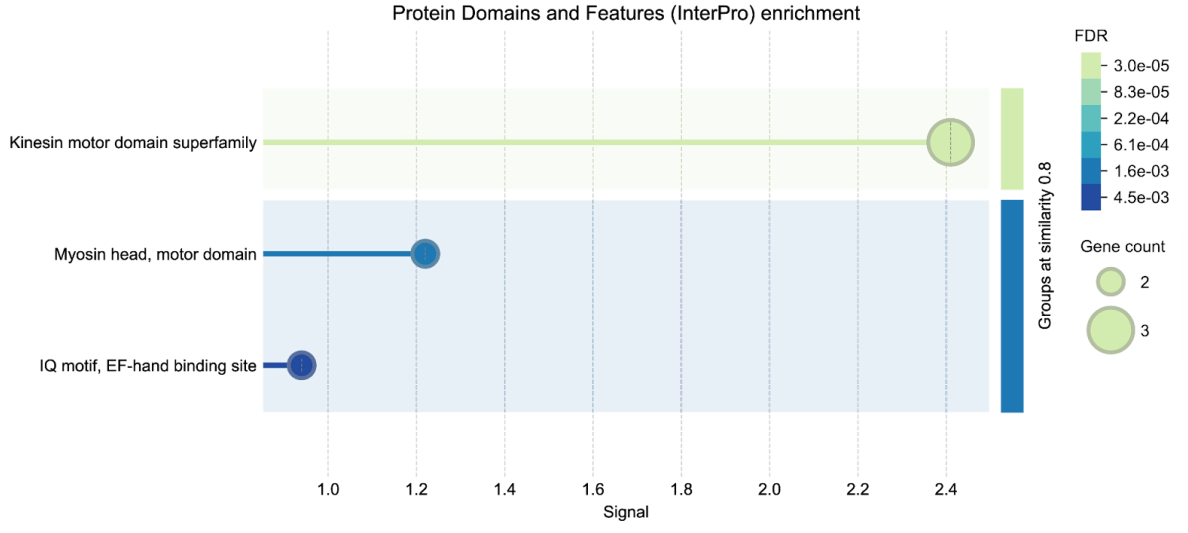

Figure 5.14: Protein Domains and Features enrichment analysis of GFP-PikA-specific interactors associated with 'Cytoskeleton Organisation'. Enrichment was calculated using STRING (v12) Reactome annotations. 'Signal' refers to the weighted harmonic mean of the observed-to-expected gene occurrence ratio and the corresponding -log(FDR) value. FDR: False Discovery Rate. 'Groups at similarity 0.8' indicates clustering based on the Jaccard index, where a value of 1 denotes complete (100%) overlap between gene sets.

Table 5.7 lists six of the 659 PikA-specific interactors identified by AP-MS that were associated with the term ‘Endocytosis’. These include VPS34-like PI3K **PikE**; **TstD**, a member of the Clathrin-interacting TSET complex (Hirst et al., 2014); **RacD**, a Rho-related protein with 54% homology to human Rac1 (Filić et al., 2021); the autophagy-related lysosome membrane protein **Lmp2B** (Xu et al., 2024); the endocytosis-associated transporter **AbcG2** (**MdrA1**) (Brazill et al., 2001); and DDB0167087 (Q8T867), an uncharacterised DNAJ-domain-containing protein potentially involved in Clathrin uncoating (Hasegawa et al., 2018). A Biological Process enrichment analysis (Figure 5.15) indicates that these interactors are involved in processes requiring coordinated regulation of membrane and cytoskeletal dynamics, including cell migration, cell motility, endocytosis, phagocytosis, and vesicle-mediated transport.

Table 5.8 highlights seven PikA-specific interactors associated with the term ‘Endosome’. In addition to PikE, these include the VPS34 modulator **Atg6B** (Beclin-1-like) (McKnight and Yue, 2013); the vesicle-SNARE **Vti1B**; the vacuolar sorting protein **Vps36**; the dynactin subunit 5 **DynE**; and the AP-4 Clathrin-adaptor complex subunit **Apm4** (de Chassey et al., 2001). Interestingly, two additional proteins were identified in association with the terms ‘Phagocytosis’ and ‘Macropinocytosis’: **MyoB** (Myosin IB heavy chain) and **ForG** (Formin-G) (data not shown).

tstD	*TSET complex member tstD. (154 aa)*
racD	*Rho-related protein racD; Belongs to the small GTPase superfamily. Rho family. (254 aa)*
pikE	*Phosphatidylinositol 3-kinase VPS34-like. (816 aa)*
DDB0167087	*Uncharacterized protein. (730 aa)*
lmpB	*Lysosome membrane protein 2-B; May act as a lysosomal receptor (By similarity). May be involved in macropinocytosis and fluid phase exocytosis; Belongs to the CD36 family. (755 aa)*
abcG2	*ABC transporter G family member 2; Required for endocytosis and endosomal pH regulation. Belongs to the ABC transporter superfamily. ABCG family. PDR (TC 3.A.1.205) subfamily. (1328 aa)*

Table 5.7: GFP-PikA-specific interactors associated with ‘Endocytosis’. Interactors were identified through STRING (v12) analysis of AP-MS data. The geneset analysed set includes proteins uniquely detected in GFP-PikA samples and absent from both GFP-PikF samples and the GFP-only control. Interactor descriptions are reproduced directly from the STRING database interface, incorporating annotations from UniProt, EnsemblProtists, and KEGG: Kyoto Encyclopedia of Genes and Genomes.

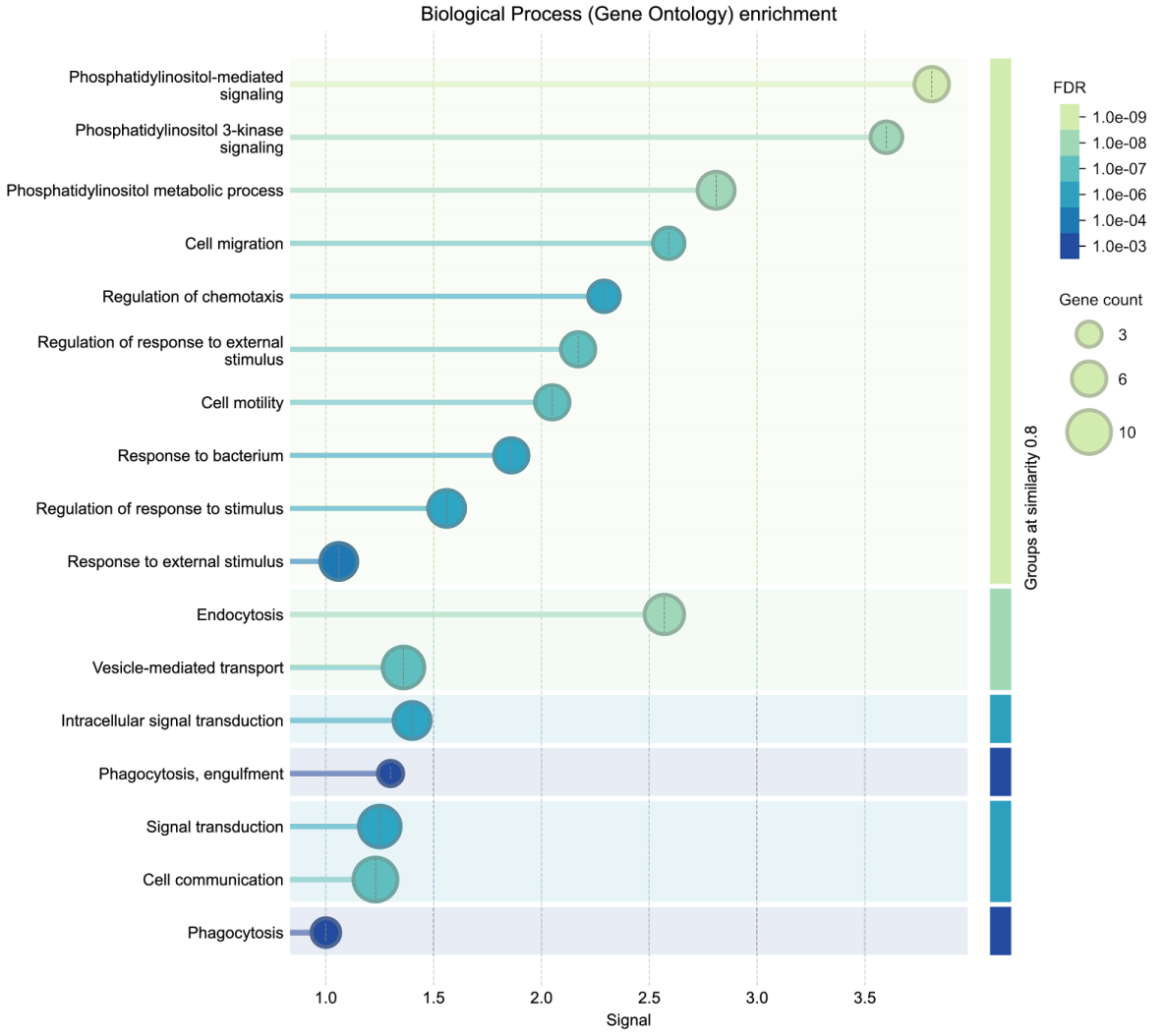

Figure 5.15: Biological Process enrichment analysis of GFP-PikA-specific interactors associated with 'Endocytosis'. Enrichment was calculated using STRING (v12) Reactome annotations. 'Signal' refers to the weighted harmonic mean of the observed-to-expected gene occurrence ratio and the corresponding -log(FDR) value. FDR: False Discovery Rate. 'Groups at similarity 0.8' indicates clustering based on the Jaccard index, where a value of 1 denotes complete (100%) overlap between gene sets.

pikE	*Phosphatidylinositol 3-kinase VPS34-like. (816 aa)*
atg6B	*Beclin-1-like protein B; Involved in autophagy. May be required to recruit the atg8-phosphatidylinositol conjugate and the atg12-atg5 conjugate to the pre- autophagosomal structure (By similarity); Belongs to the beclin family. (855 aa)*
Vti1B	*Uncharacterized protein. (269 aa)*
vps15	*Probable serine/threonine-protein kinase vps15; Belongs to the protein kinase superfamily. Ser/Thr protein kinase family. (1966 aa)*
vps36	*Vacuolar protein-sorting-associated protein 36; Component of the ESCRT-II complex, which is required for multivesicular body (MVB) formation and sorting of endosomal cargo proteins into MVBs. The MVB pathway mediates delivery of transmembrane proteins into the lumen of the lysosome for degradation (By similarity). (611 aa)*
dynE	*Dynactin subunit 5; Belongs to the dynactin subunits 5/6 family. Dynactin subunit 5 subfamily. (198 aa)*
apm4	*AP-4 complex subunit mu; Probable component of an adaptor protein complex. Adaptor protein complexes are vesicle coat components involved both in vesicle formation and cargo selection. They control the vesicular transport of proteins in different trafficking pathways. (530 aa)*

Table 5.8: GFP-PikA-specific interactors associated with ‘Endosome’. Interactors were identified through STRING (v12) analysis of AP-MS data. The geneset analysed set includes proteins uniquely detected in GFP-PikA samples and absent from both GFP-PikF samples and the GFP-only control. Interactor descriptions are reproduced directly from the STRING database interface, incorporating annotations from UniProt, EnsemblProtists, and KEGG: Kyoto Encyclopedia of Genes and Genomes.

5.2.3 PikF-Specific Interactors

AP-MS identified 398 PikF-specific interactors (Table 5.1). Among these, 15 were associated with the term ‘Cytoskeleton’ according to STRING analysis (Table 5.9). This group includes proteins involved in actin and microtubule dynamics, such as the cAMP-dependent protein kinase regulatory subunit **PkaR**; the Scar-interacting, actin-binding Profilin-2 (**ProB**) (Cvrčková et al., 2004; Seastone et al., 2001); Talin-B (**TalB**), which binds both actin filaments and PIP_3 (Tsujioka et al., 2019); and **ArpF** (**ArcC**), a subunit of the Arp2/3 complex. Several microtubule-associated proteins were also identified, including Doublecortin **DdDCX** (Sébastien et al., 2025), and the microtubule plus-end-binding proteins **Tacc1** (Samereier et al., 2010) and **DdEB1** (Rehberg and Gräf, 2002). Additional notable interactors include Actin-17 (**Act17**), Formin-F (**ForF**), and F-actin regulators such as **LimC** (Khurana et al., 2002), and the uncharacterised proteins DDB0205771 (Q54WT5, **Villin** headpiece domain) (Vardar et al., 2002), DDB0190831 (Q55CB2, **ADF-H** domain – Actin-depolymerizing factor homology) (Poukkula et al., 2011), and **GxcV** (Q54SR5, **RhoGEF** domain).

Molecular Function enrichment analysis revealed that these proteins are primarily involved in cytoskeletal protein binding (Figure 5.16), suggesting roles beyond endocytic trafficking. Supporting this, Subcellular Localisation and Biological Process enrichment analyses highlighted a broader functional scope including actin and microtubule organisation, as well as involvement in cell cycle regulation (Figures 5.17 and 5.18). Together, these findings indicate that PikF may coordinate cytoskeletal dynamics not only during macropinocytosis but also across other essential cellular processes.

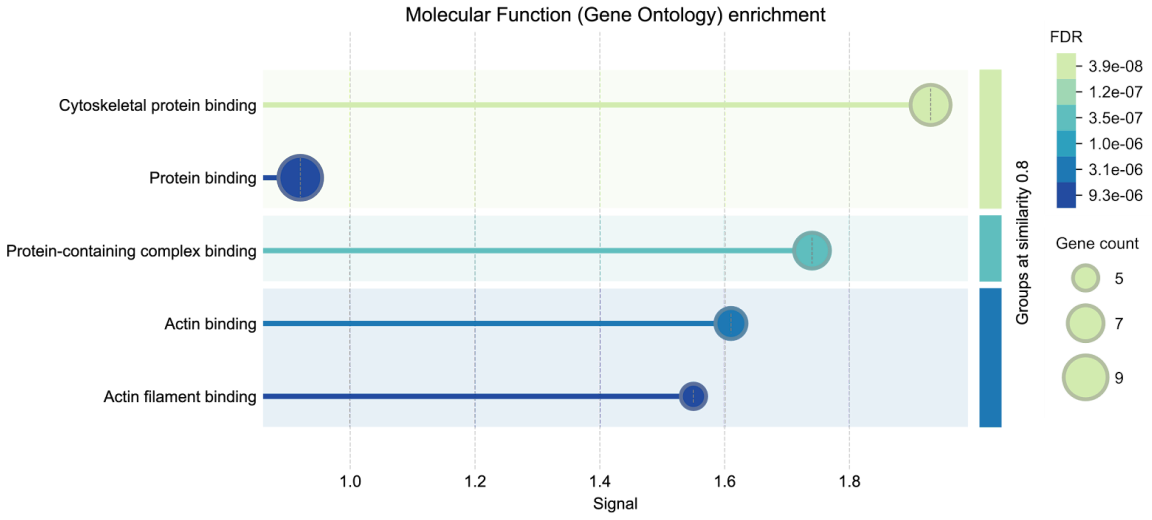

Figure 5.16: Molecular Function enrichment analysis of GFP-PikF-specific interactors associated with ‘Cytoskeleton’. Enrichment was calculated using STRING (v12) Reactome annotations. ‘Signal’ refers to the weighted harmonic mean of the observed-to-expected gene occurrence ratio and the corresponding -log(FDR) value. FDR: False Discovery Rate. ‘Groups at similarity 0.8’ indicates clustering based on the Jaccard index, where a value of 1 denotes complete (100%) overlap between gene sets.

pkaR	*cAMP-dependent protein kinase regulatory subunit. (327 aa)*
proB	*Profilin-2; Binds to actin and affects the structure of the cytoskeleton. At high concentrations, profilin prevents the polymerization of actin, whereas it enhances it at low concentrations. By binding to PIP2, it inhibits the formation of IP3 and DG. (124 aa)*
talB	*Talin-B; Actin-binding protein required for multicellular morphogenesis. Substrate of pkgB and/or pkbA. (2614 aa)*
arpF	*Actin-related protein 6. (490 aa)*
DDB0185366	*Uncharacterized protein. (652 aa)*
GxcV	*Uncharacterized protein. (481 aa)*
DDB0205771	*HP domain-containing protein. (1100 aa)*
dcx	*Protein doublecortin; Has a cytoskeleton-independent function in chemotactic signaling during development. (308 aa)*
TACC1	*Transforming acidic coiled-coil-containing protein. (1478 aa)*
act17	*Actin-17; Actins are highly conserved proteins that are involved in various types of cell motility and are ubiquitously expressed in all eukaryotic cells. Multiple isoforms are involved in various cellular functions such as cytoskeleton structure, cell mobility, chromosome movement and muscle contraction (By similarity); Belongs to the actin family. (374 aa)*
DDB0190831	*ADF-H domain-containing protein. (152 aa)*
bub2	*Putative mitotic check point protein BUB2; Part of a checkpoint which monitors spindle integrity and prevents premature exit from mitosis; Belongs to the BUB2 family. (366 aa)*
forF	*Formin-F; Formins play an important role in the nucleation of actin and the formation of linear actin filaments; Belongs to the formin homology family. Diaphanous subfamily. (1220 aa)*
eb1	*Microtubule-associated protein RP/EB family member 1; Involved in microtubule polymerization, and spindle function by stabilizing microtubules and anchoring them at centrosomes; Belongs to the MAPRE family. (506 aa)*

limC	*LIM domain-containing protein C; Binds to F-actin and may modulate the chemotactic response during early development and contribute to the maintenance of the strength of the actin cytoskeleton. (182 aa)*

Table 5.9: GFP-PikF-specific interactors associated with 'Cytoskeleton'. Interactors were identified through STRING (v12) analysis of AP-MS data. The geneset analysed set includes proteins uniquely detected in GFP-PikF samples and absent from both GFP-PikA samples and the GFP-only control. Interactor descriptions are reproduced directly from the STRING database interface, incorporating annotations from UniProt, EnsemblProtists, and KEGG: Kyoto Encyclopedia of Genes and Genomes.

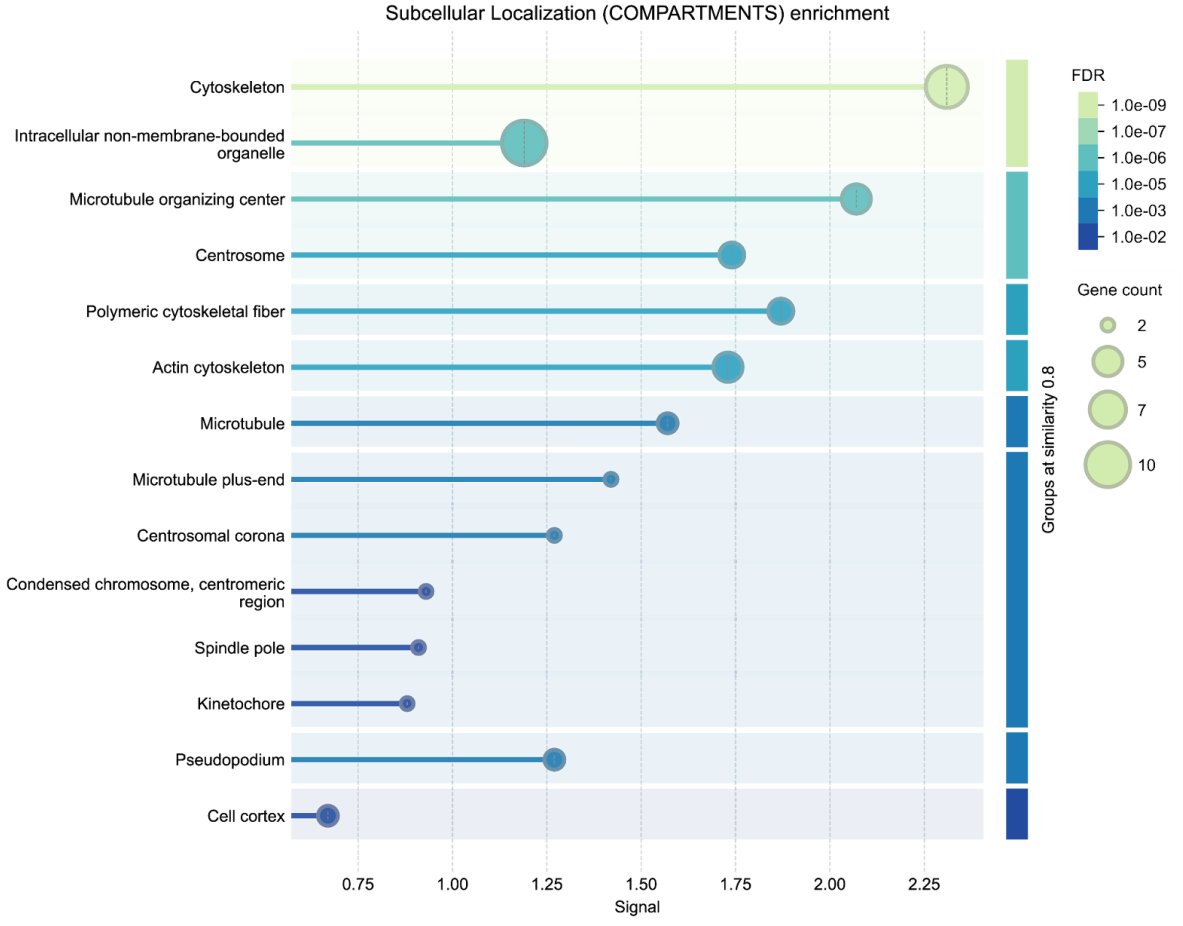

Figure 5.17: Subcellular Localisation enrichment analysis of GFP-PikF-specific interactors associated with 'Cytoskeleton'. Enrichment was calculated using STRING (v12) Reactome annotations. 'Signal' refers to the weighted harmonic mean of the observed-to-expected gene occurrence ratio and the corresponding -log(FDR) value. FDR: False Discovery Rate. 'Groups at similarity 0.8' indicates clustering based on the Jaccard index, where a value of 1 denotes complete (100%) overlap between gene sets.

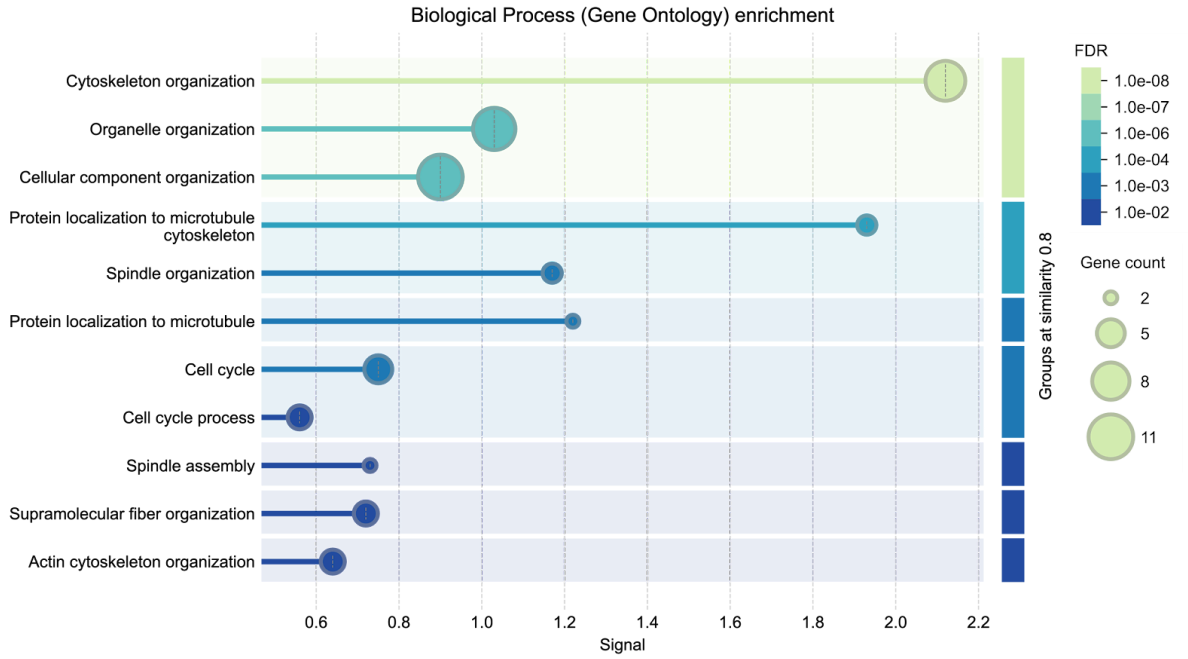

Figure 5.18: Biological Process enrichment analysis of GFP-PikF-specific interactors associated with 'Cytoskeleton'. Enrichment was calculated using STRING (v12) Reactome annotations. 'Signal' refers to the weighted harmonic mean of the observed-to-expected gene occurrence ratio and the corresponding -log(FDR) value. FDR: False Discovery Rate. 'Groups at similarity 0.8' indicates clustering based on the Jaccard index, where a value of 1 denotes complete (100%) overlap between gene sets.

Table 5.10 lists 12 of the 398 PikF-specific interactors identified through STRING analysis as being associated with 'Cytoskeleton Organisation'. Of these, nine (ProB, TalB, Tacc1, Act17, ForF, DdEB1, LimC, Q54RJ3, and Q54WT5) were also previously highlighted under the broader 'Cytoskeleton' category. The remaining three interactors are the calcium-regulated actin-bundling protein **AbpB**, the actin-depolymerisation modulator **Aip1** (Konzok et al., 1999), and the microtubule-organising, IQGAP-interacting CLIP-associating protein **CLASP** (Cao et al., 2015; Fukata et al., 2002; Jia et al., 2024). Local Network Cluster enrichment analysis revealed strong associations of these with Formin, Profilin, F-actin, the Rac3 GTPase cycle, and the Formin FH2 and FH3 domains (Figure 5.19).

Further STRING analysis identified six additional PikF-specific interactors associated with 'Regulation of Cytoskeleton Organisation' (Table 5.11). These include the Severin actin-fragmenting protein **SevA** (Yamamoto et al., 1982), the chemotaxis-regulating **CRAC** protein **DagA** (Comer et al., 2005), the probable vinculin homologue **CtnnA** (**VinA**), the villin-like domain-containing filament-bundling protein **VilD** (George et al., 2020), the Twinfilin actin polymerisation inhibitor **TwfA** (Hakala et al., 2021), and negative regulator of phagocytosis Paxillin-B (**PaxB**) (Pribic et al., 2011). Biological Process enrichment analysis associated these proteins with actin-specific cytoskeletal dynamics (Figure 5.20).

These associations were further supported by Local Network Cluster enrichment analysis, which again highlighted links to Formin, Profilin, and the Rac3 GTPase cycle, with additional associations to focal adhesions, the Talin-associated I/LWEQ domain (McCann and Craig, 1997), Filamin, and Cofilin-like domains (Figure 5.21). Finally, Protein Domains and Features enrichment analysis indicated strong representation of Gelsolin-like domains, followed by Villin-like and ADF-H (actin-depolymerising factor homology) domains (Figure 5.22), underscoring the central role of these interactors in modulating actin filament turnover and reorganisation.

abpB	*Calcium-regulated actin-bundling protein; May contribute to the structure and reorganization of filopodia and pseudopodia accompanying cell movements. (295 aa)*
proB	*Profilin-2; Binds to actin and affects the structure of the cytoskeleton. At high concentrations, profilin prevents the polymerization of actin, whereas it enhances it at low concentrations. By binding to PIP2, it inhibits the formation of IP3 and DG. (124 aa)*
aip1	*Actin-interacting protein 1; Implicated in both actin filament depolymerization and polymerization. May enhance chemotaxis by promoting cofilin-dependent actin assembly at cell leading edges. (597 aa)*
talB	*Talin-B; Actin-binding protein required for multicellular morphogenesis. Substrate of pkgB and/or pkbA. (2614 aa)*
DDB0185366	*Uncharacterized protein. (652 aa)*
DDB0205771	*HP domain-containing protein. (1100 aa)*
TACC1	*Transforming acidic coiled-coil-containing protein. (1478 aa)*
act17	*Actin-17; Actins are highly conserved proteins that are involved in various types of cell motility and are ubiquitously expressed in all eukaryotic cells. Multiple isoforms are involved in various cellular functions such as cytoskeleton structure, cell mobility, chromosome movement and muscle contraction (By similarity); Belongs to the actin family. (374 aa)*
CLASP	*CLIP-associating protein. (899 aa)*
forF	*Formin-F; Formins play an important role in the nucleation of actin and the formation of linear actin filaments; Belongs to the formin homology family. Diaphanous subfamily. (1220 aa)*

eb1	*Microtubule-associated protein RP/EB family member 1; Involved in microtubule polymerization, and spindle function by stabilizing microtubules and anchoring them at centrosomes; Belongs to the MAPRE family. (506 aa)*
limC	*LIM domain-containing protein C; Binds to F-actin and may modulate the chemotactic response during early development and contribute to the maintenance of the strength of the actin cytoskeleton. (182 aa)*

Table 5.10: GFP-PikF-specific interactors associated with 'Cytoskeleton Organisation'. Interactors were identified through STRING (v12) analysis of AP-MS data. The geneset analysed set includes proteins uniquely detected in GFP-PikF samples and absent from both GFP-PikA samples and the GFP-only control. Interactor descriptions are reproduced directly from the STRING database interface, incorporating annotations from UniProt, EnsemblProtists, and KEGG: Kyoto Encyclopedia of Genes and Genomes.

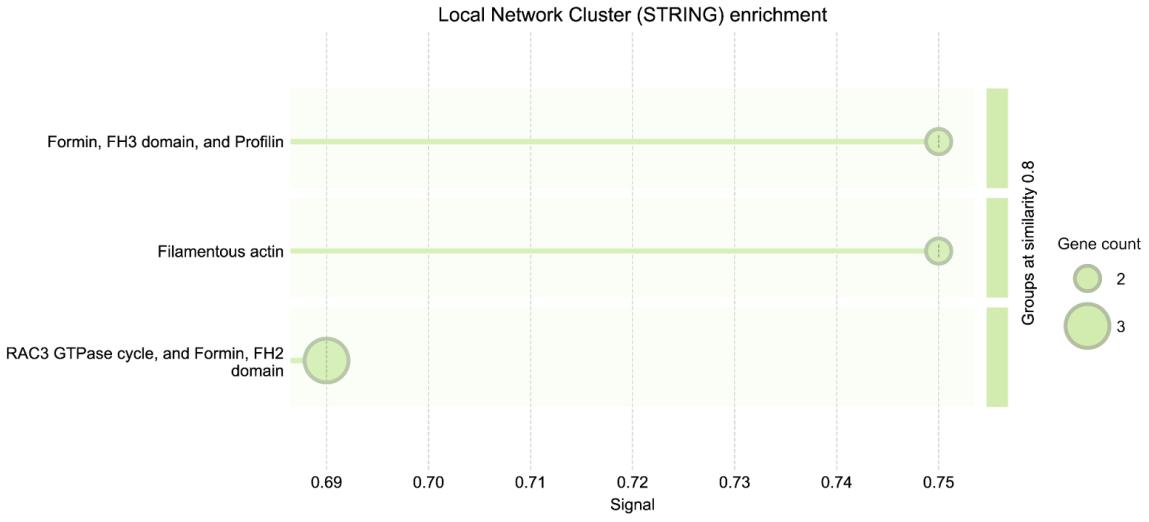

Figure 5.19: Local Network Cluster enrichment analysis of GFP-PikF-specific interactors associated with 'Cytoskeleton Organisation'. Enrichment was calculated using STRING (v12) Reactome annotations. 'Signal' refers to the weighted harmonic mean of the observed-to-expected gene occurrence ratio and the corresponding -log(FDR) value. FDR: False Discovery Rate. 'Groups at similarity 0.8' indicates clustering based on the Jaccard index, where a value of 1 denotes complete (100%) overlap between gene sets.

sevA	*Severin; Severin blocks the ends of F-actin and causes the fragmentation and depolymerization of actin filaments in a Ca(2+) dependent manner; Belongs to the villin/gelsolin family. (362 aa)*
proB	*Profilin-2; Binds to actin and affects the structure of the cytoskeleton. At high concentrations, profilin prevents the polymerization of actin, whereas it enhances it at low concentrations. By binding to PIP2, it inhibits the formation of IP3 and DG. (124 aa)*
dagA	*Protein CRAC; Couples activated G protein to adenylyl cyclase signal transduction from surface cAMP receptor. Pianissimo a cytosolic regulator and CRAC, are both essential for activation of the enzyme adenylyl cyclase. Pianissimo and CRAC do not function redundantly. Both proteins are integral components of the adenylyl cyclase activation pathway. (698 aa)*
aip1	*Actin-interacting protein 1; Implicated in both actin filament depolymerization and polymerization. May enhance chemotaxis by promoting cofilin-dependent actin assembly at cell leading edges. (597 aa)*
ctnnA	*Probable vinculin; Involved in cell adhesion. Thought to play an important role in cytokinesis B, probably by providing substrate adhesion and traction forces. Required to organize and polarize the tip epithelium during cytokinesis. Required for the normal distribution of myosin in the tip epithelium. Involved in the localization of ctxA, ctxB, dcsA, exoc6 and rgaA. Thought to form a complex with ctxA, ctxB, and rgaA which regulates myosin accumulation to the apical plasma membrane. Belongs to the vinculin/alpha-catenin family. (842 aa)*
VilD	*HP domain-containing protein. (1775 aa)*
DDB0190831	*ADF-H domain-containing protein. (152 aa)*
twfA	*Twinfilin; Actin-binding protein involved in motile and morphological processes. Inhibits actin polymerization, likely by sequestering G- actin (By similarity). (335 aa)*
paxB	*Paxillin-B; Required for cell-substrate adhesion, cell sorting, slug migration, and cell differentiation. May function upstream of limB. (569 aa)*

Table 5.11: GFP-PikF-specific interactors associated with 'Regulation of Cytoskeleton Organisation'. Interactors were identified through STRING (v12) analysis of AP-MS data. The geneset analysed set includes proteins uniquely detected in GFP-PikF samples and absent from both GFP-PikA samples and the GFP-only control. Interactor descriptions are reproduced directly from the STRING database interface, incorporating annotations from UniProt, EnsemblProtists, and KEGG: Kyoto Encyclopedia of Genes and Genomes.

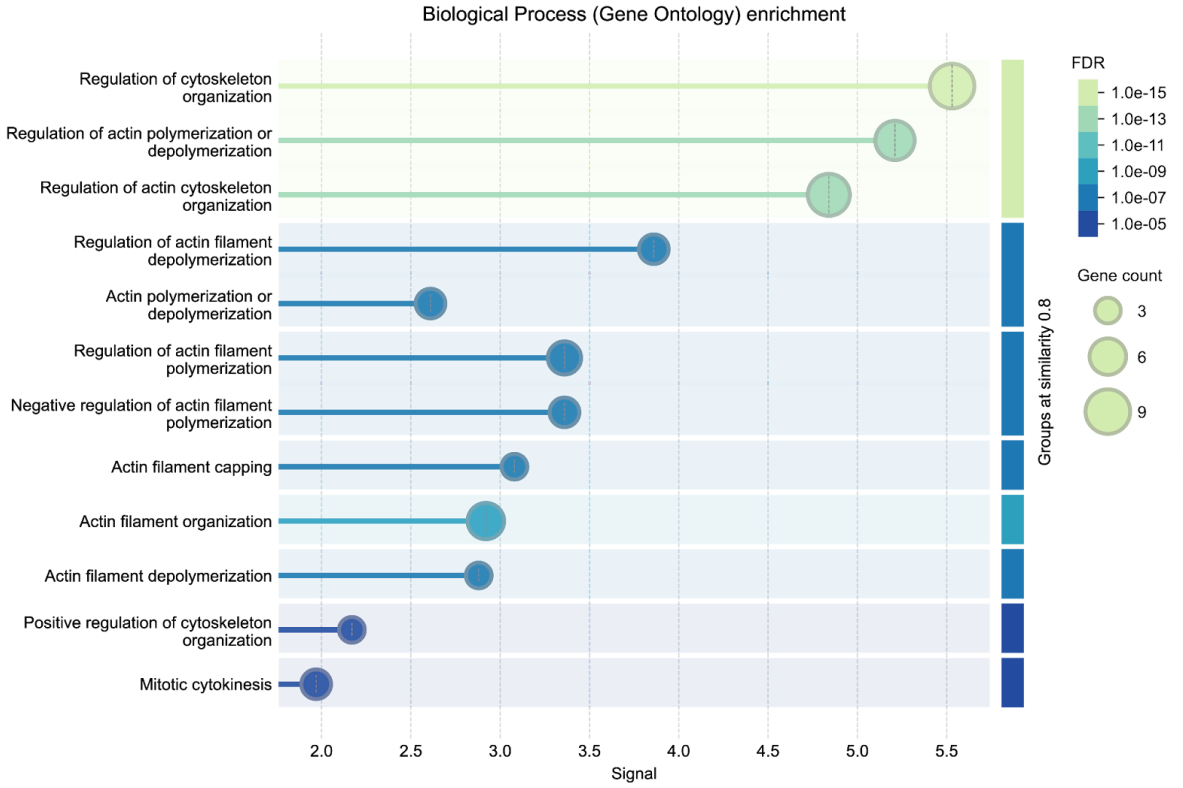

Figure 5.20: Biological Process enrichment analysis of GFP-PikF-specific interactors associated with 'Regulation of Cytoskeleton Organisation'. Enrichment was calculated using STRING (v12) Reactome annotations. 'Signal' refers to the weighted harmonic mean of the observed-to-expected gene occurrence ratio and the corresponding -log(FDR) value. FDR: False Discovery Rate. 'Groups at similarity 0.8' indicates clustering based on the Jaccard index, where a value of 1 denotes complete (100%) overlap between gene sets.

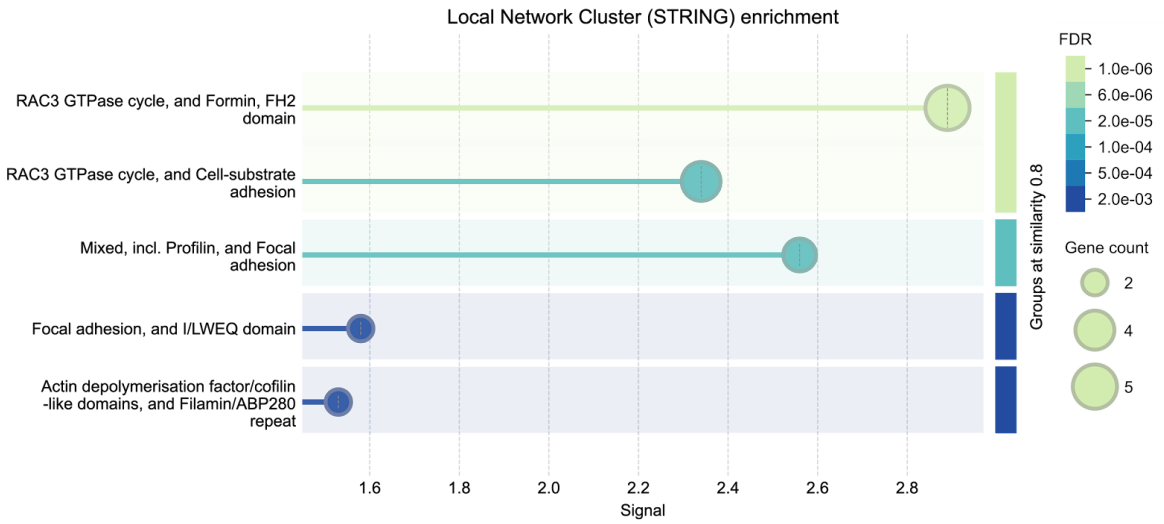

Figure 5.21: Local Network Cluster enrichment analysis of GFP-PikF-specific interactors associated with 'Regulation of Cytoskeleton Organisation'. Enrichment was calculated using STRING (v12) Reactome annotations. 'Signal' refers to the weighted harmonic mean of the observed-to-expected gene occurrence ratio and the corresponding -log(FDR) value. FDR: False Discovery Rate. 'Groups at similarity 0.8' indicates clustering based on the Jaccard index, where a value of 1 denotes complete (100%) overlap between gene sets.

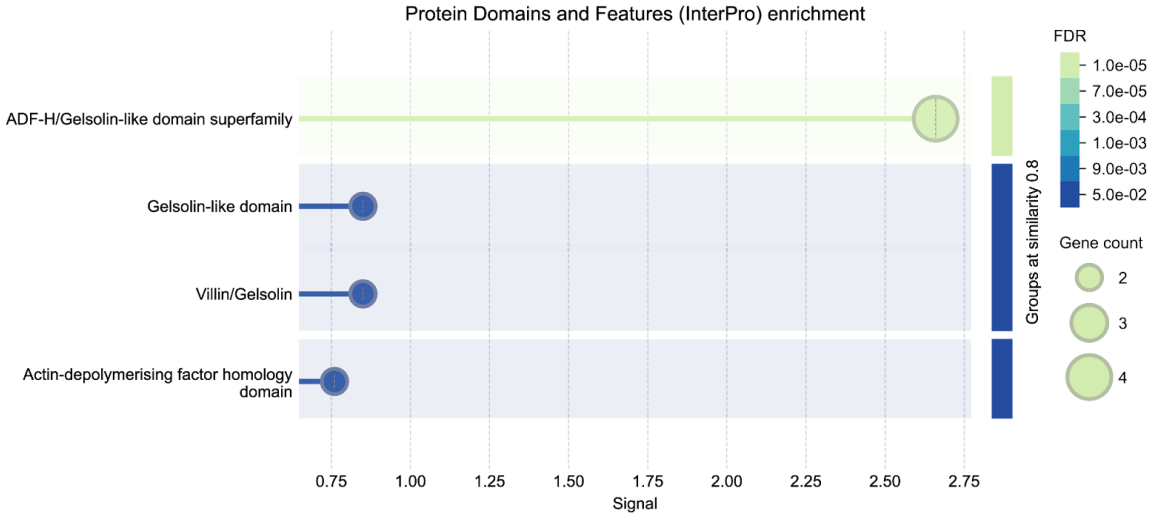

Figure 5.22: Protein Domains and Features enrichment analysis of GFP-PikF-specific interactors associated with 'Regulation of Cytoskeleton Organisation'. Enrichment was calculated using STRING (v12) Reactome annotations. 'Signal' refers to the weighted harmonic mean of the observed-to-expected gene occurrence ratio and the corresponding -log(FDR) value. FDR: False Discovery Rate. 'Groups at similarity 0.8' indicates clustering based on the Jaccard index, where a value of 1 denotes complete (100%) overlap between gene sets.

Lastly, Table 5.12 presents six PikF-specific interactors, identified via STRING analysis, that are associated with the term ‘Endosome’. These include the mTORC1-associated Roadblock/LAMTOR2 domain-containing protein **Mapbpip** (de Araujo et al., 2017); **Syn7A**, an endo-phagocytic SNARE protein homologous to mammalian syntaxin 7 (Bogdanovic et al., 2002, 2000); the Ras superfamily GTPase **Rab11B** (Dragoi and O’Halloran, 1998); the well-characterised endosomal marker **P80** (Mercanti et al., 2006; Ravanel et al., 2001); the F-actin-binding protein **LimC** (Khurana et al., 2002); and the uncharacterised protein DDB_G0291948 (Q54DY3), a putative **LAMTOR4** homolog of the lysosome-regulating Rag-Ragulator complex (Shen et al., 2016). Notably, P80 and LimC were also associated with both ‘Phagocytosis’ and ‘Macropinocytosis’ (data not shown), suggesting their involvement in specialised endocytic functions. However, no PikF-specific interactors were linked to the broader term ‘Endocytosis’, indicating a more selective association with late or specialised endosomal pathways rather than general endocytic processes.

DDB_G0291948	*Ragulator complex protein LAMTOR4 homolog; Regulator of the TOR pathway, a signaling cascade that promotes cell growth in response to growth factors, energy levels, and amino acids. As part of the Ragulator complex, may activate the TOR signaling cascade in response to amino acids (By similarity). (87 aa)*
mapbpip	*Robl_LC7 domain-containing protein. (123 aa)*
syn7A	*Syntaxin-7A; Involved in the targeting and/or fusion of transport vesicles to their target membrane during transport of proteins from the early endosome to the lysosome. Required for fusion of late endosomes with lysosomes and homotypic lysosomal fusion. May be involved in protein trafficking from the plasma membrane to the early endosome (EE) as well as in homotypic fusion of endocytic organelles. Belongs to the syntaxin family. (356 aa)*
rab11B	*Ras-related protein Rab-11B. (220 aa)*
p80	*Protein P80; Belongs to the SLC31A transporter family. (530 aa)*
limC	*LIM domain-containing protein C; Binds to F-actin and may modulate the chemotactic response during early development and contribute to the maintenance of the strength of the actin cytoskeleton. (182 aa)*

Table 5.12: GFP-PikF-specific interactors associated with ‘Endosome’. Interactors were identified through STRING (v12) analysis of AP-MS data. The geneset analysed set includes proteins uniquely detected in GFP-PikF samples and absent from both GFP-PikA samples and the GFP-only control. Interactor descriptions are reproduced directly from the STRING database interface, incorporating annotations from UniProt, EnsemblProtists, and KEGG: Kyoto Encyclopedia of Genes and Genomes.

5.3 Discussion

Isoform-specific cytoskeletal interactomes of PikA and PikF revealed by AP-MS

Our AP-MS analysis identified 4,168 putative interactors across PikA and PikF, of which 659 were unique to PikA, 398 to PikF, and 203 were shared. While preliminary – reflecting a single biological run – these data offer an initial view of isoform-specific signalling landscapes for Class I PI3Ks. The resulting interactomes point to distinct regulatory and effector sets that could underlie the non-redundant roles of PikA and PikF during macropinocytic cup formation.

A clear message emerges from this analysis: in *D. discoideum*, cytoskeletal and membrane dynamics are coordinated by broad, multi-modal networks. The same molecular players likely participate across diverse processes, including multiple endocytic pathways (clathrin-mediated, clathrin-independent, macropinocytosis, and phagocytosis), exocytosis, cell motility, division, and development – yet their process-specific orchestration remains poorly defined. Candidate components for macropinocytosis regulation include transport and motor proteins (kinesins, dyneins, dynactins, myosins), scaffolds (talins, vinculins), filament regulators (profilins, formins, severins, twinfilins), and core structural components (tubulins). Together with Chapters 3-4, these findings support an emerging view that PikA and PikF contribute non-redundantly to membrane and cytoskeletal dynamics, extending well beyond canonical PIP_3 production at the plasma membrane to spatially organised protein networks that scaffold, transport, and tune actin remodelling.

PikA-specific interactors: microtubule and motor protein complexes

GFP-PikA-specific interactors identified by AP-MS reveal a strong enrichment for cytoskeletal transport machinery, particularly microtubule-associated components, including kinesins (Kif2–Kif11), dynactin subunits (DynF, DynB, DynE), the dynein regulator NudE, and tubulin (TubC). In parallel, multiple myosins (MlcR, MyoJ, MyoG) and clathrin-associated proteins (TstD, Apm4) suggest PikA's involvement in actin-based motility and endocytic trafficking. These data point to a model in which PikA participates in a specialised cytoskeletal network that governs its recruitment, function, and recycling during macropinocytosis.

Two interactors in particular (MyoB and ForG) stand out for their known roles in actin polymerisation and cup formation. ForG contributes to actin assembly at the base of macropinocytic cups (Körber et al., 2023), while MyoB helps to both cross-link actin filaments to prevent their outward projection (like is required at the base of the cup) and mechanically propel macropinosomes into the actin cortex (Novak et al., 1995). Their enrichment supports the hypothesis that PikA is active at the base of nascent macropinocytic cups (as shown by its basal localisation in Chapter 4). In contrast, the identification of microtubule-associated transport proteins – particularly DynE, which is linked to endosomal trafficking (Mayya et al., 2022) – suggests a potential mechanism for PikA removal or recycling following its activity during the early stages of macropinocytic cup formation, as

also indicated by microscopy data presented in Chapter 4. Thus, PikA may be dynamically trafficked between intracellular compartments and the plasma membrane through the coordinated action of myosin and kinesin-dynein-dynactin motor complexes.

Taken together, these findings support a model of spatiotemporal regulation in which PikA is selectively positioned at specific sites and time points during macropinocytic cup formation. This transport-dependent localisation may be critical for distinguishing PikA's role from that of PikF, ensuring that its activity is tightly coordinated with actin assembly during the early stages of macropinocytosis. Functional validation of the proposed transport interactions will be essential to substantiate this regulatory model.

PikF-specific interactors: actin disassembly and turnover

In contrast, PikF preferentially associates with actin filament modulators such as Profilin-2, Talin-B, LimC, and Arp2/3 subunits, along with regulators of actin turnover including Aip1, Twinfilin, Severin, and Villin-domain-containing proteins. These associations support a non-redundant role for PikF in actin disassembly and macropinocytic cup closure, consistent with its localisation extending to the cup rim and previous findings (Hoeller et al., 2013). Notably, our results align with earlier studies highlighting the involvement of Aip1 and Cofilin in the later stages of macropinocytic cup formation (Konzok et al., 1999). The actin-binding protein Coronin (CorA) was enriched in association with PikF compared to PikA (Table 5.13), further supporting a role in actin filament severing. In budding yeast, Coronin (Crn1) has been shown to facilitate the recruitment of Cofilin to F-actin, thereby enhancing its severing activity (Mikati et al., 2015).

Strikingly, PikF also interacts with the IQGAP-related DGAP1 (RgaA), Cortexillin-1/2, and GacW (Table 5.13) – proteins involved in cortical tension regulation, Rac signalling, and suppression of actin polymerisation. The morphological similarity between DGAP1$^-$ and PikF$^-$ cells raises the possibility that PikF interacts with DGAP1 to spatially confine active Rac1, preventing its mislocalisation during macropinocytic cup maturation (Faix et al., 1998; Filić et al., 2014).

Together, these findings support a model in which PikF functions as a spatial regulator, directing precise Rac1 signalling to control actin dynamics during cup closure. These proposed roles for PikF align with broader insights into the functions of IQGAP-related proteins and Cortexillin, which regulate cortical mechanics downstream of Rac (Faix et al., 2001; Mondal et al., 2010). Although Rac/IQGAP/Cortexillin interactions have been most extensively studied in the context of cytokinesis and cell migration, they have also been proposed to participate in diverse feedback systems that localise PI3K activity to defined membrane regions, thereby directing cytoskeletal rearrangements (Lee et al., 2010). In mammalian cells, for example, IQGAP1 is thought to serve as a PI3K/Akt scaffolding hub that links phosphoinositide signalling with Rac-dependent cytoskeletal remodeling (Thines et al., 2023; Yerramilli et al., 2022). In *D. discoideum*, DGAP1 has been shown to bind active Rac1 and limit the availability of Rac1-GTP for effector binding, such as the SCAR/WAVE complex (Filić et al., 2014), providing a plausible mechanism for localised Rac confinement via PikF-DGAP1 interaction.

Gene	Accession	PikA LFQ Intensity	PikF LFQ Intensity	Ctrl LFQ Intensity	PikA/PikF	PikA/Ctrl	PikF/PikA	PikF/Ctrl
gacN	**Q54WY8**	**25565000**	**46350000**	**35447000**	**0.55156419**	**0.72121759**	**1.81302562**	**1.30758597**
nxnA	P24639	24618000000	42648000000	22768000000	0.57723692	1.08125439	1.73239093	1.87315531
gxcB	**Q55E26**	**14940000**	**25539000**	**0**	**0.58498767**	**#DIV/0!**	**1.70943775**	**#DIV/0!**
ctxA	**Q54HG2**	**11293000000**	**18342000000**	**9603400000**	**0.61569076**	**1.17593769**	**1.62419198**	**1.90994856**
ctxB	**Q550R2**	**8548900000**	**13700000000**	**7002200000**	**0.6240073**	**1.22088772**	**1.60254536**	**1.95652795**
gacO	**Q55GP8**	**116860000**	**182550000**	**0**	**0.64015338**	**#DIV/0!**	**1.56212562**	**#DIV/0!**
gacW	**Q54G18**	**459080000**	**691330000**	**372970000**	**0.66405335**	**1.23087648**	**1.50590311**	**1.85358072**
rgaA	**Q54K32**	**12059000000**	**18008000000**	**12457000000**	**0.66964682**	**0.96805009**	**1.49332449**	**1.44561291**
sepA	Q8T2I8	43671000	64155000	24965000	0.68071078	1.749289	1.46905269	2.56979772
svkA	O61122	101220000	147270000	100130000	0.68730902	1.01088585	1.45494961	1.47078798
forA	A0A0K2ZB59	1632700000	2366700000	1700900000	0.68986352	0.95990358	1.44956208	1.39143983
corA	**P27133**	**15364000000**	**21111000000**	**13954000000**	**0.72777225**	**1.10104629**	**1.37405624**	**1.51289953**
racI	**Q9GPR2**	**36844000**	**50554000**	**31092000**	**0.72880484**	**1.18499936**	**1.37210943**	**1.6259488**
exoc4	Q54P76	31017000	42144000	38892000	0.73597665	0.7975162	1.35873876	1.08361617
IqgC	**Q54I64**	**121940000**	**138720000**	**112050000**	**0.87903690**	**1.08826416**	**1.13760866**	**1.23801874**
rgbA	**Q55CR5**	**366060000**	**305490000**	**272870000**	**1.19827162**	**1.34151793**	**0.83453532**	**1.11954410**
racH	**Q9GPR7**	**108810000**	**79174000**	**87718000**	**1.3743148**	**1.24045235**	**0.72763532**	**0.90259695**
rapgap1	**Q75J96**	**49717000**	**34924000**	**45140000**	**1.42357691**	**1.10139566**	**0.7024559**	**0.77368188**
gefE	Q8IS18	19381000	13445000	0	1.44150242	#DIV/0!	0.69372065	#DIV/0!
fimA	P54680	289630000	194810000	44449000	1.48673066	6.51600711	0.67261679	4.38277577
pkgB	P28178	289620000	194280000	259910000	1.49073502	1.1143088	0.67081003	0.74748952
rasB	**P32252**	**358580000**	**238430000**	**383280000**	**1.50392149**	**0.93555625**	**0.66492833**	**0.62207785**
rpkA	**Q86D86**	**32668000**	**21303000**	**0**	**1.53349294**	**#DIV/0!**	**0.65210604**	**#DIV/0!**
nfaA	Q55AR6	1413700000	917200000	923180000	1.54132141	1.53133733	0.64879394	0.99352239
vilA	Q8WQ85	90114000	57368000	29711000	1.57080602	3.03301807	0.63661584	1.93086736
pgkA	Q9GPM4	2445400000	1554700000	1533600000	1.57290796	1.59454877	0.63576511	1.01375848
arfA	O00909	2190200000	1384500000	1761300000	1.58194294	1.24351331	0.63213405	0.78606711
rab1D	Q54NU2	636800000	389670000	441650000	1.6342033	1.44186573	0.61191897	0.88230499
tkt-1	Q556J0	8787900000	5290300000	4236800000	1.66113453	2.07418335	0.6019982	1.24865465
abpC	P13466	2419100000	1430100000	1919200000	1.69156003	1.26047311	0.59117027	0.74515423
myoF	P54695	268600000	156650000	88873000	1.71465049	3.02229023	0.58320923	1.76262757
pteN	Q8T9S7	71206000	41367000	38463000	1.72132376	1.85128565	0.58094823	1.07550113
rab8A	P20790	510980000	288420000	272680000	1.77165245	1.87391815	0.56444479	1.05772334
gpaB	**P16051**	**528020000**	**295970000**	**403620000**	**1.78403217**	**1.30821069**	**0.56052801**	**0.73328874**
adcA	Q54CH1	154190000	85549000	88276000	1.80235888	1.74668086	0.55482846	0.96910825
exoc2	Q54VX5	52011000	28486000	0	1.82584427	#DIV/0!	0.54769183	#DIV/0!
cdk1	P34112	503640000	252270000	412870000	1.99643239	1.21985128	0.5008935	0.61101557

Table 5.13: Tentative PikA- and PikF-enriched interactors with enrichment values below 2x. Proteins preferentially associated with PikA are highlighted in magenta, and those enriched with PikF are highlighted in blue. Interactors were identified through AP-MS. Enrichment values are based on relative detection in GFP-PikA versus GFP-PikF, and are also compared to the GFP-only control.

The role of IQGAP scaffolds in spatial PI3K signalling coordination

Among the four IQGAP-related proteins in *D. discoideum*, IqgC (DdIQGAP3) is the most closely tied to macroendocytosis, exerting RasG-dependent GAP activity (Marinović et al., 2019). Interestingly, IqgC is equally enriched with both PikA and PikF in our dataset, suggesting it may scaffold distinct Ras-PI3K complexes within different regions of the cup – with PikA localised basally and PikF toward the rim (see Chapter 3). Coincidentally, the formin ForG (a PikA-specific interactor) has been shown to be regulated by RasB and RasG, and RasB was 1.5x enriched with PikA in our AP-MS data (Table 5.13), reinforcing a possible role for IQGAP scaffolds in mediating isoform-specific PI3K recruitment and cytoskeletal coordination.

DGAP1 (RgaA), by contrast, shows preferential association with PikF (Table 5.13), and previous work shows that DGAP1 localises to cup peripheries while active Rac1 concentrates inside the cup (Šoštar et al., 2024). Although DGAP1 is proposed to dissociate from the membrane upon Rac1-GTP binding, this model does not fully explain Rac confinement. An alternative model, supported by our data, is that DGAP1 functions to deplete Rac1-GTP in peripheral zones, potentially anchored or stabilised by PikF. The similar morphological phenotypes of DGAP1$^-$ and PikF$^-$ cells further support this idea, suggesting a shared function in confining Rac signalling during cup extension and closure. This could reflect a ‘diffusion trap’ model (Welliver and Swanson, 2012), wherein localised signalling is maintained by selective sequestration or inactivation of Rac. In support of this, we also observed a 1.5x enrichment of the RhoGAP GacW in association with PikF (Table 5.13). GacW is a CARMIL-GAP that has been implicated in Rac1A regulation (Jung et al., 2022), and its PikF association suggests it may act downstream or in parallel with DGAP1 to spatially limit Rac activity. Additional PikF-associated GTPase regulators include GxcB (RhoGEF, 1.7x enriched), GacN and GacO (RhoGAPs, 1.5-1.8x enriched), and RacI (1.4x enriched) (Table 5.13), all of which are promising candidates for further investigation into Class I PI3K isoform-specific regulation of cytoskeletal dynamics during macropinocytosis.

MyoB, ForG, P80 and LimC are of particular interest

Among the PI3K isoform-specific interactors identified through STRING analysis, four proteins – MyoB and ForG (PikA-specific), and P80 and LimC (PikF-specific) – emerged as particularly relevant to macroendocytic processes, being associated with the terms ‘Phagocytosis’ and ‘Macropinocytosis’. These candidates are of considerable interest for future studies into regulatory mechanisms of macropinocytosis.

ForG, a formin involved in actin polymerisation, has been shown to promote RasB- and RasG-driven actin assembly at the base of macropinocytic cups in cooperation with RacB-regulated ForB, while being excluded from SCAR/WAVE-rich regions near the cup rim (Junemann et al., 2016; Körber et al., 2023). This pattern mirrors the spatial localisation of PikA observed in Chapter 4, where it is restricted to the base of the cup, in contrast to PikF, which extends throughout the cup and reaches the rim. Additionally, MyoB, a class I myosin, has been implicated in macropinocytosis, with MyoB$^-$ cells exhibiting fluid-phase uptake defects (Novak et al., 1995).

On the PikF side, although the molecular function of P80 remains poorly defined, it has been consistently used as a reliable marker of endosomal compartments since its identification (Ravanel et al., 2001). LimC, by contrast, is better characterised and has been previously shown to localise to macropinocytic cups (Khurana et al., 2002), in a pattern strikingly similar to that of the GFP-PikF, as presented in Chapter 4. These findings further strengthen the evidence for distinct and non-redundant roles of PikA and PikF in macropinocytosis, and suggest that the four interactors act as key effectors that mediate Class I PI3K isoform-specific regulation of macroendocytic machinery.

In summary, this chapter underscores the intricate, isoform-specific regulatory roles of Class I PI3Ks in *D. discoideum* macropinocytosis. Together with live-cell imaging (Chapter 4), the AP-MS data indicate that PikA and PikF act within distinct yet interconnected spatial domains of the macropinocytic cup, likely organised by isoform-specific interactor networks. The striking resemblance between the PikF^{-} ‘spiky’ phenotype and Rac1 overexpression (Dumontier et al., 2000) further suggests antagonistic signalling axes that shape cytoskeletal architecture at the cup rim. Collectively, our findings support a working model in which spatial segregation and differential scaffolding establish PikA and PikF specificity: PikA supporting initiation at the base and PikF confining Rac-dependent dynamics at the rim. In alignment with Hoeller *et al*. (2013) this framework explains their non-redundant roles during the transition from membrane ruffling to cup closure.

5.4 References

Bähler, M., Rhoads, A., 2002. Calmodulin signaling via the IQ motif. FEBS Lett. 513, 107–113. https://doi.org/10.1016/S0014-5793(01)03239-2

Bañuelos, S., Saraste, M., Carugo, K.D., 1998. Structural comparisons of calponin homology domains: implications for actin binding. Structure 6, 1419–1431. https://doi.org/10.1016/S0969-2126(98)00141-5

Bogdanovic, A., Bennett, N., Kieffer, S., Louwagie, M., Morio, T., Garin, J., Satre, M., Bruckert, F., 2002. Syntaxin 7, syntaxin 8, Vti1 and VAMP7 (vesicle-associated membrane protein 7) form an active SNARE complex for early macropinocytic compartment fusion in Dictyostelium discoideum. Biochem. J. 368, 29–39. https://doi.org/10.1042/bj20020845

Bogdanovic, A., Bruckert, F., Morio, T., Satre, M., 2000. A Syntaxin 7 Homologue Is Present in Dictyostelium discoideum Endosomes and Controls Their Homotypic Fusion. J. Biol. Chem. 275, 36691–36697. https://doi.org/10.1074/jbc.M006710200

Brazill, D.T., Meyer, L.R., Hatton, R.D., Brock, D.A., Gomer, R.H., 2001. ABC transporters required for endocytosis and endosomal pH regulation in Dictyostelium. J. Cell Sci. 114, 3923–3932. https://doi.org/10.1242/jcs.114.21.3923

Buckley, C.M., Pots, H., Gueho, A., Vines, J.H., Munn, C.J., Phillips, B.A., Gilsbach, B., Traynor, D., Nikolaev, A., Soldati, T., Parnell, A.J., Kortholt, A., King, J.S., 2020. Coordinated Ras and Rac Activity Shapes Macropinocytic Cups and Enables Phagocytosis of Geometrically Diverse Bacteria. Curr. Biol. 30, 2912-2926.e5. https://doi.org/10.1016/j.cub.2020.05.049

Cao, D., Su, Z., Wang, W., Wu, H., Liu, X., Akram, S., Qin, B., Zhou, J., Zhuang, X., Adams, G., Jin, C., Wang, X., Liu, L., Hill, D.L., Wang, D., Ding, X., Yao, X., 2015. Signaling Scaffold Protein IQGAP1 Interacts with Microtubule Plus-end Tracking Protein SKAP and Links Dynamic Microtubule Plus-end to Steer Cell Migration *. J. Biol. Chem. 290, 23766–23780. https://doi.org/10.1074/jbc.M115.673517

Chen, Y., Aardema, J., Corey, S.J., 2013. Biochemical and functional significance of F-BAR domain proteins interaction with WASP/N-WASP. Semin. Cell Dev. Biol. 24, 280–286. https://doi.org/10.1016/j.semcdb.2013.01.005

Comer, F.I., Lippincott, C.K., Masbad, J.J., Parent, C.A., 2005. The PI3K-Mediated Activation of CRAC Independently Regulates Adenylyl Cyclase Activation and Chemotaxis. Curr. Biol. 15, 134–139. https://doi.org/10.1016/j.cub.2005.01.007

Cvrčková, F., Rivero, F., Bavlnka, B., 2004. Evolutionarily conserved modules in actin nucleation: lessons from Dictyostelium discoideum and plants. Protoplasma 224, 15–31. https://doi.org/10.1007/s00709-004-0058-2

de Araujo, M.E.G., Naschberger, A., Fürnrohr, B.G., Stasyk, T., Dunzendorfer-Matt, T., Lechner, S., Welti, S., Kremser, L., Shivalingaiah, G., Offterdinger, M., Lindner, H.H., Huber, L.A., Scheffzek, K., 2017. Crystal structure of the human lysosomal mTORC1 scaffold complex and its impact on signaling. Science 358, 377–381. https://doi.org/10.1126/science.aao1583

de Chassey, B., Dubois, A., Lefkir, Y., Letourneur, F., 2001. Identification of clathrin-adaptor medium chains in Dictyostelium discoideum: differential expression during development.

Dragoi, I.A., O'Halloran, T.J., 1998. Cloning and characterization of a Dictyostelium gene encoding a small GTPase of the Rab11 family. J. Cell. Biochem. 70, 29–37. https://doi.org/10.1002/(SICI)1097-4644(19980701)70:1<29::AID-JCB4>3.0.CO;2-5

Faix, J., Clougherty, C., Konzok, A., Mintert, U., Murphy, J., Albrecht, R., Mühlbauer, B., Kuhlmann, J., 1998. The IQGAP-related protein DGAP1 interacts with Rac and is involved in the modulation of the F-actin cytoskeleton and control of cell motility.

Faix, J., Weber, I., Mintert, U., Köhler, J., Lottspeich, F., Marriott, G., 2001. Recruitment of cortexillin into the cleavage furrow is controlled by Rac1 and IQGAP-related proteins.

EMBO J. 20, 3705–3715. https://doi.org/10.1093/emboj/20.14.3705
Filić, V., Marinović, M., Faix, J., Weber, I., 2014. The IQGAP-related protein DGAP1 mediates signaling to the actin cytoskeleton as an effector and a sequestrator of Rac1 GTPases. Cell. Mol. Life Sci. 71, 2775–2785. https://doi.org/10.1007/s00018-014-1606-3
Filić, V., Mijanović, L., Putar, D., Talajić, A., Ćetković, H., Weber, I., 2021. Regulation of the Actin Cytoskeleton via Rho GTPase Signalling in Dictyostelium and Mammalian Cells: A Parallel Slalom. Cells 10, 1592. https://doi.org/10.3390/cells10071592
Fukata, M., Watanabe, T., Noritake, J., Nakagawa, M., Yamaga, M., Kuroda, S., Matsuura, Y., Iwamatsu, A., Perez, F., Kaibuchi, K., 2002. Rac1 and Cdc42 Capture Microtubules through IQGAP1 and CLIP-170. Cell 109, 873–885. https://doi.org/10.1016/S0092-8674(02)00800-0
George, S.P., Esmaeilniakooshkghazi, A., Roy, S., Khurana, S., 2020. F–actin-bundling sites are conserved in proteins with villin-type headpiece domains. Mol. Biol. Cell 31, 1857–1866. https://doi.org/10.1091/mbc.E20-02-0158
Hakala, M., Wioland, H., Tolonen, M., Kotila, T., Jegou, A., Romet-Lemonne, G., Lappalainen, P., 2021. Twinfilin uncaps filament barbed ends to promote turnover of lamellipodial actin networks. Nat. Cell Biol. 23, 147–159. https://doi.org/10.1038/s41556-020-00629-y
Hasegawa, T., Yoshida, S., Sugeno, N., Kobayashi, J., Aoki, M., 2018. DnaJ/Hsp40 Family and Parkinson's Disease. Front. Neurosci. 11. https://doi.org/10.3389/fnins.2017.00743
Hirst, J., Schlacht, A., Norcott, J.P., Traynor, D., Bloomfield, G., Antrobus, R., Kay, R.R., Dacks, J.B., Robinson, M.S., 2014. Characterization of TSET, an ancient and widespread membrane trafficking complex. eLife 3, e02866. https://doi.org/10.7554/eLife.02866
Hoeller, O., Bolourani, P., Clark, J., Stephens, L.R., Hawkins, P.T., Weiner, O.D., Weeks, G., Kay, R.R., 2013. Two distinct functions for PI3-kinases in macropinocytosis. J. Cell Sci. jcs.134015. https://doi.org/10.1242/jcs.134015
Jia, X., Lin, L., Guo, S., Zhou, L., Jin, G., Dong, J., Xiao, J., Xie, X., Li, Y., He, S., Wei, Z., Yu, C., 2024. CLASP-mediated competitive binding in protein condensates directs microtubule growth. Nat. Commun. 15, 6509. https://doi.org/10.1038/s41467-024-50863-3
Junemann, A., Filić, V., Winterhoff, M., Nordholz, B., Litschko, C., Schwellenbach, H., Stephan, T., Weber, I., Faix, J., 2016. A Diaphanous-related formin links Ras signaling directly to actin assembly in macropinocytosis and phagocytosis. Proc. Natl. Acad. Sci. 113, E7464–E7473. https://doi.org/10.1073/pnas.1611024113
Jung, G., Pan, M., Alexander, C.J., Jin, T., Hammer, J.A., 2022. Dual regulation of the actin cytoskeleton by CARMIL-GAP. J. Cell Sci. 135, jcs258704. https://doi.org/10.1242/jcs.258704
Khurana, B., Khurana, T., Khaire, N., Noegel, A.A., 2002. Functions of LIM proteins in cell polarity and chemotactic motility. EMBO J. 21, 5331–5342. https://doi.org/10.1093/emboj/cdf550
Konzok, A., Weber, I., Simmeth, E., Hacker, U., Maniak, M., Müller-Taubenberger, A., 1999. Daip1, a Dictyostelium Homologue of the Yeast Actin-Interacting Protein 1, Is Involved in Endocytosis, Cytokinesis, and Motility. J. Cell Biol. 146, 453–464. https://doi.org/10.1083/jcb.146.2.453
Körber, S., Junemann, A., Litschko, C., Winterhoff, M., Faix, J., 2023. Convergence of Ras- and Rac-regulated formin pathways is pivotal for phagosome formation and particle uptake in Dictyostelium. Proc. Natl. Acad. Sci. 120, e2220825120. https://doi.org/10.1073/pnas.2220825120
Lee, S., Shen, Z., Robinson, D.N., Briggs, S., Firtel, R.A., 2010. Involvement of the Cytoskeleton in Controlling Leading-Edge Function during Chemotaxis. Mol. Biol. Cell 21, 1810–1824. https://doi.org/10.1091/mbc.e10-01-0009
Loovers, H.M., Kortholt, A., de Groote, H., Whitty, L., Nussbaum, R.L., van Haastert, P.J.M.,

2007. Regulation of Phagocytosis in Dictyostelium by the Inositol 5-Phosphatase OCRL Homolog Dd5P4. Traffic 8, 618–628. https://doi.org/10.1111/j.1600-0854.2007.00546.x
Ma, X., Li, J., Liu, N., Banerjee, S., Hu, X., Wang, X., Dong, J., Liu, K., Yang, C., Dong, Z., 2024. Insights into the distinct membrane targeting mechanisms of WDR91 family proteins. Structure 32, 2287-2300.e4. https://doi.org/10.1016/j.str.2024.09.023
Marinović, M., Mijanović, L., Šoštar, M., Vizovišek, M., Junemann, A., Fonović, M., Turk, B., Weber, I., Faix, J., Filić, V., 2019. IQGAP-related protein IqgC suppresses Ras signaling during large-scale endocytosis. Proc. Natl. Acad. Sci. 116, 1289–1298. https://doi.org/10.1073/pnas.1810268116
Mayya, C., Naveena, A.H., Sinha, P., Wunder, C., Johannes, L., Bhatia, D., 2022. The roles of dynein and myosin VI motor proteins in endocytosis. J. Cell Sci. 135, jcs259387. https://doi.org/10.1242/jcs.259387
McCann, R.O., Craig, S.W., 1997. The I/LWEQ module: a conserved sequence that signifies F-actin binding in functionally diverse proteins from yeast to mammals. Proc. Natl. Acad. Sci. U. S. A. 94, 5679–5684. https://doi.org/10.1073/pnas.94.11.5679
McKnight, N.C., Yue, Z., 2013. Beclin 1, an Essential Component and Master Regulator of PI3K-III in Health and Disease. Curr. Pathobiol. Rep. 1, 231–238. https://doi.org/10.1007/s40139-013-0028-5
Mercanti, V., Blanc, C., Lefkir, Y., Cosson, P., Letourneur, F., 2006. Acidic clusters target transmembrane proteins to the contractile vacuole in Dictyostelium cells. J. Cell Sci. 119, 837–845. https://doi.org/10.1242/jcs.02808
Mikati, M.A., Breitsprecher, D., Jansen, S., Reisler, E., Goode, B.L., 2015. Coronin Enhances Actin Filament Severing by Recruiting Cofilin to Filament Sides and Altering F-Actin Conformation. J. Mol. Biol. 427, 3137–3147. https://doi.org/10.1016/j.jmb.2015.08.011
Mondal, S., Burgute, B., Rieger, D., Müller, R., Rivero, F., Faix, J., Schleicher, M., Noegel, A.A., 2010. Regulation of the Actin Cytoskeleton by an Interaction of IQGAP Related Protein GAPA with Filamin and Cortexillin I. PLoS ONE 5, e15440. https://doi.org/10.1371/journal.pone.0015440
Morris, J.H., Knudsen, G.M., Verschueren, E., Johnson, J.R., Cimermancic, P., Greninger, A.L., Pico, A.R., 2014. Affinity purification–mass spectrometry and network analysis to understand protein-protein interactions. Nat. Protoc. 9, 2539–2554. https://doi.org/10.1038/nprot.2014.164
Novak, K.D., Peterson, M.D., Reedy, M.C., Titus, M.A., 1995. Dictyostelium myosin I double mutants exhibit conditional defects in pinocytosis. J. Cell Biol. 131, 1205–1221. https://doi.org/10.1083/jcb.131.5.1205
Pankiv, S., Dahl, A.K., Aas, A., Andersen, R.L., Brech, A., Holland, P., Singh, S., Bindesbøll, C., Simonsen, A., 2024. BEACH domain proteins function as cargo-sorting adaptors in secretory and endocytic pathways. J. Cell Biol. 223, e202408173. https://doi.org/10.1083/jcb.202408173
Pollitt, A.Y., Insall, R.H., 2008. Abi Mutants in Dictyostelium Reveal Specific Roles for the SCAR/WAVE Complex in Cytokinesis. Curr. Biol. 18, 203–210. https://doi.org/10.1016/j.cub.2008.01.026
Poukkula, M., Kremneva, E., Serlachius, M., Lappalainen, P., 2011. Actin-depolymerizing factor homology domain: A conserved fold performing diverse roles in cytoskeletal dynamics. Cytoskeleton 68, 471–490. https://doi.org/10.1002/cm.20530
Pribic, J., Garcia, R., Kong, M., Brazill, D., 2011. Paxillin and Phospholipase D Interact To Regulate Actin-Based Processes in Dictyostelium discoideum. Eukaryot. Cell 10, 977–984. https://doi.org/10.1128/ec.00282-10
Ravanel, K., Chassey, B. de, Cornillon, S., Benghezal, M., al, et, 2001. Membrane sorting in the endocytic and phagocytic pathway of Dictyostelium discoideum. Eur. J. Cell Biol. 80, 754–64.
Reck-Peterson, S.L., Redwine, W.B., Vale, R.D., Carter, A.P., 2018. The cytoplasmic dynein transport machinery and its many cargoes. Nat. Rev. Mol. Cell Biol. 19, 382–398.

https://doi.org/10.1038/s41580-018-0004-3
Rehberg, M., Gräf, R., 2002. Dictyostelium EB1 Is a Genuine Centrosomal Component Required for Proper Spindle Formation. Mol. Biol. Cell 13, 2301–2310. https://doi.org/10.1091/mbc.e02-01-0054
Sala, S., Oakes, P.W., 2023. LIM domain proteins. Curr. Biol. 33, R339–R341. https://doi.org/10.1016/j.cub.2023.03.030
Samereier, M., Baumann, O., Meyer, I., Gräf, R., 2010. Analysis of Dictyostelium TACC reveals differential interactions with CP224 and unusual dynamics of Dictyostelium microtubules. Cell. Mol. Life Sci. CMLS 68, 275–287. https://doi.org/10.1007/s00018-010-0453-0
Seastone, D.J., Harris, E., Temesvari, L.A., Bear, J.E., Saxe, C.L., Cardelli, J., 2001. The WASp-like protein Scar regulates macropinocytosis, phagocytosis and endosomal membrane flow in Dictyostelium. J. Cell Sci. 114, 2673–2683. https://doi.org/10.1242/jcs.114.14.2673
Sébastien, M., Paquette, A.L., Prowse, E.N.P., Hendricks, A.G., Brouhard, G.J., 2025. Doublecortin restricts neuronal branching by regulating tubulin polyglutamylation. Nat. Commun. 16, 1749. https://doi.org/10.1038/s41467-025-56951-2
Shen, K., Sidik, H., Talbot, W.S., 2016. The Rag-Ragulator Complex Regulates Lysosome Function and Phagocytic Flux in Microglia. Cell Rep. 14, 547–559. https://doi.org/10.1016/j.celrep.2015.12.055
Singh, S.P., Thomason, P.A., Insall, R.H., 2021. Extracellular Signalling Modulates Scar/WAVE Complex Activity through Abi Phosphorylation. Cells 10, 3485. https://doi.org/10.3390/cells10123485
Šoštar, M., Marinović, M., Filić, V., Pavin, N., Weber, I., 2024. Oscillatory dynamics of Rac1 activity in Dictyostelium discoideum amoebae. PLOS Comput. Biol. 20, e1012025. https://doi.org/10.1371/journal.pcbi.1012025
Szklarczyk, D., Kirsch, R., Koutrouli, M., Nastou, K., Mehryary, F., Hachilif, R., Gable, A.L., Fang, T., Doncheva, N.T., Pyysalo, S., Bork, P., Jensen, L.J., von Mering, C., 2023. The STRING database in 2023: protein-protein association networks and functional enrichment analyses for any sequenced genome of interest. Nucleic Acids Res. 51, D638–D646. https://doi.org/10.1093/nar/gkac1000
Szklarczyk, D., Nastou, K., Koutrouli, M., Kirsch, R., Mehryary, F., Hachilif, R., Hu, D., Peluso, M.E., Huang, Q., Fang, T., Doncheva, N.T., Pyysalo, S., Bork, P., Jensen, L.J., von Mering, C., 2025. The STRING database in 2025: protein networks with directionality of regulation. Nucleic Acids Res. 53, D730–D737. https://doi.org/10.1093/nar/gkae1113
Thines, L., Roushar, F.J., Hedman, A.C., Sacks, D.B., 2023. The IQGAP scaffolds: Critical nodes bridging receptor activation to cellular signaling. J. Cell Biol. 222, e202205062. https://doi.org/10.1083/jcb.202205062
Tsujioka, M., Uyeda, T.Q.P., Iwadate, Y., Patel, H., Shibata, K., Yumoto, T., Yonemura, S., 2019. Actin-binding domains mediate the distinct distribution of two Dictyostelium Talins through different affinities to specific subsets of actin filaments during directed cell migration. PLOS ONE 14, e0214736. https://doi.org/10.1371/journal.pone.0214736
Vardar, D., Chishti, A.H., Frank, B.S., Luna, E.J., Noegel, A.A., Oh, S.W., Schleicher, M., McKnight, C.J., 2002. Villin-type headpiece domains show a wide range of F-actin-binding affinities. Cell Motil. 52, 9–21. https://doi.org/10.1002/cm.10027
Walsh, M.P., 1983. Review Article Calmodulin and its roles in skeletal muscle function. Can. Anaesth. Soc. J. 30, 390–398. https://doi.org/10.1007/BF03007862
Wang, F., Zhang, L., Zhang, G.-L., Wang, Z.-B., Cui, X.-S., Kim, N.-H., Sun, S.-C., 2014. WASH complex regulates Arp2/3 complex for actin-based polar body extrusion in mouse oocytes. Sci. Rep. 4, 5596. https://doi.org/10.1038/srep05596
Welliver, T.P., Swanson, J.A., 2012. A growth factor signaling cascade confined to circular ruffles in macrophages. Biol. Open 1, 754–760. https://doi.org/10.1242/bio.20121784
Xu, J., Gu, J., Pei, W., Zhang, Y., Wang, L., Gao, J., 2024. The role of lysosomal membrane

proteins in autophagy and related diseases. FEBS J. 291, 3762–3785. https://doi.org/10.1111/febs.16820
Yamamoto, K., Pardee, J.D., Reidler, J., Stryer, L., Spudich, J.A., 1982. Mechanism of interaction of Dictyostelium severin with actin filaments. J. Cell Biol. 95, 711–719. https://doi.org/10.1083/jcb.95.3.711
Yerramilli, V.S., Ross, A.H., Scarlata, S., Gericke, A., 2022. IQGAP1 scaffolding links phosphoinositide kinases to cytoskeletal reorganization. Biophys. J. 121, 793–807. https://doi.org/10.1016/j.bpj.2022.01.018
Zhou, Z., Sayed, N., Pyriochou, A., Roussos, C., Fulton, D., Beuve, A., Papapetropoulos, A., 2008. PROTEIN KINASE G PHOSPHORYLATES SOLUBLE GUANYLYL CYCLASE ON SERINE 64 AND INHIBITS ITS ACTIVITY. Arterioscler. Thromb. Vasc. Biol. 28, 1803–1810. https://doi.org/10.1161/ATVBAHA.108.165043

Chapter 6: Discussion

This thesis presents a comprehensive investigation into the non-redundant, isoform-specific roles of the Class I PI3Ks PikA and PikF in *Dictyostelium discoideum* macropinocytosis. Through a multidisciplinary approach combining structural analysis, protein engineering, genetic manipulation, live-cell imaging, and proteomics, this thesis provides evidence that PikA and PikF perform distinct, non-redundant functions throughout the spatial and temporal progression of macropinocytic cup formation (Hoeller et al., 2013). Our findings indicate that these functional differences do not arise from the structurally conserved catalytic domains, but rather from isoform-specific interactions primarily mediated by divergent N-terminal regions. Nonetheless, the precise roles of individual domains within the PI3K catalytic core – aside from the catalytic domain itself – remain unresolved.

Our findings, based on the successful construction and visualisation of GFP-PikA and GFP-PikF constructs, reveal that PikA is enriched at the base of the forming macropinocytic cup, whereas PikF extends throughout the cup and up to the rim, establishing a differential localisation pattern. Notably, PikF function appears to depend in part on non-catalytic mechanisms, including scaffolding roles and the feedback regulation of Rac activity. These findings are illustrated in Figure 6.1, which contextualises PikA and PikF localisation alongside published data on the distribution of F-actin, SCAR/WAVE, and RGBARG within macropinocytic cup structures (Buckley et al., 2020; Veltman et al., 2016). Additionally, live-cell imaging suggests that PikA and PikF may be differentially trafficked, with PikA appearing in vesicular compartments – offering novel insight into the dynamics of their recruitment and function. However, these trafficking behaviours require further characterisation. To our knowledge, this represents the first direct visualisation of Class I PI3K dynamics in *Dictyostelium discoideum.*

Furthermore, proteomic analyses reveal largely distinct interaction networks for each isoform. PikA preferentially associates with cytoskeletal transport machinery, including kinesins (Kif2-Kif11), dynein-dynactin components (DynF, DynB, DynE), and the dynein regulator NudE – supporting our observations of its vesicular trafficking. It also interacts with actin nucleators such as the formin ForG and the class I myosin MyoB, both of which are implicated in macropinocytic cup formation (Körber et al., 2023; Novak et al., 1995). Notably, these findings provide a potential molecular basis for previously unresolved questions, such as whether actomyosin contraction or microtubule-based transport contributes to the inward progression of macropinocytic cups. As Lutton et al. (2023) stated: “Although we observe no clear evidence for a role of actomyosin contraction or microtubule motors, we cannot completely dismiss the possibility that they contribute to the inward stretching of the cup into the cell body.” Our data now offer strong support for this possibility, implicating PikA-associated motor proteins in this process (Lutton et al., 2023).

In contrast, PikF interacts predominantly with proteins involved in actin disassembly and cortical regulation – including Profilin-2, LimC, Aip1, Twinfilin, and Severin – supporting the hypothesis that PikF functions primarily during the later stages of macropinocytic cup formation, particularly in cup closure and cytoskeletal remodelling (Hoeller et al., 2013). These isoform-specific interactomes suggest that PikA and PikF engage distinct molecular networks to coordinate different stages of macropinocytic cup formation and underscore a broader, spatially organised regulatory framework in which PI3K signalling is tightly coupled to localised cytoskeletal dynamics.

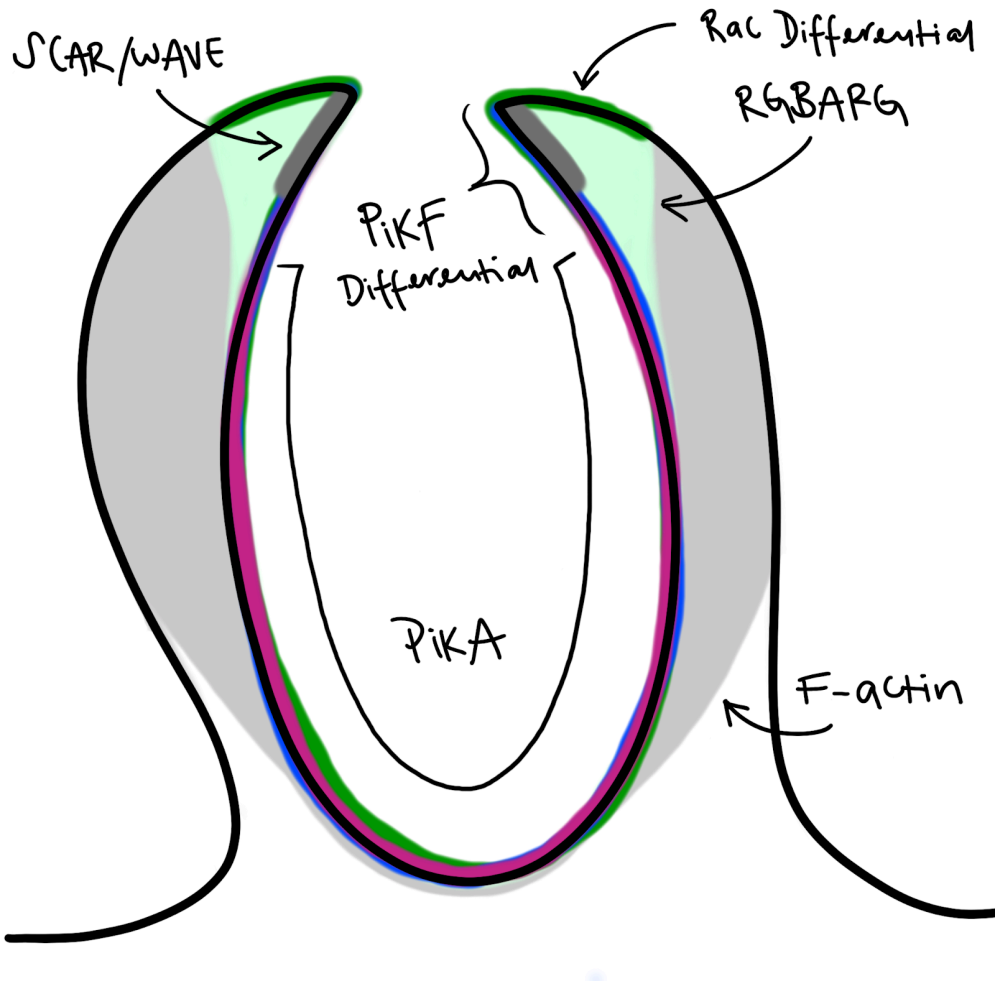

Figure 6.1: Schematic illustration of PikA and PikF localisation within macropinocytic cups, shown in relation to F-actin, SCAR/WAVE and RGBARG. PikA is depicted as enriched at the base of the cup (magenta), while PikF extends throughout the cup and up to the rim, forming a differential localisation pattern (blue). F-actin scaffolding support is indicated in grey, with SCAR/WAVE enrichment at the cup rim shown in dark grey. The “annulus” of extended Rac activity beyond the Ras domain is represented in dark green, and the area of RGBARG localisation is shown in light green. Localisation data are based on our observation of PikA and PikF dynamics, plus published findings on F-actin, SCAR/WAVE and RGBARG activity (Buckley et al., 2020; Veltman et al., 2016). Illustration created in Procreate for iPad.

Our findings challenge the prevailing view of PI3Ks as functioning solely in PIP_3 production and instead support a model in which isoform specificity arises from spatial segregation, distinct protein-protein interaction networks, and tightly regulated feedback loops involving Ras and Rac GTPases. This expanded framework repositions Class I PI3Ks as spatial coordinators of cytoskeletal dynamics, rather than merely lipid kinases.

Building on this model, Figure 6.2 illustrates how Rac dysregulation in the absence of PikF can lead to the formation of elongated, spike-like protrusions driven by unregulated linear F-actin polymerisation, uncoupled from branched actin networks. In contrast, Figure 6.3 presents a proposed mechanism for wild-type cells, in which branched and linear F-actin networks are spatially and temporally coordinated during macropinocytic cup formation. Controlled Rac activity and PI3K isoform localisation ensure that branched F-actin polymerisation occurs at the cup rim via the SCAR/WAVE complex, while linear filaments – potentially mediated by formins – support cup stability and provide upward propulsion. Areas requiring actin capping to prevent uncontrolled expansion are also highlighted, emphasising the critical role of regulated actin turnover in maintaining functional macropinocytic cup architecture.

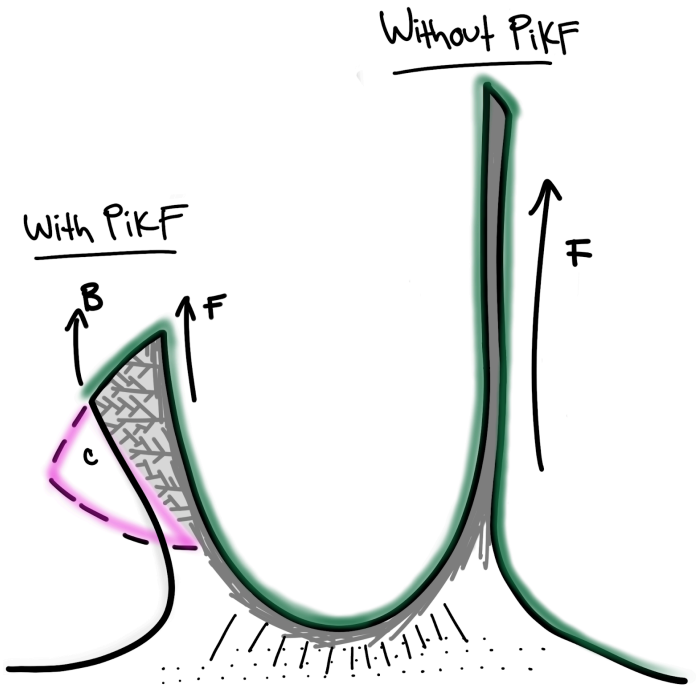

Figure 6.2: Model illustrating the effects of PikF loss on Rac regulation and actin dynamics during macropinocytic cup formation. In wild-type cells, PikF localises throughout the cup and extends to the rim – where PikA is absent – contributing to the spatial confinement of Rac activity (green). This localisation ensures the coordinated formation of branched actin networks and linear filament-driven protrusions (labelled “F”). In the absence of PikF, this regulatory feedback is disrupted, leading to uncontrolled Rac activity extending beyond the cup rim and resulting in the formation of elongated, spike-like protrusions that are uncoupled from branched actin polymerisation (labelled “B”). Regions requiring the capping of branched filaments to maintain cup integrity are indicated as “C.” Illustration created in Procreate for iPad.

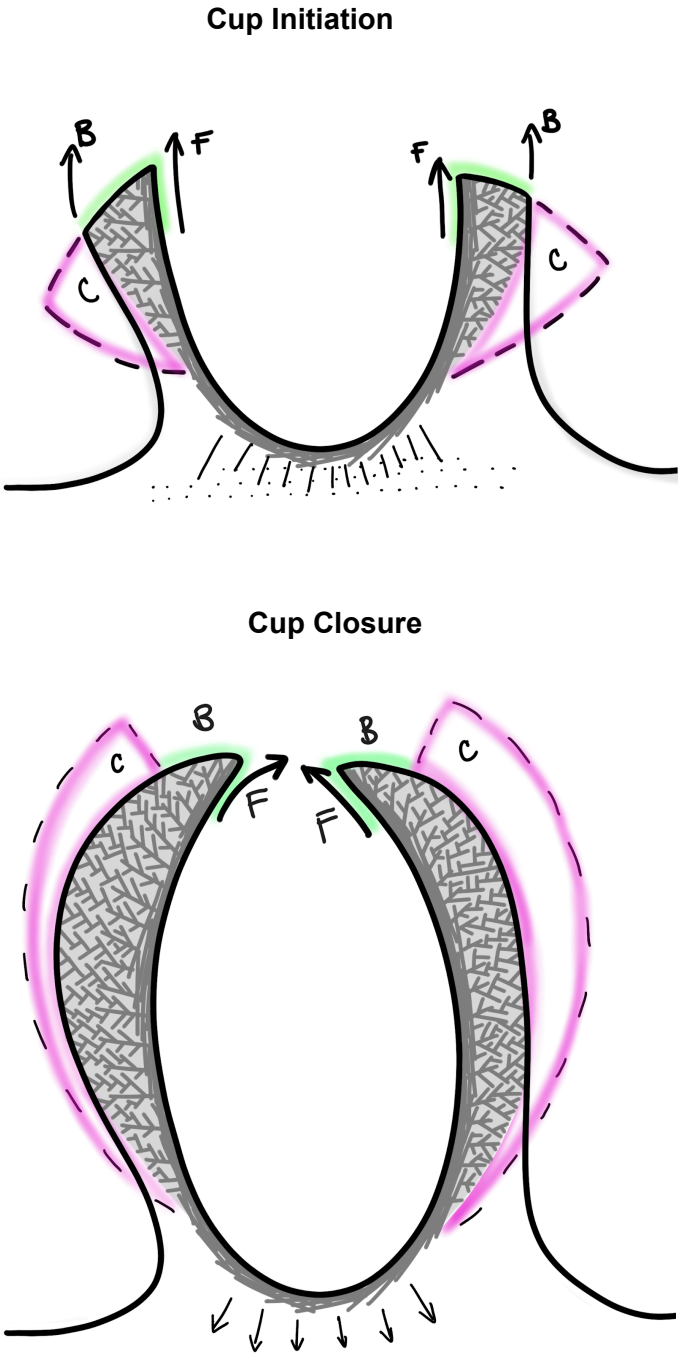

Figure 6.3: Model illustrating the coordinated regulation of branched and linear actin networks during macropinocytic cup formation in wild-type *D. discoideum* cells. Branched actin polymerisation at the cup rim (labelled “B”) is driven by SCAR/WAVE and Arp2/3 complexes, facilitating membrane ruffling and cup extension. Simultaneously, linear actin filaments (labelled “F”), likely nucleated by formins, support structural integrity and upward propulsion. Regions requiring the capping of branched actin filaments to prevent uncontrolled expansion are indicated as “C.” At the base of the cup, the illustration depicts a proposed anchoring and pulling mechanism, potentially mediated by PikA-associated myosins. Illustration created in Procreate for iPad.

References

Buckley, C.M., Pots, H., Gueho, A., Vines, J.H., Munn, C.J., Phillips, B.A., Gilsbach, B., Traynor, D., Nikolaev, A., Soldati, T., Parnell, A.J., Kortholt, A., King, J.S., 2020. Coordinated Ras and Rac Activity Shapes Macropinocytic Cups and Enables Phagocytosis of Geometrically Diverse Bacteria. Curr. Biol. 30, 2912-2926.e5. https://doi.org/10.1016/j.cub.2020.05.049

Hoeller, O., Bolourani, P., Clark, J., Stephens, L.R., Hawkins, P.T., Weiner, O.D., Weeks, G., Kay, R.R., 2013. Two distinct functions for PI3-kinases in macropinocytosis. J. Cell Sci. jcs.134015. https://doi.org/10.1242/jcs.134015

Körber, S., Junemann, A., Litschko, C., Winterhoff, M., Faix, J., 2023. Convergence of Ras- and Rac-regulated formin pathways is pivotal for phagosome formation and particle uptake in Dictyostelium. Proc. Natl. Acad. Sci. 120, e2220825120. https://doi.org/10.1073/pnas.2220825120

Lutton, J.E., Coker, H.L.E., Paschke, P., Munn, C.J., King, J.S., Bretschneider, T., Kay, R.R., 2023. Formation and closure of macropinocytic cups in Dictyostelium. Curr. Biol. 33, 3083-3096.e6. https://doi.org/10.1016/j.cub.2023.06.017

Novak, K.D., Peterson, M.D., Reedy, M.C., Titus, M.A., 1995. Dictyostelium myosin I double mutants exhibit conditional defects in pinocytosis. J. Cell Biol. 131, 1205–1221. https://doi.org/10.1083/jcb.131.5.1205

Veltman, D.M., Williams, T.D., Bloomfield, G., Chen, B.-C., Betzig, E., Insall, R.H., Kay, R.R., 2016. A plasma membrane template for macropinocytic cups. eLife 5, e20085. https://doi.org/10.7554/eLife.20085